ISSN 2786-6696 (print)
ISSN 2786-670X (online)

МІНІСТЕРСТВО ОСВІТИ І НАУКИ УКРАЇНИ

ОДЕСЬКА ДЕРЖАВНА АКАДЕМІЯ
БУДІВНИЦТВА ТА АРХІТЕКТУРИ

СУЧАСНЕ БУДІВНИЦТВО ТА АРХІТЕКТУРА

ЗБІРНИК НАУКОВИХ ПРАЦЬ

Випуск № 5
вересень 2023

ОДЕСА 2023

СУЧАСНЕ БУДІВНИЦТВО ТА АРХІТЕКТУРА
ЗБІРНИК НАУКОВИХ ПРАЦЬ
ISSN 2786-6696 (print) ISSN 2786-670X (online)

Випуск № 5, вересень 2023

Збірник наукових праць видається під назвою "Сучасне будівництво та архітектура" з 2022 р., періодичність – 4 рази на рік.

Попередня назва збірнику – Вісник Одеської державної академії будівництва та архітектури, з 2000 р.

Засновник і видавець – Одеська державна академія будівництва та архітектури, м. Одеса.

Свідоцтво про державну реєстрацію КВ №25221-15161ПР від 10 червня 2022 р.

Збірник наукових праць входить до переліку наукових фахових видань України, у яких можуть публікуватися результати дисертаційних робіт. Наказ МОН України №1643 від 28.12.2019 року (**категорія Б**).

З 2016 р. збірник наукових праць індексується в міжнародній науковометричній базі Index Copernicus.

У збірнику представлені результати наукових і експериментально-теоретичних досліджень у галузі будівництва та архітектури; будівельних конструкцій; будівельних матеріалів та технологій; гідротехнічного та транспортного будівництва; інженерних мереж та обладнання; основ та фундаментів; технології та організації будівельного виробництва.

Призначений для наукових працівників, спеціалістів проектних установ та виробничих підприємств будівельної галузі, аспірантів та магістрів навчальних закладів.

Рекомендовано до видання Вченою радою ОДАБА
Протокол № 1 від 31.08.2023 р.
Свідоцтво КВ №25221-15161ПР від 10.06. 2022 р.
Наказ МОН України №1643 від 28.12.2019 р. (категорія Б)

ISSN 2786-6696 (print)
ISSN 2786-670X (online)

ISSN 2786-6696 (print)
ISSN 2786-670X (online)

MINISTRY OF EDUCATION AND SCIENCE OF UKRAINE

ODESSA STATE ACADEMY
OF CIVIL ENGINEERING AND ARCHITECTURE

MODERN CONSTRUCTION AND ARCHITECTURE

COLLECTION OF SCIENTIFIC WORKS

Issue № 5
September 2023

ODESSA 2023

MODERN CONSTRUCTION AND ARCHITECTURE
COLLECTION OF SCIENTIFIC WORKS
ISSN 2786-6696 (print) ISSN 2786-670X (online)

Issue № 5, September 2023

Collection of scientific works has been published under name "Modern construction and architecture" since 2022, frequency – 4 times a year.

The previous title of the collection – Bulletin of Odessa State Academy of Civil Engineering and Architecture, since 2000.

Founder and publisher – Odessa State Academy of Civil Engineering and Architecture (OSACEA), Odessa**.**

Certificate of state registration КВ №25221-15161ПР, 10 June, 2022.

Collection of scientific works enters the list of scientific editions of Ukraine, in which thesis results can be published. Order of the Ministry of Education and Science of Ukraine № 1643, 28 December, 2019 (category B).

Since 2016 collection of scientific works is indexed into International scientometric base of the Index Copernicus.

Results of scientific and experimental-theoretical researches in the field of construction and architecture; building structures, building materials and techniques; hydrotechnical and transport construction; utility networks and facilities; basement and foundations; technology and organization of building production are presented in the collection.

It is assigned for scientific workers, specialists of design organizations and manufacturing enterprises of construction domain, postgraduates, masters of educational institutions.

Recommended for publication by the Academic Board of the OSACEA
Protocol № 1, 31 August, 2023.
Certificate КВ №25221-15161ПР, 10 June, 2022.
Order of Ministry of Education and Science of Ukraine № 1643, 28 December, 2019 (category B).

ISSN 2786-6696 (print)
ISSN 2786-670X (online)

ЗМІСТ

АРХІТЕКТУРА

БУДІВЕЛЬНІ КОНСТРУКЦІЇ

БУДІВЕЛЬНІ МАТЕРІАЛИ ТА ТЕХНОЛОГІЇ

ІНЖЕНЕРНІ МЕРЕЖІ ТА ОБЛАДНАННЯ

ТЕХНОЛОГІЯ ТА ОРГАНІЗАЦІЯ БУДІВЕЛЬНОГО ВИРОБНИЦТВА

CONTENTS

TECHNOLOGY AND ORGANIZATION OF BUILDING PRODUCTION

UDC 699.85 DOI: 10.31650/2786-6696-2023-5-9-15

VOLUME-PLANNING SOLUTIONS OF PRE-SCHOOL EDUCATION INSTITUTIONS WITH PLACEMENT OF SHELTERS

Zhydkova T.V., Ph.D., Associate Professor,
tavlz@ukr.net, ORCID: 0000-0001-7903-7073
National Aviation University
L. Huzara Avenue, 1, Kyiv, 03058, Ukraine

Abstract. The article highlights one of the most pressing problems of today – the protection of children in educational institutions. The author analyzes the main requirements of the current legislative and regulatory documentation on the protection of children in preschool education institutions during military operations; recommendations of the State Emergency Service; the main provisions of the concept of security of educational institutions.

The purpose of this study is to develop proposals for the placement of protected premises in preschool institutions, which will ensure the maximum possible safety, physical and psychological comfort of staying in a protected space in these conditions.

Proposals have been developed to change approaches to the space-planning solutions of preschool buildings with the arrangement of protected rooms in the middle span of the building, which will ensure the maximum possible safety, physical and psychological comfort of staying in a protected space.

The possibility of using the bedrooms of a kindergarten as a shelter is substantiated.

A comparative analysis of regulatory requirements for insolation and energy saving in preschool educational institutions is carried out. It is emphasized that there is a mismatch between the requirements of these requirements and the safety of existing premises of preschool institutions.

Proposals for new building codes for the protection of children in educational institutions, including the area of the premises per child, recommendations for the use of these premises in peacetime, and the composition of furniture and equipment, are analyzed.

If these proposals are adopted, which include the use of bedrooms as permanent premises in the protected part of the building, as well as ensuring the optimal ratio of energy saving and insolation requirements, architects will have to completely revise their approach to the space-planning solutions for kindergartens.

The new space-planning solutions will make preschool buildings more compact, which will provide energy savings, and most importantly, there will be rooms in the middle part of the building that will be enclosed by at least two main walls and, with appropriate structural strength, can be used as shelters.

The results of the research can be used in practice in the construction of shelters in preschools.

Keywords: kindergarten, protected premises, space-planning solutions, current building codes, insolation, energy saving.

Introduction. Already in the first months of the war, it became clear that educational institutions were one of the priority targets of missile strikes. Russian troops are destroying schools and universities, kindergartens and orphanages. The attacks are carried out with operational and tactical missiles, causing significant damage to buildings. According to the Ministry of Education and Science, as of the beginning of June, 3450 educational institutions were damaged by bombing and shelling, and 331 of them were completely destroyed. This disaster has not spared any region of Ukraine (Fig. 1) [11].

The mass deaths of children in educational institutions were avoided only because kindergartens were not open. After more than a year of war, we realized that life had changed forever and that we would not be safe for decades to come. From time to time, the situation will escalate, the enemy will accumulate forces and use missile attacks to destroy the population of Ukraine again.

Therefore, ensuring proper conditions for education and organizing a safe educational environment is the most pressing issue of our time.

Fig. 1. Destroyed kindergartens in different regions of Ukraine

Analysis of recent research and publications. The main provisions for protecting the population of Ukraine from military operations are clearly defined in legislation and regulations. The Civil Protection Code of Ukraine contains a list of facilities intended to protect the population. In accordance with the law, regulatory documents define the requirements for protective structures [3, 5].

In December 2021, the Institute for Public Administration and Research in Civil Protection published the State Emergency Service's guidelines "Organization of Sheltering the Population in the Civil Protection Facilities Fund". These recommendations additionally confirm the main provisions of the existing regulatory documentation [6].

In July 2022, the State Emergency Service of Ukraine published recommendations on the organization of shelter in the facilities of the fund of civil protection structures for personnel and children of educational institutions [8].

On April 7, 2023, the government adopted the Concept of Security of Educational Institutions, which contains a comprehensive strategic vision for creating a safe educational environment. The concept is based on the premise that every Ukrainian child should have access to quality education while staying in the facilities of the protective facilities fund [9].

The goal and objectives are to develop proposals for the placement of protected premises within the buildings of preschool institutions.

To achieve this goal, the following tasks were set:

– to analyze regulatory requirements, methodological documentation, recommendations of the State Emergency Service and orders of the Cabinet of Ministers on the safety of educational institutions;

– to consider options for the placement of protective premises in preschool education institutions that will ensure the maximum possible safety, physical and psychological comfort of staying in a protected space.

Research methodology. The following methods were used in the study: collection of information, study of regulatory documentation, analysis of the materials obtained and their systematization, comparative analysis of typological developments of space-planning solutions and project documentation for preschool education institutions.

Research results. The requirements of current legislative and regulatory documentation [3, 5], recommendations of the State Emergency Service [1, 6, 8], the main provisions of the concept of safety of educational institutions [7], as well as the norms that establish requirements for the design and construction of new and reconstruction of existing buildings of preschool education institutions [2] were analyzed.

Today, the process of creating new modern building codes to protect civilians, including in educational institutions, is underway.

According to the proposals to be included in the new State Building Standards, it is recommended that shelters for educational institutions be designed in the basement of the building or separately located in the underground space.

When no shelter is needed, these premises should be used to meet the needs of the educational institution, namely for creative studios, for club work with children, for parental education, for civil protection training with participants in the educational process and for practicing emergency algorithms, etc.

At the same time, the room should be equipped with bunk beds, children's tables and chairs, toy cabinets, shoe racks, etc. All this equipment has nothing to do with the use of the premises in peacetime.

Therefore, it turns out that a kindergarten should have two sets of this furniture for use in peacetime (the period between the intensification of armed aggression) and separately for shelter, as well as an additional storage room where all this should be stored. During a prolonged alert, employees should have time to remove the room's equipment (tables and chairs for adults, art studio equipment, etc.) and place children's beds and chairs.

It should be emphasized that, according to these recommendations, a kindergarten should have two sets of furniture, including children's beds – in bedrooms and in shelters.

The right decision is to use safe spaces for their main function. A safe space can be not only a separately built protective structure, but also a kindergarten bedroom located in the basement or middle section of the house. In this case, it is only necessary to reinforce the walls and ceilings of the room, which already has some protection "between the two walls" (Fig. 2).

The degree of protection of children in such a room will be not lower, but even higher than in a free-standing shelter due to the reflectivity of the building structures.

If it is impossible to place a shelter in an underground space, in case of a high groundwater level or in a catastrophic flood zone, the proposed solution may be the only way to ensure the protection of children.

An analysis of the regulatory requirements for the main premises of preschools specified in the current building codes showed that the area of bedrooms should be 2.4-2.5 m^2 per child, depending on the category of preschool education institutions [2].

At the same time, when working on the main provisions of the new state building codes, experts determined the minimum area of the main premises for preschool institutions within 3.0 m^2 per person in protective structures for new construction and 2.0 m^2 for reconstruction. As it turned out, these figures coincide with the standard for the area of sleeping rooms.

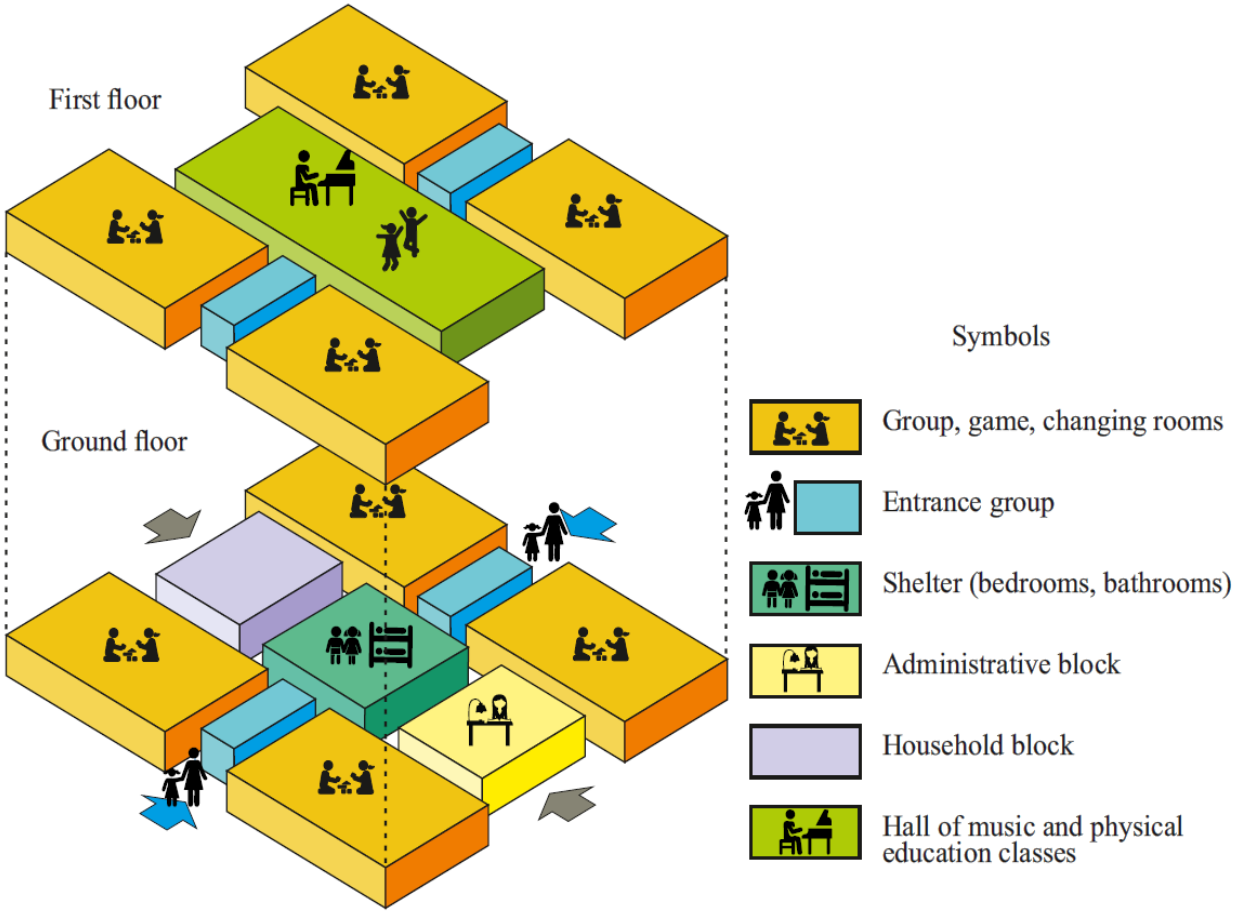

Fig. 2. Schematic diagram of the location of a shelter in preschools

The shelter should be equipped with bunk beds or transforming beds, chairs and tables for 100% of the children. Additionally, it is recommended to provide a play area, a toy closet and a shoe rack.

In accordance with the requirements of the Ministry of Education and Science, the main room of the shelter should have a rest area with children's beds, a play area with a carpet with toys, and a study area with tables and chairs.

We developed and analyzed options for the placement of this furniture within the main premises of the shelter when using three-tiered transformer beds.

In accordance with the requirements of the Ministry of Education and Science, the main room of the shelter should be divided into blocks of 60 children with the arrangement of furniture that should be equipped in such a room. A block for 60 children contains 3 groups of 20 children each). The area of the main room per group of children should be 60 m^2 at the rate of 3.0 m^2 per child.

If transforming beds are used, this area is sufficient to accommodate sleeping places and space for games, creativity and learning (Fig. 3).

Thus, children's bedrooms with transforming furniture can be a safe space in preschools. During an air raid, if children are resting at this time, they will not even hear the sounds of explosions, while at other times bedrooms can quickly turn into playrooms (Fig. 3).

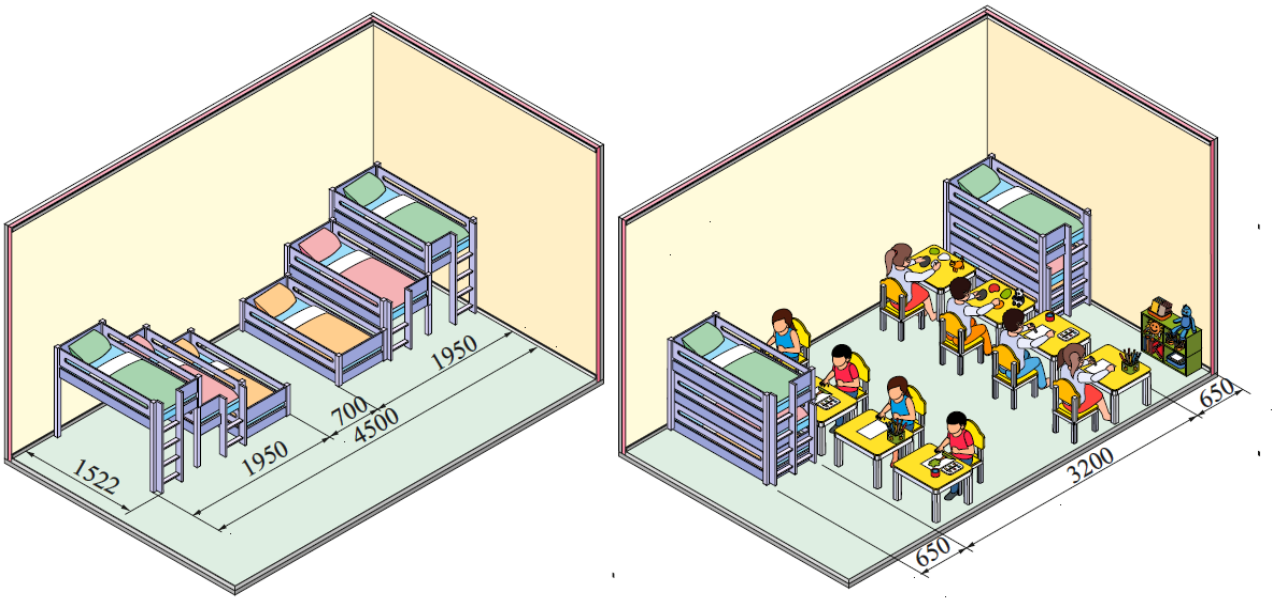

a) b)

Fig. 3. Arrangement of a fragment of the shelter:
a – during daytime rest; b – during games and studying

Thus, children's bedrooms with "transformer" furniture can be a safe space in preschools. During an air raid, if children are resting at this time, they will not even hear the sounds of explosions, while at other times bedrooms can quickly turn into playrooms (Fig. 3).

If such a solution is adopted, the bedrooms that are also shelters will not have external lighting, but, in our opinion, it is not necessary for bedrooms to have good enough ventilation.

The only obstacle to this solution is the requirements for insolation and natural light. The requirements of the sanitary regulations for preschool educational institutions determine the need for natural light for the main premises of preschool educational institutions, while the list of these premises does not include bedrooms [10].

The current building codes require at least three hours of continuous sun exposure per day for bedrooms [2].

The analysis of the layout of existing preschool buildings has shown that these buildings have a rather large area of external walls, which significantly exceeds the requirements of the calculated building compactness index, which is determined by the ratio of the total area of the internal surfaces of the external envelope of the building envelope to the volume of the building that is heated or cooled. This indicator is important in determining the degree of energy saving of a building [4].

The area of window openings is much larger than necessary to meet the regulatory requirements for lighting and insolation. In terms of safety during missile strikes, the large windows and single-bay buildings of the main premises of the kindergarten make them very vulnerable. Therefore, it is necessary to harmonize the requirements for insolation, energy saving and safety of kindergarten premises.

If these proposals are accepted, regarding the use of bedrooms as permanent premises in the protected part of the building, as well as ensuring the optimal ratio of energy saving and insolation requirements, architects will have to completely revise the approach to the space-planning solutions of kindergartens. New space-planning solutions will make preschool buildings more compact, which, first of all, will provide energy savings, and most importantly, there will be rooms in the middle part of the building that will be enclosed by at least two main walls and, with appropriate structural strength, can be used as shelters.

Conclusions.

Proposals have been developed to change approaches to the space-planning solutions of preschool educational institutions with the arrangement of protected rooms in the middle span of the building, which will ensure the maximum possible safety, physical and psychological comfort of staying in a protected space under these conditions.

A comparative analysis of the regulatory requirements for insolation and energy saving in preschool educational institutions was conducted.

If these proposals for the use of bedrooms as permanent premises in the protected part of the building are adopted, as well as ensuring the optimal ratio of energy saving and insolation requirements, architects will have to completely revise the approach to the space-planning solutions of kindergartens. The new space-planning solutions will make preschool buildings more compact, which, first of all, will provide energy savings, and most importantly, there will be rooms in the middle part of the building that will be enclosed by at least two main walls and, with appropriate structural strength, can be used as shelters.

References

[1] Alhorytm dii mistsevykh orhaniv vykonavchoi vlady Orhaniv mistsevoho samovriaduvannia, orhaniv upravlinnia osvitoiu, kerivnykiv zakladiv osvity shchodo zabezpechennia ukryttia uchasnykiv osvitnoho protsesu u fondi zakhysnykh sporud tsyvilnoho zakhystu. [Online]. Available: https://dsns.gov.ua/upload/6/2/2/0/9/6/bHq4WGc8HMHX4wGPIKG9gv4DSEgLx4uEUDgqIVGV.pdf Access date: August 8, 2023.

[2] DBN V.2.2-4:2018. Zaklady doshkilnoi osvity. Budynky i sporudy. Chynnyi vid 2018–10–01. Kyiv.: Minrehion. 2018.

[3] DBN V.2.2-5-97 Zakhysni sporudy tsyvilnoi oborony. Budynky i sporudy. Zi Zminamy [Chynnyi vid 2019-01-01]. – Kyiv : Minrehion, 2018.

[4] DBN V.2.6-31:2021 Teplova izoliatsiia ta enerhoefektyvnist budivel – Chynnyi vid 2022-09-01 – Kyiv Minirehion Ukrainy 2022.

[5] Kodeks tsyvilnoho zakhystu Ukrainy. Dokument 5403-VI, chynnyi, potochna redaktsiia vid 01.01.2023.

[6] Orhanizatsiia ukryttia naselennia u fondi zakhysnykh sporud tsyvilnoho zakhystu. Vprovadzhennia inzhenerno-tekhnichnykh zakhodiv tsyvilnoho zakhystu: seriia praktychnykh poradnykiv / O.Ia. Leshchenko, H.V. Truntsev, V.M. Mykhailov, M.V. Andriienko, V.F. Korobkin, N.M. Romaniuk, L.V. Kalynenko; za zah. red. P.B. Volianskoho, S.A. Partaliana. K. : IDU ND TsZ, 2021. Seriia 9. 63 s. [Online]. Available: https://radnuk.com.ua/pravova-baza/orhanizatsiia-ukryttia-naselennia-u-fondi-zakhysnykh-sporud-tsyvilnoho-zakhystu/ Access date: August 8, 2023.

[7] Pro skhvalennia Kontseptsii bezpeky zakladiv osvity. Rozporiadzhennia Kabinetu Ministriv Ukrainy vid 7 kvitnia 2023 r. № 301-r [Online]. Available: https://www.kmu.gov.ua/npas/pro-skhvalennia-kontseptsii-bezpeky-zakladiv-osvity-i070423-301 Access date: August 8, 2023.

[8] Rekomendatsii shchodo orhanizatsii ukryttia v obiektakh fondu zakhysnykh sporud tsyvilnoho zakhystu personalu ta ditei (uchniv, studentiv) zakladiv osvity. [Online]. Available: https://www.zakon.help/files/article/12178/Rekom.shchodo.orhanizatsiyi.ukryttya.15.06.2022.pdf. Access date: August 8, 2023.

[9] Rozvyvalne osvitnie seredovyshche v zakladi doshkilnoi osvity: metodychnyi posibnyk / ukl. L. B. Mishchenko; za red. I. V. Udovychenko. Sumy. Niko: 2021. 52 s.

[10] SR 234, Sanitarnyi rehlament dlia doshkilnykh navchalnykh zakladiv [Online]. Available: https://zakon.rada.gov.ua/laws/show/z0563-16#Text Access date: August 8, 2023.

[11] Zaklady osvity, shcho postrazhdaly vid bombarduvan ta obstriliv [Online]. Available: https://mon.gov.ua/ua. Access date: August 8, 2023.

ОБ'ЄМНО-ПЛАНУВАЛЬНІ РІШЕННЯ ЗАКЛАДІВ ДОШКІЛЬНОЇ ОСВІТИ З РОЗМІЩЕННЯМ УКРИТТІВ

Жидкова Т.В., к.т.н., доцент,
tavlz@ukr.net, ORCID: 0000-0001-7903-7073
Національний авіаційний університет
проспект Л. Гузара, 1, Київ, 03058, Україна

Анотація. У статті висвітлено одну з найактуальніших проблем сьогодення – захист дітей в закладах освіти. Проаналізовано основні вимоги чинної законодавчої та нормативної документації, щодо захисту дітей в закладах дошкільної освіти під час воєнних дій; рекомендації Державної служби з надзвичайних ситуацій; основні положення концепції безпеки закладів освіти.

Метою даного дослідження є розробка пропозицій щодо розміщення захищених приміщень в дитячих дошкільних закладах, які забезпечать максимально можливу в цих умовах безпеку, фізичну та психологічну комфортність перебування в захищеному просторі.

Розроблено пропозиції щодо зміни підходів до об'ємно-планувальних рішень будинків дошкільних закладів освіти з влаштуванням захищених приміщень в середньому прогоні будинку, забезпечить максимально можливу в цих умовах безпеку, фізичну та психологічну комфортність перебування в захищеному просторі.

Обґрунтовано можливість використання під укриття спальних кімнат дитячого садочку.

Проведено порівняльний аналіз нормативних вимог щодо інсоляції та енергоощадження в дошкільних закладах освіти. Наголошено на невідповідності зазначених вимог й безпеки наявних приміщень дитячих дошкільних закладів.

Проаналізовано пропозиції до нових будівельних норм, щодо захисту дітей в закладах освіти, зокрема площу приміщення з розрахунку на одну дитину, рекомендації, щодо використання цих приміщень в мирний час, склад меблів та обладнання.

В разі прийняття зазначених пропозицій, щодо використання спальних кімнат як приміщень постійного призначення в захищеній частині будинку, а також забезпечення оптимального співвідношення вимог енергоощадження й інсоляції, архітекторам доведеться повністю переглянути підхід до об'ємно-планувальних рішень дитячих садочків.

Нові об'ємно-планувальні рішення зроблять будинки дошкільних закладів освіти більш компактними, що забезпечить енергоощадження, а головне, з'являться приміщення в серединній частині будинку, які будуть огороджені щонайменше двома капітальними стінами й, при відповідній міцності конструкцій, зможуть використовуватись як укриття.

Результати досліджень можуть бути використані на практиці при влаштуванні укриття в дитячих дошкільних закладах.

Ключові слова: дитячий дошкільний заклад, захищені приміщення, об'ємно-планувальні рішення, чинні будівельні норми, інсоляція, енергоощадження.

Стаття надійшла до редакції 14.07.2023

УДК 711.1 DOI: 10.31650/2786-6696-2023-5-16-23

КОМПЛЕКСНИЙ АНАЛІЗ ТА ОЦІНКА ТЕРИТОРІЙ МІСТА ЯК ПЕРШОЧЕРГОВЕ ВИЗНАЧЕННЯ ПОТРЕБ ДЛЯ ФОРМУВАННЯ КОМФОРТНОГО ТА БЕЗПЕЧНОГО МІСЬКОГО ПРОСТОРУ

[1]**Нижник О.В.**, д.т.н., професор,
alnyzhnyk@gmail.com, ORCID: 0000-0002-2672-1987
[1]**Завальний О.В.**, к.т.н., професор,
azavalniy@i.ua, ORCID: 0000-0002-6191-2893
[1]*Харківський національний університет міського господарства ім. О.М. Бекетова*
вул. М. Бажанова, 17, м. Харків, 61002, Україна

Анотація. Формування міського простору, яке в експлуатації є комфортним та безпечним для його користувачів – найвища мета сучасної містобудівної науки. Після аналізу існуючих практик планування було встановлено, що першочерговою передумовою формування міського простору є визначення потреб місцевості, які встановлюються після комплексних аналізів та оцінки територій. Саме потреби визначають напрям їх розвитку.

В даній роботі розглянуті існуючі методи аналізу та оцінки територій, та визначені їх характерні ознаки, які потребують аналізу та оцінки для встановлення більш чітких дій для покращення простору. В даній статті було досліджено питання щодо комплексного аналізу та оцінки територій міста, та їх вплив на формування, реформування та реконструкції міського простору. Ціллю даного дослідження була систематизація знань щодо аналізу та оцінки міських територій. На базі виявлених проблем відбувається встановлення передумов для формування комфортного міського простору для всіх рівнів потреб його мешканців та користувачів.

В сучасному місті відбувається багато процесів одночасно, які впливають на функціональний поділ територій відповідно до домінуючих діяльностей на них. Сформульовані чіткі містобудівні задачі для рішення допомагають: зберегти позитивні та змінити негативні характеристики міського простору, взяти до уваги погляди місцевих жителів та користувачів простору, проаналізувати інвестиційні можливості, вперш за все, для розуміння матеріальних перспектив місцевостей.

Комплексний аналіз та оцінка територій міста дозволяє виявити проблеми або конфліктні ситуації у міському просторі, які негативно впливають на його функціонування, розвиток та комфортність. Зазвичай визначення комфортності міста визначають як окремий критерій оцінки, але на думку автора, саме формування комфортного міського простору і є головним завданням для урбаністів, яке включає в себе багато критеріїв, що забезпечують безпечність, екологічність, ідентичність та сучасність простору відповідно до потреб місцевої громади.

В результаті наукового дослідження було встановлено, що доповнення існуючих практик і методик аналізу та оцінки міського простору відповідно до сучасних потреб містобудування дозволить більш якісно та актуально формувати той простір міста, який необхідний мешканцю та його користувачу.

Ключові слова: міський простір, комплексний аналіз, інтегральна оцінка, індекс якості міського простору, формування територій міста, комфортність міського простору.

Вступ. Життя у будь-якому урбанізованому просторі має ряд як позитивних, так і негативних особливостей. В даній статті, розглянуті аспекти при встановленні передумов до формування комфортного і міського простору. Саме повно визначені характеристики території міста при їх комплексному аналізі та оцінці обґрунтовують першочергові передумови для формування, реформування або повної реконструкції міського простору в залежності від потреб простору. Саме проаналізувавши та оцінивши стан, визначивши перспективи розвитку – це дасть змогу якісно та практично сформувати завдання на

проєктування планованої місцевості. Без чіткого завдання і покроковим рішенням містобудівних проблем, які безпосередньо впливають на комфортність міського простору, формування міських територій буде не повним та не якісним. Тому формулювання чітких задач для рішення перед початком планування територій є саме визначення позитивних та негативних характеристик міського простору, поглядів місцевих жителів та користувачів простору і інвестиційних можливостей для розуміння матеріальних перспектив місцевостей.

Аналіз останніх досліджень. Аналізом проблем формування міст та їх територій, планувальної організації та оцінкою якості міського простору займались багато вчених урбаністів. В даній роботі були проаналізовані деякі роботи, які безпосередньо мають вплив на визначення комфортності міського простору, а особливо його аналізу та оцінки.

На якість аналізу та повноту оцінки міського простору впливають багато факторів. Міський простір – це динамічна система, яка постійно змінюється під впливом домінуючих чинників. Вплив соціально-економічних чинників на містобудівні процеси відображається системою зав’язків прикладання праці та селищних зон, їх зв'язок між ними та територіальними особливостями, що детально було розглянуто в роботі М. М. Дьоміна.

В роботі [10] узагальнені моделі естетичного сприйняття і їх інтерпретації до сприйняття міського середовища. В науковій роботі [4] детально висвітлені соціологічні підходи до вивчення міського простору, які були проаналізовані в історичній перспективі. Автором роботи було запропоновано використовувати комплексний підхід до аналізу сучасного міста, основою якого є аналіз сприйняття мешканцями місцевості.

В монографії [2] розглянуте міське середовище як містобудівна система, яка включає зовнішні і внутрішні функції та їх узгодження між собою. Автором було визначено п’ять вимірів такі як: L – людський, P – функціональний, X – умови, G – геометричний, T – часовий. Кожен з вимірів є багатокомпонентним і поділяються на складові залежно від ієрархії простору та характеру містобудівних завдань. Саме така містобудівна модель зможе принципово реформувати інформаційну базу містобудування, структурувати її під містобудівні завдання та орієнтувати на використання комп’ютерних технологій за аналогією з цифровими картами.

В монографії [11] висвітлені теоретичні засади оцінки планувальних рішень на базі розширеної системи містобудівних критеріїв за ознаками ефективності, інтенсивності та керованості забудовою. Були розкритті питання виявлення конфліктних зон та функціонально-просторової організації міста. Саме такий опис функціонально-планувальної оптимізації використання міських територій дав змогу виявляти визначати містобудівні рішення для покращення комфортності міського простору для всіх рівнів потреб.

Детально в роботі [3] були послідовно розглянуті теоретичні основи формування містобудівного кадастру або містобудівного банку даних. Саме такий погляд та організація структури системи інформаційного забезпечення містобудівної діяльності дасть змогу більш ретельно та якісно провести аналіз та оцінки міських територій.

В дисертаційному дослідженні [6] були розроблені методологічні засади оцінювання готовності громад України до впровадження концепції «розумності» на основі диференціації регіонів України за рівнем розвитку інформаційного суспільства шляхом адаптації міжнародної методики розрахунку територіального індексу розвитку ІКТ (ICT Development Index). Дані засади на думку автора забезпечить якісне управління розвитком «розумних» сталих міст та впровадить інформаційно-комунікаційні технології, які дозволять регулювати міських простір відповідно до сучасних потреб.

В науковій роботі [8] розглядаються основні фактори, що зумовлюють стан міського середовища та методи оцінки якості міського середовища у складі інженерного благоустрою міських територій. В роботі були детально розглянуті основні фактори, що впливають на навколишнє середовище. Було встановлено, що спрямованість методів оцінки якості міського середовища визначається питаннями благоустрою, що дозволить більш комплексно підвищити якість існуючого міського середовища.

Метою статті є узагальнити та систематизувати дані щодо комплексного аналізу та оцінки територій міста в сучасних практиках, та проаналізувати передумови формування

комфортного та безпечного міського простору для підготовки дієвого рішення при проєктуванні визначеної місцевості.

Матеріали та методи досліджень. Виконання даного наукового дослідження базувалось на емпіричному методі, що включав в себе спостереження та порівняння існуючих практик аналізу та оцінки міських територій. Також в досліджені використовувався метод моделювання для визначення прогнозованих передумов розвитку міського простору.

Основний матеріал і результати. В міжнародному рейтингу «Economist Intelligence Unit» [15] аналізують та оцінюють близько 140 міст світу. Рейтинг щорічно базується на основі досліджень 30 найважливіших факторів, які впливають на комфортність проживання, наприклад, такі як:

– безпечність;

– доступність медичного обслуговування та освіти;

– якість їжі, доріг та громадського транспорту;

– можливість весело провести час, відпочиваючи в місті.

В рейтингу Найзручніші міста світу у 2023 році [14] був показаний індекс якості міського простору, який включив в себе оцінювання стабільності, якості сфери охорони здоров'я, сфери культури, стану навколишнього середовища, якості сфери освіти та інфраструктури. Оцінювання умов життя було розроблено, щоб допомогти компаніям розрахувати надбавки за важкі умови праці для співробітників, які переїжджають у нове – і, можливо, менш стерпне місто. Також завдяки рейтингу можливо зробити короткий огляд найбільш і найменш бажаних міст для життя, якщо ви емігрант. Відень, з його чудовим поєднанням стабільності та культурних розваг, надійною інфраструктурою, очолює рейтинг в четвертий раз за п'ять років. Копенгаген, місто такого ж розміру з багатьма такими ж характеристиками, посідає друге місце. Мельбурн, який у минулому році очолював рейтинг, посідає третє місце. Загалом дев'ять із першої десятки малих та середніх міст, і навіть більшість із топ-50, знаходяться в багатих країнах. Лондон – опустився на 12 позицію порівняно з минулим роком – займає 46-е місце, а Нью-Йорк опустився на десять позицій до 69-го. З п'яти категорій, охоплених оцінюванням Найзручніші міста світу у 2023 році в середньому знизився лише показник стабільності. Показники стабільності в багатьох містах Східної Європи, які з 2022 року впали через те, що вони розташовані поблизу України, цього року зросли. Страйк робітників у Греції, протести щодо пенсійного забезпечення у Франції та смертельні сутички в Ізраїлі та Перу знизили показники в цих країнах [14]. Рейтинг Найзручніших міст світу у 2023 році показаний на рис. 1.

Рис. 1. Рейтинг Найзручніші міста світу у 2023 році (розроблено The Economist)

Оцінювання міського простору поєднане з процесом його аналізу і визначенням певних критеріїв оцінки. При комплексному аналізі територій міста найчастіше визначають послідовно вид робіт, в яких характеризують населений пункт, місце знаходження в структурах, види діяльності, розвиненість і стан навколишнього середовища та природних ресурсів. Даний аналіз повинен проводитись з прийнятою періодичністю, бо місто – це динамічна система, яка змінює міське середовище кожен день.

В даному досліджені розглянуті сучасні практики аналізу міського простору. На протиріч, існуючим методикам аналізу територій міста з'являються нові більш практичні методи аналізу, які описані та проаналізовані в таблиці 1, визначені їх характерні ознаки та принципи дії.

Принципи дії, кожного з розглянутого сучасного методу дослідження та аналізу міського простору, вказують на гуманістичний та позитивний підхід до формулювання ідей досліджень і дає змогу поєднати людину і простір в одному вимірі. На думку автора, включення принципів проаналізованих методів існуючих методик аналізу територій міста зможе сформувати потреби сучасного мешканця та середовища навколо.

Найзастосованіший підхід щодо оцінки якості міського простору є індикативний, який дозволяє працювати з кількісними кваліметричними показниками [14]. Але в даному підході є деякі труднощі при розгляді параметрів естетичності, зручності, комфорту та інші.

При оцінці територій міста зазвичай використовують індекс якості міського простору як інструмент оцінки матеріальної складової досліджуваного простору. Даний метод оцінювання базується на визначені індикаторів, які безпосередньо впливають на формування міського простору. Індикатори встановлюються відповідно до загальноприйнятих чинних документів, наприклад як програма ООН по розвитку населених пунктів [16]. Всі визначені індикатори складають в матрицю оцінки, тим самим отримуючи індекс якості міського простору. Види індикаторів, які можуть бути оціненими:

– безпечність (площа аварійних будівель та споруд, площа загальнодоступного озеленення, частка освітлених частин вулиць та інші, безпека пересування та інші);

– комфортність (площа будівель та споруд з наявністю інж. комунікацій, рівень озеленення, різновид послуг, культурно-дозвіллєвої та спортивної інфраструктури, доступність зупинок громадського транспорту та інші);

– екологічність (стан зелених насаджень, завантаження доріг та інші);

– ідентичність та різновид (різноманіття забудови, привабливість територій, наявність об'єктів культурної спадщини та інші);

–сучасність та актуальність (різноманітність послуг, озеленення, рівень розвитку громадських просторів та інші);

– ефективність керування простором (наявність зовнішнього оформлення міського простору, рівень прибирання та ремонту громадських територій та інші).

Будь яка оцінка починається визначення питання, що оцінюється та по відношенню до чого. Загалом в містобудуванні об'єктом оцінювання є територія, її природні умови і ресурси та безпосередньо простір, створений цією територією. Але в сучасному світі, міський простір набирає багатовимірних характеристик, таких як час, культурні компоненти, емоційні відчуття. Тому при оцінці міського простору необхідно звертати увагу не лише на економічні, екологічні, соціально-культурні, містобудівні, інфраструктурні, а й на естетичні та чуттєві характеристики простору.

Відповідно до піраміди потреб за А. Маслоу [13], простір не може бути розглянутий без аналізу всіх рівнів людських потреб. На базі цього можливо встановити якісно-модально та якісно-середовищні параметри міського простору, що допоможуть оцінити ментальне, інстинктивне та візуальне сприйняття місцевості.

Виходячи з цього, додатково оцінити міський простір можливо через:

– аналіз міста через зорові кадри та кути зору – спирається на кути зору під якими сприймається верхня межа архітектурних об'єктів та простору;

– сприйняття міста як інформаційний процес – архітектура подається як система, яка, теоретично, за наявності певних вихідних даних може оброблятись комп'ютером, інформаційна система «людина – штучне середовище», де людина – це отримувач інформації, архітектор – творець, архітектурні об'єкти – джерело інформації.

Таблиця 1 – Сучасні методи дослідження та аналізу міського простору [7]

Методи дослідження та аналізу міського простору	Принцип дії
Метод Go-along	Дослідження та аналіз відбувається відповідно до засобів пересування. Walk along – під час руху пішки, ride along – на машині або на велосипеді. Інтерв'юер пересувається містом разом із респондентом, ставлячи уточнювальні запитання щодо того, на що вони подивилися, куди пішли, яким є їхній досвід пересування цими маршрутами тощо. При використанні методу go-along відчуття місця загострюється завдяки тому, що пересування по ньому здійснюється в даний момент. Очевидний недолік цього методу полягає у впливі інтерв'юера на сприйняття міського простору і пересування ним. Так, для когось наявність лавок не проблема, а ось порожні клумби або недоглянутий газон становитимуть дискомфорт.
Метод ментальних карт	Дослідження та аналіз відбувається на базі ментальних карт, які відображають образ міста виходячи з отриманої з різних непрямих та прямих джерел інформації про нього. Метою низки досліджень є вивчення того, як під час пересування містом змінюється уявлення людини про простір, що її оточує, і змінюється та доповнюється ментальна карта.
Метод автоетнографії	Дослідження та аналіз проблеми полягає в тому, що дослідник фіксує досвід свого руху і сприйняття міського простору, а потім аналізує його. Даний метод пов'язаний із вивченням дослідником власного досвіду для розуміння культурного досвіду. Передбачається, що дослідник сам є носієм певної культури, а отже, опис його власного досвіду є одночасно описом самої культури.
Метод аналізу відеозаписів	Дослідження та аналіз відбувається на базі відеозаписів. Даний метод аналізу відеозаписів не дає змоги вивчити сприйняття міського простору. Якоюсь мірою воно може дати інформацію про практики пересування ним, але не про сприйняття. Навіть якщо на відео ми спостерігаємо, що людина протягом тривалого часу дивиться на щось, ми не можемо зробити висновок про те, що саме цей об'єкт її зацікавив. Використовувати метод аналізу відеозаписів можна тільки в тому разі, якщо за цим слідує інтерв'ю з носієм досліджуваної практики
Опитування населення	Дослідження та аналіз відбувається на базі опитування місцевих мешканців або користувачів досліджуваного простору. Анкета опитування повинна повно відображати проблеми та питання, які безпосередньо пов’язані з формування та реформуванням простору.
Аналіз статистики	Дослідження базується на аналізі, зіставлення, порівняння отриманих даних (між собою та з іншими даними), їх узагальнення, тлумачення та формулювання наукових і практичних висновків щодо міського простору.
Спостереження	Аналіз відбувається на базі дослідження конкретних об'єктів спостереження.
Інструментальне обстеження	Дослідження та аналіз відбувається на базі встановлених методик обстеження з покроковою інструкцією.

Результати досліджень. Комплексний аналіз та оцінка територій міста дозволяє виявити проблеми або конфліктні ситуації у міському просторі, які негативно впливають на його функціонування, розвиток та комфортність. Зазвичай, визначення комфортності міста визначають як окремий критерій оцінки, але на думку автора, саме формування комфортного міського простору і є головним завданням для урбаністів, яке включає в себе багато критеріїв, що забезпечують безпечність, екологічність, ідентичність та сучасність простору відповідно до потреб місцевої громади. Тому виявлення сучасних передумов формування міського простору сучасними методами аналізу та оцінки його стану зможе повно наповнити міські території та якісно регулювати, обслуговувати та експлуатувати їх відповідно до потреб громади і їх відношенню до місцевості.

Висновки та перспективи подальших досліджень. В даній статті було досліджено питання щодо комплексного аналізу та оцінки територій міста, їх вплив на формування, реформування та реконструкції міського простору. Було встановлено, що аналіз та оцінка територій міста є першочерговою передумовою для створення завдання на проєктування з визначеними негативними сторонами та проблемами, які впливають на комфортність ведення життєдіяльності населення на певній досліджуваній території. Доповнення існуючих практик та методик аналізу та оцінки міського простору сучасними практичними методами дозволить більш якісно та актуально, відповідно до потреб місцевості, формувати той простір міста, який необхідний сучасному мешканцю та його користувачу. Автор планує у подальшому більш детально визначити фактори передумов формування комфортного міського простору.

Література

1. Биваліна М. В. Містобудівні методи оцінки якості міського середовища. Містобудування та територіальне планування. 2010. № 37. С. 61–63.

2. Габрель М. М. Просторова організація містобудівних систем : монографія. Київ : А.С.С, 2004. 400 с.

3. Дёмин М. М. Управление развитием градостроительных систем. Київ : Будівельник, 1991. 184 с.

4. Денисюк А. І. Вивчення міського простору: історичний огляд та перспективи аналізу. Вісник Харківського національного університету імені В.Н. Каразіна. 2010. № 889. С. 138–141.

5. Дьомін М. М., Сингаївська О. І. Містобудівні інформаційні системи. Містобудівний кадастр. Первинні елементи структури об’єктів містобудування та територіального планування. Київ : Фенікс, 2015. 216 с.

6. Корепанов О. С. Методологічні засади статистичного забезпечення управління розвитком «розумних» сталих міст в Україні: дис. … д-ра екон. наук: 08.00.10. Київ, 2018. 638 с.

7. Методы иследования пространства городской среды - Із будівництва. Останні новини, нормативи та публікації - ДБНУ - Державні будівельні норми України - норми: ДБН, ДСТУ, СНиП, ГОСТ, СН, ВБН. URL: https://dbn.co.ua/publ/metody_isledovanija_prostranstva_gorodskoj_sredy/2-1-0-485 (дата звернення: 9.08.2023).

8. Містобудівні методи оцінки якості міського середовища. / А. А. Лютіков та ін. Містобудування та територіальне планування. 2015. № 58. С. 273–277.

9. Модель планування території новостворених об’єднаних територіальних громад / К. І. Вяткін та ін. “Science progress in European countries: new concepts and modern solutions” : Papers of the 10th international scientific conference, м. Stuttgart, 25 жовт. 2019. С. 84–92.

10. Осиченко Г. О. Модель естетичного сприйняття міського середовища. Сучасні проблеми архітектури та містобудування. 2012. № 29. С. 263–270. URL: https://repositary.knuba.edu.ua/server/api/core/bitstreams/4d839a4a-2114-475f-a4fa-84139b566595/content (дата звернення: 9.08.2023).

11. Плешкановська А. М. Функціонально-планувальна оптимізація використання міських територій : Монографія. Київ : Ін-т Урбаністики, 2005. 190 с.

12. Рыбак А. И., Балдук Г. П., Базарова И. Б. Модель оценки качества городской среды.

Вісник Криворізького національного університету. 2019. № 48. С. 23–31.

13. Учасники проектів Вікімедіа. Піраміда потреб Абрагама Маслоу – Вікіпедія. Вікіпедія. URL: https://uk.wikipedia.org/wiki/Піраміда_потреб_Абрагама_Маслоу (дата звернення: 9.08.2023).

14. The Economist. The world's most liveable cities in 2023. The Economist. URL: https://www.economist.com/graphic-detail/2023/06/21/the-worlds-most-liveable-cities-in-2023 (дата звернення: 9.08.2023).

15. The Economist. Vienna overtakes Melbourne as the world's most liveable city. The Economist. URL: https://www.economist.com/graphic-detail/2018/08/14/vienna-overtakes-melbourne-as-the-worlds-most-liveable-city (дата звернення: 9.08.2023).

16. UN-Habitat - A better urban future | un-habitat. UN-Habitat - A Better Urban Future | UN-Habitat. URL: https://unhabitat.org/ (дата звернення: 9.08.2023).

References

[1] M.V. Byvalina, "Mistobudivni metody otsinky yakosti miskoho seredovyshcha", *Mistobuduvannia ta terytorialne planuvannia*, no. 37, pp. 61–63, 2010.

[2] M.M. Habrel, *Prostorova orhanizatsiia mistobudivnykh system*. Kyiv: A.S.S, 2004.

[3] M.M. Dëmyn, *Upravlenye razvytyem hradostroytelnыkh system*. Kyiv: Budivelnyk, 1991.

[4] A.I. Denysiuk, "Vyvchennia miskoho prostoru: istorychnyi ohliad ta perspektyvy analizu", *Visnyk Kharkivskoho natsionalnoho universytetu imeni V.N. Karazina*, no. 889, pp. 138–141, 2010.

[5] M.M. Domin, O.I. Synhaivska, *Mistobudivni informatsiini systemy. Mistobudivnyi kadastr. Pervynni elementy struktury obiektiv mistobuduvannia ta terytorialnoho planuvannia*. Kyiv: Feniks, 2015.

[6] O.S. Korepanov, "Metodolohichni zasady statystychnoho zabezpechennia upravlinnia rozvytkom «rozumnykh» stalykh mist v Ukraini": dys. … d-ra ekon. nauk: 08.00.10. Kyiv, 2018.

[7] Metodы ysledovanyia prostranstva horodskoi sredы - Iz budivnytstva. Ostanni novyny, normatyvy ta publikatsii - DBNU - Derzhavni budivelni normy Ukrainy - normy: DBN, DSTU, SNyP, HOST, SN, VBN. [Online]. Available: https://dbn.co.ua/publ/metody_isledovanija_prostranstva_gorodskoj_sredy/2-1-0-485. Accessed on: August 9, 2023.

[8] A.A. Liutikov ta in., "Mistobudivni metody otsinky yakosti miskoho seredovyshcha", *Mistobuduvannia ta terytorialne planuvannia*, no. 58, pp. 273–277, 2015.

[9] K.I. Viatkin ta in., "Model planuvannia terytorii novostvorenykh obiednanykh terytorialnykh hromad", *"Science progress in European countries: new concepts and modern solutions", Papers of the 10th international scientific conference*, 2019, pp. 84–92.

[10] H.O. Osychenko, "Model estetychnoho spryiniattia miskoho seredovyshcha", *Suchasni problemy arkhitektury ta mistobuduvannia*, no. 29, pp. 263–270, 2012. [Online]. Available: https://repositary.knuba.edu.ua/server/api/core/bitstreams/4d839a4a-2114-475f-a4fa-84139b566595/content. Accessed on: August 9, 2023.

[11] A.M. Pleshkanovska, *Funktsionalno-planuvalna optymizatsiia vykorystannia miskykh terytorii* : Monohrafiia. Kyiv: In-t Urbanistyky, 2005.

[12] A.Y. Rыbak, H.P. Balduk, Y.B. Bazarova, "Model otsenky kachestva horodskoi sredы", *Visnyk Kryvorizkoho natsionalnoho universytetu*, no. 48, pp. 23–31, 2019.

[13] Uchasnyky proektiv Vikimedia. Piramida potreb Abrahama Maslou – Vikipediia. Vikipediia. [Online]. Available: https://uk.wikipedia.org/wiki/Piramida_potreb_Abrahama_Maslou. Accessed on: August 9, 2023.

[14] The Economist. The worlds most liveable cities in 2023. The Economist. [Online]. Available: https://www.economist.com/graphic-detail/2023/06/21/the-worlds-most-liveable-cities-in-2023. Accessed on: August 9, 2023.

[15] The Economist. Vienna overtakes Melbourne as the worlds most liveable city. The

Economist. [Online]. Available: https://www.economist.com/graphic-detail/2018/08/14/vienna-overtakes-melbourne-as-the-worlds-most-liveable-city. Accessed on: August 9, 2023.
[16] UN-Habitat - A better urban future | un-habitat. UN-Habitat - A Better Urban Future | UN-Habitat. [Online]. Available: https://unhabitat.org/. Accessed on: August 9, 2023.

COMPREHENSIVE ANALYSIS AND ASSESSMENT OF THE CITY'S TERRITORIES AS A PRIORITY IDENTIFICATION OF NEEDS FOR THE FORMATION OF A COMFORTABLE AND SAFE URBAN SPACE

[1]**Nyzhnyk Oleksandr,** Doctor of Technical Sciences, Professor,
alnyzhnyk@gmail.com, ORCID: 0000-0002-2672-1987
[1]**Zavalniy Oleksandr**, Ph.D, Associate Professor,
azavalniy@i.ua, ORCID: 0000-0002-6191-2893
[1]*O.M. Beketov National University of Urban Economy in Kharkiv*
17, Marshal Bazhanov Street, Kharkiv, 61002, Ukraine

Abstract. The formation of urban space that is comfortable and safe for its users is the highest goal of modern urban planning science. After analysing existing planning practices, it was found that the primary prerequisite for the formation of urban space is to determine the needs of the area, which are established after comprehensive analyses and assessment of the territories. The needs determine the direction of their development.

This paper reviews the existing methods of analysis and assessment of territories and identifies their characteristic features that require analysis and assessment to establish clearer actions to improve the space. This article investigates the issue of comprehensive analysis and assessment of urban areas and their impact on the formation, reform and reconstruction of urban space. The purpose of this study was to systematize knowledge on the analysis and assessment of urban areas. Based on the identified problems, the prerequisites for the formation of a comfortable urban space for all levels of needs of its residents and users are established.

In a modern city, many processes take place simultaneously, which affect the functional division of territories in accordance with the dominant activities on them. Formulating clear urban planning tasks helps to: preserve the positive and change the negative characteristics of urban space, take into account the views of local residents and space users, analyse investment opportunities, primarily to understand the material prospects of the area.

A comprehensive analysis and assessment of the city's territories allows identifying problems or conflict situations in the urban space that negatively affect its functioning, development and comfort. Usually, the definition of city comfort is defined as a separate assessment criterion, but in the author's opinion, it is the formation of a comfortable urban space that is the main task for urbanists, which includes many criteria that ensure the safety, environmental friendliness, identity and modernity of the space in accordance with the needs of the local community.

As a result of the research, it was found that supplementing the existing practices and methods of analyzing and assessing urban space in accordance with the current needs of urban planning would allow for a better and more relevant formation of the urban space that is needed by the resident and its user.

Keywords: urban space, comprehensive analysis, integral assessment, urban space quality index, formation of city territories, comfort of urban space.

Стаття надійшла до редакції 12.07.2023

UDC 621.86.065 DOI: 10.31650/2786-6696-2023-5-24-35

DEPENDENCE OF TENSILE FORCE OF THE ELASTIC LIMIT STATE OF ROPES FROM THE BENDING PARAMETER ON THE DRUM

[1]**Vovk P.E.,** Graduate student,
vovk.pavel.1995@gmail.com, ORCID: 0000-0001-6156-1686
[1]**Chaiun I.M.**, DSc., Professor,
i.m.c@ukr.net, ORCID: 0000-0003-0867-8791
[1]*Odessa National Polytechnic University*
Shevchenko avenue, 1, Odessa, 65044, Ukraine

Abstract. Based on the method previously developed by the authors for the analytical determination of the ultimate elastic state of the ropes, the dependence of the $P(\overline{D})$ tensile force with the winding of the rope on the drum on the parameter $\overline{D} = D_d/d_r$ (the ratio of the diameters of the drum and the rope) in the interval $\overline{D} = 10 - 120$. Dependence $P(\overline{D})$ was determined for two loading schemes of rope: stretching of the rope with winding on the drum with a freely suspended load and stretching of the rope with winding on the drum with the load in the guides. Based on the developed method, the dependence of $P(\overline{D})$ was performed for 16 kantais of different designs. The tensile strength is presented in the relative form $\overline{P}(\overline{D}) = P(\overline{D})/P_t$ (P_t total breaking strength of the rope wires). The effort $\overline{P}(\overline{D})$ significantly depends on the construction of the rope and the bending parameter $\overline{D}$. In the section $40 \le \overline{D} \le 120$ the force $\overline{P}(\overline{D})$ increases monotonically and practically linearly, reaching the value corresponding to the calculation scheme of stretching a straight rope. For different structures with the parameter $\overline{D} = 40$ change in force $\Delta\overline{D} = 0.723 - 0.578 = 0.145$ with $\overline{D} = 120 \cdot \Delta\overline{P} = 0.765 - 0.677 = 0.08$. In the section $40 \ge \overline{D} \ge 20$ the dependence $\overline{P}(\overline{D})$ is not linear, at $\overline{D} = 40 \cdot \Delta\overline{P} = 0.663 - 0.418 = 0.245$. The section $20 \ge \overline{D} \ge 10$ is characterized by a sharp change in force $\overline{P}(\overline{D})$, with the bending parameter $\overline{D} = 10 \cdot \Delta\overline{P} = 0.416$. For most rope designs at $\overline{D} < 10$ the forces $\overline{P}(\overline{D})$ are close to zero values. When stretching with a freely suspended load, the forces $\overline{P}(\overline{D})$ are 1.6–1.7 times lower than when stretching in guides. For twisting ropes (one-way winding), the ratio is 2.5–3.4 times. In the normative methods of calculations of lifting ropes, the characteristics P_t or $P_a = 0.83P_t$ are used, which do not take into account the peculiarities of the deformation and construction of the ropes. We believe that the given information is appropriate in solving the issue of building a methodology for calculating the static strength of lifting ropes based on the characteristics of their ultimate elastic state, which will ensure stable optimality of the use of ropes, will allow you to rationally choose the type of rope construction and its dimensions.

Keywords: rope, strength characteristics, calculation scheme, bending parameter when winding on a drum, calculation method for static strength.

Introduction. The strength calculations of lifting ropes use characteristics corresponding to extremely simplified calculation schemes [1–4]. One of them, the most simplified, is the total breaking force:

$$P_t = F_t\sigma_b, \quad (1)$$

where F_t – total area of all wires of the rope;
σ_b – wire strength limit (marked rope group).
The second is the aggregate breaking force of the rope as a whole:

$$P_a = kP_t, \quad (2)$$

where k is a coefficient, which in various sources [1–4] has close, slightly different numerical

values. So, in [1, 2, 4] $k = 0.83$ in [3] $k = 0.75 - 0.90$ (a smaller value refers to three-layer double-wound ropes, more to single-wound ropes).

In the European standard EN 12385-2, 10 indicators of strength characteristics are established for ropes. Two of them fully correspond to the specified characteristics P_t and P_a, the others are based on these two characteristics and are also not connected by real load schemes of the lifting ropes. According to the content, it seems that the characteristics of EN 12385-2 are intended for comprehensive control of rope manufacturing technology.

Such inaccuracy (simplification) of the calculation schemes of the ropes is compensated by an increase in the level of normative safety margins, the interval of which is $[m] = 3 - 13$, according to [1, 2, 4]. We consider the statement in [4, p. 96] that high values of [m] "reflect greater responsibility of steel ropes". Of course, the responsibility, but no less important is the factor of extreme simplicity of the calculation scheme of the ropes. Under such conditions, the calculation of ropes cannot be stably optimal.

Research analysis. In work [1], the calculation of the strength of mine lifting ropes is reduced to a comparison of the normative margin of strength [m] with the estimated:

$$m = \frac{P_t}{S} = \frac{qg\sigma_b}{(Q_k + qL)\gamma}, \quad (3)$$

where S estimated static load;

q – linear rope mass, kg/m;

g – acceleration of free fall, m/s^2;

$\gamma = q/F_t 10^6$ – fictitious (reduced) density;

$Q_k = Q_b + Q_c$ – final mass, which includes the mass of the cargo and the mass of all suspended elements;

L – lift height.

Formula (3) does not take into account the bending of the rope on the drum and blocks.

In Rules [2], the calculation is reduced to checking the selected rope according to the formula:

$$P_a \geq z_p S, \quad (4)$$

where $P_a -$ the second is the aggregate breaking force of the rope as a whole; S – the greatest tension of the rope branch; z_p – minimum utilization factor (safety factor).

In the Rules [2], the influence of rope bending is somewhat taken into account by assigning the minimum diameters of drums, blocks and leveling blocks according to the formulas:

$$D_1 \geq b_1 d;\ D_2 \geq b_2 d;\ D_3 \geq b_3 d, \quad (5)$$

where $D_1; D_2; D_3$ – diameters of drums and blocks;

$b_1; b_2; b_3$ – assignment coefficients for drum and block diameters; d – rope diameter.

Table 1, which combines two tables from the Rules [2], shows the correspondence between the normative safety margins and the parameters $\overline{D} = D_d/d_r$. But this correspondence is not sufficient, because it does not take into account the construction of the ropes, the deformed-stressed state and does not give the connection of the parameter $\overline{D}$ with their strong characteristics.

Table 1 – Minimum safety margins and rope bending parameters $\overline{D}$

Mechanism class according to ISO 4301/1	M_1	M_2	M_3	M_4	M_5	M_6	M_7	M_8
Coefficients of margin of strength of the rope z_p	3.15	3.35	3.55	4	4.5	5.6	7.10	9
$b_1(\overline{D} = D_d/d_r)$	11.2	12.5	14	16	18	20	22.5	25.0
$b_2(\overline{D} = D_d/d_r)$	12.5	14.0	16.0	18.0	20	22.4	25.0	28.0
$b_3(\overline{D} = D_d/d_r)$	11.2	12.5	12.5	14	14	16	18	18

In article [3], where the current state of the ropes in crane installations is analyzed, their calculation for static strength is reduced to a condition of the form (4), but with a different interpretation of the component z_p (he is named "minimum design factor", although in terms of the terms (4) – this is a normative safety factor, it is also taken depending on the class of the mechanism and the type of rope).

In article [4] the calculation is reduced to the appointment of the diameter of the rope according to the condition:

$$[F_0] \geq F_0 = F_{\max} z_p,$$

where $F_0 -$ the second is the aggregate breaking force of the rope as a whole;

$F_{max} -$ the calculated maximum force in the rope; $z_p -$ is the safety coefficient, which is also based on the formula (4).

This means that in the methods considered in the works [3, 4], the strength characteristics of the ropes are taken, which also do not take into account the bending deformation when the rope is wound onto the drum.

In work [5], on the basis of formula (4), it is proposed to determine the value of the breaking force, according to which the rope is selected, taking into account operational features (diameters of the drum, blocks, method of securing the rope, intensity of work, etc.). But here the deformed-stressed state of the ropes is not taken into account too.

In Germany [6], in order to increase the service life of the ropes, it is recommended to assign the parameter $\overline{D}$ depending on the lifting speed: at a speed greater than 4 m/s, the parameter $\overline{D} \geq 100$ at a speed lower than 4 m/s, the parameter $\overline{D} \geq 60$ These ratios apply to ropes of all structures except closed, for which $\overline{D} \geq 120$ is recommend.

In the USA, according to the Federal Law "Occupational Safety and Safety", the following standards are established for mining installations designed for the transportation of people: $\overline{D} \geq 60$ when the diameter of the rope is less than 25.4 mm; $\overline{D} \geq 80$ when the diameter of the rope is more than 25.4 mm; $\overline{D} \geq 100$ for closed ropes.

Similar offers are also indicated by rope manufacturers. So, the English company "Bridon" recommends a parameter $\overline{D}$ in the range of 100-120 for closed ropes of its production. In the past, the Khartsyz steel wire and rope plant for closed lifting ropes with a diameter of 20-38 mm GOST 10506 recommended the following ratios: for ropes with a diameter of $d \geq 27$ mm parameter $\overline{D} \geq 90$ for ropes with a diameter of $d \geq 30$ mm parameter $\overline{D} \geq 120$.

It can be seen from the given analysis: consideration of the bending of lifting ropes is somewhat assumed, but without connection with their design, with the external and internal deformed-tension state of the ropes, and there is no connection of the parameter $\overline{D}$ with the corresponding strength characteristics of the ropes.

Aim of the study. The aim of the work is an analytical study of the dependence of the tensile force of the ropes (those their strength characteristics) in the limiting elastic state of the bending parameter associated with winding on the drum under conditions of loading with a load in the guides and with free suspension. Ultimately, the aim is subordinated to the proposal to use such characteristics in the methods for calculating ropes for static strength. This will provide a significant increase in the accuracy of the design scheme of the ropes in comparison with the existing regulated methods, which are based on the strength characteristics that do not correspond to the loading schemes of the ropes.

Research materials and methods. The finite element method was used to study the strained state of the rope. Two schemes of rope loading are considered: stretching of the rope with winding on the drum with a freely suspended load and stretching of the rope with winding on the drum with the load in the guides.

Research results. In this work, on the basis of external and internal deformed states, it is proposed to study the dependence of the tensile force $P_e(\overline{D})$ of the limit elastic state of the rope on the bending parameter $\overline{D} = D_d/d_r$ when winding on a drum. Fig. 1 shows the schemes of the

loaded and deformed state of the lifting rope, which are characterized by the bending parameter $\overline{D}$ and internal force factors (IFF) in sections: N – longitudinal force; M, L, Γ torque and bending moments. The solution of the given task is based on the theoretical foundations of works [6, 7]. Let's consider their relationship with the final formula of dependence $P_e(\overline{D})$ on the basis of the deformed state corresponding to the diagrams (Fig. 1) of the rope load.

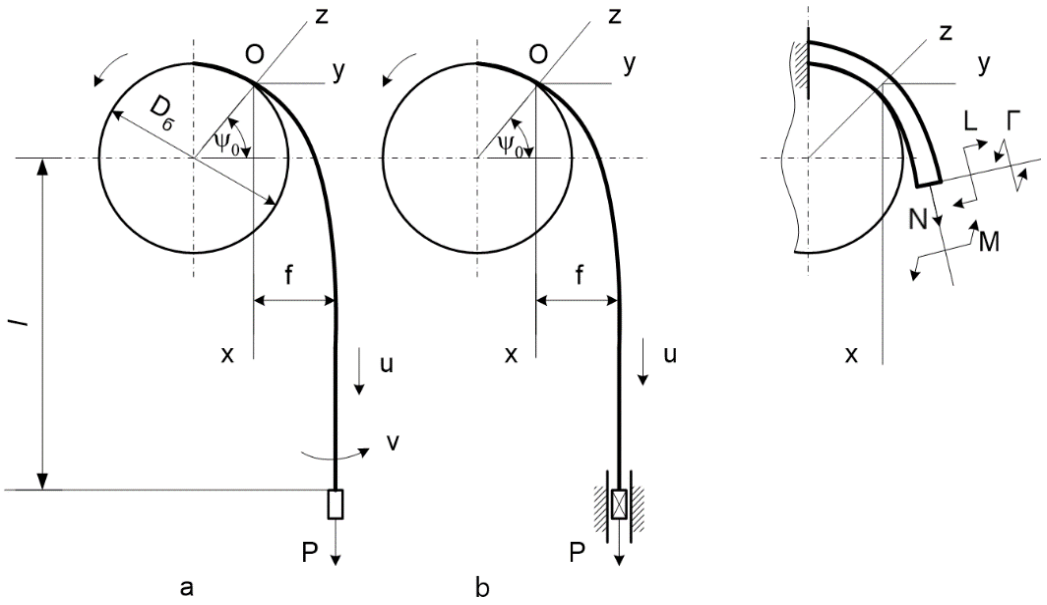

Fig. 1. Rope load schemes:
a – the load is freely suspended; b – the load is in the guides

The external deformed state of the rope is expressed by the vector of deformations:

$$|DK| = |\varepsilon\theta\chi\xi| = |G|^{-1}|F|. \quad (6)$$

Here $\varepsilon, \theta, \chi, \xi$ – according to stretching, torsion, and bending deformations (in the elastic state, the components of the vector $|F|$ IFF are proportional to them;

$|G|$ – global stiffness matrix of the rope section:

$$|G| = \begin{vmatrix} G_{11} & G_{12} & G_{13} & G_{14} \\ G_{21} & G_{22} & G_{23} & G_{24} \\ G_{31} & G_{32} & G_{33} & G_{34} \\ G_{41} & G_{11} & G_{43} & G_{44} \end{vmatrix} = \sum_1^S sc\ \alpha_i\ sc\beta_i |K|_i \begin{vmatrix} \Phi_{p_i} & & & 0 \\ & \Phi_{t_i} & & \\ & & \Phi_{u_i} & \\ 0 & & & \Phi_{u_i} \end{vmatrix} |K|_i^T, \quad (7)$$

where $G_{11}, G_{22}, G_{33}, G_{44}$ – the main stiffnesses of the rope section (longitudinal, torsional, bending);

$G_{12} = G_{21};\ G_{13} = G_{31}$ etc. – severity of impact;

$\Phi_{p_i} = \mathrm{E}\pi\delta^2/4;\ \Phi_{t_i} = \mathrm{E}\pi\delta^4/80; \Phi_{u_i} = \mathrm{E}\pi\delta^4/64$ – stiffness of the cross section of the wires (longitudinal, torsional, bending; E – modulus of elasticity; δ – diameter of the wires).

Matrix $|K|_i$ specific deformations of the *i*-th wire:

$$|K|_i = \begin{vmatrix} K_{e\varepsilon} & K_{t\varepsilon} & K_{b\varepsilon} & K_{n\varepsilon} \\ K_{e\theta} & K_{t\theta} & K_{b\theta} & K_{n\theta} \\ K_{e\chi} & K_{t\chi} & K_{b\chi} & K_{n\chi} \\ K_{e\xi} & K_{t\xi} & K_{b\xi} & K_{n\xi} \end{vmatrix} = |KT|_i \cdot |KF|_i = \quad (8)$$

$$|K|_i = \begin{vmatrix} \overline{K}_{E\varepsilon} & \overline{K}_{T\varepsilon} & \overline{K}_{B\varepsilon} & 0 \\ \overline{K}_{E\theta} & \overline{K}_{T\theta} & \overline{K}_{B\theta} & 0 \\ \overline{K}_{E\chi} & \overline{K}_{T\chi} & \overline{K}_{B\chi} & \overline{K}_{N\chi} \\ \overline{K}_{E\xi} & \overline{K}_{T\xi} & \overline{K}_{B\xi} & \overline{K}_{N\xi} \end{vmatrix} \cdot \begin{vmatrix} K_{eE} & K_{tE} & K_{bE} & 0 \\ K_{eT} & K_{tT} & K_{bT} & 0 \\ K_{eB} & K_{tB} & K_{bB} & K_{nB} \\ K_{eN} & K_{tN} & K_{bN} & K_{nN} \end{vmatrix};$$

$|KT|_i$ – matrix of specific deformations of the strands in the rope, which includes the *i*-th wire; $|KF|_i$ – matrix of specific deformations of the *i*-th wire in the strand.

In the elements of the matrix $|K|_i$, the first index indicates the deformation of the wire in the rope (e – longitudinal; t – torsion; b and n – bending), and the second – the deformation of the rope, from which this deformation of the wire is obtained.

In the elements of the matrix $|KT|_i$, the first index indicates the deformation of the strand in the rope, which includes the i-th wire (E – longitudinal; T – torsional; B and N – bending), and the second index indicates the deformation of the rope, from which this deformation of the strand occurs.

In the elements of the matrix $|KF|_i$, the first index indicates the deformation of the wire in the strand, and the second – the deformation of the strand, with which this deformation of the wire is associated (for a single winding rope, the first index is the deformation of the wire, and the second – the deformation of the rope, for example, $K_{e\chi} = \nu cos^2\alpha\, cos\varphi$).

The elements of the matrix $|KF|_i$ and $|KT|_i$ are obtained on the basis of geometric equations of deformations, respectively, of wires in a single-twist rope (strand) and strands in a double-twist rope [8], taking into account transverse narrowing and friction [6].

Vector $|F|$ of internal power factors in formula (6):

$$|F| = |NML\Gamma|^T, \tag{9}$$

here $N = Pcos\psi$ longitudinal force, $N = Pcos\psi - M = M_H cos\psi$ – torque moment, $L = Pfe^{-kx}$; $\Gamma = M_H sin\psi$ – bending moments;

where $k = (P/G_{33})^{0.5}$;

$$f = G_{33}/PR; \tag{10}$$

x and ψ – linear and angular coordinates of the cross-section of the rope:

$$\psi = (G_{33}/PR^2)^{0.5}e^{-kx}; \tag{11}$$

$M_H = -PA_{12}/A_{22}$ guide reaction (A_{12} and A_{22} algebraic additions of the stiffness matrix G). Bending curvature in the plane of winding on the drum (curvature of the bent axis of the rope):

$$\chi = R^{-1}e^{-kx}. \tag{12}$$

The maximum values of the curvatures and the angle of rotation of the rope section at point O (Fig. 1):

$$\chi_O = \left|2(D_d + d_r)^{-1} = 2\left(d_r\left(\overline{D} + 1\right)\right)^{-1}\right|;\ \psi_O = (G_{33}/PR^2)^{0.5}. \tag{13}$$

The internal deformed state of the rope is expressed by a matrix formula:

$$|D\Pi| = |DK||K|, \tag{14}$$

where $|D\Pi|$ – block matrix $1 \times s$ (s – number of wires in the rope).

Matrix components (14):

$$|D\Pi_i| = |e\ t\ b\ n|,\ i = 1,2,\dots,s, \tag{15}$$

where e, t, b, n – strains of stretching, torsion, bending of wires.

The calculation formula $P_e(\overline{D})$ tensile strength of the ultimate elastic state of ropes for 2 load schemes (Fig. 1) (note that the same formula looks the same for 2 straight rope load schemes) is obtained on the basis of the proportionality between the longitudinal deformation e (15) of the wires in the rope and the elastic limit ε_{lim} of the corresponding wire:

$$P_e\left(\overline{D}\right) = \varepsilon_{lim}/max\overline{e}_i;\ i = 1,2,\dots,s, \tag{16}$$

where ε_{lim} – deformation of the elastic limit of the cable wire according to the diagram $\sigma - \varepsilon$ tensile testing of its samples;

$max\overline{e}_i$ – the largest value among all s wires of the rope of the specific tensile strain at the final load $\overline{P} = 1$.

$$max\overline{e}_i = \overline{\varepsilon}K_{e\varepsilon_i} + \overline{\theta}K_{e\theta_i} + \overline{\chi}K_{e\chi_i} + \overline{\xi}K_{e\xi_i}, \tag{17}$$

$\overline{\varepsilon}, \overline{\theta}, \overline{\chi}, \overline{\xi}$ – specific deformations of stretching, twisting, and bending of the rope from $\overline{P} = 1$ for the load schemes (Fig. 1), which are obtained on the basis of the matrix formula (6) using all subsequent dependencies (6) – (13):

$$|DK| = \begin{vmatrix} \varepsilon \\ \theta \\ \chi \\ \xi \end{vmatrix} = \frac{1}{|D|} \begin{vmatrix} A_{11} & A_{12} & A_{13} & A_{14} \\ A_{21} & A_{22} & A_{23} & A_{24} \\ A_{31} & A_{32} & A_{33} & A_{34} \\ A_{41} & A_{42} & A_{43} & A_{44} \end{vmatrix} \cdot \begin{vmatrix} N \\ M \\ L \\ \Gamma \end{vmatrix}, \quad (18)$$

where the determinant of the stiffness matrix of the rope section:

$$|D| = G_{11}A_{11} + G_{12}A_{12} + G_{13}A_{13} + G_{14}A_{14};$$

algebraic additions:

$$A_{11} = G_{22}(G_{33}G_{44} - G_{34}^2) - G_{23}(G_{23}G_{44} - G_{34}G_{24}) + G_{24}(G_{23}G_{34} - G_{33}G_{24})$$

. . . . . .

. . . . . .

$$A_{44} = G_{11}(G_{22}G_{33} - G_{23}^2) - G_{12}(G_{12}G_{33} - G_{23}G_{13}) + G_{13}(G_{12}G_{23} - G_{22}G_{13}).$$

On the basis of (18), the deformations of the rope at a unit load are determined $\overline{P} = 1$.

In the case of stretching when the load is freely suspended (Fig. 1, a):

$$\overline{\varepsilon} = (A_{11}cos\psi + A_{13}fe^{-kx})/|D|; \overline{\theta} = (A_{12}cos\psi + A_{23}fe^{-kx})/|D|; \quad (19)$$

$$\overline{\chi} = (A_{13}cos\psi + A_{33}fe^{-kx})/|D|; \overline{\xi} = (A_{14}cos\psi + A_{34}fe^{-kx})/|D|. \quad (20)$$

In the case of stretching in the guides (Fig. 1, b):

$$\overline{\varepsilon} = (A_{11}cos\psi - A_{12}(A_{12}cos\psi + A_{14}sin\psi)/A_{22} + A_{13}fe^{-kx})/|D|; \quad (21)$$

$$\overline{\theta} = (A_{23}fe^{-kx} - A_{24}\frac{A_{12}}{A_{22}}sin\psi)/|D|; \quad (22)$$

$$\overline{\chi} = (A_{13} - A_{12}(A_{23}cos\psi + A_{34}sin\psi)/A_{22} + A_{33}fe^{-kx})/|D|; \quad (23)$$

$$\overline{\xi} = (A_{14}cos\psi - A_{12}(A_{24}cos\psi + A_{44}sin\psi)/A_{22} + A_{34}fe^{-kx})/|D|. \quad (24)$$

In the works [4-5], considered above in the analysis, data are given on the relationship of the bending parameter $\overline{D}$ with the tension force of the rope in the guides, according to the scheme on Fig. 1, b. Therefore, in the future, the main attention is paid to this scheme.

Table 2 for the load scheme (Fig. 1, b) shows the results of calculations of the relative $\overline{P}1 = P1/P_t$ stretching forces of the ultimate elastic state of the ropes based on formula (16) at the standard bending parameters [2] $b_1(\overline{D}) = 11.2 - 25$ and at $\overline{D} = 120$, as well as the force $\overline{P}3$ corresponding to the scheme of pure stretching [8] (stretching of a straight rope in guides). The characteristics of ropes No. 1–3 are presented in Table 3.

Table 4 shows the relative values $\overline{P}1 = P1/P_t$ for ropes of various designs from Table 3 with bending parameters $\overline{D}$ in the full range $\overline{D} = 10 - 120$. Along with the numerical value of the force $\overline{P}1$, the numbers of the wires that determine the ultimate elastic state of the rope are indicated. For example, in Fig. 2, No. 123 and No. 2 are shaded, and in Fig. 3, No. 2, No. 8, and No. 1 are wires whose deformation (17) determines the ultimate elastic state of the rope at different values of the bending parameter $\overline{D}$. Table 5 refers to the ultimate elastic state of ropes when loaded with a freely suspended load (Fig. 1, a).

Table 2 – Relative stretching forces $\overline{P}1 = P1/P_t$ of ropes in guides (Fig. 1, b) with normative parameters $b_1(\overline{D})$ [2] of bending in winding on a drum

Mechanism class		M1	M2	M3	M4	M5	M6	M7	M8	$\overline{D}$	$\overline{P}3$
№	$b_1(\overline{D})$	11.2	12.5	14	16	18	20	22.5	25	120	
1	Stretching with winding on a drum	0.563	0.585	0.607	0.630	0.648	0.663	0.677	0.690	0.765	0.765
2		0.201	0.257	0.309	0.367	0.412	0.447	0.481	0.512	0.741	0.741
3		0.211	0.265	0.316	0.370	0.412	0.447	0.481	0.510	0.717	0.725

Table 3 – Characteristics of ropes: geometric, strength and rigidity

№	Design designation: 12×(…): 6×(…) – the number of strands; 1/0.6; 6/0.6...//7/1.3...//6/1.5 – the number of wires in the layers of strands and their diameter	d_r, mm	P_t, kN	Stiffness of the section × 10^{-4}			
				G_{11}, N	G_{12}, Nmm	G_{22}, Nmm^2	G_{33}, Nmm^2
1	12×(1/0.6–6/0.6) - 6×(1/0.6+6/0.6)+o.c.	9.3	57.0	515	359.8	620.3	179
2	12×(1/1.4–6/1.4–6(1/0.8+6/0.8+12/0.8)+o.c.	20.5	289.5	2867	45856	19121	4815
3	6×(1/2.4+7/1.8+7/1.8//7/1.3+14/2.2)+ o.c.; GOST 7668–80	39	985.5	8216	48533	292924	5903
4	6×(1/1.2+7/0.9+7/0.9//7/0.65+14/1.1)+ +o.c ;GOST 7668–80	20	246.4	2048	6087	18487	390.4
5	6×(1/1.5+6/1.4+6/1.15//6/1.5)+o.c.; GOST 2688–80	21	267.2	2271	5794	15346	662.7
6	6×(1/2.4+7/1.8+7/1.8//7/1.3+14/2.2) +7×(1/1.7+6/1.6); GOST 7669–80	39	1146	11267	54828	296982	5982
7	6×(1/1.2+6/1.1)+o.c.; GOST 3069–80	10.5	64.25	560	734	1029	70.4
8	6×(1/1.2–6/1.1)+o.c.;GOST 3069–80	10.5	64.25	553	503	523	70.4
9	6×(1/1.2+6/1.1)+ 1× (1/1.2+6/1.1); GOST 3066–80	10	74.95	715	571	602	63.1
10	1/1,15+6/1	3.15	9.2	100	25.8	15.1	25.7
11	1/1.15+6/1+12/1; GOST 3063–80	5.15	24.28	261	123	84.6	22.7
12	1/1.15–6/1+12/1; GOST 3063–80	5.15	24.28	261	72.5	85.8	22.7
13	1+7/2.4+7/1.8//7/1.8+14/2.2; GOST 7668–80	12.7	164	1790	1837	2938	844
14	1/1.9+6/1.8+12/1.8+18/1,8; GOST 3064–80	12.5	151	1472	1618	2563	667
15	1/1.9+6/1.8–12/1.8+18/1.8; GOST 3064–80	12.5	151	1472	630	2503	667
16	1/1.3-6/1.2–(6/1+6/1.3)+18/1.1	7.9	60.63	630	136	443	62.3

Table 4 – Dependence of the tensile strength $\overline{P}1 = P1/P_t$ of the ultimate elastic state of the ropes on the bending parameter $\overline{D}$ when winding on a drum

$\frac{\overline{D}}{№\ r.}$	10	20	30	40	50	60	70	80	90	100	120	$\overline{P}3$
1	0.537 №123	0.663 №123	0.708 ″	0.723 ″	0.747 ″	0.757 ″	0.765 №2	0.765 ″	0.765 ″	0.765 ″	0.765 ″	0.765 №2
2	0.343 №107	0.547 №107	0.625 ″	0.667 ″	0.692 ″	0.709 №195	0.719 ″	0.726 ″	0.732 №189	0.737 №189	0.741 №116	0.741 116
3	0.149 №139	0.447 ″	0.553 ″	0.607 ″	0.640 ″	0.662 ″	0.678 ″	0.690 ″	0.700 ″	0.707 №139	0.717 №121	0725 №2
4	0.148 №139	0.447 ″	0.554 ″	0.608 ″	0.641 ″	0.663 ″	0.670 ″	0.691 ″	0.701 ″	0.708 №121	0.711 №121	0.728 №2
5	0.141 №51	0.405 №51	0.511 ″	0.567 ″	0.602 ″	0.626 ″	0.643 ″	0.656 ″	0.666 ″	0.674 ″	0.687 ″	0.713 2

$\frac{\overline{D}}{№\ r.}$	10	20	30	40	50	60	70	80	90	100	120	$\overline{P}3$
6	0.241 №187	0.533 ″	0.636 ″	0.689 ″	0.712 №1	0.712 ″	0.712 ″	0.712 ″	0.712 ″	0.712 ″	0.712 ″	0.712 ″
7	0.405 № 27	0.580 ″	0.642 ″	0.673 ″	0.693 ″	0.706 ″	0.716 ″	0.723 ″	0.728 ″	0.733 ″	0.738 №2	0.738 №2
8	0.408 №3	0.584 ″	0.647 ″	0.679 ″	0.698 ″	0.711″	0.721 ″	0.728 ″	0.730 №2	0.730 ″	0.730 ″	0.730 ″
9	0.483 №2	0.575 ″	0.608 ″	0.625 ″	0.635 ″	0.642 ″	0.647 ″	0.651 ″	0.653 ″	0.656 ″	0.659 ″	0.677 №1
10	0 №2	0.161 №2	0.391 ″	0.509 ″	0.581 ″	0.630 ″	0.666 ″	0.691 ″	0.711 ″	0.728 ″	0.753 ″	0.788 №1
11	0.041 №2	0.432 №2	0.572 ″	0.644 ″	0.687 №8	0.715 ″	0.736 ″	0.751 ″	0.763 ″	0.772 ″	0.778 № 1	0.778 №1
12	0.041 №2	0.432 №2	0.572 ″	0.644 ″	0.687 №8	0.715 ″	0.736 ″	0.751 ″	0.763 ″	0.772 ″	0.778 №1	0.778 №1
13	0 № 23	0.266 №23	0.465 ″	0.567 ″	0.626 ″	0.670 ″	0.700 ″	0.722 №9	0.734 ″	0.743 ″	0.758 ″	0.789 №1
14	0 №8	0.227 №8	0.400 ″	0.490 ″	0.544 ″	0.580 ″	0.607 ″	0.626 ″	0.642 ″	0.654 ″	0.673 ″	0.711 №1
15	0 №8	0.227 №8	0.400 ″	0.490 ″	0.544 ″	0.580 ″	0.607 ″	0.626 ″	0.642 ″	0.654 ″	0.673 ″	0.711 №1
16	0.694 №1	….	….	….	….	….	….	….	….	….	….	0.694 №1

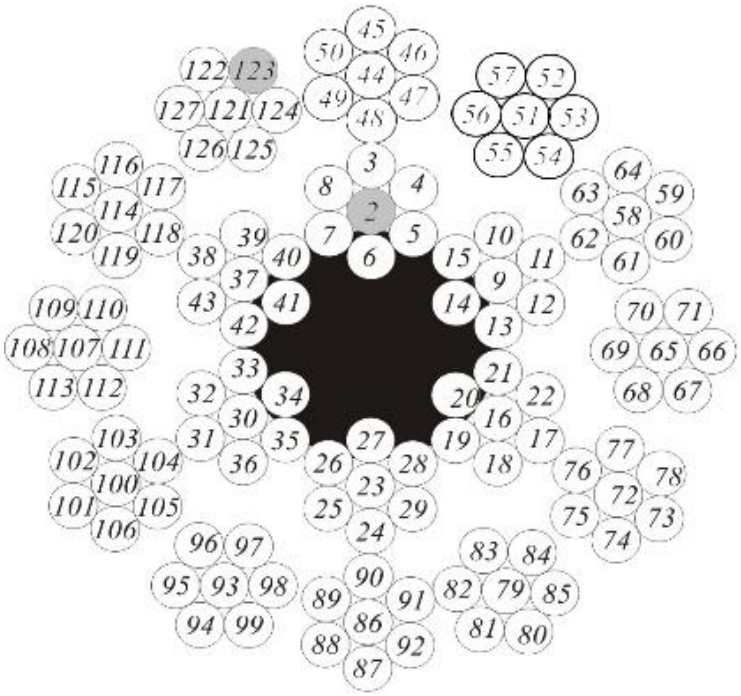

Fig. 2. Rope No. 1: 12(1–6) – 6(1+6) +o.c

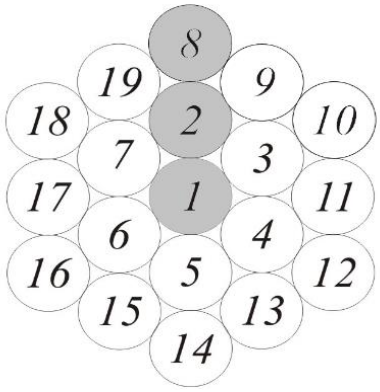

Fig. 3. Rope No. 11: 1+6+12

Table 5 – Dependence of tensile forces $\overline{P}2 = P2/P_t$ of the ultimate elastic state of the ropes on the parameter $\overline{D}$ when the load is freely suspended

$\frac{\overline{D}}{№\ r.}$	10	20	30	40	50	60	70	80	90	100	120	$\overline{P}4$
11	0.02 №2	0.243 №1	〃	〃	〃	〃	〃	〃	〃	〃	0.243 〃	0.243 №1
12	0.03 №2	0.263 №2	0.347 〃	0.389 〃	0.416 〃	0.433	0.446 〃	0.455 〃	0.463 〃	0.469 〃	0.471 〃	0.523 №2
16	0.04 №2	0.593 №8	〃	〃	〃	〃	0.592	〃	〃	0.592	〃	0.592

Let us consider the factors that affect the deformation components (17). The first component $\overline{\varepsilon}K_{e\varepsilon_i}$ is the stretching deformation of the wires, which is related to the stretching deformation ε of the rope. The second component $\pm\overline{\theta}K_{e\theta_i}$ is related to the deformation θ of the twisting of the rope ("+" sign for layers of wires, the direction of twisting of which coincides with the direction of twisting θ and the opposite sign is "-"). When the rope is stretched in the guides, regardless of the construction of the rope, the torsional deformation $\theta = 0$ component $\overline{\theta}K_{e\theta_i} = 0$. When the load is freely suspended (Fig. 1, a) the component $\overline{\theta}K_{e\theta_i}$ depends on the construction of the rope.

In the case of free stretching of a straight rope, the constructive sign of the absence of torsional deformation θ is the zero value of impact stiffness, $G_{12} = 0$. The degree of torsion of the rope is determined by the parameter [8]: $\psi = G_{12}/maxG_{12} \leq 1$, where $maxG_{12}$ – is the maximum possible value for this type of rope construction. So, for the rope No. 11 of construction 1+6+12 $\psi = 1$ and for the rope No. 12 of construction 1– 6+12 $\psi = G_{12}/maxG_{12} = 725/1230 = 0.589$.

Tables 4 and 5 and Fig. 6 show a significant influence of the rope design (partly parameter) on the force $\overline{P}2$ of the limit elastic state with a freely suspended load. For the same ropes, the data in Table 4 and Figs. 4 and 5 show the uniformity of the force $\overline{P}1$ of the ultimate elastic state with the load in the guides.

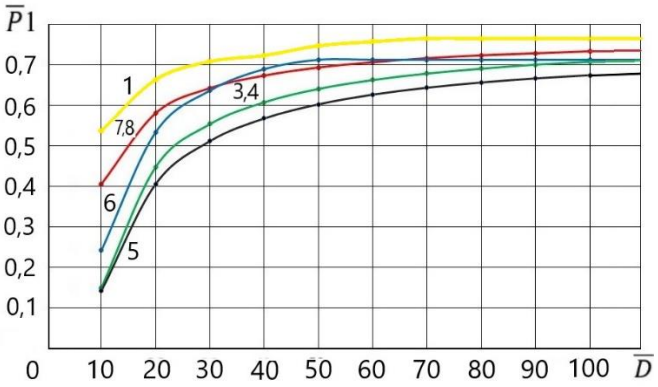

Fig. 4. Dependence $\overline{P}1(\overline{D})$ of double twist ropes

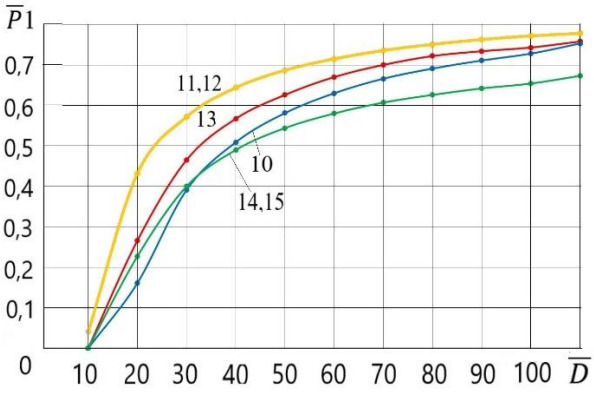

Fig. 5. Dependence $\overline{P}1(\overline{D})$ of single twist ropes

The component $\overline{\chi}K_{e\chi_i}$ in the specific strain (17) represents the stretching from the bending strain $\overline{\chi}$ of the rope. This component is given by the parameter $\overline{D}$ and is related to interelement friction. The mechanics of the formation of this deformation is described in [6]:

$$K_{e\chi} = \nu cos^2\alpha\ cos\varphi, \tag{25}$$

where $\nu(\overline{D})$ – is the coefficient due to interelement friction.

We accept on the basis of [9]: $\nu = 0.2 - 0.1$ respectively for the wires of the inner and outer layers and $\nu = 0$ for the central wires.

Somewhat anomalous values of forces $\overline{P}1$ and $\overline{P}2$ are associated with this feature ($\nu = 0$) their constant values, independent of the bending parameter $\overline{D}$. Table 4 shows several calculation results of this feature. Thus, for the rope No. 1 at $\overline{D} = 70 - 120$ the independence of the force from the bending parameter $\overline{P}1 = 0.765$ due to the fact that the limit state is determined by the central wire No. 2, Fig. 3, for which $\nu = 0$. A similar situation for the rope No. 8: in the interval $\overline{D} = 90 - 120$ the force of the ultimate elastic state under load in the guides is unchanged ($\overline{P}1 = 0.730$).

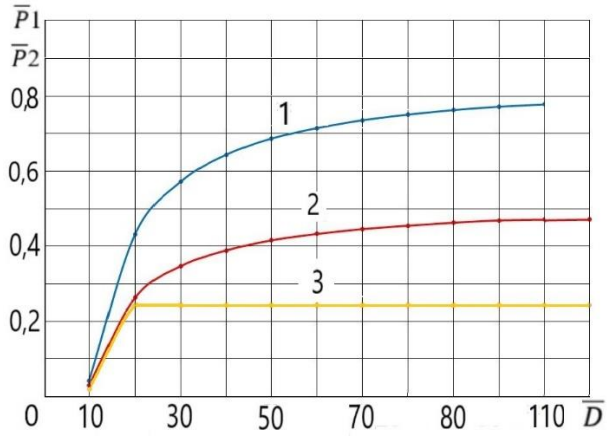

Fig. 6. Dependence $\overline{P}1(\overline{D})$ and $\overline{P}1(\overline{D})$ of ropes 1+6+12 and 1– 6+12:
1 – ropes №11, 12 force $\overline{P}1$; 2 – rope №12, force $\overline{P}2$; 3 – rope №11, force $\overline{P}2$

The same peculiarity is manifested with a freely suspended load. As an example, this is shown in Table 5 for the rope No. 11 at $\overline{D} = 20 - 120$ ($\overline{P}2 = 0.243$), due to the fact that the limit state is determined by the central wire No. 1, which does not receive stretching from the bending of the rope, $\nu = 0$.

The component $\overline{\xi}K_{e\xi_i}$ in the specific deformation (17) should take into account the stretching of the wires from the bending deformation $\overline{\xi}$ of the rope in the plane orthogonal to the winding on the drum. Such a deformation occurs with asymmetry in the cross-section of the rope, when its impact stiffnesses G_{14}, G_{24}, G_{34} are not zero. This happens if the wires are broken. This work does not consider such a state.

Fig. 4 shows a graphical representation of the dependence $\overline{P}1(\overline{D})$ for the double-twist ropes specified in Table 3 (numbers: 1; (7. 8); 6; (3, 4), 5). Fig. 5 shows a similar representation for single winding ropes (numbers: (11, 12); 13; 10; (14, 15)).

Fig. 6 shows the dependences $\overline{P}1(\overline{D})$ and $\overline{P}2(\overline{D})$ of the limit elastic state for load schemes in guides (Fig. 1, b) and free suspension of the load (Fig. 1, a). The graphs are constructed for ropes of construction 1+6+12 and 1–6+12 (No. 11 and No. 12 according to Table 3).

Conclusions. Analysis of Table data 2 and 4 graphs of Fig. 4 – 6 leads to the following conclusions.

For ropes of the same design, the relative tensile forces under loading in the guides $\overline{P}1$ of the limit elastic state are practically the same.

Efforts $\overline{P}1$ differ significantly for different designs. For double-twisted ropes, at $\overline{D} = 10$ the greatest force value $\overline{P}1$ has construction 12(1–6)±6(1+6)+o.c., GOST 7681–80 (No. 1 according to Table 3). The effort $\overline{P}1$ of this design is 3.8 times greater compared to designs No. 3, 4, 5 (GOST 7668–80 and GOST 2688–80). For other structures (No. 6 according to Table 3, GOST 7668–80 and No. (7, 8) GOST 3069–80), the forces differ by 2.2 and 1.3 times, respectively. For other structures (No. 6 according to Table 3, GOST 7668–80 and No. (7, 8) GOST 3069–80), the forces differ by 2.2 and 1.3 times, respectively. As the bending parameter $\overline{D}$ increases, the indicated ratios decrease. So, at $\overline{D} = 20 - 120$ the effort ratio $\overline{P}1$ of the specified structures being only 1.48-1.07.

With the bending parameter $\overline{D} \geq 120$ the limit elastic force $\overline{P}1$ (according to the load scheme in the guides (Fig. 1, b)) is practically equal to the force $\overline{P}3$ of the loaded straight rope in the guides (pure stretching).

We believe that this theoretical study reveals the practical validity of the recommendations in Germany [5] regarding the assignment of the parameter $\overline{D} \geq 100 - 120$ for mine installations in order to increase the service life of ropes.

Among single twist ropes, the design 1+6+12, GOST 3063–80 (No. 11 and No. 12 according to Table 3) shows the greatest effort $\overline{P}1$. In comparison with the design 1/1.9+6/1.8+12/1.8+18/1.8; GOST 3064–80 and construction 1+7/2.4+7/1.8//7/1.8+14/2.2 (No. 14 and No. 13 according to Table 3) the ratio of efforts $\overline{P}1$ at $\overline{D} = 20$ is 1.9-1.6. As the bending parameter $\overline{D}$ increases, these ratios decrease. So, when $\overline{D} = 120$ the effort ratio $\overline{P}1$ is 1.15-1.03.

The smallest possible (suitable) values of the bending parameter for double-twisted ropes $\overline{D} = 10$ and for single-twisted ropes $\overline{D} = 15$.

When stretching with bending in the guides, the forces $\overline{P}1$ as well as during pure stretching $\overline{P}3$ are the same for single-sided and cross-winding ropes (No. 11 and No. 12 according to Table 3).

The tensile strength of the ultimate elastic state when the load is freely suspended is much smaller compared to the load scheme in the guides, especially for torsion ropes, which makes such structures unsuitable for such a load scheme.

Ropes with a metal core have a stress of ultimate elastic state $\overline{P}1$ 15-17% lower compared to similar designs of ropes with organic cores.

Twisted ropes show the forces of the elastic limit state $\overline{P}2$ when the load is freely suspended by 1.7–2.9 times less compared to the force $\overline{P}1$ when loaded in the guides. This indicator is extremely important for the practice of using ropes.

We believe that the research data are appropriate in solving the issue of building a methodology for calculating the static strength of lifting ropes based on the characteristics of their ultimate elastic state, which will ensure stable optimality of the use of ropes.

References

[1] V.I. Berezhinskiy, A.N. Shatilo, *Zvukoizolyaciya pod styazhku pola kotoraya luchKanaty shahtnyh pod"emnyh ustanovok.* Univesitetskaya kniga, Moskva, 2015.

[2] *Pravila ustrojstva i bezopasnoj ekspluatacii gruzopod"yomnyh kranov.* Fort, Har'kov, 2007.

[3] J. Reinl and M. Golder, "Wire Ropes in Crane Applications – Current State of the Standardization Work of ISO/WD 16625", *InnoTRAC Journal*, vol. 1, pp. 37–46, 2020, doi.org/10.14464.

[4] S.B. Budrin, A.I. Ilyin, V.V. Ovsyannikov, O.A. Smirnov, "Assessing the Integrity of Steel Ropes for Lifting Machines Based on Testing Data", *IOP Conf. Series: Materials Science and Engineering*, vol. 1079, 2021, doi:10.1088/1757-899X/1079/5/052013.

[5] DIN-Taschenbuch. Drahtseile: Normen. Berlin-Koln, Beuth, 1990.

[6] V.O. Malinovsky, *Stal'nye kanaty: analiticheskij spravochnik.* Odessa: Astroprint, 2016.

[7] Die Technischen Anforderungen an Schacht-und Schragforderanlagen (TAS). Stand: Dez. 2005 Bezirksregirung Arnsberg: Abt. Bergbau und Energie in NRW. Dortmund, 2005.

[8] I.M. Chaiun, *Nesushchaya sposobnost' pod"emnyh kanatov i lent.* Odessa, Astroprint, 2003.

[9] P.E. Vovk, I.M. Chaiun, "Rope limit state characteristics", *Materials of conference «Actual problems of engineering mechanics»*, vol. 8, pp. 115-119, 2021.

[10] M.F. Glushko, *Stal'nye pod"yomnye kanaty*. Odessa, Astroprint, 2013.

[11] I.M. Chaiun, "Eksperimental'naya proverka modeli formirovaniya izgibnoj zhestkosti kanata", *Stal'nye kenaty*, vol. 3, pp. 56-63, 2003.

ЗАЛЕЖНІСТЬ ЗУСИЛЛЯ РОЗТЯГАННЯ ГРАНИЧНОГО ПРУЖНОГО СТАНУ КАНАТІВ ВІД ПАРАМЕТРА ЗГИНАННЯ НА БАРАБАНІ

[1]**Вовк П.Є.,** аспірат,
vovk.pavel.1995@gmail.com, ORCID: 0000-0001-6156-1686
[1]**Чаюн І.М.**, д.т.н., професор,
i.m.c@ukr.net, ORCID: 0000-0003-0867-8791
[1]*Національний університет «Одеська політехніка»*
пр. Шевченко 1, Одеса, 65044, Україна

Анотація. На основі раніше розробленого методу аналітичного визначення граничного пружного стану канатів досліджена залежність $P(\overline{D})$ зусилля розтягання з навиванням каната на барабан від параметра $\overline{D} = D_d/d_r$ (відношення діаметрів барабана і каната) в інтервалі $\overline{D} = 10 - 120$. Залежіть $P(\overline{D})$ визначалась для двох схем навантаження канату: розтягання канату з навиванням на барабан вільно підвішеним вантажем та розтягання канату з навиванням на барабан вантажем в напрямних. На основі розробленого методу представлено залежність $P(\overline{D})$ для 16-ти кантаів різних конструкцій. Зусилля розтягання представлено в відносній формі $\overline{P}(\overline{D}) = P(\overline{D})/P_t$ (P_t – сумарне розривне зусилля дротів канату). Зусилля $\overline{P}(\overline{D})$ суттєво залежить від конструкції канату і параметра $\overline{D}$ згинання. На ділянці $40 \le \overline{D} \le 120$ зусилля$\overline{P}(\overline{D})$ монотонно практично лінійно зростає доходячи до значення відповідного розрахунковій схемі розтягання прямого канату. Для різних конструкцій при параметрі $\overline{D} = 40$ зміна зусилля $\Delta\overline{P} = 0{,}723 - 0{,}578 = 0{,}145$ при $\overline{D} = 120$ зусилля $\Delta\overline{P} = 0{,}765 - 0{,}677 = 0{,}08$. На ділянці $40 \ge \overline{D} \ge 20$ залежність $\overline{P}(\overline{D})$ не лінійна, при $\overline{D} = 40$ зусилля $\Delta\overline{P} = 0{,}663 - 0{,}418 = 0{,}245$. Ділянка $20 \ge \overline{D} \ge 10$ характерна різкою зміною зусилля $\overline{P}(\overline{D})$, при параметрі згинання $\overline{D} = 10$ зусилля $\Delta\overline{P} = 0{,}416$ Для більшості конструкцій канатів при $\overline{D} < 10$ зусилля $\overline{P}(\overline{D})$ близькі до нульових значень. При розтяганні вільно підвішеним вантажем мало крутних канатів зусилля $\overline{P}(\overline{D})$ в 1,6 –1,7 разів менші в порівнянні з розтяганням в напрямних. Для канатів крутних (одностороннього звивання) співвідношення складає 2,5–3,4 рази. В нормативних методиках розрахунків піднімальних канатів використовуються характеристики P_t або $P_a = 0{,}83P_t$, які не враховують особливості деформування і конструкції канатів. Вважаємо, що наведена інформація є доцільною в вирішенні питання побудови методики розрахунку піднімальних канатів на статичну міцність на основі характеристик їх граничного пружного стану, що забезпечить стабільну оптимальність використання канатів, дозволить раціонально обирати вид конструкції канату та його розміри.

Ключові слова: канат, міцнісні характеристики, розрахункова схема, параметр згинання при навиванні на барабан, методика розрахунку на статичну міцність.

Стаття надійшла до редакції 30.07.2023

UDC 621.372.543.2 DOI: 10.31650/2786-6696-2023-5-36-51

THE USE OF MECHANICAL FILTER MODELS IN THE ANALYSIS OF FORMING AND COMPACTION PROCESSES OF FORMATION AND COMPACTION OF BUILDING/CONCRETE MIXTURES BY VIBRATING FIELD

[1]**Chovnyuk Yurii,** Ph.D., Associate Professor,
ychovnyuk@ukr.net, ORCID: 0000-0002-0608-0203
[1]**Priymachenko Aleksey,** Ph.D., Associate Professor,
pryimachenko.ov@knuba.edu.ua, ORCID: 0000-0001-5125-8472
[1]**Cherednichenko Petro,** Associate Professor,
petro_che@ukr.net, ORCID: 0000-0001-7161-661X
[1]**Ostapushchenko Olga,** Ph.D., Associate Professor,
olga_ost_17@ukr.net, ORCID: 0000-0001-8114-349X
[1]*Kyiv National University of Construction and Architecture*,
Povitroflotsky prospect, 31, Kyiv, 03037, Ukraine

Abstract. The paper describes the use of various types of mechanical filter models, which are used for the analysis of the processes of formation and compaction of the construction/concrete mixtures of building/concrete mixtures by means of vibrating fields. The values of resonant frequencies and equivalent masses for different resonators modeling the propagation in the latter of vibrating-wave formations have been established. The analysis of the influence of a vibrating field on the processes of formation and compaction of concrete/concrete mixtures in this study is based on the methods of mathematical physics, classical variation calculus, physics of oscillations and waves and methodology of solution of ordinary differential equations and partial differential equations. The conditions and main integral characteristics of resonance phenomena, the possibility of occurrence of which is conditioned by: 1) the geometry of the initial boundary-edge problem (it is The so-called "geometric resonances" of the considered system with distributed parameters simulating the mixture to be processed); 2) the working rheological model of the mixture involved in the study (these are the so-called "rheological resonances").

The approach developed and scientifically substantiated in this work allows us to establish the main parameters and opportunities for the use of energy-saving modes of operation of vibration systems intended for the formation and vibration compaction of the above mixtures. The results obtained in the work The results obtained can be further used to clarify and Improvement of existing engineering methods of calculation of vibration systems for the formation and compaction of concrete/concrete mixtures in order to optimize the operating modes of their functioning both at the design stage and in the modes of real operation.

Keywords: modeling, mechanical filters, vibration resonators, analysis, formation processes, compaction, construction and concrete mixtures, vibration field, resonances, equivalent masses.

Problem formulation. Mechanical circuit diagrams are quite often used in modeling the compaction and forming processes of concrete/construction mixtures. In particular, equivalent circuits simplify the calculation process or make the operation of mechanical filters more understandable [1]. Say, the distributed mechanical circuit of a piezoceramic transducer operating on flexural vibrations is often transformed in scientific research into a mechanical circuit with concentrated elements formed by springs and masses. The mechanical circuit is then converted into its electrical counterpart. The conversion from a plate resonator to a system of masses and springs simplifies the circuit, but this conversion is not exact. A plate resonator has an infinite number of natural frequencies, while the number of resonances of an equivalent circuit with concentrated parameters is determined by the number of springs, masses, and the way they are connected. Since mechanical filters are devices with a narrow frequency bandwidth, this fact does not cause large errors, and equivalent circuits with concentrated elements are very useful.

The second type of equivalent circuits are electrical analogs of mechanical circuits. This equivalence promotes understanding and facilitates the analysis of not only the converter but also the entire filter. In the initial stage of system design, the filter user may deal with the mechanical filter as if it were a LC – filter, or more generally, a resonator stage circuit. Let us first consider mechanical schematic diagrams and the very subject of analogies and equivalent circuits.

Both mechanical circuit diagrams and mechanical analogies may be used to describe physical systems. Mechanical circuit diagrams may have concentrated elements, such as masses and springs, or capacitances and inductances, or transmission lines (elements with common parameters), which are characterized by wave impedance and propagation constant (wave propagation).

Mathematical modeling of such systems can be expressed through differential equations or equations of change of state. In all cases, the starting point is a physical system, which in turn is expressed by a kinematic scheme [1].

A kinematic diagram is simply a representation in the form of a drawing of the main features of a real device. It is most often used to describe a mechanical device and acts as a bridge between the real device and its mechanical circuit diagram.

For example, the simplest kinematic diagram of a mechanical single resonance filter has the form of a mass M, which is connected to a stiffness spring K, and to this mass is connected in parallel damping element D.

The resonant frequency of such a system is determined from the relation:

$$\Omega = 2\pi f = \sqrt{K/M}\,, \tag{1}$$

where: Ω is cyclical, f – linear frequency.

The equivalent mass of such a system is the apparent mass of the resonator measured at a point on the resonator and in a particular direction. In other words, we have replaced the resonator with a spring-mass combination that has the same resistance near the resonant frequency. The equation of state for the resonator through the force is F and velocity $\dot{x} = \dfrac{dx}{dt}$, where x – displacement of mass M in space, t – is time, written as:

$$F = j\omega M\dot{x} + \left(\frac{K}{j\omega}\right)\cdot\dot{x} + D\dot{x},\ \ j^2 = -1. \tag{2}$$

The differential equation (essentially a Proportional-Integral-Differential (PID) controller equation for force F at its harmonic variation in time) will have the form:

$$F\sin\omega t = M\frac{d\dot{x}}{dt} + K\int \dot{x}dt + D\dot{x}\,. \tag{3}$$

Proceeding from equation (2), after passing to complex variables (find $\dot{x}(t) = x_0\exp(j\omega t)$), one has:

$$\dot{x}(t) = \frac{F(t)}{\left(j\omega M + \dfrac{K}{j\omega} + D\right)}. \tag{4}$$

Resonance value $\dot{x}_{res}$ will be under the condition of the minimum value of the denominator of formula (4), namely, when:

$$j\omega M + \frac{K}{j\omega} = 0 \Leftrightarrow \omega_{res} = \Omega_{res} = \sqrt{\frac{K}{M}};\ \dot{x}_{res}(t) = F(t)/D\,. \tag{5}$$

Consequently, such a simple model of the mechanical system exhibits resonant properties and has a resonant frequency $\omega_{res} = \Omega_{res}$. Note that the circuit diagram (for such a kinematic scheme)

turns into three in parallel: mass M, stiffness K, and damping element D. In the electromechanical analogy, the equivalent of velocity becomes voltage V and force becomes current I. Therefore, writing (2) and (3) in electrical quantities, we obtain:

$$I = j\omega CV + \left(1/\, j\omega L\right)V + GV; \tag{6}$$

$$I\sin\omega t = C\frac{dV}{dt} + \frac{1}{L}\int Vdt + GV, \tag{7}$$

where: G is permeability, L – inductiveness, C – capacitance. Therefore, the following equivalence of mechanical and electrical parameters arises: $M \leftrightarrow C;\ D \leftrightarrow G;\ K \leftrightarrow L^{-1}$.

Quite often in the literature, researchers also use longitudinal oscillation resonator models.

In the case when one of the resonator dimensions becomes much larger than the other two, the vibration types are simplified and become ideal types of longitudinal compression-extension vibrations. The wave equation for such vibrations of rods and strips have second order with respect to the length coordinate, i.e.:

$$\left(\frac{E}{\rho}\right)\cdot\frac{\partial^2 u}{\partial x^2} = \frac{\partial^2 u}{\partial t^2}, \tag{8}$$

where: $u\left(x,t\right)$ – moving the section point with the coordinate x, at a point in time t, ρ – material density, E – is the elasticity modulus of this material. After introducing complex variables, we consider that $u = A\cdot\exp(i\omega t)$, where $i^2 = -1$, ω – is the cyclic frequency of oscillations. Then from (8) we have:

$$\left(\frac{E}{\rho}\right)\cdot\frac{\partial^2 u}{\partial x^2} = -\omega^2 u. \tag{9}$$

We find the solution of (9) in the form:

$$u\left(x\right) = A\sin kx + B\cos kx, \tag{10}$$

where: x – distance from the rod end, k – is the wave propagation constant in the rod. We consider that the ends of the rod oscillate freely, then we have for the constants undefined in (10) A and B two boundary conditions if the rod has finite length l:

$$\left.\frac{\partial u}{\partial x}\right|_{x=0} = 0;\ \left.\frac{\partial u}{\partial x}\right|_{x=l} = 0. \tag{11}$$

Substituting (10) into the first limiting condition, we obtain:

$$A = 0. \tag{12}$$

Therefore,

$$u\left(x\right) = B\cos kx. \tag{13}$$

From the second boundary condition (11) we have:

$$\sin\left(kl\right) = 0. \tag{14}$$

Equation (14) is the resulting frequency equation and has the following roots:

$$k_n l = n\pi,\ n = 1,2,3,\ldots\left(n \in N\right). \tag{15}$$

Next, we establish the relationship between and frequency by substituting the solution (13) into the wave equation (9) and differentiating the left part by x. After contracting the value $\cos\left(kx\right)$ one obtains:

$$k = \omega\cdot\sqrt{\rho/E}, \tag{16}$$

that is, we obtain the so-called dispersion equation of the resonator. Note that the phase velocity of the waveforms:

$$v_{phase} = v_p = \frac{\omega}{k} = \left(\frac{E}{\rho}\right)^{1/2}, \quad (17)$$

and the group velocity of wave formation:

$$v_{group} = v_g = \frac{d\omega}{dk} = \left(\frac{E}{\rho}\right)^{1/2}, \quad (18)$$

independent of frequency ω, and therefore the longitudinal type of oscillations is nondispersive. Then we substitute the values k_n from (15) into the dispersion equation (16); this gives us a relation for determining the resonant frequencies of the rod:

$$f_n = \frac{\omega_n}{2\pi} = \left(\frac{n}{2l}\right) \cdot \sqrt{E/\rho}, \; n \in N. \quad (19)$$

For each mode of wave formations in the rod by substituting the value of k_n from (15) into equation (13) the distribution of displacements can be found $u(x)$. The result is:

$$u(x) = B\cos\left(n\pi x/l\right). \quad (20)$$

The above approaches known in the scientific literature are used in this study.

Analyzing the study's publications. Rheological models of media to which concrete/construction mixtures belong are considered in [2-13], and the idea of using models of mechanical filters to analyze wave processes and determine the integral characteristics of mixtures (concrete or construction) is presented in [1]. However, the authors of these works practically do not investigate exactly the resonance properties of their proposed rheological models of media that support wave formation of various types (in particular, longitudinal waves). Therefore, this particular study is devoted to the problem of determining possible resonance phenomena (geometric and rheological) and the conditions for their occurrence in media that are treated by vibratory fields. Concrete/construction mixtures belong to such media.

The aim of the work is to establish the conditions and characteristics of resonances that are possible in concrete/construction mixtures when studying the processes of their vibration compaction and formation within the framework of classical rheological models of visco-elastic-plastic media in the presence of longitudinal wave formation in the latter. To achieve the goal of this work, the model of a rod supporting longitudinal wave formation is used.

Research Methodology. The following methods are chosen as research techniques: 1) models and mathematical apparatus of solid deformed body mechanics; 2) methods of solving differential equations describing linear wave processes in visco-elastic deformed bodies (in the presence of various dissipation mechanisms); 3) methods of mathematical physics; 4) methods and models of linear acoustics used in the analysis of impedance (including resonance) properties of media supporting waves of different physical nature; 5) discrete-continuum models and methods of analyzing linearly deformed media (including resonance) properties of media supporting waves of different physical nature; 6) discrete-continuum models and methods for analyzing linearly deformed media.

Outlining the main content of the study. Let us consider wave formation in a rod of finite length, when it is necessary to take into account dissipative processes that occur in this rod. It should be noted that the rod model is popular in studies of vibration compaction of concrete mixtures.

1. Investigation of absolute (in time) stability of wave formation in the rod.

Proceeding from (16), we feed the dispersion relation as follows:

$$\frac{\omega}{k} = \left(\frac{\tilde{E}}{\rho}\right)^{1/2}, \; \omega = \omega' + i\omega'', \; i^2 = -1, \; \tilde{E} = E' + iE'', \quad (21)$$

where: ω' – characterizes the frequency of wave propagation in the rod material, ω'' – characterizes the attenuation of this wave formation in time t (specifically, $(\omega'')^{-1} = \tau_{att}$, where τ_{att}

– time period for which the amplitude of wave formation decays in the e-times), E' – characterizes the elastic properties of the rod (its material), E'' – its dissipative properties, with k we shall hereinafter understand the expression k_n, $n \in N$ (15). For the wave formation to be absolutely stable, i.e., not increasing with time, it is necessary that the $\omega'' > 0$. (It should be noted that, ω' describes the so-called frequency of (cyclic) filling of wave formation, and the true frequency of wave formation Ω is expressed as follows:

$$\Omega = \left\{ \left(\omega'\right)^2 - \left(\omega''\right)^2 \right\}^{1/2}, \tag{22}$$

that is, in fact, ω' characterizes the frequency (cyclic) of wave propagation in the rod (in its material) in the absence of dissipative processes – that is, we mean a rod of ideal material (in which there is no dissipation).

Relationship (21) can be represented as follows:

$$\frac{\left(\omega' + i\omega''\right)}{k_n} = \left(\frac{E' + iE''}{\rho} \right)^{1/2}. \tag{23}$$

The solution of this equation in the complex plane allows us to write the following (for each n-mode of wave formation):

$$\omega_n' = \left\{ \left[\left(\frac{E'}{\rho} \cdot \frac{k_n^{\,2}}{2} \right)^2 + \left(\frac{E''}{\rho} \right)^2 \cdot \frac{k_n^{\,4}}{4} \right]^{1/2} + \frac{E'}{\rho} \cdot \frac{k_n^{\,2}}{2} \right\}^{1/2}, \quad n \in N. \tag{24}$$

$$\omega_n'' = \left\{ \left[\left(\frac{E'}{\rho} \cdot \frac{k_n^2}{2} \right)^2 + \left(\frac{E''}{\rho} \right)^2 \cdot \frac{k_n^4}{4} \right]^{1/2} - \frac{E'}{\rho} \cdot \frac{k_n^2}{2} \right\}^{1/2}, \; n \in N. \tag{25}$$

Expressions (24), (25) taking into account (15) can be presented as follows:

$$\omega_n' = \frac{n\pi}{\sqrt{2}l} \cdot \left\{ \frac{E'}{\rho} + \frac{\left[\left(E'\right)^2 + \left(E''\right)^2 \right]^{1/2}}{\rho} \right\}^{1/2}, \; n \in N, \tag{26}$$

$$\omega_n'' = \frac{n\pi}{\sqrt{2}l} \cdot \left\{ \frac{\left[\left(E'\right)^2 + \left(E''\right)^2 \right]^{1/2}}{\rho} - \frac{E'}{\rho} \right\}^{1/2}, \; n \in N. \tag{27}$$

For the value Ω_n we have the following expression (exact formula):

$$\Omega_n = \frac{n\pi}{l} \cdot \left\{ \frac{E'}{\rho} \right\}^{1/2}, \; n \in N. \tag{28}$$

We further consider that the deformation $\varepsilon(t)$ and $\sigma(t)$ – stresses related to each other by the linear Hooke's law, which takes into account dissipative processes in the rod material:

$$\sigma = \left(E' + iE''\right) \cdot \varepsilon; \; \sigma_0 = \varepsilon_0 \cdot \sqrt{\left(E'\right)^2 + \left(E''\right)^2}, \tag{29}$$

where: $(\sigma_0, \varepsilon_0)$ – stress and strain amplitudes, provided that $\sigma(t)$ and change over time as follows: $\varepsilon(t) = \varepsilon_0 \sin \omega t; \; \sigma(t) = \sigma_0 \sin(\omega t + \varphi); \; tg\varphi = \left(\frac{E''}{E'} \right)$. (30)

For the time variations given by (30) ε and σ let us calculate the work done by the wave formation/vibrations in the rod material during the time t (per unit area of the cross section of the rod S):

$$A = \int_0^t \sigma d\varepsilon = \omega\sigma_0\varepsilon_0 \cdot \left[\cos\varphi \cdot \int_0^t \left(\sin\omega t \cdot \cos\omega t\right) dt + \sin\varphi \cdot \int_0^t \sin^2 \omega t dt \right] = \tag{31}$$

$$= U + Dt,$$

where: U – fully recoverable work of elastic forces, which can be written as follows:

$$U = \sigma_0\varepsilon_0 \cdot \left[0,5\cos\varphi \cdot \sin^2\psi + 0,25\sin\varphi \cdot \sin 2\psi\right], \varphi = \omega t; \tag{32}$$

and D the following relationship can be found:

$$D = 0,5\omega\sigma_0\varepsilon_0 \cdot \sin\varphi. \tag{33}$$

In essence Dt is irreversible/unrecoverable work per unit time.

The power of elastic forces can be found as follows:

$$\frac{dU}{dt} = 0,5\omega\sigma_0\varepsilon_0 \cdot \sin\left(2\omega t + \varphi\right). \tag{34}$$

From (34) it can be seen that the maximum values of the elastic force power reach at the moments of time t^*, which can be found from the ratio:

$$2\omega t^* + \varphi = \frac{\pi}{2} + 2\tilde{n}\pi, \ \tilde{n} = 0,1,2, \ldots; \tag{35}$$

For t^* one has:

$$\left(\frac{dU}{dt}\right)_{\max} = 0,5\omega\sigma_0\varepsilon_0. \tag{36}$$

Maximum value U is achieved under the condition:

$$2\psi = \pi - \varphi. \tag{37}$$

In this case we have:

$$U_{\max} = \frac{1}{4}\sigma_0\varepsilon_0 \cdot \left(1 + \cos\varphi\right). \tag{38}$$

If we introduce the concept of inverse goodness of fit (Q^{-1}) as the ratio of the energy that is dissipated during the time when the phase of wave formation/vibration changes by 1 radian to the maximum value of free energy in the oscillation cycle (period of this cycle $T = 2\pi/\omega$), and take into account that the change ψ by one radian occurs in the time ($1/\omega$), then you can have it:

$$Q^{-1} = \frac{D}{\omega U_{\max}} = \frac{0,5\omega\sigma_0\varepsilon_0 \sin\varphi}{\omega \cdot \frac{1}{4}\sigma_0\varepsilon_0 \cdot \left(1 + \cos\varphi\right)} = \frac{2\sin\varphi}{\left(1 + \cos\varphi\right)} = 2 \cdot tg\frac{\varphi}{2}. \tag{39}$$

Since $tg\varphi = E''/E'$, with (39) one has:

$$Q^{-1} = -2 \cdot \left(\frac{E'}{E''}\right) + 2 \cdot \sqrt{\left(\frac{E'}{E''}\right)^2 + 1}. \tag{40}$$

Expression, for Q^{-1} (40) is exact, but $\varphi << 1$ one can write:

$$Q^{-1} = \frac{2\sin\varphi}{1 + \cos\varphi} \approx \frac{2\sin\varphi}{2} = \sin\varphi \approx tg\varphi = \frac{E''}{E'}. \tag{41}$$

D gains maximum value when:

$$\sin\varphi = 1 \Rightarrow \varphi = \frac{\pi}{2}. \tag{42}$$

Then:

$$Q^{-1} = 2, \tag{43}$$

and: $E'' >> E'$.

Also, it follows from relation (42) that: $E'' >> E'$. (44)

Then for Ω_n one gets the equality (28), which will be accurate for the resonant frequency of the waveformation/vibration propagating in the rod material. In this sense, such a frequency of wave formation can be called the resonant frequency, since it is at this frequency that the maximum energy absorption by the rod material from the existing wave formations in it occurs.For ω'_n and ω''_n one can obtain:

$$\omega'_n \approx \omega''_n \approx \frac{n\pi}{\sqrt{2}\cdot l}\cdot\left\{E''/\rho\right\}^{1/2}. \tag{45}$$

So, the wave formation in the rod, which leads to the maximum absorption by its material of the energy of this wave formation, has all the features of a dissipative wave, with a "resonant" (in this sense of maximum absorption) frequency (28), the filling frequency of the envelope of this wave ω'_n (45) and amplitude, which decreases in time (envelope wave) according to the law proportional to $\exp(-\omega''_n \cdot t)$. Moreover, as the mode number increases, this damping of the envelope wave increases. Practically, only the first and second modes are excited, since all higher modes (in terms of the mode number n) will quickly decay. Therefore, the conclusion is as follows: in a rod of finite length l only a few dissipative waveforms are excited, which have the following parameters:

$$n = 1,2,3;\ \tilde{\Omega}_n = \frac{n\pi}{l}\cdot\left\{\frac{E'}{\rho}\right\}^{1/2};\ \tilde{\omega}'_n \approx \tilde{\omega}''_n \approx \frac{n\pi}{\sqrt{2}\cdot l}\cdot\left\{E''/\rho\right\}^{1/2}. \tag{46}$$

Models of elastic-plastic material (rod) in the theory of internal friction are considered in detail by the author [2], where the values of the E' and E'' for many such models. The vast majority of works on amplitude-dependent friction, particularly in metals, are devoted to the study of harmonic or near-harmonic deformation laws (such as the one discussed above). This applies equally to both experimental and theoretical works. The main reason preventing the theoretical study of nonharmonic motions relevant for applied problems is the lack of an analytical expression for the external (forced) force at an arbitrary deformation law in time. Note that the available expressions of this force [2, 3] refer exclusively to the harmonic law of change of deformation, and it is not clear how to define or remake these dependencies so that they appear to be valid under an arbitrary law. At the same time, the ideas necessary for this purpose have been expressed in the literature.

In 1938, N.N. Davydenkov on the basis of the experimental works carried out at that time and at that level put forward a hypothesis according to which internal friction at significant material stresses is an effect of microplastic deformations. Even a direct indication that internal friction should be studied using the equations of Mises-Henky plasticity theory is known. However, this rational idea was realized by N.N. Davydenkov only for the case of cyclic deformation under uniaxial stress state and with a partial view of the material loading curve. As a result, the well-known formula of the hysteresis loop was proposed, according to which the energy losses in the material per oscillation cycle depend according to the step law on the amplitude of deformation or stress.

This view of the main role of the theory of plasticity for the applied theory of energy dissipation is explicitly or implicitly shared by many modern authors. Thus, the formula of N.N. Davydenkov and its generalization are intensively used in the studies of G.S. Pisarenko and other members of the Kiev school. The same formula was the basis for the creation of simpler applied theories of internal friction, of which the theory of J.G. Panovka is the most widespread.

The direct use of the equations of plasticity theory to analyze internal friction under uniaxial stress state and again for harmonic deformation was carried out by E.S. Sorokin in 1960 [2].

Thus, the most popular formulas of the theory of energy dissipation under intense stresses are based on the ideas of the theory of plasticity [2].

The fruitfulness of this approach also manifests itself in the fact that it is possible to unambiguously solve one more important problem for the applied theory of energy dissipation – generalization to the case of a complex stress state. The fact that this problem is relevant for the theory of energy dissipation is evidenced by direct indications in the book [2] and numerous ways of its solution exactly for the case of harmonic oscillations. In the literature it was suggested to carry out this generalization by methods of the theory of linear viscoelasticity [3], with the help of the superposition principle, using the hypothesis that the energy dissipation in a unit volume per oscillation cycle depends on the amplitude value of the potential energy density and, finally, by methods of the theory of plasticity . Only the last of these methods can be correctly generalized to nonharmonic motions [2, 3].

Let us dwell on the question of choosing the variant of plasticity theory that is suitable for the description of internal friction. The point of view of N.N. Davydenkov was mentioned above, according to which the amplitude-dependent internal friction represents the effect of microplastic deformations. Microplastic deformations are understood as such plastic deformations that occur at any stress level, including stresses less than the macroscopic yield strength of the material. From this point of view, the application of the theory of microplastic deformations by V.V. Novozhilov and Yu. Novozhilov and Y.I. Kadashevich, where, for example, the simplest of the microplasticity theories – the theory of elastic-plastic bodies – is systematically used, and the general theory of plasticity with linear hardening (which can be used to describe the cyclic deformation of concrete/construction mixtures) is considered in the works of this author.

In the following we will use expressions for E' and E'', which follow, in particular, from the consideration of the uniaxial stressed state of the material in the framework of the models of A.Y. Ishlinsky, E.S. Sorokin [2], G.S. Pisarenko, and Y.G. Panovka.

For the main parameters of wave formations arising in the rod material when dissipation processes are taken into account ($\tilde{\Omega}_n$, $\tilde{\omega}'_n$, $\tilde{\omega}''_n$ (46)) and (Ω_n (28)), (ω'_n (26), ω''_n (27)), one should determine E' and E'' – parameters of the complex modulus of elasticity (at known E – Young's modulus of the material, its density ρ geometric length of the rod l) for different models of visco-elastic-plastic materials. We have the following results:

a) A.Y. Ishlinsky's model:

$$E' = E\left(1 - ra^{\alpha}\right);\ E'' = Ega^{\alpha}, \tag{47}$$

where notations are introduced:

$$r = \frac{2H}{(2+\alpha)} \cdot n^{-\alpha};\ g = \frac{\alpha H}{2} \cdot n^{-\alpha} \cdot B\left(\frac{\alpha+1}{2}, \frac{3}{2},\right),\ n = \frac{4}{\pi}, \tag{48}$$

a – amplitude of cyclic (harmonic) deformation of material, B – Euler's beta function, $(H, \alpha) > 0$ – some positive constants describing the distribution function of defects in the region of their small values:

$$F(h) = Hh^{\alpha}, \tag{49}$$

where: h – dimensionless yield strength of the rod material;

b) E.S. Sorokin's model [2]:

$$E' = E \cdot \frac{(1-\gamma^2/4)}{(1+\gamma^2/4)},\ E'' = E \cdot \frac{\gamma}{(1+\gamma^2/4)}, \tag{50}$$

where: $\gamma = \gamma(a)$ – dissipation parameter (dissipation coefficient, characterizing the ratio of energy quantity ΔW, which is dissipated in the rod material during its oscillation cycle, to W – of

all elastic energy stored in the rod material during the oscillation cycle, i.e. $\gamma = \Delta W/W$). As a general rule $0 < \gamma << 1$, therefore we can write:

$$E' \approx E\left(1-\gamma^2/2\right),\ E'' \approx E\gamma\,. \tag{51}$$

c) G.S. Pisarenko's model:

$$\left\{E' = E\cdot(1-r\cdot a^{\alpha}),\ \ E'' = E\cdot g\cdot a^{\alpha}\right\} \Leftrightarrow E' = E - \frac{r}{g}\cdot E'';$$
$$\frac{r}{g} = \frac{n\cdot 2^{2n}}{(n-1)}\cdot\frac{[G(n+1/2)]^2}{G(2n+1)}. \tag{52}$$

Note that in contrast to the model of A.Y. Ishlinsky, in the model of G.S. Pisarenko another value of $\frac{r}{g}$. In (52) G (z) – gamma function of the argument z.

In A.Y. Ishlinsky's model we have:

$$\frac{r}{g} = 4\cdot\left[\alpha\left(2+\alpha\right)\cdot B\left(\frac{\alpha+1}{2},\frac{3}{2}\right)\right]^{-1}. \tag{53}$$

d) Y.G. Panovka's model:

$$E' = E,\ E'' = Ega^{\alpha}\,. \tag{54}$$

In [3] it is shown that the theories of G.S. Pisarenko, Y.G. Panovk and A.Yu. Ishlinsky lead to practically the same results, and the existing differences in the formulas for the E' and E'' caused by different methods of averaging and linearization.

2. Investigation of convective (in space) stability of wave formations in a rod. We consider (in the field of complex quantities) the deformation, which propagates in the rod, as a quantity proportional to $\exp\left\{i\left(\omega t - \bar{k}_n x\right)\right\}$, where $\bar{k}_n = k_n' + ik_n'', 0x$ – axis along which the deformation wave propagates in the rod (thus ω – purely real value). For this deformation wave to be convectively stable, i.e., not growing in space along the propagation axis, the condition must be fulfilled:

$$k_n'' < 0\,. \tag{55}$$

To determine k_n' and k_n'' it is necessary to solve the dispersion equation in the complex plane:

$$\frac{\omega_n}{k_n' + ik_n''} = \left(\frac{E' + iE''}{\rho}\right)^{1/2}. \tag{56}$$

Physical meaning k_n' is that this quantity characterizes the wave vector of wave formation propagating in the rod material, and $\left(k_n''\right)^{-1}$ – at what length along the axis of the rod the amplitude 0x of wave formation in space decreases to $e-$ times.

For convectively stable wave formation we have:

$$k_n' = \left\{\frac{\omega_n^2\rho}{2\left[\left(E'\right)^2+\left(E''\right)^2\right]}\cdot\left[E' + \sqrt{\left(E'\right)^2+\left(E''\right)^2}\right]\right\}^{1/2}; \tag{57}$$

$$k_n'' = -\left\{\frac{\omega_n^2\rho}{2\left[\left(E'\right)^2+\left(E''\right)^2\right]}\cdot\left[\sqrt{\left(E'\right)^2+\left(E''\right)^2} - E'\right]\right\}^{1/2}. \tag{58}$$

3. Equivalent mass and the method of its calculation.

The equivalent mass (of a resonator) is defined as the equivalent distributed parameter of a rod

or plate, concentrated at a given point and determined for a particular natural frequency. In other words, we replace the equivalent transmission line circuit described above with a mass and spring that are resonant at frequency.

One method of finding the equivalent mass of a resonator that oscillates in the longitudinal direction is to calculate the kinetic energy, which is the product of the mass by half the square of the velocity in a given direction and at a given point [1]. This is a consequence of the fact that the kinetic energy of the rod is invariant, that is, the kinetic energy is independent of the point or direction of reference chosen to calculate the equivalent mass. Thus, it is possible to equate the kinetic energy in a spring-mass system to that of the rod resonator. From equation (13) and equation $V_x = du(x)/dt$ gives:

$$\frac{1}{2}\cdot M_{eqvx}\cdot {V_x}^2 = \frac{1}{2}\cdot\int_0^l (V_0\cdot\cos k_n x)^2\cdot\rho\cdot S dx, \tag{59}$$

where: M_{eqvx} – equivalent mass in point x, linked to velocity V_x in the direction of axis x. V_0 is the velocity at the point $x=0$, ρ – core material density, S – is the cross-sectional area. Therefore, the equivalent mass reduced to the ends of the rod is equal to:

$$M_{eqv0,l} = \frac{\frac{1}{2}\cdot\rho\cdot S\cdot {V_0}^2\cdot\int_0^l \left(\cos^2 k_n x\right)dx}{\frac{1}{2}\cdot {V_0}^2}, \tag{60}$$

and after substitution $k_n = n\pi/l$ in (60) and integration:

$$M_{eqv0,l} = \rho\cdot l\cdot S/2 = M_{st}/2. \tag{61}$$

Consequently, the equivalent mass given to the end of a longitudinally vibrating resonator in the direction of the plate or rod axis is simply half its static mass ($M_{st} = \rho\cdot S\cdot l$).

Example. We solve the problem of finding the fundamental resonance frequency and equivalent mass of a longitudinal oscillating resonator with length, $l = (1...3)m,\ S = 0{,}4m^2,\ \rho = 2\cdot 10^3 kg/m^3$.

Table 1 shows the values of the first resonant frequency, which is expressed by relation (19), for different grades of concrete (M200...M800), as well as the value of the $M_{eqv0,l}$ for different l.

Table 1 – Value of the first resonant frequency f_1, Hz and $M_{eqv0,l}$, kg, for different grades of concrete and different resonator lengths l, м

Type of concrete	$E,\ N/m^2 \equiv Pa$	l,m;/ $M_{eqv0,l}$, kg		
		l =1m; 400 kg	l =2m; 800 kg	l =3m; 1200 kg
M200	$2\cdot 10^7$	50 Hz	25 Hz	17 Hz
M300	$3\cdot 10^7$	61 Hz	30.5 Hz	20.3 Hz
M400	$4\cdot 10^7$	70.7 Hz	35.4 Hz	23.6 Hz
M500	$5\cdot 10^7$	79.1 Hz	39.6 Hz	26.4 Hz
M600	$6\cdot 10^7$	86.6 Hz	43.3 Hz	28.9 Hz
M700	$7\cdot 10^7$	93.5 Hz	46.8 Hz	31.2 Hz
M800	$8\cdot 10^7$	100 Hz	50 Hz	33 Hz

Formula (19) allows us to state that for the longitudinal wave resonators we have resonances at frequencies corresponding to the half-wave resonator, since wavelength λ_w and the length of the resonator l are related by the relations:

$$\lambda_w{}^{(n)} = \frac{2\pi}{k_n} = \frac{2\pi}{(n\cdot\pi/l)} = \frac{2l}{n},\quad f_n = \frac{n}{2l}\cdot v_w,\quad v_w = \sqrt{\frac{E}{\rho}}, \tag{62}$$

where: v_w – propagation velocity of the longitudinal wave in the resonator. Knowing f_n with (62) (they correspond to the conditions of excitation of standing waves and "resonances" of the half-wave resonator), it is possible to create conditions under which effectively, at these frequencies ($n=1,2,3,...$), where an integer number of half-waves is inserted, will be absorbed by the resonator material the energy from wave formation, which propagates in it. Let us finally consider the solution for the case of a non-thin rod. First we define the effective radius r_{eff} of a rod resonator whose cross section is rectangular with sides: b – width, h – height:

$$\pi r_{eff}^2 = bh \Leftrightarrow r_{eff} = \sqrt{\frac{bh}{\pi}}. \tag{63}$$

Consider the case when the radius $r_{eff} > 0{,}1 \cdot \lambda_w^{(n)}$, that is:

$$r_{eff} > 0{,}1 \cdot \frac{2l}{n} = \frac{0{,}2l}{n},\ n=1,2,3,.... \tag{64}$$

In this case, the rod cannot be considered thin and a correction factor must be introduced into the wave equation. Relay [2] and Maison [3] showed that the displacement along the axis of the rod is expressed in the form:

$$u_x = z(r) \cdot \sin(k_n x), \tag{65}$$

where $z(r)$ – distance function r from the axis of the rod. At resonant frequencies f_n constant dissemination $k_n = n\pi/l$, $n \in N$, and $\lambda_w^{(n)}$ is found from (62). Taking into account only the main correction, which leaves only the compression-expansion inertia in the direction perpendicular to the rod axis, the frequency equation takes the following form:

$$f_n = \frac{n}{2l} \cdot \sqrt{\frac{E}{\rho}} \cdot \left[1 - \left(\frac{n\mu\pi r_{eff}}{2l}\right)^2\right], \tag{66}$$

where: μ – Poisson's ratio. The frequency equation transforms into the thin rod equation (equation (19)) when $r_{eff} \to 0$. Meson showed that when the rod diameter is very large. d_{eff} ($d_{eff} = 2r_{eff} >> 0{,}1 \cdot \lambda_w^{(n)}$) the higher order terms should be included in equation (66). From the point of view of calculating the equivalent mass, the effect of transverse inertia (i.e., the effect of taking into account the kinetic energy associated with motion in the direction perpendicular to the axis of the rod) is to increase this mass with respect to the value determined by the relation (61). The reason for the increase is as follows: the kinetic energy associated with oscillations along the axis is slightly less than the total kinetic energy of the rod (the numerator of relation (60), which determines the equivalent mass). Accordingly, the ratio of the total energy to the term in the denominator, which consists of the square of the velocity in the direction of the axis, increases. On the contrary, the equivalent mass in the direction perpendicular to the axis decreases when the ratio of the diameter to the term in the denominator is (d_{eff}) to the length increases (assuming that the static mass remains constant).

Let us consider further the influence of boundary conditions on the formation of the spectrum of natural frequencies of the resonator.

A. Both ends of the rod ($x=0;\ x=l$) free of stress:

$$\left.\frac{\partial u}{\partial x}\right|_{x=0} = \left.\frac{\partial u}{\partial x}\right|_{x=l} = 0 \Leftrightarrow f_n = \frac{n}{2l} \cdot v_w = \frac{n}{2l} \cdot \sqrt{\frac{E}{\rho}},\quad n \in N. \tag{67}$$

B. Both ends of the rod ($x=0;\ x=l$) are fixed:

$$u|_{x=0} = u|_{x=l} = 0 \Leftrightarrow f_n = \frac{n}{2l} \cdot v_w = \frac{n}{2l} \cdot \sqrt{\frac{E}{\rho}},\ n \in N. \tag{68}$$

C. One end of the rod is fixed and the other end is stress free:

$$u\big|_{x=0} = \left.\frac{\partial u}{\partial x}\right|_{x=l} = 0 \Leftrightarrow f_n = \frac{(2n-1)}{4l}\cdot v_w = \frac{(2n-1)}{4l}\cdot\sqrt{\frac{E}{\rho}},\ \ n \in N. \tag{69}$$

Consequently, the first two types of boundary conditions (67), (68) lead to the frequency (eigenfrequency) spectrum of the half-wave resonator, and conditions (69) lead to the frequency (eigenfrequency) spectrum of the quarter-wave resonator. f_n, except for the geometric dimensions of the resonator (l, r_{eff}) is also determined by the density of the rod material (ρ) and its elastic properties (Young's modulus – E). Note that $M_{eqv0,l}$ remains the same regardless of the boundary conditions and is described by (61).

4. Resonance properties of linear viscoelastic bodies.

4.1. Maxwell's viscoelastic fluid.

Defining dependence $\sigma_x(\varepsilon_x)$ gives:

$$\dot{\varepsilon}_x = \frac{1}{E_G}\cdot\dot{\sigma}_x + \frac{1}{\eta_v}\cdot\sigma_x,\ \ \dot{\varepsilon}_x = d\varepsilon/dt,\ \ \dot{\sigma}_x = d\sigma_x/dt, \tag{70}$$

where: E_G – Young's modulus of elasticity, η_v – coefficient of (bulk) viscosity.

With $(\sigma_x, \varepsilon_x) \sim \exp(i\omega t)$, $i^2 = -1$, from (70) one obtains:

$$i\omega\varepsilon_x = \frac{1}{E_G}\cdot i\omega\sigma_x + \frac{1}{\eta_v}\cdot\sigma_x \Leftrightarrow \sigma_x = \frac{\left(\omega^2/E_G\right)\cdot\varepsilon_x}{(1/\eta_v)^2 + (\omega/E_G)^2} + \frac{i\cdot(\omega/\eta_v)\cdot\varepsilon_x}{(1/\eta_v)^2 + (\omega/E_G)^2}. \tag{71}$$

Let us introduce the complex modulus of elasticity $\tilde{E}$ by ratios:

$$\tilde{E} = E' + iE'';\ \ E' = \frac{\left(\omega^2/E_G\right)}{(1/\eta_v)^2 + (\omega/E_G)^2};\ \ E'' = \frac{(\omega\cdot\eta_v)}{(1/\eta_v)^2 + (\omega/E_G)^2}. \tag{72}$$

Physical meaning of the dynamic modulus of elasticity E' (which coincides in phase with the applied strain ε_x) is that it characterizes the elastic dynamic properties of a material that is in a harmonic deformation field.

Physical meaning of the dynamic loss modulus E'' (which lags in phase from the applied strain ε_x at an angle φ) is that the tangent of the angle of loss φ or dissipative factor (ratio of mechanical energy dissipated during one cycle to the stored energy) is determined by the alternation between E'' and E':

$$tg\varphi = E''/E' \Leftrightarrow \varphi = arctg\left(E''/E'\right). \tag{73}$$

Since $E'' = E''(\omega)$, then its maximum value determines the "resonance frequency" at which the maximum amount of mechanical energy is absorbed during 1 cycle of oscillations. We call this "resonance frequency" based on the rheological model adopted for the study. It may differ from the "resonance frequency", which is caused by boundary conditions and dimensions, density and the given material as a half-wave or quarter-wave resonator specified above (formulas (67)-(69)). Studies show that such "rheological resonance frequency" within the framework of Maxwell's model for the medium has the form:

$$\omega_{res}{}^* = \sqrt{E_G/\eta_v}. \tag{74}$$

4.2. The Kelvin-Feugt elastically coherent body.

$$\sigma_x = E_G\cdot\varepsilon_x + \eta_v\cdot\dot{\varepsilon}_x;\ \ E' = E_G;\ \ E'' = \omega\cdot\eta_v. \tag{75}$$

From the last expression in (75) it can be seen that the "rheological resonance frequency" for this model lies at infinity, i.e:

$$\omega^*_{res} \to \infty. \tag{76}$$

4.3. Poynting-Thomson elastically coherent body (A.Yu. Ishlinsky).

$$\sigma_x + \dot{\sigma}_x \cdot \tau_{re} = E_G \cdot (\varepsilon_x + \dot{\varepsilon}_x \cdot \tau_{sl}), \tag{77}$$

where: $\tau_{re} = (\eta_v / E_M)$ – time of relaxation, E_M – modulus of elasticity in the viscous piston branch; $\tau_{sl} = \frac{(E_M + E_G)}{E_M \cdot E_G} \cdot \eta_v$ – during sliding.

For this model we have:

$$E' = \frac{E_G \cdot \left(1 + \omega^2 \cdot \tau_{re} \cdot \tau_{sl}\right)}{(1 + \omega^2 \cdot {\tau_{re}}^2)}; \quad E'' = \frac{E_G \cdot \omega \cdot (\tau_{sl} - \tau_{re})}{(1 + \omega^2 \cdot {\tau_{re}}^2)}. \tag{78}$$

$$\omega_{res}{}^* = 1/\tau_{re} = E_M / \eta_v. \tag{79}$$

4.4. Ziner's elastically coherent body [2].

$$\sigma_x + \dot{\sigma}_x \cdot \tilde{\tau}_{re} = \tilde{E}_G \cdot (\varepsilon_x + \dot{\varepsilon}_x \cdot \tilde{\tau}_{sl}); \quad \tilde{\tau}_{re} = \frac{\eta_v}{E_f}; \quad \tilde{\tau}_{sl} = \frac{\left(\tilde{E}_G + E_f\right)}{\tilde{E}_G \cdot E_f} \cdot \eta_v, \tag{80}$$

where: E_f – elastic modulus of the branch parallel to the viscous piston branch; $\tilde{E}_G$ – elastic modulus of the branch, which is connected in series with two parallel branches (viscous piston and elastic branch with E_f).

For this model we have:

$$E' = \frac{\tilde{E}_G \cdot \left(1 + \omega^2 \cdot \tilde{\tau}_{sl} \cdot \tilde{\tau}_{re}\right)}{(1 + \omega^2 \cdot \tilde{\tau}_{re}{}^2)}; \quad E'' = \frac{\tilde{E}_G \cdot \omega \cdot (\tilde{\tau}_{sl} - \tilde{\tau}_{re})}{(1 + \omega^2 \cdot \tilde{\tau}_{re}{}^2)}. \tag{81}$$

$$\omega_{res}{}^* = 1/\tilde{\tau}_{re} = E_f / \eta_v. \tag{82}$$

4.5 Brankov elastic-viscous body [4].

This rheological model consists of three parallel branches (connected in parallel), to which a fourth branch with a purely elastic element having an elastic modulus is connected in series E_G. In the first of the parallel branches there are elasticities with modulus of elasticity E_M, which is connected in series with a viscous piston η'_v. The second of the parallel branches contains only a viscous piston η''_v. In the third of the parallel branches there is a purely elastic element with modulus of elasticity E_f.

The constitutive equation for the (rheological) Brankov model has the form [4]:

$$a_1 \ddot{\sigma}_x + a_2 \dot{\sigma}_x + a_3 \sigma_x = b_1 \ddot{\varepsilon}_x + b_2 \dot{\varepsilon}_x + b_3 \varepsilon_x, \tag{83}$$

where:

$$\ddot{\sigma}_x = d^2\sigma_x / dt^2; \quad \ddot{\varepsilon}_x = d^2\varepsilon_x / dt^2; \quad a_1 = \frac{\eta''_v}{E_G \cdot E_M}; \quad a_2 = \left(\frac{1}{E_G} + \frac{1}{E_M} + \frac{E_f}{E_G \cdot E_M} + \frac{\eta''_v}{E_G \cdot \eta'_v}\right);$$

$$a_3 = \left(\frac{1}{\eta'_v} + \frac{E_f}{E_G \cdot \eta'_v}\right); \quad b_1 = \frac{\eta''_v}{E_M}; \quad b_2 = \left(1 + \frac{E_f}{E_M} + \frac{\eta''_v}{\eta'_v}\right); \quad b_3 = \frac{E_f}{\eta'_v}.$$

The values of the real and imaginary parts of the elastic modulus in the Brankov model are follows:

$$E'_{(\omega)} = \frac{\left[\left(-\omega^2 b_1 + b_3\right) \cdot \left(-\omega^2 a_1 + a_3\right) + \omega^2 a_2 b_2\right]}{\left[\left(-a_1\omega^2 + a_3\right)^2 + a_2^2\omega^2\right]}; \tag{84}$$

$$E''_{(\omega)} = \frac{\left[\left(-a_1 b_2 + a_2 b_1\right)\omega^3 + \left(a_3 b_2 - a_2 b_3\right)\omega\right]}{\left[\left(-a_1\omega^2 + a_3\right)^2 + a_2^2\omega^2\right]}. \tag{85}$$

Since $E''(\omega) \to 0$ with $\omega \to 0$ and $\omega \to \infty$, then $E''(\omega)$ there exists an extremum (like a maximum), which determines the ω^*_{res} for this model. Finding (ω^*_{res}) we need to solve the equation:

$$d\left\{E''(\omega)\right\}/d\omega = 0. \quad (86)$$

It can be shown that equation (86) with respect to ω^2 of the third degree:

$$\tilde{A}z^3 + \tilde{B}z^2 + \tilde{C}z^1 + \tilde{D} = 0,\ z = \omega^2, \quad (87)$$

where: $\tilde{A}, \tilde{B}, \tilde{C}, \tilde{D}$ – coefficients, which are expressed in terms of $a_j,\ j = \overline{(1,3)},\ b_k,\ k = \overline{(1,3)}$. Equation (87) can be solved using Cardano's formula. In this case, one of the possible valid (positive) solutions of this equation (87) will be the one that corresponds to the case: the (cubic) equation has three roots, of which one is valid and two are complex-conjugate. To establish and determine this real root it is necessary to investigate this cubic equation according to standard methods. (This solution is not given here because it is rather cumbersome).

5. Resonance properties of linear viscoelastic bodies, which are described by defining dependencies $\sigma_x(\varepsilon_x)$ integrally.

5.1. Buergers model. As per [5-8] the rheological properties of asphalt concrete are well described by the so-called Bürgers model, which consists of two successively connected links: the Maxwell model and the Kelvin-Feugt model [2]. The differential equations relating stress and strain for the Bürgers model are of the form [8]:

$$\frac{\eta_2}{E_1}\cdot\dot{\sigma} + \left(1 + \frac{E_2}{E_1} + \frac{\eta_2}{\eta_1}\right)\cdot\sigma + \frac{E_2}{\eta_1}\cdot\int_t \sigma dt = \eta_2\dot{\varepsilon} + E_2\varepsilon. \quad (88)$$

If we differentiate by t (88), then we obtain:

$$\frac{\eta_2}{E_1}\cdot\ddot{\sigma} + \left(1 + \frac{E_2}{E_1} + \frac{\eta_2}{\eta_1}\right)\cdot\dot{\sigma} + \frac{E_2}{\eta_1}\cdot\sigma = \eta_2\ddot{\varepsilon} + E_2\dot{\varepsilon}, \quad (89)$$

where: (η_1, E_1) – coefficient of dynamic viscosity and modulus of elasticity of the link, which corresponds to the Maxwell model; (η_2, E_2) – dynamic viscosity coefficient and elastic modulus of the link, which corresponds to the Kelvin-Foigt model. This Bürgers model fits into the reasoning of Sect. 4.5 related to the elastic-viscous body of Brankov [4], and therefore it also has an extremum of the maximum type for the $E''(\omega)$ and sets ω^*_{res}.

5.2. Brankow's model of $\tau_{re} << \tau_{sl}$ $(\ddot{\sigma}_x << E_G \cdot \ddot{\varepsilon}_x)$.

Single integration over t of the rheological law describing the deformation processes of the Brankov body [4], provided that $\tau_{re} << \tau_{sl}$ (relaxation time/duration is much smaller than the time/duration of the creep process), allows us to present this model of body deformation as an integral one, and in differential form it will already look as follows:

$$a_2\dot{\sigma}_x + a_3\sigma_x = b_1\ddot{\varepsilon}_x + b_2\dot{\varepsilon}_x + b_3\varepsilon_x, \quad (90)$$

where all coefficients (90) a_2, a_3, b_1, b_2, b_3 introduced in 4.5 above.

Let's define for this model ω^*_{res}. According to [4], in order for the rheological model to make physical sense of the degree polynomials of the differential operators σ_x and ε_x must either coincide, or for ε_x be 1 more than for σ_x.

The analysis shows that for this case. $\omega^*_{res} \to \infty$.

Findings:

1. In this study, the conditions of occurrence and the main integral characteristics of resonance phenomena (of geometric and rheological types) that are possible in the processes of vibro-compaction and formation of concrete/construction mixtures, which are modeled by visco-elastic-plastic rods of finite length, are determined. The (classical) rheological models known

in the scientific literature, which are scientifically valid and widely used, are used.

2. The results obtained in the paper can be further used to refine and improve the existing engineering methods of calculation of vibration systems for compaction of concrete/construction mixtures both at the design stage and during their actual operation. In addition, such an approach in the technologies of formation and vibration compaction of concrete/construction mixtures will be useful in establishing the conditions of energy-saving functioning and modes of operation of such systems.

References

[1] R. Dzhonson, *Mekhanycheskye fyltry v elektronyke*. M.: Myr, 1986.

[2] E.S. Sorokyn, *K teoryy vnutrenneho trenyia pry kolebanyiakh upruhykh system*. M.: Hosstroiyzdat, 1960.

[3] V.S. Postnykov, *Vnutrennee trenye v metallakh*. M.: Metallurhyia, 1969.

[4] D. Kolarov, A. Baltov, N. Boncheva, *Mekhanyka plastycheskykh sred*. M.: Myr, 1979.

[5] *Konstruyrovanye y raschet nezhestkykh dorozhnykh odezhd*. Pod red. N.N. Yvanova. M.: Transport, 1973.

[6] Z.P. Shulman, Ya.N. Kovalev, E.A. Zaltsyndler, *Reofyzyka konhlomeratnykh materyalov*. Mynsk: Nauka y tekhnyka, 1978.

[7] V.O. Bohomolov, V.K. Zhdaniuk, V.M. Riapukhin, S.V. Bohomolov, "Reolohichna model roboty asfaltobetonu pry styskanni", *Avtoshliakhovyk Ukrainy*, no. 3, pp. 34-37, 2010.

[8] R. Sheremeta, "Ohliad reolohichnykh modelei", *Visnyk Lvivskoho natsionalnoho ahrarnoho un-tu. Ahroinzhenerni doslidzhennia*, no. 22, pp. 22-30, 2021.

[9] D.V. Savielov, "Doslidzhennia rezhymu roboty dynamichnoi systemy «vibratsiina plyta – polimernyi beton» pid chas poverkhnevoho ushchilnennia", *Vibratsii v tekhnitsi ta tekhnolohiiakh*, no. 4(103), pp. 33-40, 2021.

[10] A.H. Maslov, D.V. Savelov, "Teoretichne viznachennya zakonomirnosti zmini napruzhen, yaki vinikayut u polimernomu betoni pri jogo ushchilnenni vibracijnoyu plitoyu", *Transactions of Kremenchuk Mykhailo Ostrohradskyi National University*, Issue 4/2021 (129), pp. 135-141, 2021. https://doi.org/10.30929/1995- 0519.2021.4.135-141.

[11] O. Maslov, D. Savielov, Y. Salenko, M. Javadova, "Theoretical Study of the Dynamic System «Vibration Platform − Polymer Concrete» Stress–Strain State", *Proceedings of the 3rd International Conference on Building Innovations. ICBI 2020*. *Lecture Notes in Civil Engineering*, vol. 181, pp. 191-201, 2022. https://doi.org/10.1007/978-3-030-85043- 2_19.

[12] N.M. Sudarshan, Rao T. Chandrashekar, "Vibration Impact on Fresh Concrete of Conventional and UHPFRC", *International Journal of Applied Engineering Research*, vol. 12, pp. 1683–1690, 2017.

[13] H.B. Koh, D. Yeoh, S. Shahidan, "Effect of revibration on the compressive strength and surface hardness of concrete", *IOP Conf. Series: Materials Science and Engineering*, vol. 271, 012057, pp. 1–6, 2017.

ВИКОРИСТАННЯ МОДЕЛЕЙ МЕХАНІЧНИХ ФІЛЬТРІВ У АНАЛІЗІ ПРОЦЕСІВ ФОРМУВАННЯ ТА УЩІЛЬНЕННЯ БУДІВЕЛЬНИХ/БЕТОННИХ СУМІШЕЙ ВІБРАЦІЙНИМ ПОЛЕМ

[1]**Човнюк Ю.В.,** к.т.н., доцент,
ychovnyuk@ukr.net, ORCID: 0000-0002-0608-0203
[1]**Приймаченко О.В.,** к.т.н., доцент,
pryimachenko.ov@knuba.edu.ua, ORCID: 0000-0001-5125-847
[1]**Чередніченко П.П.,** доцент,
petro_che@ukr.net, ORCID: 0000-0001-7161-661X
[1]**Остапущенко О.П.,** к.т.н., доцент,
olga_ost_17@ukr.net, ORCID: 0000-0001-8114-349X
[1]*Київський Національний університет будівництва та архітектури*
Повітрофлотський пр., 31, м. Київ, 03037, Україна

Анотація. Використані моделі механічних фільтрів різних типів, які застосовуються для аналізу процесів формування та ущільнення будівельних/бетонних сумішей за допомогою вібраційних полів. Встановлені значення резонансних частот та еквівалентних мас для різноманітних резонаторів, що моделюють розповсюдження у останніх вібраційно-хвильових утворень. У основу аналізу впливу вібраційного поля на процеси формування та ущільнення бетонних/будівельних сумішей у даному дослідженні покладені методи математичної фізики, класичного варіаційного числення, фізики коливань і хвиль та методологія розв'язку звичайних диференціальних рівнянь й диференціальних рівнянь у частинних похідних. Встановлені умови та основні інтегральні характеристики резонансних явищ, можливість виникнення котрих обумовлена: 1) геометрією поставленої початково-крайової задачі (це так звані «геометричні резонанси» розглядуваної системи з розподіленими параметрами, що моделює оброблювану суміш); 2) задіяною у дослідженні робочою реологічною моделлю суміші (це так звані «реологічні резонанси»). Розвинутий і науково обґрунтований у роботі підхід дозволяє встановити основні параметри і можливості використання енергоощадних режимів функціонування вібраційних систем, призначених для формування й вібраційного ущільнення вказаних вище сумішей. Отримані у роботі результати можуть бути у подальшому використані для уточнення й вдосконалення існуючих інженерних методів розрахунку вібраційних систем для формування й ущільнення бетонних/будівельних сумішей з метою оптимізації робочих режимів їх функціонування як на стадії проектування, так і у режимах реальної експлуатації.

Ключові слова: моделювання, механічні фільтри, резонатори коливань, аналіз, процеси формування, ущільнення, будівельні та бетонні суміші, вібраційне поле, резонанси, еквівалентні маси.

Стаття надійшла до редакції 27.07.2023

UDC 621.873.01 DOI: 10.31650/2786-6696-2023-5-52-59

IMPROVEMENT OF THE GENERALIZED FORCE CRITERION OPTIMIZATION OF OVERHEAD CRANES MOVEMENT MODES

[1]**Chovnyuk Yurii,** Ph.D., Professor,
ychovnyuk@ukr.net, ORCID: 0000-0002-0608-0203
[1]**Priymachenko Aleksey,** Ph.D., Associate Professor,
pryimachenko.ov@knuba.edu.ua, ORCID: 0000-0001-5125-8472
[1]**Cherednichenko Petro,** Associate Professor,
petro_che@ukr.net, ORCID: 0000-0001-7161-661X,
[1]**Shudra Nataliia,** Senior Lecturer,
Shudra_n@ukr.net, ORCID: 0000-0001-5416-7680
[1]*Kyiv National University of Construction and Architecture*
Povitroflotsky prospect, 31, Kyiv, 03037, Ukraine

Abstract. During the operation of overhead cranes, pendulum oscillations of the payload are often observed, which causes uneven movement of these cranes, their trolleys, loads on the ropes and power elements of the cranes, which, in turn, create various inconveniences during their operation, reduce the reliability of the functioning of both the crane as a whole and its individual elements. It is clear that all of these factors must be taken into account in the refined calculations of cranes (especially in the modes of their optimal (with the minimum driving force required for this) start/braking).

The paper uses a standard methodology and scheme for calculating pendulum oscillations of a payload on the cables of an overhead crane, which are usually carried out within a two-mass model of a crane system. Further refinements and improvements to the above methodology have been made on the basis of a well-founded generalized force criterion for the quality of crane movement. The dependencies describing the law of motion of the crane system and the law of change in time of the applied driving force during the startup/braking stages were obtained, which satisfy the above-mentioned power criterion and ensure high-quality (smooth) movement of the system during its startup or braking.

The law of motion of the crane rotation mechanism (crane drive) at its stopping, as well as the law of motion of the cargo at its lifting by the corresponding crane mechanism and sharp braking, at which the dynamic loads in the drive and in the crane rope, respectively, are minimized, is established. The results obtained in the work can be further used to clarify and improve the existing engineering methods for calculating the start-up modes of overhead cranes both at the stages of their design and in the modes of real operation.

Keywords: improvement, generalized force criterion, optimization, motion modes, starting, braking, overhead cranes, two-axle model.

Introduction. During the operation of overhead travelling cranes the oscillations of load are observed which cause unequal motion of overhead travelling cranes or their trolleys, additional loads on the power elements of these cranes, create inconveniences in their operation, which, of course, must be carefully considered in refined calculations of both cranes themselves and (mechatronic) control systems by them.

The existing methods of the analysis of forced (including pendulum) oscillations of cargo on the ropes according to the classical scheme of the mathematical analysis and the simplest model of the crane system (two-mass) for different laws of change in time (t) of the driving/forced force (F(t)) require, in the opinion of the authors of this investigation, further specification and perfection with the purpose of optimization (minimization of force and kinematic characteristics of motion) as the control systems of cranes at their start/braking, as well as the search of new economically proved methods.

Analysis of the latest research sources and publications. The calculation of load oscillations is usually carried out according to the simplest scheme of two-mass system [1-14], at that, considering that angle of ropes deflection from vertical does not exceed 10° ... 12° (so called small oscillations). It is also considered that the period of pendulum oscillations of load on flexible ropes is more or the same order as the period of acceleration (braking) of the crane, and the driving force of the driving motor of the travel mechanism is constant and equal to the average starting (braking) value [8, 9].

To substantiate the force (generalized) criterion for quality of motion of an overhead crane in start-up/braking modes, the approach of the authors [1, 14] has been applied. In addition, the results of research of the authors [15] have been used in the paper.

Aim and objectives. The aim of this paper consists in substantiation of the kinematic-force criterion (generalized) for optimization of modes and quality of bridge crane movements under their start/braking which provides high quality of such movements (minimization of kinematic and force characteristics of movements) as well as in definition of values of the specified parameters and duration of transients for these (stated by this investigation) optimal modes of such crane systems functioning.

Research methodology. We have used the apparatus of mathematical physics, methods of the classical calculus of variations and methods of the solution of the ordinary linear differential equations.

Statement of basic contents of research. In [8, 9] it has been established that within the framework of two-mass model of the bridge crane ("cargo" – "load carriage", connected by a rope), the swinging of cargo at start-up/braking is described by the following equation:

$$\ddot{x} + \omega^2 \cdot x = (P - W)/m_1, \tag{1}$$

where: X is the horizontal movement of the load relative to the moving point of the load suspended on the rope to the load carriage; $\omega = \sqrt{\frac{(m_1 + m_2)\cdot g}{m_1 \cdot H}}$ – natural frequency of pendulum oscillations of the crane's load during the acceleration period; g=9.81 m/s^2 – acceleration of free fall; m_1 – mass of the crane or trolley, given to translational motion of the crane or trolley; m_2 – mass of the load; H – length of the ropes; P – total traction/braking force of the crane or trolley drive wheels; W – resistance force to movement of the crane or trolley; $x = x_1 - x_2$, where are horizontal displacements of masses m1 and m_2, respectively. It should be noted that in equation (1) the specified variant of motion of the load carriage and the load on the rope, when $(\dot{x}_1 - \dot{x}_2) = \dot{x} > 0$ otherwise the sign in front of the force W is reversed, i.e. at $\dot{x} < 0$ $(\dot{x}_2 > \dot{x}_1)$. Assuming that the drag force against the movement of the crane or trolley is the Coulomb (dry) friction force, it can be added in general as follows:

$$F_{on.} = -W \cdot sign(\dot{x}_1 - \dot{x}_2) = -W \cdot sign(\dot{x}), \;\; W > 0. \tag{2}$$

(It is clear that in notation (2) $F_{on.}$ multiplier W denotes the amplitude of the dry friction force). At zero initial conditions:

$$x\big|_{t=0} = \dot{x}\big|_{t=0} = 0. \tag{3}$$

solution (1) has the form [8, 9]:

$$x = A \cdot (1 - \cos\omega t), \;\; A = (P - W) \cdot H/[g \cdot (m_1 + m_2)]. \tag{4}$$

After acceleration to a steady-state movement of the trolley with constant speed V $(\dot{x}_1\big|_{t=t_{II}} = V)$ the load must have zero velocity (the vibrations disappear $\dot{x}_2\big|_{t=t_{II}} = 0)$, where t_{II} – is the duration of the start-up process, so we have:

$$t = t_{II} \Rightarrow (\dot{x}_1 - \dot{x}_2)\big|_{t=t_{II}} = V - 0 = V. \tag{5}$$

This condition makes it easy to determine t_{II}:

$$\dot{x} = (\dot{x}_1 - \dot{x}_2), \;\; \dot{x}\big|_{t=t_{II}} = V. \tag{6}$$

Given (4), we have:

$$\dot{x} = \omega \cdot A \cdot \sin \omega t \Rightarrow V = \omega \cdot A \cdot \sin(\omega t_{II}). \tag{7}$$

Hence:

$$t_{II} = (1/\omega) \cdot \arcsin(V/(A \cdot \omega)). \tag{8}$$

The path the trolley will take in time t_{II} can be found from the relation [8, 9]:

$$m_1 \cdot \ddot{x}_1 + c \cdot (x_1 - x_2) = P - W, \;\; c = m_2 \cdot g / H. \tag{9}$$

Then for $\ddot{x}_1$ (9) we have:

$$\ddot{x}_1 = (P - W) - c \cdot x = (P - W) - c \cdot A \cdot (1 - \cos \omega t). \tag{10}$$

Then at zero initial conditions for x_1:

$$x_1\big|_{t=0} = \dot{x}_1\big|_{t=0} = 0, \tag{11}$$

from (10) it is easy to obtain the distance L that the crane trolley travels to reach a steady state (with speed V=const.) at the end of the acceleration period ($t = t_{II}$):

$$x_1\big|_{t=t_{II}} = \frac{(P - W - c \cdot A) \cdot {t_{II}}^2}{2} + \frac{c \cdot A}{\omega^2} \cdot \left\{ \sqrt{1 - \left(\frac{V}{A \cdot \omega} \right)^2} - 1 \right\}. \tag{12}$$

In order to find the minimum effective motive force $F_{mf}^{(eff)}$ to accelerate the system and reach a steady speed V, the following criterion for the quality of motion of the crane trolley during the acceleration period must be fulfilled:

$$F_{mf}^{(eff)} = \frac{(P - W)}{m_1} \Rightarrow \min, \tag{13}$$

which is equivalent to the condition:

$$\int_0^{t_{II}} \left\{ F_{mf}^{(eff)} \right\}^2 dt \Rightarrow \min, \tag{14}$$

or, using equation (1), criterion (14) can be represented as:

$$\int_0^{t_{II}} \left(\ddot{x} + \omega^2 \cdot x \right)^2 dt \Rightarrow \min. \tag{15}$$

Criterion (15) can be realized if the law of motion satisfies the Euler-Poisson equation:

$$x^{(IV)} + 2\omega^2 \cdot \ddot{x} + \omega^4 \cdot x = 0. \tag{16}$$

Solve (16) under the following initial and final conditions:

$$x\big|_{t=0} = \dot{x}\big|_{t=0} = 0; \;\; \ddot{x}\big|_{t=t_{II}} = 0; \;\; \dot{x}\big|_{t=t_{II}} = V, \tag{17}$$

as follows:

$$x(t) = C_1 \cdot \sin \omega t + C_2 \cdot \cos \omega t + C_3 \cdot t \cdot \sin \omega t + C_4 \cdot t \cdot \cos \omega t. \tag{18}$$

Undefined constants C_i, $i = \overline{(1.4)}$, we find from conditions (17), then we have:

$$\begin{cases} C_2 = 0; \;\; \omega \cdot C_1 + C_4 = 0; \\ \omega \cdot C_1 \cdot \cos \omega t_{II} + C_3 \cdot (\sin \omega t_{II} + \omega t_{II} \cdot \cos \omega t_{II}) + C_4 \cdot (\cos \omega t_{II} - \omega t_{II} \cdot \sin \omega t_{II}) = V; \\ -\omega^2 \cdot C_1 \cdot \sin \omega t_{II} + C_3 \cdot \left\{ 2\omega \cdot \cos \omega t_{II} - \omega^2 \cdot t_{II} \cdot \sin \omega t_{II} \right\} + C_4 \cdot \left\{ -2\omega \cdot \sin \omega t_{II} - \omega^2 \cdot t_{II} \cdot \cos \omega t_{II} \right\} = 0. \end{cases} \tag{19}$$

As a result of solving the system of equations (19) with respect to C_i, $i = \overline{(1.4)}$, by Cramer's rule we have:

$$\begin{cases} C_2 = 0; \;\; C_1 = -C_4 / \omega; \;\; C_3 = \dfrac{V \cdot (\sin \omega t_{II} + \omega t_{II} \cdot \cos \omega t_{II})}{\left(\sin^2 \omega t_{II} + \omega^2 \cdot {t_{II}}^2 \right)}; \\ C_4 = \dfrac{V \cdot (2 \cos \omega t_{II} - \omega t_{II} \cdot \sin \omega t_{II})}{\left(\sin^2 \omega t_{II} + \omega^2 \cdot {t_{II}}^2 \right)}. \end{cases} \tag{20}$$

The law of optimum (in the sense of the motion quality criterion (13)-(15)) motion $x(t)$ becomes:

$$x(t) = C_1 \cdot \sin\omega t + C_3 \cdot t \cdot \sin\omega t + C_4 \cdot t \cdot \cos\omega t. \tag{21}$$

The law of optimum load carriage movement takes on the following form:

$$\dot{x}_1 = (P-W)t - c\left\{C_1\omega^{-1}\cdot(1-\cos\omega t) + C_3\left[-t\cdot\omega^{-1}\cdot\cos\omega t + \omega^{-2}\cdot\sin\omega t\right] + C_4\left[\frac{t}{\omega}\sin\omega t + \frac{\cos\omega t}{\omega^2} - \omega^{-2}\right]\right\} + \overline{C_1}. \tag{22}$$

Given the initial conditions (11) for $\overline{C_1}$ we have a ratio:

$$\overline{C_1} = 0. \tag{23}$$

The final optimum time variation of the load carriage speed $V_{bogie} = x_1(t)$ over the run-up period $(0 < t \le t_n)$ takes the following form:

$$\dot{x}_{1opt}(t) = (P-W)\cdot t - \frac{c}{\omega}\cdot\left\{C_1(1-\cos\omega t) + C_3(-t\cos\omega t + \frac{\sin\omega t}{\omega}) + C_4\left(t\sin\omega t + \frac{\cos\omega t}{\omega} - \omega^{-1}\right)\right\}. \tag{24}$$

Optimum law of motion of the trolley in time t $x_1(t) \equiv x_{1opt}(t)$ assumes the following form:

$$x_{1opt}(t) = \frac{(P-W)\cdot t^2}{2} - c\cdot\left\{\frac{C_1}{\omega}\left(t - \frac{\sin\omega t}{\omega}\right) + \frac{C_3}{\omega}\left(-\frac{2\cos\omega t}{\omega^2} + \frac{2}{\omega^2} - \frac{t}{\omega}\cdot\sin\omega t\right) + \frac{C_4}{\omega}\left(\begin{array}{l} -\frac{t}{\omega} + \frac{2\sin\omega t}{\omega^2} - \\ -\frac{t}{\omega}\cos\omega t \end{array}\right)\right\} + \overline{\overline{C_2}}. \tag{25}$$

Using the initial conditions (11) for $\overline{\overline{C_2}}$ we have the following relationship:

$$\overline{\overline{C_2}} = 0. \tag{26}$$

Therefore, finally, the law of motion of the trolley in time t when the motion quality criteria (13) -(15) are fulfilled is as follows:

$$x_{1opt}(t) = \frac{(P-W)t^2}{2} - c\cdot\left\{\begin{array}{l} \frac{C_1}{\omega}\left(t - \frac{\sin\omega t}{\omega}\right) + \frac{C_3}{\omega}\left(-\frac{2\cos\omega t}{\omega^2} + \frac{2}{\omega^2} - \frac{t}{\omega}\sin\omega t\right) + \\ + \frac{C_4}{\omega}\left(-\frac{t}{\omega} + \frac{2\sin\omega t}{\omega^2} - \frac{t}{\omega}\cos\omega t\right) \end{array}\right\}. \tag{27}$$

The equivalent scheme for calculation of dynamic loads arising at stopping of crane rotation mechanisms can be presented in the form of a single-mass system with a walled elastic link [3]. Applying the D'Alamber principle it is easy to see that the motion of such a system is described by a differential equation:

$$J\cdot\ddot{\varphi} + c'\cdot\varphi = M_p, \quad \ddot{\varphi} = d^2\varphi/dt^2, \tag{28}$$

where: J – the reduced moment of inertia of the crane rotating mechanism (e.g. moment of inertia of the mechanism drive or moment of inertia of the machine/crane rotating part), φ – twisting angle of the elastic link, c' – is the angular stiffness of the elastic link, M_p – driving torque. This equation (28) can be reduced to the following:

$$\ddot{\varphi} + k^2\cdot\varphi = M_p/J, \quad k^2 = c'/J. \tag{29}$$

Integrating the last equation (29) over time for the initial conditions:

$$\varphi|_{t=0} = M_p/c', \quad \dot{\varphi}|_{t=0} = \omega, \tag{30}$$

where: ω – is the circular speed of the mechanism, we shall have:

$$\varphi = \frac{\omega}{k}\cdot\sin kt + M_p/c'. \tag{31}$$

The corresponding dynamic load of the crane rotating mechanism (torque from elastic forces) is defined as the product of the elastic deformation φ) of the machine to its angular stiffness c':

$$M_F = \frac{c' \cdot \omega}{k} \cdot \sin kt + M_p \Leftrightarrow M_F = \omega \cdot \sqrt{c' \cdot J} \cdot \sin kt + M_p. \quad (32)$$

The maximum dynamic load is:

$$M_{F\max} = \omega \cdot \sqrt{c' \cdot J} + M_p. \quad (33)$$

This load occurs at points in time t_n :

$$t_n = \left\{ \frac{(-1)^n \cdot \pi/2 + \pi \cdot n}{k} \right\}, \ n \in N. \quad (34)$$

In order to reduce the aforementioned dynamic loads during the time that the locking process lasts τ_l (meaning $t \in [0, \tau_l]$), determine the law of motion $\varphi(t)$, at which the quality criterion for this movement will be met:

$$I = \sqrt{\frac{1}{\tau_l} \cdot \int_0^{\tau_l} (c' \cdot \varphi)^2 dt} \Rightarrow \min. \quad (35)$$

The physical meaning of the motion quality criterion (35) is that its implementation minimizes the mean-square dynamic load on the crane mechanism which takes part in the rotary movement during the time that the stopping process lasts.

Using equation (29), criterion (35) can be represented as follows:

$$I = \sqrt{\left\{ \frac{c'}{k^2} \right\} \cdot \frac{1}{\tau_l} \cdot \int_0^{\tau_l} \left(M_p / J - \ddot{\varphi} \right)^2 dt} \Rightarrow \min. \quad (36)$$

A prerequisite for realizing this criterion (provided that $M_p = const$) is the Euler-Poisson equation:

$$\varphi^{(IV)} = 0. \quad (37)$$

We will search for the solution of equation (37) under the following initial/end (so-called terminal) conditions, which make physical sense and follow from the adopted model of motion:

$$\varphi\big|_{t=0} = M_p / c'; \ \dot{\varphi}\big|_{t=0} = \omega; \ \ddot{\varphi}\big|_{t=0} = 0; \ \dot{\varphi}\big|_{t=\tau_l} = 0. \quad (38)$$

Let's feed the solution of equation (37) as a cubic spline on t :

$$\varphi(t) = a_0 + a_1 \cdot t + a_2 \cdot t^2 + a_3 \cdot t^3. \quad (39)$$

Uncertain constants (a_0, a_1, a_2, a_3) are easily found from (39) and the terminal conditions (38). We have:

$$a_0 = M_p / c'; \ a_1 = \omega; \ a_2 = 0; \ a_3 = -\omega/(3 \cdot \tau_l^2). \quad (40)$$

So, the law of motion $\varphi(t)$, at which the quality of movement criterion is realized I (35), (36), is of the form:

$$\varphi(t) = M_p / c' + \omega \cdot t - \frac{\omega \cdot t^3}{3 \cdot \tau_l^2}. \quad (41)$$

Value $M_F(t)$ for the law of motion $\varphi(t)$ (41) takes on the following meanings:

$$M_F(t) = M_p + c' \cdot \omega \cdot t - \frac{c' \cdot \omega \cdot t^3}{3 \cdot \tau_l^2}. \quad (42)$$

So, first of all, the advantage of the law of motion of the system (41) as compared to (31) is that the dynamic loads on the crane system (42) have a smooth character over time rather than oscillating as in (32).

Its maximum value $M_F(t)$ (42) acquires at a point in time $t = \tau_l$ and amounts to:

$$M_{F\max} = M_p + \frac{2}{3} \cdot c' \cdot \omega \cdot \tau_l. \quad (43)$$

Of course, under such circumstances, the value of $M_{F\max}$ decreases compared to (33), because by improving the locking mechanism (e.g. by using mechatronic control systems for this process), it is possible to reduce significantly τ_l $(\tau_l \to 0)$ and it always becomes an attainable condition:

$$\frac{2}{3}\cdot\frac{\tau_l}{k}<1. \tag{44}$$

That is, if the condition is met (44) $M_{F\max}$ (43) is less than $M_{F\max}$ (33). This is another advantage of the mode of motion (41) in comparison with the mode of motion (31).

It should be noted that in the most general case this is the total reduced moment of inertia of all the moving parts of the crane drive located between the motor and the crane actuator, and M_p – the torque created by the crane motor.

If a safety coupling is installed in the crane drive, then the calculation scheme and all the above defined dependencies remain the same when the coupling is activated, but the value is equal to the total reduced moment of inertia of only those drive elements which are placed between the coupling slave part and the actuator of the crane mechanism (rotation), and the value M_p is equal to the moment at which the coupling slips.

The formulas (31) to (33) can also be used to determine the dynamic loads (on the rope) when the crane hoist is suddenly braked [3]. For this purpose, instead of M_p the static moment from the drag force (load), and for forward motion of the mass m_0 – static load (weight $G_0 = m_0 \cdot g$, $g = 9.81 м/с^2$); in the latter case the dynamic force F is determined according to the formula [3]:

$$F = \frac{c_0 \cdot v}{\beta}\cdot \sin \beta t + G_0, \tag{45}$$

where: $\beta = \sqrt{c_0 / m_0}$; c_0 – the stiffness of the crane rope material; v – lifting speed of the crane (normalized parameter).

To optimize the dynamic loads on the crane rope during sudden braking (braking time is τ_b, meaning $t \in [0, \tau_b]$) The above approach and considerations regarding the lifting mechanism of the crane (namely, to minimize the above loads) can be applied $M_F, M_{F\max}$, but already for F, $F_{\max}$, and make the following replacements:

$$c' \leftrightarrow c_0; \omega \leftrightarrow v; k \leftrightarrow \beta; J \leftrightarrow m_0; M_p \leftrightarrow G_0; \varphi \leftrightarrow Y; \ddot{\varphi} \leftrightarrow \ddot{Y}; \tau_l \leftrightarrow \tau_b. \tag{46}$$

(46) $Y, \ddot{Y}$ – symbolize the upward movement along the rope axis and the acceleration along this direction, respectively.

Conclusions:

1. Improved generalized force criterion for optimizing crane movements (start-up) is justified, minimizing the driving force during the transition process.

2. The law of a crane trolley movement and the law of change in time of its speed, which enable to fulfil the above criterion, have been determined analytically.

3. The law of motion of the crane rotation mechanism (drive of the crane) at its stopping and the law of motion of the cargo at its lifting by the proper mechanism of the crane and abrupt braking at which dynamic loads in the drive and in the crane rope are minimized, respectively, has been established.

3. The results obtained in the work can be further used to clarify and improve the existing engineering methods for calculating the starting modes of overhead cranes both at the stages of their design and in the modes of actual operation.

Referencts

[1] V.S. Loveikin, Yu.V. Chovniuk, M.H. Dikteruk, K.I. Pochka, "Analitychnyi pidkhid u analizi uzahalnenoho enerhosylovoho kryteriiu optymizatsii rezhymiv rukhu mostovykh kraniv", *Sbornyk nauchnыkh trudov. Stroytelstvo. Materyalovedenye. Mashynostroenye. Yntensyfykatsyia robochykh protsessov stroytelnыkh y dorozhnыkh mashyn. Seryia: Podъёmno-transportnые, stroytelnые y dorozhnые mashynы y oborudovanye,* no. 72, pp. 251-257, 2013.

[2] F.K. Ivanchenko, *Pidiomno-transportni mashyny*. K.: Vyshcha shkola, 1993.

[3] S.N. Kozhevnykov, *Dynamyka mashyn s upruhymy zveniamy*. K.: Yzd-vo AN USSR, 1961.

[4] V.S. Loveikin, Yu.V. Chovniuk, M.H. Dikteruk, S.I. Pastushenko, *Modeliuvannia dynamiky mekhanizmiv vantazhopidiomnykh mashyn.* K. Mykolaiv: RVV MDAU, 2004.

[5] V.S. Loveikin, A.P. Nesterov, *Dynamichna optymizatsiia pidiomnykh mashyn*. Kh.: KhNADU, 2002.

[6] V.S. Loveikin, Yu.O. Romasevych, Yu.V. Chovniuk, I.O. Kadykalo, *Dynamika y optymizatsiia pidiomno-transportnykh mashyn*. *Monohrafiia*. K.: TsP «KOMPRINT», 2019.

[7] S.N. Kozhevnykov, *Dynamyka nestatsyonarnыkh protsessov v mashynakh*. K.: Naukova dumka, 1986.

[8] V.S. Loveikyn, *Raschёtы optymalnыkh rezhymov dvyzhenyia mekhanyzmov stroytelnыkh mashyn*. K.: UMK VO, 1990.

[9] V.S. Loveikin, "Minimizatsiia dynamichnykh navantazhen v pruzhnykh elementakh vantazhopidiomnykh mashyn", *Hirnychi, budivelni, dorozhni i melioratyvni mashyny*. vol. 52, pp. 63-68, 1998.

[10] S.M. Novak, A.S. Lohvynets, *Zashchyta ot vybratsyy y shuma v stroytelstve: Spravochnyk*. K.: Budivelnyk, 1990.

[11] F.K. Yvanchenko, V.S. Bondarev, N.P. Kolesnyk, V.Ia. Barabanov, *Raschёtы hruzopodъёmnыkh y transportyruiushchykh mashyn*. K.: Vyshcha shkola, 1978.

[12] L.Ia. Budykov, *Mnohoparametrycheskyi analyz dynamyky hruzopodъёmnыkh kranov mostovoho typa*. Luhansk: Yzd-vo VUTU, 1997.

[13] B.P. Rumiantsev, L.Ia. Budykov, *Yssledovanye vlyianyia otdelnыkh parametrov krana na velychynu dynamycheskykh nahruzok. Lokomotyvostroenye*, vol. 4, pp. 28-35, 1972.

[14] V.S. Loveikin, Yu.V. Chovniuk, M.H. Dikteruk, K.I. Pochka, "Universalnyi metod analizu vymushenykh kolyvan elementiv mostovykh kraniv u protsesakh yikh pusku pid vplyvom shvydkozminnykh syl. Stroytelstvo. Materyalovedenye. Mashynostroenye. Yntensyfykatsyia rabochykh protsessov stroytelnыkh y dorozhnыkh mashyn", *Sbornyk nauchnыkh trudov. Seryia: Podъёmno-transportnые, stroytelnые y dorozhnые mashynы y oborudovanye*, no. 72, pp. 257-265, 2013.

[15] L.D. Landau, E.M. Lyfshyts, *Teoretycheskaia fyzyka*. T.1. Mekhanyka. M.: Nauka, 1965.

ВДОСКОНАЛЕННЯ УЗАГАЛЬНЕНОГО СИЛОВОГО КРИТЕРІЮ ОПТИМІЗАЦІЇ РЕЖИМІВ РУХУ МОСТОВИХ КРАНІВ

[1]**Човнюк Ю.В.,** к.т.н., доцент,
ychovnyuk@ukr.net, ORCID: 0000-0002-0608-0203
[1]**Приймаченко О.В.,** к.т.н., доцент,
pryimachenko.ov@knuba.edu.ua, ORCID: 0000-0001-5125-8472
[1]**Чередніченко П.П.,** доцент,
petro_che@ukr.net, ORCID: 0000-0001-7161-661X
[1]**Шудра Н.С.,** ст. викладач,
Shudra_n@ukr.net, ORCID: 0000-0001-5416-7680
[1]*Київський Національний університет будівництва та архітектури*
Повітрофлотський пр., 31, м. Київ, 03037, Україна

Анотація. При роботі мостових кранів часто спостерігаються маятникові коливання вантажу, що є причиною нерівномірного руху вказаних кранів, їх вантажних візків, навантажень на канати та силові елементи кранів, які, у свою чергу, створюють різноманітні незручності при їх експлуатації, зменшують надійність функціонування як крану у цілому, так і його окремих елементів. Зрозуміло, що всі ці фактори необхідно враховувати при уточнених розрахунках кранів (особливо в режимах їх оптимального (з мінімальною необхідною для цього рушійною силою) пуску/гальмування).

У роботі використана стандартна методика та схема розрахунку маятникових коливань вантажу на канатах мостового крану, які проводяться зазвичай у межах двомасової моделі кранової системи. Здійснені подальші уточнення й вдосконалення вказаної вище методики на основі обґрунтованого узагальненого силового критерію якості руху крану. Отримані залежності, що описують закон руху кранової системи та закон зміни у часі прикладеної рушійної сили на етапах пуску/гальмування, що задовольняють вищезгаданий силовий критерій і забезпечують якісний (плавний) рух системи у період її пуску чи гальмування.

Встановлений закон руху механізму обертання крана (приводу крана) при його стопорінні, а також закон руху вантажу при його підйомі відповідним механізмом крана й різкому гальмуванні, за яких мінімізуються динамічні навантаження у приводі та у канаті крана, відповідно. Отримані у роботі результати можуть бути у подальшому використані задля уточнення й вдосконалення існуючих інженерних методів розрахунку режимів пуску мостових кранів як на етапах їх проектування, так і у режимах реальної експлуатації.

Ключові слова: вдосконалення, узагальнений силовий критерій, оптимізація, режими руху, пуск, гальмування, мостові крани, двомасова модель.

Стаття надійшла до редакції 21.06.2023

UDC 666.96:699.844 DOI: 10.31650/2786-6696-2023-5-60-68

RESEARCH OF ACOUSTIC PROPERTIES OF MATERIALS FOR FOUNDATIONS UNDER THE FLOOR

[1]**Kersh V. Ya.,** Ph.D., Professor,
kersh@ogasa.org.ua, ORCID: 0000-0001-6085-5260
[1]**Zamula M.O.,** postgraduate student,
zamulamichailodaba@gmail.com, ORCID: 0000-0001-8737-0933
[1]*Odessa State Academy of Civil Engineering and Architecture*
4, Didrikhson str., Odessa, 65029, Ukraine

Abstract. The most important components of comfortable conditions for people on the premises of residential and public buildings are thermal (temperature) and acoustic comfort. By the regulatory documents of Ukraine, high requirements are imposed on the thermal and sound insulation qualities of external and internal building envelopes, especially on interfloor floors. While the problem of insufficient thermal protection primarily concerns floors over cold basements and passageways, poor sound insulation of floors is a problem for all apartments in high-rise buildings. This article analyzes the causes of acoustic discomfort in buildings. A person indoors is exposed to three types of noise: airborne, impact, and structural. The most difficult problem to solve is an impact noise through the floors. It is emphasized that despite the different noise sources, the mechanisms of propagation of structural and impact noise are similar – through the structural elements of the building. Therefore, measures to reduce impact noise can simultaneously reduce the level of structural noise. The most common methods of reducing sound transmission through floors are analyzed. It is proposed to replace the conventional screed in the floor structure with a heat and sound-insulating screed based on a gypsum-cement-pozzolana binder. This paper considers only an acoustic aspect of the problem. According to the theory of acoustic dissipation, it is assumed that the effect of sound energy dissipation is enhanced by the introduction of aggregates into the mixture, which increases the number of structural heterogeneities and interfaces. The aggregates used in the mixture are expanded polystyrene granules, cork chips, and granular waste from the production of foam glass. In order to experimentally verify this assumption, laboratory methods and devices were developed for a comparative assessment of the soundproofing properties of the developed compositions. Based on the results of measuring the acoustic properties of the prototypes, experimental and statistical (ES) models were constructed, and the best combinations of mixture components were determined in terms of sound insulation. ES models of noise properties were used in the multi-criteria optimization of the composition of the composite mixture.

Keywords: interfloor floors, floors, acoustics, impact sound, sound insulation, acoustic measurements, planed experiment, modeling.

Introduction. An important task of civil engineering is to provide comfortable conditions for people to stay in buildings. The main components of a comfortable stay of people in residential and public buildings are thermal (temperature) and acoustic comfort. In accordance with the regulatory documents of Ukraine [1-3], rather high requirements are imposed on the thermal and sound insulation qualities of external and internal building envelopes, especially on interfloor floors. Insufficient thermal insulation of floors leads to increased heat loss and higher heating costs. If insufficient thermal protection is manifested primarily in rooms with floors over cold basements or passageways, then acoustic discomfort as a result of poor sound insulation of interfloor floors in residential buildings, especially from impact noise, is a problem for all apartments in high-rise buildings [4].

Despite the differences in the physical phenomena of heat and sound transmission through building structures, a significant improvement in the thermal and sound insulation of floors can be

achieved by using special materials with a set of specified properties as floor substrates. The requirements for such materials for some properties are multidirectional, for example, improving sound insulation characteristics by increasing density is accompanied by a deterioration in thermal protection properties. While meeting the requirements of standards for a number of other important properties such as strength, moisture resistance, shrinkage, and fire safety, these materials must also be environmentally friendly and inexpensive.

These requirements are met by water-resistant gypsum-based composite materials, a distinctive feature of which is the consideration of the physical and chemical capabilities of each of the components of building mixtures, their interaction with each other and their predominant influence on certain operational and technological characteristics. Synthesis of a suitable material under many non-coincident conditions is a non-trivial but important task of construction materials science. Thus, the development of a composition of multicomponent gypsum-containing materials for floor substrates with an optimal set of operational and technological properties is an urgent task. This paper considers one of the aspects of creating comfortable indoor conditions – providing acoustic protection against the penetration of airborne noise and, especially, impact noise through the floors.

Analysis of recent research and publications. The problem of heat and sound insulation of not only interfloor floors, but also other building envelopes, both external and internal – walls, partitions, windows and doors – arose with the beginning of mass construction of panel and block buildings using large-sized precast concrete products, in particular, floor slabs [5]. The first Soviet projects of that time included gypsum slabs, and sometimes panels the size of an entire room, which were laid on the floor under a screed. They served as soundproofing and, partially, thermal insulation of the floors, and they did their job quite well. The disadvantage of such gypsum bases was their low water resistance. Plumbing accidents and flooding of the premises with water during firefighting led to soaking of the gypsum bases, loss of strength, cracking, and loss of sound insulation properties. During the renovation, these slabs were dismantled to increase the height of the room, and the sound insulation was completely eliminated. Another solution to the problem of soundproofing the floors was the installation of floors with elastic gaskets. As a material for elastic pads, products made of silicate fibers (glass, mineral) were used, which were intended mainly for thermal insulation purposes. The main disadvantage of all these products as elastic gaskets is their high compressibility during operation [6]. The problem of sound insulation of premises became especially acute with the advent of frame-monolithic buildings, where, in an effort to reduce the weight of structures, the thickness of floors and partitions was reduced to the minimum permissible strength. This has led to a decrease in the soundproofing properties of the enclosures and a sharp increase in complaints from residents about increased noise in their apartments.

There are three types of acoustic impact on humans indoors: airborne noise, impact noise, and structural noise. Airborne noise is noise that spreads through the air, such as loud conversation, media devices, traffic noise, and the operation of machinery under the window. Impact noise is any impact that is perceived by a building structure element and propagates through the premises over a wide area – the sound of heels on a tiled floor, a nail being driven into a wall, a hammer drill, etc. Structural noise is caused by the vibration of communications in the building – the "growling" of the water supply system, the noise of water running down, the operation of elevator equipment, knocks in ventilation shafts, etc. It should be noted that, despite the different noise sources, the mechanism of structural noise propagation is similar to the mechanism of impact noise propagation (Fig. 1) – through the structural elements of the building [7]. Therefore, measures to reduce impact noise can simultaneously reduce the level of structural noise.

The sound insulation of the floor is mainly affected by the value of the total mass of 1 m^2 of the interfloor ceiling with the floor, and if it is greater than 350 kg/m^2, the required sound insulation of airborne noise is generally provided [8]. For impact noise insulation, the mass of the floor is also important, but to meet the standards, it must be several times greater than for airborne noise standards, which is neither technically nor economically feasible. In this case, it is more efficient to use special floor structures [9].

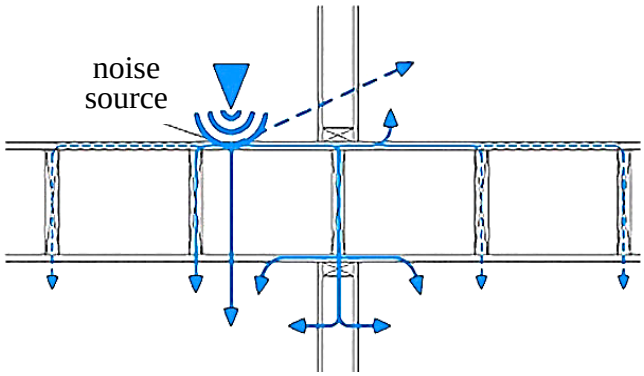

Fig. 1. Scheme of impact noise transmission

Typically, a common floor structure for panel buildings includes the following elements (Fig. 2): coating, screed, and a reinforced concrete slab base.

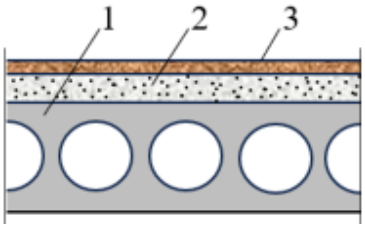

Fig. 2. Elements of the floor structure:
1 – reinforced concrete slab; 2 – screed (underlying layer); 3 – coating

Let us take a closer look at layer 2 – the screed as an element of the floor structure, which is most appropriate to use as a soundproofing base. A screed is a layer that levels the floor surface and also serves to create a flat surface for the coating. Depending on the materials used, screeds are divided into solid (monolithic) and prefabricated.

The composition of solid screeds includes: cement-sand mortars, concrete, expanded clay concrete, gypsum concrete, and cement fiber. Almost all of these types of screeds can be used as self-leveling screeds. A self-leveling screed is a ready-mix that, after pouring, self-distributes and levels without the need for additional leveling or adjustment, making the installation process faster and easier. In flooring technologies with prefabricated screeds, the following materials are mainly used: fiberboard, chipboard, gypsum fiber sheets and plywood.

The list of screeds used shows that their functions do not include the formation of thermal and acoustic protection of the floor.

Existing solutions for soundproofing floors are mainly constructive in nature. To increase the sound insulation of building envelopes, multilayer structures are used - floating floors, suspended ceilings, with the use of elastic roll materials [10]. Obviously, the most effective is the sound insulation of structures from the side of the noise source. However, it is practically impossible to implement sound insulation measures in existing buildings in operation, since they are of no interest to the occupants of the "noisy" upper floors. Therefore, measures for acoustic protection of premises should be provided for at the design stage and implemented during construction, or reconstruction and overhaul.

It is possible to provide both heat and sound insulation properties of floor substrates using special materials and technologies.

In particular, materials with low thermal conductivity, such as extruded polystyrene foam (XPS), extruded polyurethane foam (XPU) or mineral wool, can be used for thermal protection. These materials can be laid under the screed.

For soundproofing, materials such as acoustic mineral wool boards, gypsum board, or rubber mats can be used, which can be placed either under the screed or under the floor covering. However, the above recommendations imply the use of leveling screeds in any case.

In view of the above, it may be considered productive to replace a conventional screed, such as a cement-sand screed, with a heat and sound insulating base for the final coating. It is proposed to use environmentally friendly and energy-efficient building gypsum as the main binder, but not in its pure form, but to increase water resistance, in the form of a gypsum-cement-pozzolan mixture with the addition of ash as a pozzolanic additive. To impart heat and sound insulating properties, expanded polystyrene granules, cork chips, and granular waste from the production of foam glass were introduced into the mixture [11]. It is technologically and economically feasible to make such screeds from self-leveling mixtures, adjusting the setting time over time by means of additives.

The assumption that the introduction of aggregates with soundproofing properties into the mixture should improve the acoustic characteristics of the flooring is based on the theory of acoustic dissipation, which explains the attenuation of sound waves in the propagation medium by the conversion of sound energy into heat energy as a result of molecular friction during the process of scattering on small inhomogeneities [12]. This process occurs in all environments, but its intensity depends on the properties of the environment and the frequency of sound waves. For example, air has a low capacity for acoustic dissipation, so sound energy in air is not actively converted into heat. However, in denser environments, such as concrete, acoustic dissipation is more pronounced, leading to a more intense conversion of sound energy into heat. It can be assumed that the introduction of aggregates into the mixture increases the number of structural inhomogeneities and interfaces, which, according to the theory of acoustic dissipation, enhances the effect of sound energy dissipation and, consequently, its absorption by the material.

Purpose and objectives. The aim of the study is to substantiate the choice of methods for determining the acoustic properties of materials developed as heat and sound insulating floor bases and to analyze the effect of various aggregates on sound insulation properties.

It should be noted that standard methods for measuring airborne and impact noise are designed to study real structures with regulation of the size of the rooms separated by these structures and a certain standard set of equipment [13].

Thus, it can be concluded that there is currently no standardized, generally accepted methodology for determining the soundproofing properties of materials in the form of samples of the compositions being developed. Consequently, there is a need to develop a methodology and laboratory equipment for determining the acoustic properties of samples of relatively small sizes made in large quantities, for example, during planned experiments [14]. Obviously, the results obtained in this way will not correspond to standard sound insulation indicators. However, these results may well be used for a comparative assessment of the sound insulation properties of an array of prototypes of experimental compositions and the selection of the best ones according to the specified quality criteria.

Research methods and materials. The following methods and experimental setups were used to determine the characteristics of airborne and impact noise.

Airborne noise. During laboratory measurements, the soundproofing ability of the material of the samples against airborne noise is taken as the sound transmission, which is the ratio of the power of sound energy that passed through the sample to the power of energy incident on it.

The experimental setup for measuring sound transmission (Fig. 3) is a chamber with wooden walls, separated by a partition with a slot for installing the sample. To eliminate the indirect transmission of sound through the walls of the chamber, its interior is filled with soundproofing material, and the outer walls of the chamber are also covered with it from the outside.

To study the sound processes, we used the Spectralab program, which allows us to measure the spectral power of sound, both at individual frequencies and integral. The sound power corresponding to the voltage of the alternating component at the sound card input in millivolts was determined without the sample *Efal* and with the sample *Etrans*. The sound transmission coefficient was defined as $K_{air\ noise} = Efal/Etrans$.

The determination was performed at different frequencies – from 100 to 2000 Hz. Each experiment was performed three times with the sample reinstalled, and the results were then averaged.

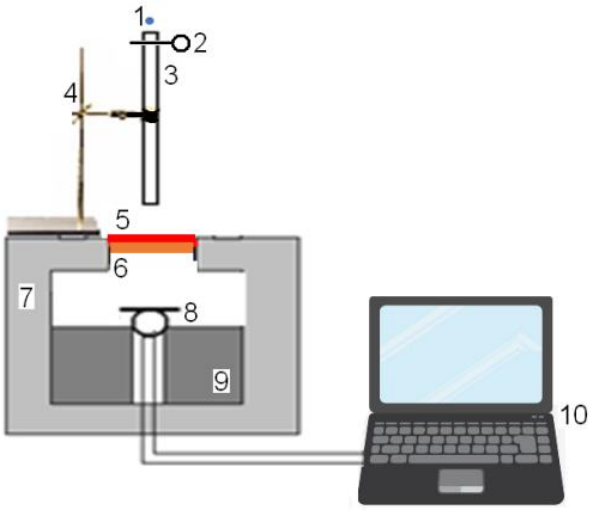

Fig. 3. Device for measuring the sound transmission coefficient:
1 – sound generator; 2 – sound chamber; 3 – sound emitter (speaker); 4 – dynamic microphone; 5 – test sample; 6 – computer with sound card

Impact noise. The proposed method for determining the soundproofing ability of a material uses the effect of converting the kinetic energy of a metal ball falling vertically from a constant height onto an impact surface that contacts the test sample and simulates a finish coating into an electrical signal measured by a computer. A diagram of the test setup is shown in Fig. 4.

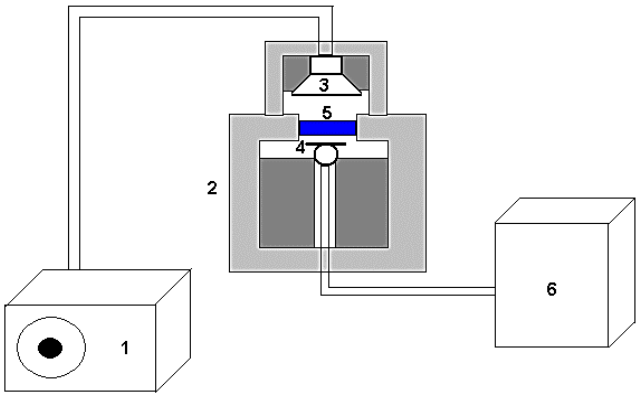

Fig. 4. Device for measuring impact sound:
1 – metal ball; 2 – shutter mechanism; 3 – guide tube; 4 – laboratory tripod; 5 – impact surface; 6 – test sample; 7 – sound chamber; 8 – dynamic microphone; 9 – soundproofing filling; 10 – laptop with sound input (sound card)

In this case, the measured parameter is the amplitude of the electrical signal proportional to the sound energy that has passed through the sample. The best materials are those with the lowest signal amplitude, i.e., the highest sound absorption. As mentioned earlier, this measured parameter does not directly correspond to standard sound insulation characteristics, such as the impact noise insulation index, although such a transition is possible using the material of structures that have passed standard tests. However, this study did not set such a task. For the development of compositions with improved acoustic properties, a relative measurement method is sufficient, in which the actual characteristic of the sound insulation ability to impact noise is proportional (with a certain constant proportionality factor) to those measured by various types of sound analyzers. The relative method makes it possible to correctly perform the most important task of the study – to optimize the composition and technological factors of the material.

Production of prototypes. For the production of prototypes, a comprehensive experiment plan with three dependent (aggregates) and one independent (fly ash/cement ratio) factors was adopted, the so-called "Triangles on a linear segment" plan (Fig. 5). The amount of binding components – gypsum and cement – was fixed, and the ash-cement ratio varied from 30 to 40%. The content of mixed components – polystyrene foam, cork and foam glass – varied at three levels, the gold-cement ratio at two levels: 1.11 (level -1) and 1.65 (level +1). Since the plan is mixed, without technological factors, we consider it possible to denote all factors by X: the amount of expanded polystyrene is X_1, the amount of cork is X_2, the amount of foam glass is X_3, and the amount of ash is X_4. The factors and their levels of variation are shown in Table 1.

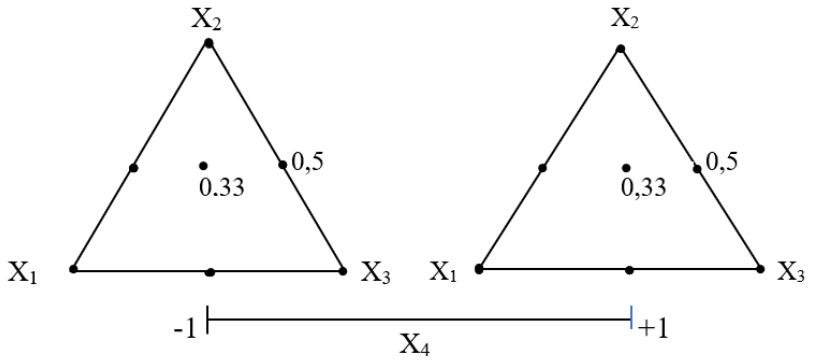

Fig. 5. Scheme of the research plan (levels of variation for X_2 are indicated, for X_1 and X_3 they are symmetrical)

Table 1 – Factors and levels of their variation

Factors	Levels of variation at:								
	$X_4 = -1$					$X_4 = +1$			
X_1, X_2, X_3	Coded	0	0.33	0.5	1	0	0.33	0.5	1
	Natural, g	0	61.9	92.9	185.8	0	59.1	88.65	177.3

In accordance with the adopted experimental plan, samples of fourteen formulations were made in the form of standard beams for measuring mechanical and thermophysical properties, as well as in the form of plates measuring 205×100×20 mm for acoustic tests.

Research results and their interpretation. According to the results of measurements of acoustic characteristics, graphs of dependence of the sound permeability coefficient (Fig. 6, a) and impact sound amplitude (Fig. 6, b) on the average density of the material are plotted. The analysis of these graphs shows that density is not the main factor that determines the ability of a material to resist airborne noise, let alone impact sound.

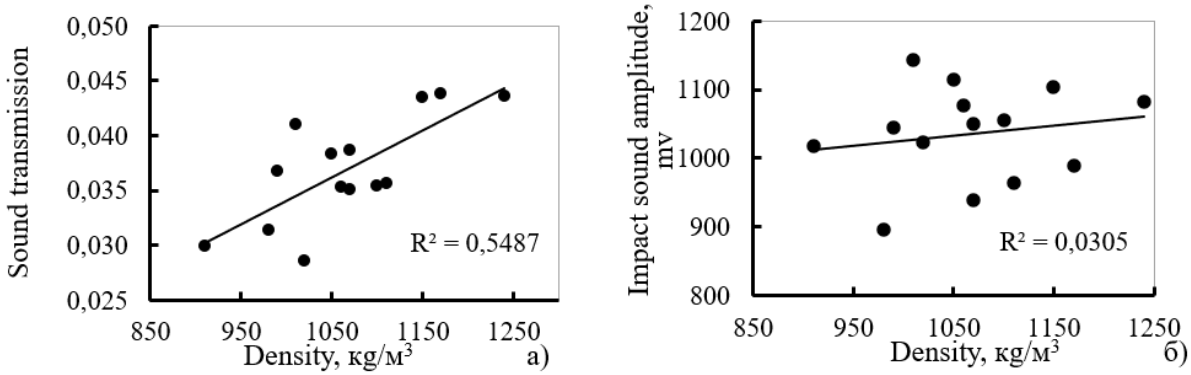

Fig. 6. Dependence of sound transmission (a) and impact sound amplitude (b) on density

The results of the measurements of acoustic properties were used to build experimental and statistical models (ES-models) of sound transmission and impact sound amplitude.

ES model of sound transmission for airborne sound after exclusion of insignificant coefficients:

$$K_{air\ noise} = +0.0924 \cdot X_1 + 0.0404 \cdot X_2 + 0.0392 \cdot X_3 + 0.0048 \cdot X_2 \cdot X_4 + 0.0046 \cdot X_3 \cdot X_4 \quad (1)$$

The final ES model of the impact sound amplitude A blow noise, normalized to the largest value, in relative units:

$$A_{blownoise} = +0.910 \cdot X_1 + 0.0931 \cdot X_2 + 0.938 \cdot X_3 - 0.906 \cdot X_1 \cdot X_2 \quad (2)$$

As an example, the ES model of the impact sound is graphically displayed on a triangle (Fig. 7), the vertices of which correspond to the maximum content of the respective aggregate (the amount of ash – X_4 is fixed at the minimum level).

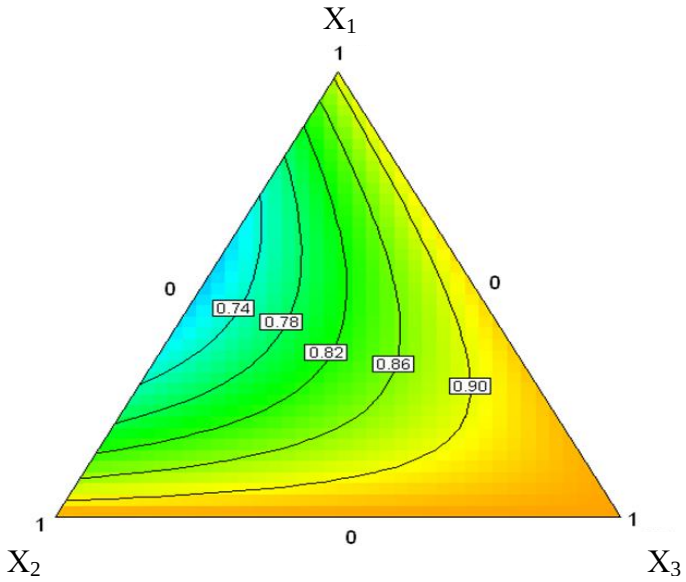

Fig. 7. Dependence of the normalized impact sound amplitude in relative units on the number of aggregates: X_1 – expanded polystyrene, X_2 – cork, X_3 – foam glass

Conclusions and prospects for further research. The analysis of model (1) allows us to conclude that all the introduced components worsen the soundproofing properties of the material, but to varying degrees. Expanded polystyrene has a relatively significant impact, which confirms the information on the deterioration of the sound insulation ability against airborne noise of walls insulated with expanded polystyrene.

The ES model of impact sound (2) shows that the introduction of the accepted components into the mixture separately also slightly increases the sound transmission of the material. The minimum signal value, i.e., the highest sound insulation against impact noise, corresponds to the composition that includes a combination of expanded polystyrene and cork. This can be attributed to two effects: a decrease in the thickness of the matrix material partitions, through which impact noise mainly propagates, and the dissipation of strain energy on elastic inclusions and its conversion into heat at the interfaces in the material. The amount of ash in the studied factor space does not affect the sound transmission from impact sound.

However, it should be understood that the study of acoustic characteristics is a rather limited task of creating materials for floor substrates that must meet a wide range of requirements for thermal conductivity, water resistance, strength, etc. The obtained experimental and statistical models for airborne and impact noise are used for further multicriteria compromise optimization of the gypsum composition by a set of properties.

Further research involves a comprehensive selection of plasticizing and retarding additives to ensure the required mobility of the mixture, as well as the regulation of setting times.

References

[1] DBN V.1.1-31:2013. Zakhist teritorij, budinkiv i sporud vid shumu. K.: Minregion Ukraïni, 2014.

[2] DBN V.2.6-31:2021. Teplova izolyatsiya ta energoefektivnist' budivel'. K.: Ministerstvo rozvitku gromad ta teritorij Ukraïni, 2022.

[3] DSTU-N B V.1.1-34:2013. Nastanova z rozrakhunku ta proektuvannya zvukoizolyatsiï ogorodzhuval'nikh konstruktsij zhitlovikh i gromads'kikh budinkiv. K.: Minregion Ukraïni, 2014.

[4] I.L. Shubin, V.A. Aistov, M.A. Porozhenko, "Zvukoizolyatsiya ograzhdayuschikh konstruktsij v mnogoetazhnykh zdaniyakh. Trebovaniya i metody obespecheniya", *Stroitel'nye materialy*, no. 3, pp. 33-43, 2019.

[5] O.V. Startseva, S.N. Ovsyannikov, "Teoreticheskie i eksperimental'nye issledovaniya zvukoizolyatsii peregorodok", *Vestnik Tomskogo gosudarstvennogo arkhitekturno-stroitel'nogo universiteta*, no. 2 (39), pp. 176-184, 2013.

[6] A.S. Polevschikov, "Zvukoizolyatsiya mezhduetazhnykh perekrytij v zhilykh zdaniyakh", *Zhilischnoe stroitel'stvo*, no 7, pp. 55-57, 2015.

[7] Zvukoizolyaciya pod styazhku pola kotoraya luchshe. [Online]. Available: https://7tg.com.ua/zvukoizolyaciya-pid-styazhku-pidlogi-yaka-krashhe/ Accessed on: July 5, 2023.

[8] V.A. Gorin, V.V. Klimenko, M.A. Porozhenko, "Issledovanie zvukoizolyatsii mnogoslojnykh mezhduetazhnykh perekrytij", *Stroitel'stvo i rekonstruktsiya*, no. 3 (77), pp. 46-50, 2018.

[9] I.N. Babij, A.N. Gostrik, E.Yu. Kal'chenya, "Mnogokriterial'nyj analiz pri vybore tekhnologii ustrojstva zvukoizolyatsii mezhduetazhnykh monolitnykh perekrytij", *Visnik Pridniprovs'koï derzhavnoï akademiï budivnitstva ta arkhitekturi*, no. 4, pp. 79-84, 2018.

[10] A.M. Senan, "K otsenke zvukoizolyatsii mezhduetazhnykh perekrytij", *Ekologicheskij vestnik nauchnykh tsentrov Chernomorskogo ekonomicheskogo sotrudnichestva*, Spetsvypusk, pp. 151–153, 2006.

[11] V.Ya. Kersh, A.V. Kolesnikov, M.O. Zamula, "Podbor sostavov teplozvukoizoliruyuschikh kompozitsij", *Materiali mizhnarodnoï naukovo-praktichnoï konferentsiï «Energoefektivne misto. XXI stolittya»*, ODABA, pp. 39-41, 2020.

[12] M.A. Musakaev, "*Issledovanie protsessov dissipatsii akusticheskoj energii v pogranichnom sloe tvyordoj poverkhnosti pri vzaimodejstvii s nej stoyachej zvukovoj volny*": dis. k.f.m. nauk, S-Pb., 2013.

[13] DSTU B V.2.6-86:2009. Konstruktsiï budinkiv i sporud. Zvukoizolyatsiya ogorodzhuval'nikh konstruktsij. Metodi vimiryuvannya. K.: Minregionbud Ukraïni, 2010.

[14] T.V. Lyashenko, V.A. Voznesenskij, *Metodologiya recepturno-tekhnologicheskih polej v komp'yuternom stroitel'nom materialovedenii*. Odessa: Astroprint, 2017.

ДОСЛІДЖЕННЯ АКУСТИЧНИХ ВЛАСТИВОСТЕЙ МАТЕРІАЛІВ ДЛЯ ОСНОВ ПІД ПІДЛОГИ

[1]**Керш В.Я.,** к.т.н., професор,
kersh@ogasa.org.ua, ORCID: 0000-0001-6085-5260
[1]**Замула М.О.,** аспірант,
zamulamichailodaba@gmail.com, ORCID: 0000-0001-8737-0933
[1]*Одеська державна академія будівництва та архітектури*
вул. Дідріхсона, 4, м. Одеса, 65029, Україна

Анотація. Найважливішими складовими комфортних умов перебування людей у приміщеннях житлових і громадських будівель є тепловий (температурний) і акустичний комфорт. Відповідно до нормативних документів України, до теплоізоляційних і звукоізоляційних якостей зовнішніх і внутрішніх огороджувальних конструкцій будівель висуваються високі вимоги, особливо щодо міжповерхових перекриттів. Якщо проблема недостатнього теплового захисту стосується насамперед підлог на перекриттях над холодними підвалами і проїздами, то погана звукоізоляція перекриттів – це проблема всіх квартир у багатоповерхових будинках. У цій статті аналізуються причини акустичного дискомфорту в будівлях. Людина в приміщенні піддається впливу трьох різновидів шуму – повітряного, ударного і структурного. Показано, що найбільш складно розв'язуваною проблемою є зниження ударного шуму через перекриття. Акцентовано на тому, що незважаючи на різні джерела шуму, механізми поширення структурного та ударного шуму є аналогічними – по конструктивних елементах будівлі. Тому заходи щодо зниження ударного шуму одночасно дають змогу знизити рівень структурного шуму. Проаналізовано найпоширеніші методи зниження звукопередачі через перекриття. Запропоновано замінити звичайну стяжку в конструкції підлоги на тепло-звукоізолюючу на основі гіпсоцементно-пуцоланового в'яжучого з відповідними заповнювачами. У цій роботі розглядається тільки акустичний аспект проблеми. Згідно з теорією акустичної дисипації, зроблено припущення про посилення ефекту розсіювання звукової енергії за рахунок введення заповнювачів у суміш, що збільшує кількість структурних неоднорідностей і поверхонь розділу. Як заповнювачі до суміші взято гранули пінополістиролу, коркову крихту і гранульовані відходи виробництва піноскла. З метою експериментальної перевірки цього припущення було розроблено лабораторні методики і пристрої для порівняльної оцінки звукоізолюючих властивостей розроблюваних складів. За результатами вимірювання акустичних властивостей дослідних зразків побудовано експериментально-статистичні (ЕС) моделі і визначено найкращі поєднання компонентів суміші з точки зору звукоізоляції. Шумові ЕС моделі використано при багатокритеріальної оптимізації складу композитної суміші.

Ключові слова: міжповерхові перекриття, підлоги, акустика, ударний звук, звукоізоляція, акустичні вимірювання, планований експеримент, моделювання.

Стаття надійшла до редакції 19.07.2023

УДК 691.3; 691.57 DOI: 10.31650/2786-6696-2023-5-69-78

ЛУЖНЕ АЛЮМОСИЛІКАТНЕ ПОКРИТТЯ ДЛЯ ЗАХИСТУ БЕТОНУ ВІД ТРАНСПОРТУ Cl^--ІОНІВ ПРИ ПЕРІОДИЧНИХ ЦИКЛАХ ЗВОЛОЖУВАННЯ І ВИСУШУВАННЯ

[1]**Кривенко П.В.**, д.т.н., професор,
pavlo.kryvenko@gmail.com, ORCID: 0000-0001-7697-2437
[1]**Руденко І.І.,** д.т.н., с.н.с.,
igor.i.rudenko@gmail.com, ORCID: 0000-0001-5716-8259
[1]**Константиновський О.П.,** к.т.н., доцент,
alexandrkp@gmail.com, ORCID: 0000-0002-7936-5699
[1]**Кириченко В.М.**, студент,
kirichenkovladislav051@gmail.com, ORCID: 0009-0000-4487-0233
[1]*Науково-дослідний інститут в'яжучих матеріалів ім. В.Д. Глуховського, Київський національний університет будівництва і архітектури*
пр. Повітрофлотський, 31, м. Київ, 03037, Україна

Анотація. Забезпечення довговічності конструкцій є актуальною світовою тенденцією будівельної галузі. Відомо, що найбільший ризик корозії сталевої арматури в залізобетонних конструкціях викликає періодичний вплив хлор-вміщуючого водного середовища і карбонізація під дією вуглекислоти повітря. Розвиток процесу карбонізації призводить до вивільнення зв'язаних Cl^--іонів, які були зв'язані продуктами гідратації. Підвищений транспорт Cl^--іонів обумовлює корозію сталевої арматури. Таким чином, актуальним для досліджень є засіб запобігання транспорту агресивних іонів у бетон, який функціонує в умовах впливу агресивного середовища з комбінацією класів XD3 та XC4. Покриття на основі лужних алюмосилікатних зв'язуючих запропоновані для захисту залізобетону від проникнення агресивних іонів, що обумовлено здатністю їх зв'язування цеолітоподібними фазами.

Метою роботи було визначення ефективності покриття на основі лужного алюмосилікатного в'яжучого складу $(0{,}2K_2O+0{,}8Na_2O)\cdot 4{,}5SiO_2\cdot Al_2O_3\cdot nH_2O$ як захисту залізобетону від транспорту Cl^-, CO_3^{2-}-іонів при періодичних циклах зволожування і висушування. За авторською методикою здійснено оцінку захисних властивостей запропонованого покриття в реальних умовах експлуатації при періодичних циклах зволожування і висушування в хлор-вміщуючому водному середовищі.

Повний захист бетону після 90 циклів зволожування в 5 % розчині NaCl і висушування за відсутності слідів транспорту Cl^--іонів забезпечується при нанесенні покриття товщиною 3 мм. Високі захисні властивості покриття підтверджено збереженням його адгезивних властивостей, а також високою корозійною стійкістю захищеного бетону при дії агресивного середовища з комбінацією класів XD3 та XC4. Високі захисні властивості покриття обумовлені зв'язуванням іонів Cl^- і CO_3^{2-} водостійкими цеолітоподібними матрицями.

Ключові слова: лужне алюмосилікатне зв'язуюче, захисне покриття, сталева арматура, транспорт іонів.

Вступ. Підвищення довговічності будівельних конструкцій, особливо в умовах дії агресивних середовищ, є актуальною світовою тенденцією розвитку сучасного матеріалознавства [1-3]. Особливої уваги з огляду на підвищення довговічності потребують залізобетонні конструкції, які функціонують в умовах періодичного впливу хлор-вміщуючого водного середовища (морська вода, рідкі промислові відходи, технічні води) і карбонізації під дією вуглекислоти повітря [4]. До прикладів залізобетонних конструкцій, що зазнають дії вказаного агресивного середовища відносяться споруди, що експлуатуються в морській воді (причали, пірси, берегоукріплюючі споруди, греблі), споруди для хімічної промисловості, споруди сільськогосподарських підприємств тощо. Агресивний вплив вказаного середовища на

залізобетонні конструкції класифікується комбінацією класів XD3 (періодичний вплив хлор-вміщуючого водного середовища) і XC4 (вплив вуглекислого газу при періодичному контакті з водою) згідно з [5].

Відомо, що карбонізація, яка супроводжується зниженням показника pH порової рідини бетону до значень близьких до 9 [6], а також дифузія (транспорт) Cl^--іонів в структуру, є процесами, які призводять до корозії сталевої арматури [7]. Сумісний вплив хлор-вміщуючого водного середовища і карбонізації на залізобетон спричинює складні фізико-хімічні процеси, які по різному впливають на транспортні властивості бетону в часі і, відповідно, пасивний стан арматури [8]. Так, ущільнення поверхневого шару бетону на початку карбонізації через утворення $CaCO_3$, як продукту взаємодії портландиту $Ca(OH)_2$ з CO_2 повітря, обумовлює гальмування транспорту Cl^--іонів в структуру [9]. Однак, подальший розвиток процесу карбонізації призводить до вивільнення в поровий розчин Cl^--іонів, які були вже зв'язані гелевими фазами (хемосорбція) і фазами сімейства двошарових гідроксидів (наприклад, солі Фріделя) [10, 11]. Підвищений транспорт Cl^--іонів в структуру бетону, який функціонує при впливі вказаного агресивного середовища, обумовлює запровадження ефективних заходів попередження корозії сталевої арматури, серед яких обов'язковим є поверхневий захист [12].

Аналіз останніх досліджень та публікацій. Використання поверхневого захисту бетону є економічно ефективним і відносно простим рішенням щодо захисту вже збудованих споруд від проникненню агресивних для сталевої арматури іонів. В залежності від хімічної природи, захисні покриття поділяються на органічні і неорганічні [13]. До недоліків органічних покриттів, які наносяться тонким шаром (100…400 мкм), є зменшення терміну експлуатації під впливом ультрафіолетового випромінювання [14].

Серед неорганічних покриттів розповсюдження отримали неорганічні захисні покриття на основі лужних алюмосилікатних зв'язуючих (далі, лужні алюмосилікатні покриття) для захисту бетону [15]. Такі покриття можуть розглядатись як альтернатива органічним через їх високі сульфато-, хлоридостійкістю, стійкістю в органічних і неорганічних кислотах тощо [16]. Відомо, що лужні алюмосилікатні покриття характеризуються низькою водонепроникністю [17], високими показниками морозостійкості [18], а також адгезії до різних основ, в тому числі до бетону [19].

Підвищена довговічність і високі захисні властивості лужних алюмосилікатних покриттів до дії агресивних середовищ обумовлені формуванням в складі продуктів реакції новоутворень, які є аналогами природних мінералів типу цеолітів та фельдшпатоїдів [20]. Обмеження транспорту агресивних іонів в структуру бетону внаслідок зв'язування цеолітоподібними матрицями лужного алюмосилікатного зв'язуючого, які формуються, дозволяє прогнозувати ефективність використання покриттів на його основі для забезпечення пасивного стану сталевої арматури.

Основним обмежуючим фактором щодо використання захисних лужних алюмосилікатних покриттів є необхідність тверднення при підвищених температурах (>40 °C) для формування водостійкого штучного каменю, фазовий склад якого представлений цеолітоподібними новоутвореннями [21]. Показано можливість синтезу водостійких цеолітоподібних фаз (жисмондін ($CaSi_2Al_2O_8 \cdot 4H_2O$), томпсоніт ($NaSi_5Al_5O_{20} \cdot 6H_2O$), натрієвий ($Na_6Si_{27}Al_{36}O_{72} \cdot 24H_2O$) і калієвий гейландит ($K_6Si_{27}Al_{36}O_{72} \cdot 24H_2O$)) в складі продуктів реакції лужного алюмосилікатного зв'язуючого за нормальних температур (t= 20±2 ^oC) шляхом оптимізації співвідношення оксидів системи Na_2O-K_2O-Al_2O_3-SiO_2-H_2O [22] і використання кальцій-вміщуючого модифікатора [23]. Формування вказаних новоутворень створює передумови для отримання корозійностійкого штучного каменю [24]. Покриття, розроблене на основі отриманого зв'язуючого, характеризується високими захисними властивостями до дії сульфатних середовищ. Зменшення негативного впливу вказаного середовища на бетон пояснено включенням агресивних SO_4^{2-}-іонів шляхом хемосорбції і хімічного зв'язування цеолітоподібними фазами, які синтезуються, наприклад, нозеан $Na_8(Al_6Si_6O_{24})(SO_4) \cdot H_2O$, бьякеллаіт $(Na,Ca,K)_8(Si_6Al_6O_{24})(SO_4)_2(OH)_{0.5} \cdot H_2O$), канкрініт $(Na,Ca)_8(Al_6Si_6)O_{24}(CO_3,SO_4)_2 \cdot 2H_2O$) тощо, що супроводжується підвищенням ступеня їх

кристалічності [25]. Висока щільність мікроструктури, обумовлена підвищеним вмістом кристалічних цеолітоподібних гідроалюмосилікатів і субмікрокристалічних гідросилікатів кальцію, також є фактором високого опору дифузії агресивних іонів [26].

Наведені дані дозволяють прогнозувати підвищений захист залізобетонних конструкцій від транспорту агресивних іонів в умовах впливу агресивного середовища з комбінацією класів XD3 і XC4 при використанні лужного алюмосилікатного покриття. Реалізація вказаного розвитку структуроутворення передбачає можливість включення до складу сформованих цеолітоподібних мінералів при хемосорбції і хімічному зв'язуванні також Cl^--іонів з формуванням хлор-вміщуючих фаз, подібних за структурою до Cl-шабазіту ($Al_2CaCl_2O_8Si_2$), Cl-содаліту ($Al_6Cl_2Na_8O_{24}Si_6$) тощо [27]. Відома здатність цеолітів також до адсорбції CO_3^{2-}-іонів [28]. Це може обумовити обмеження карбонізації бетону навіть в умовах поєднання класів агресивного впливу оточуючого середовища. При цьому, об'єктивна оцінка ефективності такого рішення потребує застосування методики, що враховує комплексний вплив вказаних факторів, якому піддається залізобетонна конструкція в реальних умовах експлуатації.

Мета та завдання. Метою роботи є визначення ефективності лужного алюмосилікатного покриття для захисту залізобетонних конструкцій від транспорту іонів Cl^- та CO_3^{2-} при періодичних циклах зволожування в хлор-вміщуючому водному середовищі і висушування при дії вуглекислоти повітря.

Для досягнення мети вирішувалась задача визначення глибини проникнення іонів Cl^- в структуру бетону, захищеного захисним покриттям, залежно від показників якості покриття (міцність зчеплення з основою, коефіцієнт корозійної стійкості), при періодичних циклах зволожування і висушування при природній концентрації CO_3^{2-}-іонів повітря.

Матеріали та методики дослідження. Лужне алюмосилікатне зв'язуюче загальною формулою $(0.8Na_2O+0.2K_2O)\cdot Al_2O_3\cdot 4.5SiO_2\cdot nH_2O$ використано як основу захисних покриттів.

Як основі компоненти лужного алюмосилікатного зв'язуючого використано:

– метакаолін ARGICAL-M 1200S (Франція) (вміст оксидів, %: CaO – 0.60, SiO_2 – 55.00, Al_2O_3 – 39.00, Fe_2O_3+FeO – 1.80, K_2O+N_2O – 1.00; в.п.п. – 1.00 %), пуцолановий індекс – 1247 мг $Ca(OH)_2$/г (Chapelle test), густина – 2400 кг/м^3; питома поверхня $S_{пит}$ – 2000 м^2/кг (за Блейном);

– натрієве рідке скло, модуль M_c= 2,8, густина= 1430 кг/м^3.

Для коригування складу лужного алюміносилікатного зв'язуючого за основними оксидами використано:

– трепел (Коноплянське родовище, Україна) (вміст оксидів, %: CaO – 0.86, SiO_2 – 85.12, TiO_2 – 2.10, Al_2O_3 – 6.40, Fe_2O_3+FeO – 3.25, MgO – 0.98, K_2O+N_2O – 0.69, SO_3 – 0.40; в.п.п. – 0.20 %), питома поверхня $S_{пит}$= 800 м^2/кг (за Блейном);

– розчин гідроксиду калію KOH (CAS 1310-58-3), густина – 1420 кг/м^3.

В ролі кальційвміщуючої модифікуючої добавки, яка сприяє конденсації рідкого скла за нормальної температури, використано гідроксид кальцію (CAS 1305-62-0).

В якості функціональних добавок (наповнювачі) використано:

– зола-винесення (Ладижинська ТЕЦ, Україна) (вміст оксидів, %: CaO – 2.94, SiO_2 – 52.38, TiO_2 – 0.97, Al_2O_3 – 25.25, Fe_2O_3 – 13.62, MgO – 2.04, K_2O+N_2O – 0.71, SO_3 – 0.41; в.п.п. – 1.68 %), фракція $\leq$ 0,16 мм;

– піски кварцові фракцій 0…0,315 та 0,315…0,63 мм згідно з ДСТУ Б В.2.7-32-95.

Для регулювання технологічних властивостей розчинової суміші (консистенція, відкритий час) використано комплексну добавку, яка містить тринатрійфосфат натрію $Na_3PO_4\cdot 12H_2O$ (CAS № 7601-54-9) і глюконат натрію (CAS № 527-07-1).

Водоутримувальну здатність при необхідній консистенції розчинової суміші забезпечено добавкою карбоксиметилцелюлози («Gabrosa HV» AkzoNobel, Нідерланди).

Для приготування розчинової суміші при отриманні лужного алюмосилікатного покриття окремо готували рідку та суху частину матеріалу. Рідка частина (лужний розчин) складається з рідкого натрієвого скла і розчину KOH; суха частина – усі сухі компоненти покриття. Після приготування рідкої та сухої частин, їх сумісно перемішували за допомогою

змішувача типу HOBART впродовж 3 хв на швидкості 140 $хв^{-1}$.

Розтічність, термін придатності і водоутримувальна здатність розчинової суміші визначали згідно з ДСТУ Б В.2.7-126:2011.

Міцність на згин і на стиск лужного алюмосилікатного покриття визначали згідно з ДСТУ Б В.2.7-187:2009.

Міцність зчеплення лужного алюмосилікатного покриття з бетонною основою, а також водонепроникність і морозостійкість вказаного покриття визначали згідно з ДСТУ Б В.2.6-181:2011.

Моделювання зміни властивостей лужного алюмосилікатного покриття в реальних умовах експлуатації при періодичному впливі хлор-вміщуючого водного середовища і карбонізації під дією вуглекислоти повітря, тобто при комбінації класів впливу XD3 і XC4, здійснено за запропонованою авторами методикою. Покриття наносили на бокові поверхні зразків дрібнозернистого бетону 40×40×160 мм (портландцемент:пісок) шаром 3 мм і витримували впродовж 28 діб за умов t= 20±2 °С та W= 60±5 %. Після цього, зразки, як захищені покриттям, так і незахищені (для порівняння), витримували в умовах перемінного зволожування (21 год повного занурення в 5 %-му водному розчині NaCl; вміст Cl^--іонів – 30 г/л) і висушування на повітрі (3 год витримування в сушильній шафі при температурі 105 ± 3 °С). В контрольний термін (90 циклів зволожування в 5 %-му розчині NaCl і висушування) визначали експлуатаційні властивості покриття (міцність зчеплення з бетонною основою, коефіцієнт корозійної стійкості), а також глибину проникнення (транспорт) Cl^--іонів. Вказаний контрольний термін обрано за аналогією з методикою корозійних випробувань сталевої арматури в бетоні, викладеної в ДСТУ Б В.2.6-181:2011.

Коефіцієнт корозійної стійкості зразків бетону визначали як відношення міцності на згин зразків, які зазнавали дії агресивного середовища впродовж терміну випробування, до міцності на згин аналогів, які зберігали за умов t= 20±2 °С та W= 60±5 %. Вказана методика визначення коефіцієнту корозійної стійкості, викладена в ДСТУ Б В.2.7-214:2009, враховує більшу чутливість показника міцності на згин зразків бетону до корозії порівняно з міцністю на стиск. Згідно з ДСТУ Б В.2.7-288:2011 бетони поділяють на нестійкі (Кст < 0,3), малостійкі (0,3 ≤ Кст < 0,5), стійкі (0,5 ≤ Кст < 0,8) та високостійкі (Кст ≥ 0,8) в корозійних середовищах.

Глибину проникнення Cl^--іонів визначали за результатом якісної реакції шляхом розприскування водного розчину $AgNO_3$ (концентрація 0,1 Н) на переріз зразків бетону відразу після розрізання його навпіл. Для підтвердження результатів якісної реакції, глибину проникнення вказаних іонів визначали за допомогою методу зондового аналізу на растровому електронному мікроскопі-мікроаналізаторі (REMMA 102-02, SELMI, Україна). В якості зразків для цього методу використано тонкі пластинки, отримані розрізанням бетону в перерізі.

Результати досліджень. Для досліджень обрано лужне алюмосилікатне покриття, ефективність якого в стаціонарних умовах впливу агресивного сульфатного середовища (концентрація SO_4^{2-}-іонів – 30000 мг/л) показано в роботі [25]. Склад покриття, %: натрієве рідке скло – 23,75, метакаолін – 11,62, гідроксид калію (суха речовина) – 1,11, трепел – 1,04, гідроксид кальцію – 0,81, тринатрійфосфат натрію – 0,96, глюконат натрію – 0,41, карбоксиметилцелюлоза – 0,06, пісок кварцовий фракції 0…0,315 мм – 20,07, пісок кварцовий фракції 0,315…0,63 мм – 23,27, зола-винесення – 13,56.

Визначено технологічні та експлуатаційні властивості покриття; розтічність – 20 см, термін придатності термін придатності – 90 хв, водоутримувальна здатність – 98 %, міцність на згин – 3,7, 6,5 і 8,3 МПа на 2, 7 і 28 добу тверднення, міцність на стиск – 19,8, 37,6 і 42,5 МПа на 2, 7 і 28 добу тверднення, міцність зчеплення з бетонною основою – 1,2 МПа, марка за водонепроникністю W10, марка за морозостійкістю F300.

Досліджено ефективність вказаного покриття щодо запобігання транспорту Cl^--іонів в структуру бетону в перемінних умовах впливу агресивного середовища з комбінацією класів XD3 і XC4. Згідно результатам якісної реакції після обробки поверхні розчином нітрату срібла ($AgNO_3$) (див. рівняння хімічної реакції 1) глибина проникнення Cl^--іонів в структуру бетону

без покриття після 90 циклів зволожування в 5 %-му розчині NaCl і висушування в середньому становить 8 мм (рис. 1). При нанесенні захисного покриття товщиною 3 мм транспорт іонів в структуру відсутній.

$$NaCl + AgNO_3 \rightarrow AgCl\downarrow + NaNO_3 \quad (1)$$

Ефективність покриття для захисту бетону від транспорту агресивних іонів підтверджується також результатами зондового аналізу. Так, вміст Cl^--іонів на глибині 0,1 мм зразків незахищеного бетону становив 4,19 % (рис. 2), на глибині 10 мм його вміст мінімізований – 0,08 % (рис. 3). В зразках бетону, захищених покриттям товщиною 3 мм, на глибині 0,1 мм вміст Cl^-- іонів становить 0,0 %, що свідчить про відсутність транспорту при використанні покриття (рис. 4). Сповільнення транспорту Cl^--іонів може бути обумовлено їх зв'язуванням цеолітоподібними фазами лужної алюмосилікатної матриці [25]. В свою чергу, зв'язування CO_3^{2-}-іонів за таким самим механізмом також сприяє обмеженню проникнення хлоридів.

Вивчено зміну експлуатаційних властивостей захисного покриття після 90 циклів зволожування в 5 %-му розчині NaCl і висушування. Так, міцність зчеплення покриття з бетонною основою після впливу вказаного агресивного середовища становить 1,1 МПа, що незначно менше (на 8,3 %) порівняно з аналогом, що зберігався впродовж вказаного терміну за умов t= 20±2 °C та W= 60±5 %. Отримані результати корелюють з даними щодо високих адгезивних властивостей лужних алюмосилікатних покриттів навіть в умовах впливу агресивного середовища [15, 25, 26].

Рис. 1. Фотографії перерізів половинок зразків бетону після розприскування нітрату срібла: з покриттям (ліворуч) і без покриття (праворуч)

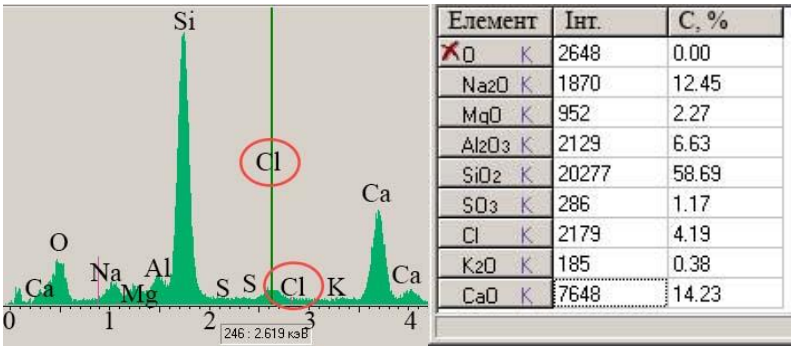

Елемент	Інт.	C, %
O K	2648	0.00
Na2O K	1870	12.45
MgO K	952	2.27
Al2O3 K	2129	6.63
SiO2 K	20277	58.69
SO3 K	286	1.17
Cl K	2179	4.19
K2O K	185	0.38
CaO K	7648	14.23

Рис. 2. Зондовий аналіз на глибині 0,1 мм зразку незахищеного бетону після 90 циклів зволожування в 5 %-му розчині NaCl і висушування

Захист бетону лужним алюмосилікатним покриття призводить до підвищення коефіцієнту корозійної стійкості після 90 циклів зволожування в 5 %-му розчині NaCl і висушування порівняно з незахищеним аналогом з 0,74 до 0,96 (на 30 %). Деградація незахищеного бетонного зразку обумовлена обмінною реакцією хлориду натрію NaCl з портландитом з утворенням хлориду кальцію $CaCl_2$, що призводить до зменшення основності високоосновних гідросилікатів кальцію як основних структуроутворюючих гідратів в

фазовому складі портландцементу [29]. Підвищення корозійної стійкості бетону, захищеного покриття, підтверджує відсутність транспорту Cl^--іонів в структуру.

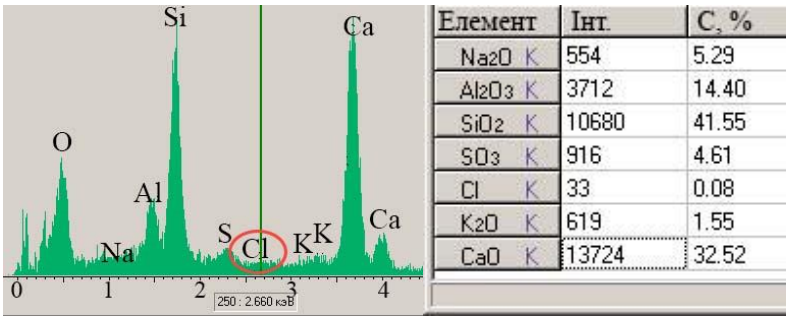

Елемент	Інт.	C, %
Na_2O K	554	5.29
Al_2O_3 K	3712	14.40
SiO_2 K	10680	41.55
SO_3 K	916	4.61
Cl K	33	0.08
K_2O K	619	1.55
CaO K	13724	32.52

Рис. 3. Зондовий аналіз на глибині 8 мм зразку незахищеного бетону після 90 циклів зволожування в 5 %-му розчині NaCl і висушування

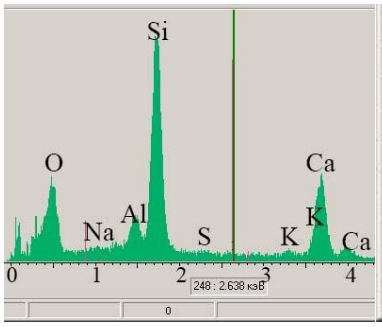

Елемент	Інт.	C, %
Na K	405	2.50
Al K	2437	3.94
Si K	13271	17.49
S K	289	0.42
Cl K	-30	0.00
K K	102	0.16
Ca K	4796	5.79

Рис. 4. Зондовий аналіз на глибині 0,1 мм зразку захищеного бетону (товщина покриття – 3.0 мм) після 90 циклів зволожування в 5 %-му розчині NaCl і висушування

Висновки:

1. Доведено ефективність покриття на основі лужного алюмосилікатного зв'язуючого формули $(0{,}2K_2O+0{,}8Na_2O)\cdot 4{,}5SiO_2\cdot Al_2O_3\cdot nH_2O$ для захисту залізобетонних конструкцій, які функціонують в умовах комплексного впливу агресивних факторів - періодичного впливу хлор-вміщуючого водного середовища і карбонізації під дією вуглекислоти повітря. Запобігання транспорту агресивних іонів (Cl^-, CO_3^{2-}) обумовлює забезпечення пасивного стану сталевої арматури в бетоні, захищеного запропонованим покриттям.

2. Підтверджено збереження адгезивних властивостей лужного алюмосилікатного покриття і підвищення корозійної стійкості захищеного бетону при дії вказаних факторів впливу. Повний захист бетону при відсутності ознак транспорту Cl^--іонів після 90 циклів зволожування в 5 %-му розчині NaCl і висушування при дії вуглекислоти повітря забезпечується при нанесенні покриття товщиною 3 мм.

Подяка. Автори висловлюють подяку за фінансову підтримку роботи, яка виконується в рамках сумісного проєкту Наукової ради Литви та Міністерства освіти і науки України «Протидія транспорту агресивних іонів SO_4^{2-} і Cl^- в армованому сталевою арматурою портландцементному бетоні для морського будівництва», код проекту S-LU-22-7.

Література

1. Hu J.Y., Zhang S.S., Chen E., Li W.G. A review on corrosion detection and protection of existing reinforced concrete (RC) structures. Construction and Building Materials. 2022. Vol. 325. 126718. doi.org/10.1016/j.conbuildmat.2022.126718.

2. Li J., Wu Z., Shi C., Yuan Q., Zhang Z. Durability of ultra-high performance concrete – A review. Construction and Building Materials. 2020. Vol. 255. 119296. doi.org/10.1016/j.conbuildmat.2020.119296.

3. Qiu Q. A state-of-the-art review on the carbonation process in cementitious materials: Fundamentals and characterization techniques. Construction and Building Materials. 2020. Vol. 247. 118503. doi.org/10.1016/j.conbuildmat.2020.118503.

4. Zhu X., Zi G., Cao Z., Cheng X. Combined effect of carbonation and chloride ingress in concrete. Construction and Building Materials. 2016. Vol. 110. pp. 369-380. dx.doi.org/10.1016/j.conbuildmat.2016.02.034.

5. ДСТУ Б В.2.7-176:2008. Будівельні матеріали. Суміші бетонні та бетон. Загальні технічні умови. [Чинний з 2010-04-01]. К.: Мінрегіонбуд України, 2010. 109 с.

6. Fuhaid A.F.A., Niaz A. Carbonation and corrosion problems in reinforced concrete structures. Buildings. 2022. Vol. 12. 586. doi.org/10.3390/buildings12050586.

7. Krishna B.M., Asrith P.S., Tezeswi T.P. Creep, chloride, carbonation and sulphate attack on concrete. IOP Conference Series: Earth and Environmental Science. 2022. Vol. 982. 012002. doi.org/10.1088/1755-1315/982/1/012002.

8. Xu L., Zhang Y., Zhang S., Fan S., Chang H. Effect of carbonation on chloride maximum phenomena of concrete subjected to cyclic wetting–drying conditions: a numerical and experimental study. 2022. Materials. Vol. 15. 2874. doi.org/10.3390/ma15082874.

9. Malheiro R., Camões A., Meira G., Amorim M.T., Castro-Gomes J. Interaction of carbonation and chloride ions ingress in concrete. RILEM Technical Letters. 2020. Vol. 5. pp. 56-62. doi.org/10.21809/rilemtechlett.2020.126.

10. Chang H.L., Feng P., Lyu K., Liu J. A novel method for assessing C-S-H chloride adsorption in cement pastes. Construction and Building Materials. 2019. Vol. 225. pp. 324-331. doi.org/10.1016/j.conbuildmat.2019.07.212.

11. Geng J., Easterbrook D., Liu Q.F., Li L.Y. Effect of carbonation on release of bound chlorides in chloride contaminated concrete. Magazine of Concrete Research. 2016. Vol. 68. pp. 353-363. doi.org/10.1680/jmacr.15.00234.

12. Goyal A., Pouya H.S., Ganjian E., Claisse P. A review of corrosion and protection of steel in concrete. Arabian Journal for Science and Engineering. 2018. Vol. 43. pp. 5035-5055. doi.org/10.1007/s13369-018-3303-2.

13. Pan X., Shi Z., Shi C., Ling T.-C., Li N. A review on concrete surface treatment Part I: Types and mechanisms. Construction and Building Materials. 2017. Vol. 132. pp. 578-590. doi.org/10.1016/j.conbuildmat.2016.12.025.

14. Wang H., Feng P., Lv Y., Geng Z., Liu Q., Liu X. A comparative study on UV degradation of organic coatings for concrete: Structure, adhesion, and protection performance. Progress in Organic Coatings. 2020. Vol. 149. 105892. doi.org/10.1016/j.porgcoat.2020.105892.

15. Krivenko P.V., Guziy S.G., Kyrychok V.I. Geocement-based coatings for repair and protection of concrete subjected to exposure to ammonium sulfate. Advanced Materials Research. 2014. Vol. 923. pp. 121–124. doi.org/10.4028/www.scientific.net/amr.923.121.

16. Sikora S., Gapys E., Michalowski B., Horbanowicz T., Hynowski M. Geopolymer coating as a protection of concrete against chemical attack and corrosion. 2018. E3S Web of Conferences. Vol. 49. 00101. doi.org/10.1051/e3sconf/20184900101.

17. Jiang C., Wang A., Bao X., Chen Z., Ni T., Wang Z. Protective geopolymer coatings containing multi-componential precursors: Preparation and basic properties characterization. *Materials*. 2020. Vol. 13. 3448. doi.org/10.3390/MA13163448.

18. Duan P., Yan C., Zhou W. A novel water permeable geopolymer with high strength and high permeability coefficient derived from fly ash, slag and metakaolin. Advanced Powder Technology. 2017. Vol. 28(5). pp. 1430-1434. doi.org/10.1016/j.apt.2017.03.009.

19. Zhang Z., Yao X., Zhu H. Potential application of geopolymers as protection coatings for marine concrete, I. Basic properties. Applied Clay Science. 2010. Vol. 49(1-2). pp. 1-6. doi.org/10.1016/j.clay.2016.10.029.

20. Krivenko P.V. Why alkaline activation – 60 years of the theory and practice of alkali-activated materials. Journal of ceramic science and technology. 2017. Vol. 8. pp. 323-334. doi.org/10.4416/JCST2017-00042.

21. Krivenko P., Kyrychok V., Advances in geopolymer-zeolite composites – synthesis and characterization: Monograph, in: P. Vizureanu, P. Krivenko (Eds.), IntechOpen, London, 2021. doi.org/10.5772/intechopen.93360.

22. Kryvenko P., Kyrychok V., Guzii S. Influence of the ratio of oxides and temperature on the structure formation of alkaline hydro-aluminosilicates. Eastern-European Journal of Enterprise Technologies. 2016. Vol. 5(5 (83). pp. 40-48. doi.org/10.15587/1729-4061.2016.79605.

23. Kyrychok V., Kryvenko P., Guzii S. Influence of the CaO-containing modifiers on the properties of alkaline alyumosilicate binders. Eastern-European Journal of Enterprise Technologies. 2019. Vol. 2(6 (98). pp. 36-42. doi.org/10.15587/1729-4061.2019.161758.

24. Pang X.R.W., Yu J., Huo Q., Chen J. Chemistry of zeolites and related porous materials: synthesis and structure, John Wiley & Sons (Asia) Pte Ltd. 2007.

25. Киричок В.І. Лужні алюмосилікатні зв'язуючі з підвищеною сульфатостійкістю та покриття на їх основі для захисту бетону. – На правах рукопису: автореф. дис. … канд. техн. наук: 05.23.05. Київ, 2018. 22 с.

26. Kryvenko P., Guzii S., Kovalchuk O., Kyrychok V. Sulfate Resistance of Alkali Activated Cements. Materials Science Forum. 2016. Vol. 865. pp. 95-106. doi.org/10.4028/www.scientific.net/msf.865.95.

27. Jun Y., Yoon S., Oh J.E. A Comparison Study for Chloride-Binding Capacity between Alkali-Activated Fly Ash and Slag in the Use of Seawater. Appl. Sci. 2017. Vol. 7. 971. doi.org/10.3390/app7100971.

28. Indira V., Abhitha K. A review on recent developments in Zeolite A synthesis for improved carbon dioxide capture: Implications for the water-energy nexus. Energy Nexus. 2022. Vol. 7. 100095. doi.org/10.1016/j.nexus.2022.100095.

29. Stark J., Wicht B. Dauerhaftigkeit von Beton: der Baustoff als Werkstoff (Birkhäuser, Berlin, Deutschland, 2001), p. 293

References

[1] J.Y. Hu, S.S. Zhang, E. Chen, W.G. Li, "A review on corrosion detection and protection of existing reinforced concrete (RC) structures", *Construction and Building Materials*, vol. 325, 126718, 2022. doi.org/10.1016/j.conbuildmat.2022.126718.

[2] J. Li, Z. Wu, C. Shi, Q. Yuan, Z. Zhang, "Durability of ultra-high performance concrete – A review", *Construction and Building Materials*, vol. 255. 119296, 2020. doi.org/10.1016/j.conbuildmat.2020.119296.

[3] Q. Qiu, "A state-of-the-art review on the carbonation process in cementitious materials: Fundamentals and characterization techniques", *Construction and Building Materials*, vol. 247, 1185032020. doi.org/10.1016/j.conbuildmat.2020.118503.

[4] X. Zhu, G. Zi, Z. Cao, X. Cheng, "Combined effect of carbonation and chloride ingress in concrete", *Construction and Building Materials*, vol. 110., pp. 369-380, 2016. http://dx.doi.org/10.1016/j.conbuildmat.2016.02.034.

[5] DSTU B.V.2.7-176:2008. Budivelni materialy. Sumishi betonni ta beton. Zahalni tekhnichni umovy. K.: Minrehionbud Ukrainy, 2010.

[6] A.F.A. Fuhaid, A. Niaz, "Carbonation and corrosion problems in reinforced concrete structures", *Buildings*, vol. 12, 586, 2022. doi.org/10.3390/buildings12050586.

[7] B.M. Krishna, P.S. Asrith, T.P. Tezeswi, "Creep, chloride, carbonation and sulphate attack on concrete", *IOP Conference Series: Earth and Environmental Science*, vol. 982, 012002, 2022. doi.org/10.1088/1755-1315/982/1/012002.

[8] L. Xu, Y. Zhang, S. Zhang, S. Fan, H. Chang, "Effect of carbonation on chloride maximum phenomena of concrete subjected to cyclic wetting–drying conditions: a numerical and experimental study", *Materials*, vol. 15, 2874, 2022. doi.org/10.3390/ma15082874.

[9] R. Malheiro, A. Camões, G. Meira, M.T. Amorim, J. Castro-Gomes, "Interaction of

carbonation and chloride ions ingress in concrete", *RILEM Technical Letters*, vol. 5., pp. 56-62, 2020. doi.org/10.21809/rilemtechlett.2020.126.

[10] H.L. Chang, P. Feng, K. Lyu, J. Liu, "A novel method for assessing C-S-H chloride adsorption in cement pastes", *Construction and Building Materials*, vol. 225., pp. 324-331, 2019. doi.org/10.1016/j.conbuildmat.2019.07.212.

[11] J. Geng, D. Easterbrook, Q.F. Liu, L.Y. Li, "Effect of carbonation on release of bound chlorides in chloride contaminated concrete", *Magazine of Concrete Research*, vol. 68. pp. 353-363, 2016. doi.org/10.1680/jmacr.15.00234.

[12] A. Goyal, H.S. Pouya, E. Ganjian, P. Claisse, "A review of corrosion and protection of steel in concrete", *Arabian Journal for Science and Engineering*, vol. 43., pp. 5035-5055, 2018. doi.org/10.1007/s13369-018-3303-2.

[13] X. Pan, Z. Shi, C. Shi, T.-C. Ling, N. Li, "A review on concrete surface treatment Part I: Types and mechanisms. Construction and Building Materials", vol. 132. pp. 578-590, 2017. doi.org/10.1016/j.conbuildmat.2016.12.025.

[14] H. Wang, P. Feng, Y. Lv, Z. Geng, Q. Liu, X. Liu, "A comparative study on UV degradation of organic coatings for concrete: Structure, adhesion, and protection performance", *Progress in Organic Coatings*, vol. 149, 105892, 2020. doi.org/10.1016/j.porgcoat.2020.105892.

[15] P.V. Krivenko, S.G. Guziy, V.I. Kyrychok, "Geocement-based coatings for repair and protection of concrete subjected to exposure to ammonium sulfate", *Advanced Materials Research*, vol. 923, pp. 121–124, 2014. doi.org/10.4028/www.scientific.net/amr.923.121.

[16] S. Sikora, E. Gapys, B. Michalowski, T. Horbanowicz, M. Hynowski, "Geopolymer coating as a protection of concrete against chemical attack and corrosion", E3S Web of Conferences, vol. 49, 00101, 2018. doi.org/10.1051/e3sconf/20184900101.

[17] C. Jiang, A. Wang, X. Bao, Z. Chen, T. Ni, Z. Wang, "Protective geopolymer coatings containing multi-componential precursors: Preparation and basic properties characterization", *Materials*, 13, 3448, 2020. doi.org/10.3390/MA13163448.

[18] P. Duan, C. Yan, W. Zhou, "A novel water permeable geopolymer with high strength and high permeability coefficient derived from fly ash, slag and metakaolin", *Advanced Powder Technology*, vol. 28(5), pp. 1430-1434, 2017. doi.org/10.1016/j.apt.2017.03.009.

[19] Z. Zhang, X. Yao, H. Zhu, "Potential application of geopolymers as protection coatings for marine concrete", *I. Basic properties. Applied Clay Science*, vol. 49(1-2), pp. 1-6, 2010. doi.org/10.1016/j.clay.2016.10.029.

[20] P.V. Krivenko, "Why alkaline activation – 60 years of the theory and practice of alkali-activated materials", *Journal of ceramic science and technology*, vol. 8, pp. 323-334, 2017. doi.org/10.4416/JCST2017-00042.

[21] P. Krivenko, V. Kyrychok, *Advances in geopolymer-zeolite composites – synthesis and characterization*: Monograph, in: P. Vizureanu, P. Krivenko (Eds.). London: IntechOpen, 2021. doi.org/10.5772/intechopen.93360.

[22] P. Kryvenko, V. Kyrychok, S. Guzii, "Influence of the ratio of oxides and temperature on the structure formation of alkaline hydro-aluminosilicates", *Eastern-European Journal of Enterprise Technologies*, vol. 5(5 (83), pp. 40-48, 2016. doi.org/10.15587/1729-4061.2016.79605.

[23] V. Kyrychok, P. Kryvenko, S. Guzii, "Influence of the CaO-containing modifiers on the properties of alkaline alyumosilicate binders", *Eastern-European Journal of Enterprise Technologies*, vol. 2(6 (98), pp. 36-42, 2019. doi.org/10.15587/1729-4061.2019.161758.

[24] X.R.W. Pang, J. Yu, Q. Huo, J. Chen, *Chemistry of zeolites and related porous materials: synthesis and structure*. John Wiley & Sons (Asia) Pte Ltd, 2007.

[25] V. Kyrychok, "Luzhni aliumosylikatni zviazuiuchi z pidvyshchenoiu sulfatostiikistiu ta pokryttia na yikh osnovi dlia zakhystu betonu", avtoref. dis. na zdobuttya nauk. stupenya k-ta tekhn. nauk: 05.23.05. Kyiv, 2018.

[26] P. Kryvenko, S. Guzii, O. Kovalchuk, V. Kyrychok, "Sulfate Resistance of Alkali

Activated Cements", *Materials Science Forum*, vol. 865, pp. 95-106, 2016. doi.org/10.4028/www.scientific.net/msf.865.95.

[27] Y. Jun, S. Yoon, J.E. Oh, "A Comparison Study for Chloride-Binding Capacity between Alkali-Activated Fly Ash and Slag in the Use of Seawater", *Appl. Sci.*, vol. 7, 971, 2017. doi.org/10.3390/app7100971.

[28] V. Indira, K. Abhitha, "A review on recent developments in Zeolite A synthesis for improved carbon dioxide capture: Implications for the water-energy nexus", *Energy Nexus*, vol. 7, 100095, 2022. doi.org/10.1016/j.nexus.2022.100095.

[29] J. Stark, B. Wicht, *Dauerhaftigkeit von Beton: der Baustoff als Werkstoff*. Berlin, 2001.

ALKALINE ALUMINOSILICATE COATING TO PROTECT CONCRETE AGAINST THE TRANSPORT OF Cl^--IONS UNDER PERIODICAL CYCLES OF WETTING/DRYING

[1]**Krivenko P.V.**, DSc., Professor,
pavlo.kryvenko@gmail.com, ORCID: 0000-0001-7697-2437
[1]**Rudenko I.I.,** DSc., Leading Researcher,
igor.i.rudenko@gmail.com, ORCID: 0000-0001-5716-8259
[1]**Konstantynovskyi O.P.,** PhD, Associate Professor
alexandrkp@gmail.com, ORCID: 0000-0002-7936-5699
[1]**Kirichenko V.M.**, student,
kirichenkovladislav051@gmail.com, ORCID: 0009-0000-4487-0233
[1]*Scientific Research Institute for Binders and Materials,*
Kyiv National University of Construction and Architecture
Povitroflotskyi prospect 31, Kyiv 03037, Ukraine

Abstract. To ensure the durability of constructions is current world tendency of building industry. It's well known that the periodical effect of chlorine-containing aqueous environment and carbonation under the action of atmospheric carbonic gas causes the most risk of the corrosion of steel reinforcement. The carbonation contributes toward releasing the bound Cl^--ions adsorbed on hydration products. The advanced transport of Cl^--ions ensures the corrosion of steel reinforcement. Thus, the mean to prevent the transport of aggressive ions in concrete from aggressive environment with combination of exposure classes XD3 and XC4 is actual for investigations. The coatings based on alkaline aluminosilicate binders were proposed for protection of reinforced concrete against the ingress of aggressive ions because of their well-known capability to ones bind in the zeolite-like phases.

The aim of this research was to determine the effectiveness of coating based on alkaline aluminosilicate binder of the composition $(0.2K_2O+0.8Na_2O)\cdot 4.5SiO_2\cdot Al_2O_3\cdot nH_2O$ as protection of reinforced concrete from transport of Cl^-, CO_3^{2-}-ions under periodical cycles of wetting/drying. The evaluation of protective properties of proposed coating in real operating conditions under cyclic drying-wetting in chlorine-containing aqueous environment was determined using the author's methodology.

Total protection of concrete after 90 cycles of drying-wetting in a 5 % solution of NaCl in the absence of traces of Cl^--ions transport can be ensured by 3 mm of the coating. High protective properties of the coating were confirmed by the retention of its adhesion as well as high corrosion resistance of coated concrete under the action of specified aggressive environment. High protective properties of the coating are caused by binding Cl^- and CO_3^{2-} ions in the water-resistant zeolite-like matrices.

Keywords: alkali-activated slag concrete, sodium nitrate, carbonization, sea water, pore structure.

Стаття надійшла до редакції 3.06.2023

UDC 691.32 DOI: 10.31650/2786-6696-2023-5-79-89

STRENGTH OF CONCRETE FOR BASES OF ROAD CLOTHES ON DIFFERENT TYPES OF SECONDARY GRAVEL AND SAND

[1]**Kroviakov S.O.,** Doctor of Engineering, Professor,
skrovyakov@ukr.net, ORCID: 0000-0002-0800-0123
[1]**Chystiakov A.O.**
artemchis@gmail.com, ORCID: 0000-0002-8424-842X
[1]*Odessa State Academy of Civil Engineering and Architecture*
4, Didrichson street, Odessa, 65029, Ukraine

Abstract. The task of developing of concrete for the bases of road clothing using secondary concrete aggregates is relevant for an economic and ecological reasons. The properties of concrete were compared with different types of coarse aggregate of 8-16 mm fraction: granite river gravel, secondary crushed stone from recycled reinforced concrete structures, secondary crushed stone from recycled brickwork and ceramic tiles. Three types of sand with a fraction of 0-4 mm were also used: quartz, secondary sand from recycled reinforced concrete structures, secondary sand from recycled brickwork. 2 series of experiments were conducted. During the first series of experiments Portland cement CEM II/B-S 32.5 R and superplasticizer Soudal Soudaplast was used (1% from weight of cement). For the second series of experiments Portland cement CEM II/B-S 42.5 R and superplasticizer Berament HT28 was used (1.2% from weight of cement). The mobility of all mixtures was equal to S1.

Concretes with Berament HT28 superplasticizer had a lower W/C ratio of mixture than concretes with similar aggregates composition and Soudal Soudaplast superplasticizer. The use of secondary crushed stone requires an increasing of the W/C ratio of the mixture. The simultaneous use of secondary sand additionally increases W/C. Due to the lower W/C, the concretes of the second series have a higher average density than the similar concretes of the first series of the experiment. Concretes based on granite gravel and quartz sand have the highest average density (2369-2465 kg/m^3). When using secondary crushed stone from reinforced concrete structures, the average density decreases by 3-5%. When using secondary crushed stone from brickwork and ceramic tiles – decreases by 8-9%. Concretes based on secondary crushed stone and sand from reinforced concrete structures have a 6-9% lower average density compared to concretes on granite gravel. Concretes based on secondary crushed stone and sand from recycled brickwork and ceramic tiles have the lowest average density – from 2015 to 2061 kg/m^3.

Due to the use of higher grade cement and a more effective superplasticizer, the strength of the concretes of the second series of the experiment at the age of 3 days was 69-190% higher than the strength of similar concretes of the first series, at the age of 28 days – higher by 67 to 147%. When using quartz sand, concrete based on secondary crushed stone from reinforced concrete structures has the greatest strength. At the age of 3 days up to 17.97 MPa and 30.33 MPa, at the design age (28 days) up to 32.07 and 53.41 MPa for the first and second series, respectively. The lowest strength (about 16 MPa in the first series of experiments and 27 MPa in the second) had concretes using only low-strength secondary aggregates from recycled brickwork and ceramic tiles.

In general, all the studied concretes on secondary aggregates were characterized by sufficient strength for their use in the bases of hard road clothes.

Keywords: secondary crushed stone, secondary sand, secondary concrete aggregates, superplasticizer, base of road clothes, strength.

Introduction. The task of processing and reusing of the remains of demolished buildings and structures is becoming more and more relevant for most countries of the world every year. For Ukraine, such task is even more urgent due to the presence of a significant amount of destruction caused by hostilities. Among the entire mass of concrete scrap arising from the dismantling of

buildings and structures, the remains of reinforced concrete structures and brick walls should be separated. They can serve as high-quality raw materials for the production of crushed stone and sand.

The recycling of demolished and destroyed structures can provide the production of significant volumes of secondary concrete aggregates, but the main disadvantage of such aggregates is their relatively low homogeneity. Taking this into account, the use of secondary aggregates for concrete for the bases of road clothes can be considered promising. Requirements for the strength and frost resistance of these concretes are relatively not strict, but the volumes of concreting in the foundations of roads are significant. The use of rigid bases of road clothing allows to achieve high durability and functional quality of roads with a cement concrete coating. It is also possible to use cement-concrete basement for roads with an asphalt concrete surface.

Thus, the task of developing concretes for the bases of road clothing using secondary concrete aggregates is relevant both from the economic and ecological points of view. At the same time, it is necessary to develop such concretes taking into account modern modifiers (superplasticizers) and cements of local production available on the market.

Analysis of recent research and publications. The volumes of waste from the dismantling of buildings and structures are constantly growing [1, 2]. Every year, it threatens the environment and human health more and more [3]. Due to the increase in the use of secondary aggregates for concrete producing, it is possible to solve the problem of processing not only "new" concrete waste, but also potentially carry out reclamation of construction waste landfills [4].

A promising industry for the use of concrete on secondary aggregates is road construction, namely the installation of concrete foundations for highways. The basis of road clothing is designed to reduce the pressure on additional layers of road clothing and the soil of the ground surface. This happens due to the redistribution of loads from the wheels of transport on a larger area [5]. When designing rigid road clothing according to ДБН В.2.3-4 "it is necessary to provide the using of the of local materials and industrial waste" [5].

According to ГБН В.2.3-37641918-557, the foundation layers are made from low-strength cement concrete. It is recommended to use concretes with a design class of B_{tb} 1.0 and B_{tb} 1.2 in terms of tensile strength when bending [6]. And according to ДБН В.2.3-4, for a monolithic bases, the minimal class is B_{tb} 0.8 (10 kgf/cm^2), frost resistance at the average monthly temperature of the coldest month from 0 to minus 5°C – F25, from minus 5 to minus 10°C – F50 [5]. Thus, the relatively non-strict requirements for the strength and frost resistance of road wear bases concretes open up the possibility of their wide use as part of secondary concrete aggregates, in particular low-strength aggregates.

Some experience has been accumulated in the use of secondary crushed stone in road construction. In [7] it was established that when replacing up to 30% of granite crushed stone with secondary concrete crushed stones, the strength of concrete remained sufficient for the construction of road surfaces. At the same time, four variants of the state of use of the secondary aggregate were compared: initial, saturated superficially dry, fully saturated, dried. It was established that the saturated surface-dry state of the aggregate gives the best results in terms of concrete strength, and the lowest strength is observed when fully saturated crushed stone is used.

In [8], concrete for the bases of road clothing with a compressive strength of up to 6 MPa was obtained using secondary concrete aggregates and blast furnace slag as a binder. Such a material has a minimal carbon footprint due to the fact that it is produced only from waste. Material similar in properties to the foundations of rural roads was obtained in the study [9]. When using secondary aggregates, lime and fly ash, a strength of up to 3 MPa was achieved. In [10], the effectiveness of the use of building demolition waste for the concrete of highway foundations, which are laid by the rolling method, is shown. Due to the use of dispersed reinforcement in [11], concrete based on secondary aggregates was obtained, which meets the requirements for the installation of rigid road surfaces.

However, as shown in [12], the use of secondary concrete aggregates in road construction is limited due to their heterogeneity, low resistance to fragmentation, and high water absorption. In

particular, it reduces the wear resistance of concrete. That is, concrete on secondary aggregates is effective precisely for the foundations and lower layers of road clothing, taking into account the conditions of their operation.

The aim of the work is to determine the influence of secondary crushed stone and sand, made from dismantled reinforced concrete structures, as well as brickwork and ceramic tiles, on the properties of the concrete bases of road wear.

Materials and methods of research. For the production of concrete, the following types of coarse aggregate of the same size, fraction 8-16 mm, were used (Fig. 1):

– granite river gravel mined in the Slovak part of the Danube River. Bulk density of gravel ρ_b=1570 kg/m^3, water absorption 0.70%;

– secondary crushed stone from recycled reinforced concrete structures. Bulk density of this crushed stone ρ_b = 1260 kg/m^3, water absorption 5.94%;

– secondary crushed stone from recycled brickwork and ceramic tiles. Bulk density of this crushed stone ρ_b = 1150 kg/m^3, water absorption 8.53%.

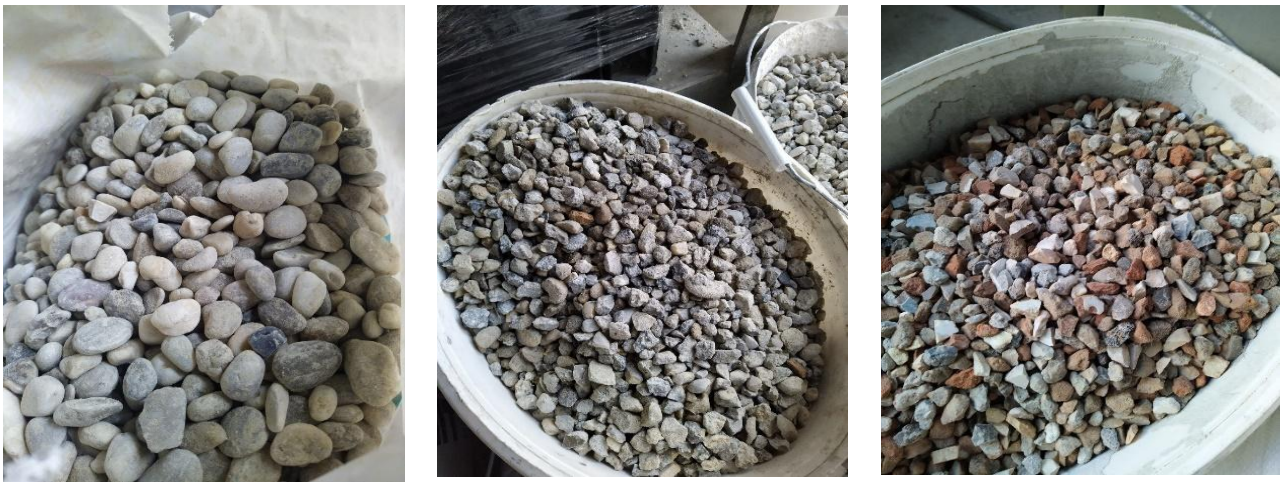

granite river gravel | secondary crushed stone from recycled reinforced concrete structures | secondary crushed stone from recycled brickwork and ceramic tiles

Fig. 1. Types of coarse aggregate used for concrete production

In addition, three types of sand fraction 0-4 mm were used (Fig. 2):

– quartz sand with a coarseness modulus of 3.19. Bulk density of sand ρ_b = 1935 kg/m^3;

– secondary sand from recycled reinforced concrete structures. The coarseness module of this sand is 3.83, bulk density ρ_b = 1500 kg/m^3;

– secondary sand from recycled brickwork and ceramic tiles. The coarseness module of this sand is 3.72, bulk density ρ_b = 1375 kg/m^3.

2 series of experiments were conducted. In the first series (formulations №1a – №5a, №1b – №5b) was used Portland cement CEM II/B-S 32.5 R manufactured by the Slovak company Cementaren Ladce (brand 400, containing up to 35% blast furnace slag) and additive superplasticizer polycarboxylate type Soudal Soudaplast, manufactured Soudal (Czech Republic). The amount of additive was 1% of the weight of cement.

In another series (formulations №1c – №5c, №1d – №5d) was used Portland cement CEM II / B-S 42.5 N produced by the Slovak company Cementaren Ladce (brand 500, containing up to 21% blast-furnace slag) and additive superplasticizer polycarboxylate type Berament HT 28, production BetonRacio (Slovakia). The amount of additive was 1.2% of the weight of the cement.

The rational quantity for both additives of superplasticizers was determined by the results of previous experiments.

quartz sand | secondary sand from recycled reinforced concrete structures | secondary sand from recycled brickwork and ceramic tiles

Fig. 2. Types of sand used for concrete production

In each series, concretes based on granite gravel and quartz sand (basic composition), secondary crushed stone from reinforced concrete structures and quartz sand, secondary crushed stone from brickwork and quartz sand, secondary crushed stone from reinforced concrete structures and secondary sand from reinforced concrete structures, secondary crushed stone from brickwork and ceramic tiles and secondary sand from brickwork have been researched.

According DBN B.2.3-4 [5], when using a concrete paver with a sliding formwork, the mobility of the concrete mixture of the base of the road clothing should be from 1 to 5 cm, depending on the speed of the concrete paver. It is also possible to use mixtures with hardness from 3 to 10 s. Accordingly, the mobility of all the studied mixtures was in the range of cone subsidence from 1 to 2 cm. To ensure the necessary mobility with different compositions of concrete, the amount of water varied. The compositions of all the studied concretes of the base of road clothing are shown in Table 1.

Table 1 – Compositions of the investigated road surface concretes

№	Cement (type, kg/m^3)	Coarse aggregate (type, kg/m^3)	Sand (type, kg/m^3)	Additive (type, kg/m^3)	Water (l/m^3)	W/C
First series of the experiment						
1a	CEM II/B-S 32.5 R, 300	granite gravel, 1245	quartz, 735	Soudal Soudaplast, 3	132	0.440
2a		secondary from reinforced concrete constructions, 1100			142	0.473
3a		secondary from brickwork, 980			180	0.600
4a		secondary from reinforced concrete constructions, 1100	secondary from reinforced concrete constructions, 665		169	0.563
5a		secondary from brickwork, 980	secondary from brickwork, 580		231	0.770
1b	CEM II/B-S 32.5 R, 350	granite gravel, 1230	quartz, 695	Soudal Soudaplast, 3.5	144	0.411
2b		secondary from reinforced concrete constructions, 1085			146	0.417
3b		secondary from brickwork, 965			192	0.549
4b		secondary from reinforced concrete constructions, 1085	secondary from reinforced concrete constructions, 625		174	0.497
5b		secondary from brickwork, 965	secondary from brickwork, 530		242	0.691

№	Cement (type, kg/m^3)	Coarse aggregate (type, kg/m^3)	Sand (type, kg/m^3)	Additive (type, kg/m^3)	Water (l/m^3)	W/C
Second series of the experiment						
1c	CEM II/B-S 42.5 R, 300	granite gravel, 1252	quartz, 762	Berament HT28, 3.6	124	0.413
2c		secondary from reinforced concrete constructions, 1122			138	0.460
3c		secondary from brickwork, 982			175	0.583
4c		secondary from reinforced concrete constructions, 1070	secondary from reinforced concrete constructions, 755		168	0.560
5c		secondary from brickwork, 803	secondary from brickwork, 765		229	0.762
1d	CEM II/B-S 42.5 R, 350	granite gravel, 1233	quartz, 727	Berament HT28, 4.2	136	0.389
2d		secondary from reinforced concrete constructions, 1112			141	0.403
3d		secondary from brickwork, 968			183	0.523
4d		secondary from reinforced concrete constructions, 992	secondary from reinforced concrete constructions, 752		166	0.474
5d		secondary from brickwork, 789	secondary from brickwork, 704		232	0.663

Research results. Due to the use of different types of aggregates, two types of cement in the amount of 300 and 350 kg/m^3 of mixture, as well as two types of superplasticizers, the water consumption of concrete mixtures differed significantly. Accordingly, the W/C of the mixtures changed, as shown in Fig. 3 diagrams.

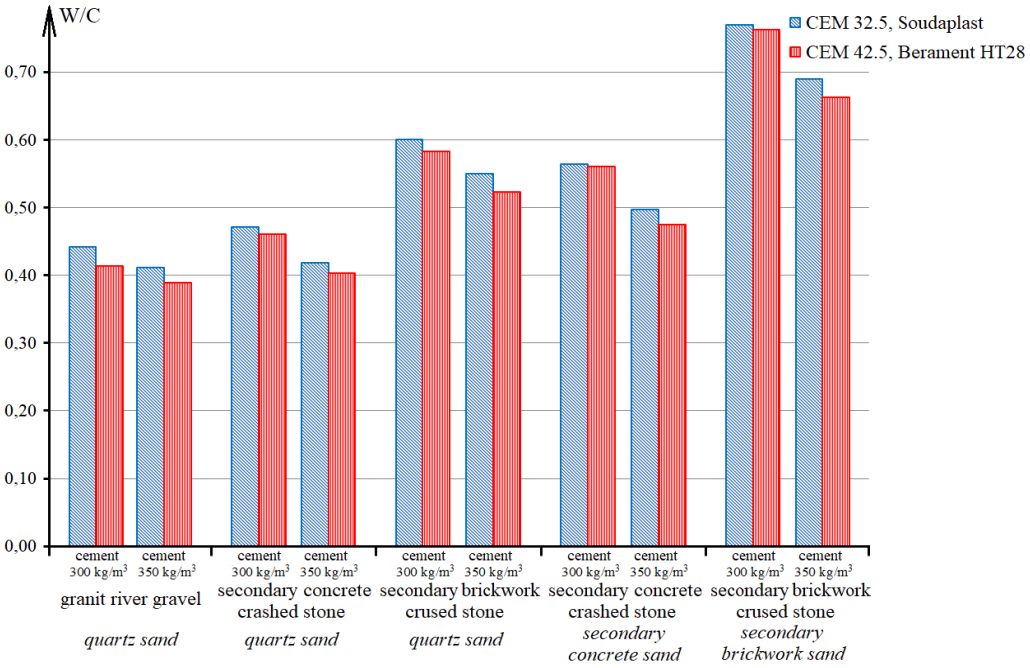

Fig. 3. Effect of concrete composition on W/C of mixtures (cone subsidence =1…2 cm)

As can be seen from the diagram and the data in Table 1, concretes with Berament HT28 superplasticizer have a lower W/C of mixture than concretes with similar aggregates when using Soudal Soudaplast superplasticizer. The different effectiveness of the additives may also be due to the different types of cement used in the first and second series of the experiment [13, 14].

Concretes based on granite gravel and quartz sand were expected to have the least W/C. When using secondary crushed stone from reinforced concrete structures, the W/C of the mixtures increased due to the absorption of part of the water by the aggregate. Accordingly, the use of secondary crushed stone from brickwork and ceramic tiles made it necessary to increase the W/C of the mixture even more. When secondary crushed stone was used simultaneously with secondary sand, the W/C of the mixtures increased further and was the maximum for concretes based on crushed stone and sand from brickwork and ceramic tiles. It should be noted that a significant part of the water in concrete on secondary aggregates, which are porous, is spent precisely on the saturation of the aggregate. This has a rather ambiguous effect on the structure of concrete: on the one hand, it increases the total porosity of the composite material, on the other hand, it improves the conditions of concrete hardening and the adhesion between the aggregate and the cement matrix [14, 15]. At the same time, the strength and porosity of the aggregate, in turn, have a significant impact on the properties of concrete.

For all studied concretes, their average density and compressive strength at the age of 3 and 28 days were determined. The results of determining these indicators are shown in Table 2.

Table 2 – Properties of the investigated concretes for the bases of road wear

№	Average density, kg/m^3	Compressive strength at the age of 3 days, MPa	Compressive strength at the age of 28 days, MPa
First series of the experiment			
1a	2369	12.21	23.88
2a	2303	14.78	25.35
3a	2171	8.28	16.88
4a	2214	10.40	20.27
5a	2015	4.39	10.95
1b	2373	14.21	29.57
2b	2298	17.97	32.07
3b	2164	11.70	24.85
4b	2224	13.85	22.40
5b	2030	6.39	16.07
Second series of the experiment			
1c	2458	28.28	47.99
2c	2341	29.45	49.16
3c	2238	21.29	41.63
4c	2288	15.61	35.47
5c	2061	13.04	27.05
1d	2465	29.81	50.18
2d	2358	30.33	53.41
3d	2238	22.23	42.66
4d	2247	23.62	39,77
5d	2034	13.85	27,65

At Fig. 4 is a diagram showing the average density of the tested concretes for pavement bases.

Analysis of the diagram and the data in Table 2 shows that the concretes of the second series (Portland cement CEM II/B-S 42.5 N, superplasticizer Berament HT28) have a higher average density than the concretes of the first series of the experiment, which are similar in terms of the type of aggregates. This is explained by the lower W/C of the mixtures due to the use of a more effective superplasticizer. Both for the first and for the second series of experiments, the amount of Portland cement does not significantly affect the average density of concrete.

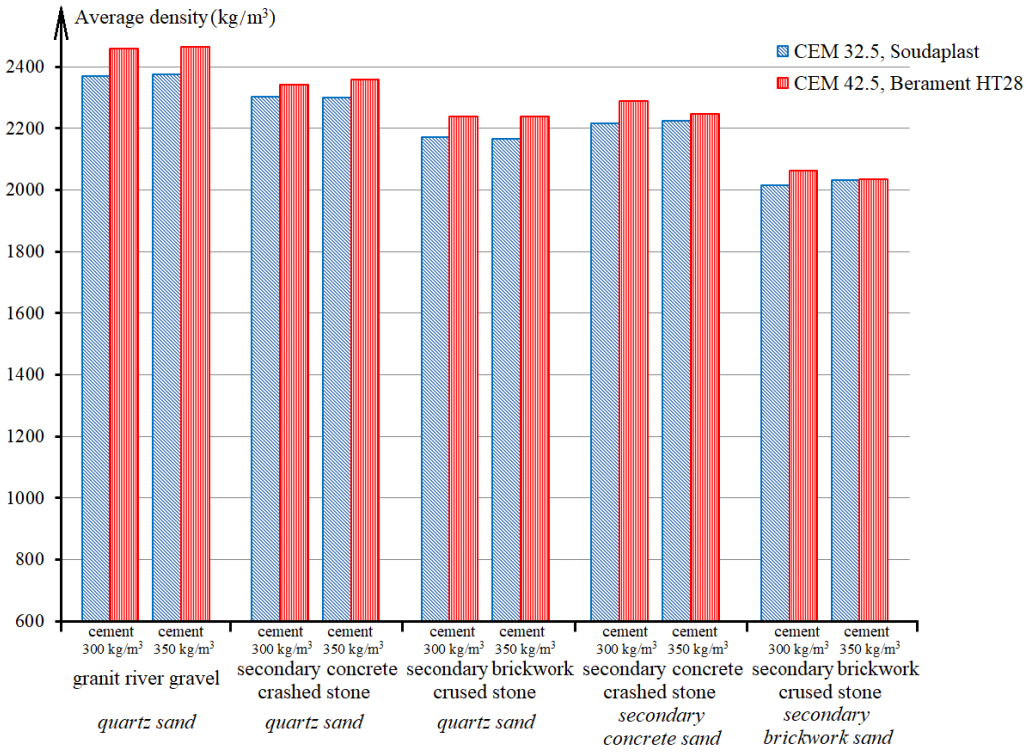

Fig. 4. Average density of the studied concretes

The general effect of the type of aggregate on the average density of concrete is similar for both series of the experiment. Concretes based on granite gravel and quartz sand have the highest density. When using secondary crushed stone from reinforced concrete structures, the average density decreases by 3-5%. When using secondary rubble from brickwork and ceramic tiles – by 8-9%. Concretes based on secondary crushed stone and sand from reinforced concrete structures have a 6-9% lower average density compared to "basic" compounds on granite gravel. The smallest average density (from 2015 to 2061 kg/m^3) has concretes based on secondary crushed stone and sand from recycled brickwork and ceramic tiles. This is 14-17% less than the average density of "basic" concretes on granite gravel. Such influence of aggregates is expected and is explained by their own average density and porosity [16]. To confirm this, in the second series of experiments, the water absorption of the tested concretes was determined, which is actually their open porosity and is shown in Table 3.

Table 3 – Water absorption of the tested concretes of the second series of the experiment (% by volume)

№	1c	2c	3c	4c	5c	1d	2d	3d	4d	5d
Water absorption	6.2	7.6	9.7	7.8	13.9	5.6	7.6	8.7	7.7	12.4

However, the type of Portland cement, superplasticizer and aggregates has a significantly greater influence on the strength of the studied concretes than on the average density. The compressive strength of the studied concretes for the foundations of road clothing at the age of 3 and 28 days is shown in the diagrams in Fig. 5.

Analysis of the diagrams and data in Table 2 shows that the strength of the concretes of the second series of the experiment was much higher in comparison with the strength of the aggregates similar in type to the concretes of the first series. At the age of 3 days, the difference was from 69 to 190%, at the age of 28 days – from 67 to 147%. This is explained by the use of cement with a higher grade and, at the same time, a more effective superplasticizer, which provided a lower W/C of the mixtures.

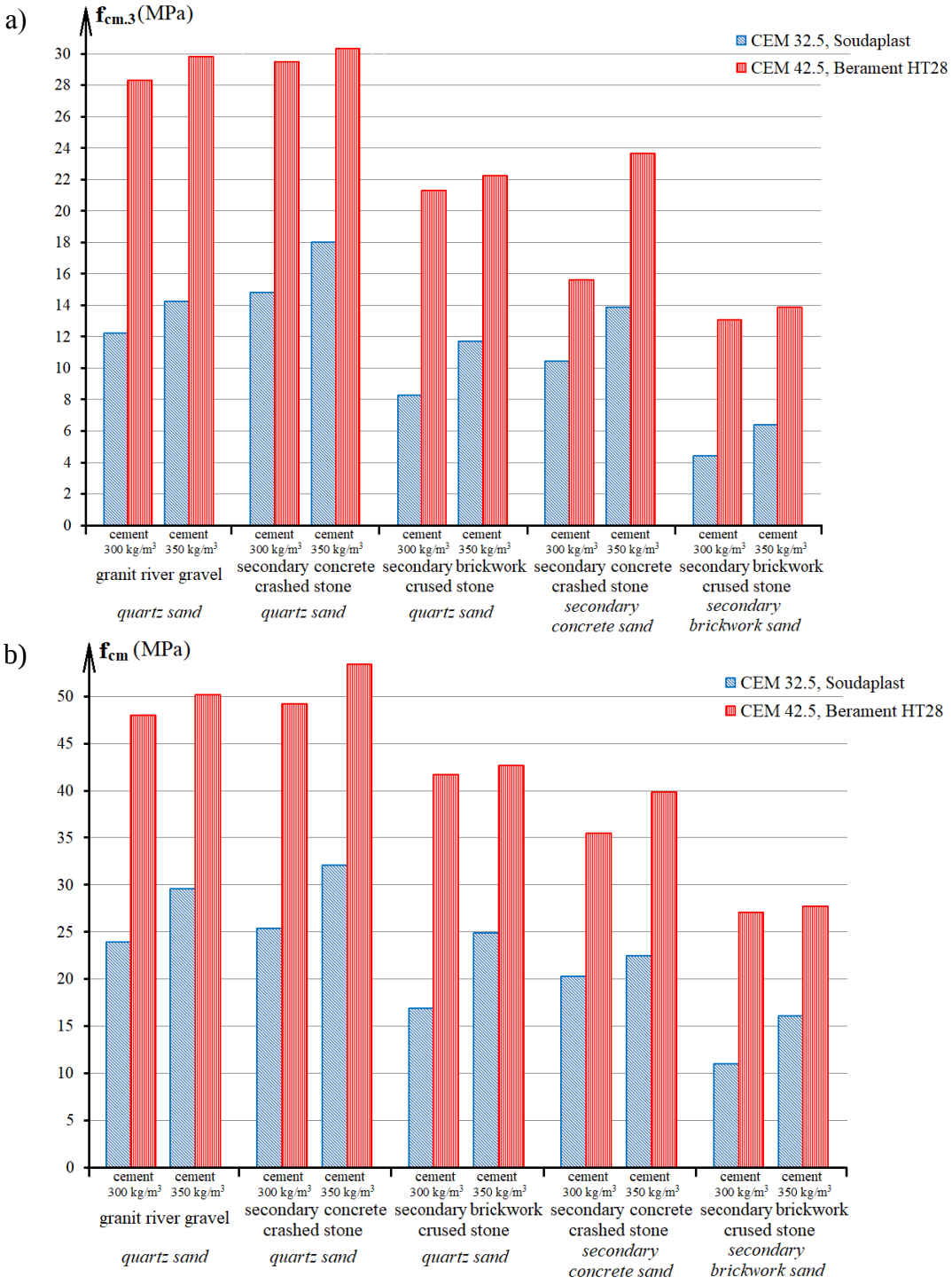

Fig. 5. Strength of the studied concretes at the age of 3 days (a) and 28 days (b)

At the same time, the general trends of the influence of the type of aggregate on strength were similar for the concretes of the first and second series of the experiment. When using quartz sand, concretes based on secondary crushed stone from reinforced concrete structures have the highest strength at the age of 3 and 28 days – up to 30.3 MPa and 53.4 MPa, respectively. At the design age, the strength of concrete on such secondary crushed stone is 2-8% higher than the strength of concrete on granite gravel. At the age of 3 days for the first series of experiments, the difference in strength was even greater. This effect is explained primarily by the use in concrete of "basic" compositions of granite gravel, which has a rolled shape. It is known that gravel has less adhesion to the cement-sand matrix, which affects the strength of the composite [14]. Secondary crushed stone has a non-rolled shape and, as noted above, relatively high porosity, which ensures sufficient

adhesion with the matrix and improves concrete hardening conditions [15]. However, for many European countries, river gravel is the main type of coarse aggregate for concrete.

When using secondary crushed stone from brickwork and ceramic tiles (quartz sand as a fine aggregate), the strength of concrete becomes lower compared to concrete on granite gravel by 18-32% at the age of 3 days and by 13-29% at the age of 28 days. This is explained by the fact that this coarse aggregate has the lowest strength among those used in research.

When using secondary crushed stone from reinforced concrete structures simultaneously with secondary sand, the strength of concrete decreases by 15-26% compared to concrete of "basic" compositions. This can be explained by a decrease in the strength of the cement-sand matrix due to the use of porous sand and a corresponding increase in the W/C of the mixture.

When using secondary crushed stone and sand from brickwork and ceramic tiles, the strength of concrete is 44-56% less than the strength of similar concretes of "basic" compositions on granite gravel, that is, approximately twice. However, even such concretes with the use of only low-strength secondary aggregates due to the use of an effective superplasticizer (the second series of the experiment) have a strength at the design age of about 27 MPa, which satisfies the requirements for the material of the road wear base. It should be noted that the tensile strength of such concretes during bending was determined in additional studies. Its value was from 2.8 to 2.9 MPa, which also confirms the possibility of using such concrete in road construction.

In general, all the studied concretes on secondary aggregates were characterized by sufficient strength for their use in the basements of hard road wear. At the same time, the concretes of the second series of experiments based on secondary crushed stone and sand from reinforced concrete structures, as well as on the basis of any crushed stone and quartz sand, have strength that allows such materials to be considered as an alternative to "traditional" concrete when arranging the bottom layer of a two-layer hard coating. However, for use not only in basements, but also directly in road surfaces, concrete must meet sufficiently high frost resistance requirements (F100, F150) [5]. When using secondary aggregates, it is quite difficult to achieve this level of frost resistance and it requires additional research.

Conclusions and prospects for further research. The conducted studies confirmed the prospects of using concrete on secondary aggregates for the arrangement of the bases of hard road clothing. When using an effective superplasticizer, even concretes based on low-strength aggregates from recycled brickwork and ceramic tiles have sufficient strength for such structures.

Further research is planned to determine the flexural strength and frost resistance of concrete on secondary aggregates. It is also planned separately to determine the degree of homogeneity of the properties of such concretes, which is important given the potentially high heterogeneity of the composition and properties of secondary aggregates.

References

[1] M. Yazdani, K. Kabirifar, B.E. Frimpong, M. Shariati, M. Mirmozaffari, A. Boskabadi, "Improving construction and demolition waste collection service in an urban area using a simheuristic approach: A case study in Sydney, Australia", *Journal of Cleaner Production*, 280(1), 124138, 2021. https://doi.org/10.1016/j.jclepro.2020.124138.

[2] A. Saad, M. Bal, J. Khatib, "The need for a proper waste management plan for the construction industry: a case study in Lebanon", *Sustainability*, 14, 12783, 2022. https://doi.org/10.3390/su141912783.

[3] H. Zheng, X. Li, X. Zhu, Y. Huang, Z. Liu, Y. Liu, J. Liu, X. Li, Y. Li, C. Li, "Impact of recycler information sharing on supply chain performance of construction and demolition waste resource utilization", *International Journal of Environmental Research and Public Health*, 19(7), 3878, 2022, https://doi.org/10.3390/ijerph19073878.

[4] V.W.Y. Tam, M. Soomro, A.C.J. Evangelista, "A review of recycled aggregate in concrete applications (2000–2017) ", *Construction and Building Materials*, 172, pp. 272-292, 2018. https://doi.org/10.1016/j.conbuildmat.2018.03.240.

[5] DBN B.2.3-4:2015. Avtomobil′ni dorohy. Sporudy transportu. Chastyna I. Proektuvannya. Chastyna II. Budivnytstvo. Minrehionbud Ukrayiny, 2015.
[6] HBN V.2.3-37641918-557:2016. Avtomobil′ni dorohy. Dorozhniy odyah zhorstkyy. Proektuvannya. Ministerstvo infrastruktury Ukrayiny, 2016.
[7] A. Jindal, R.N. G.D. Ransinchung, P. Kumar, "Study of pavement quality concrete mix incorporating beneficiated recycled concrete aggregates", *Road Materials and Pavement Design*, 18 (5), pp. 1159-1189, 2017. https://doi.org/10.1080/14680629.2016.1207556.
[8] F. Juveria, P. Rajeev, P. Jegatheesan, J. Sanjayan, "Impact of stabilisation on mechanical properties of recycled concrete aggregate mixed with waste tyre rubber as a pavement material", *Case Studies in Construction Materials*, 18, e02001, 2023. https://doi.org/10.1016/j.cscm.2023.e02001.
[9] G.S. Kumar, S. Shankar, "Strength and durability characteristics of lime fly ash-stabilized recycled concrete aggregate for use in low-volume rural roads", *Indian Geotechnical Journal*, 53, pp. 78–92, 2023. https://doi.org/10.1007/s40098-022-00659-3.
[10] L. Courard, F. Michel, P. Delhez, "Use of concrete road recycled aggregates for Roller Compacted Concrete", *Construction and Building Materials*, 24(3), pp. 390-395, 2010. https://doi.org/10.1016/j.conbuildmat.2009.08.040.
[11] R. Chan, M.A. Santana, A.M. Oda, R.C. Paniguel, L.D. Vieira, A.D. Figueiredo, I. Galobardes, "Analysis of potential use of fibre reinforced recycled aggregate concrete for sustainable pavements", *Journal of Cleaner Production*, 218, pp. 183-191, 2019. https://doi.org/10.1016/j.jclepro.2019.01.221.
[12] O. Dokić, A. Radević, D. Zakić, D. Dokić, "Potential of natural and recycled concrete aggregate mixtures for use in pavement structures", *Minerals*, 10, 744, 2020. https://doi.org/10.3390/min10090744.
[13] M. Sanytsky, U. Marushchak, Y. Olevych, Y. Novytskyi, "Nano-modified ultra-rapid hardening portland cement compositions for high strength concretes", *Lecture Notes in Civil Engineering*, 47, pp. 392–399, 2020. https://doi.org/10.1007/978-3-030-27011-7_50.
[14] L.Y. Dvorkin, *Mitsnist' betonu*. K.: Kondor, 2021.
[15] V. Volchuk, S. Kroviakov, V. Kryzhanovskyi, "Strength assesment of lightweight concrete considering metric variance of the structural elements", *Romanian Journal of Materials*, 52(2), pp. 185-193, 2022.
[16] S.O. Kroviakov, A.O. Chystiakov, A.O. Bershadskyi, T.I. Shevchenko, "Concretes on secondary crushed stone as a promising material for the rigid pavement base", *Bulletin of Odessa State Academy of Civil Engineering and Architecture*, 87, pp. 85-91, 2022. https://doi.org/10.31650/2415-377X-2022-87-85-91.

МІЦНІСТЬ БЕТОНІВ ОСНОВИ ДОРОЖНЬОГО ОДЯГУ НА РІЗНИХ ВИДАХ ВТОРИННОГО ЩЕБЕНЮ І ПІСКУ

[1]**Кровяков С.О.,** д.т.н., професор,
skrovyakov@ukr.net, ORCID: 0000-0002-0800-0123
[1]**Чистяков А.О.**
artemchis@gmail.com, ORCID: 0000-0002-8424-842X
[1]*Одеська державна академія будівництва та архітектури*
вул. Дідріхсона, 4, м. Одеса, 65029, Україна

Анотація. Задача розробки бетонів для основи дорожнього одягу з використанням вторинних заповнювачів є актуальною з економічної та екологічної точок зору. Порівняно властивості бетонів з різними типами крупного заповнювача фракції 8-16 мм: гранітного річкового гравію, вторинного щебеню з перероблених залізобетонних конструкцій, вторинного щебеню з переробленої цегляної кладки та керамічної плитки. Також

використовувалося три типу пісків фракції 0-4 мм: кварцовий, вторинний пісок з перероблених залізобетонних конструкцій, вторинний пісок з переробленої цегляної кладки. Проведено 2 серії експериментів. У першій серії використовувався портландцемент CEM II/B-S 32.5 R та суперпластифікатор Soudal Soudaplast (1% від маси цементу). У другій серії використовувався портландцемент CEM II/B-S 42.5 R та суперпластифікатор Berament HT28 (1,2% від маси цементу). Рухомість всіх суміші була рівною S1.

Бетони з суперпластифікатором Berament HT28 мали меншу В/Ц суміші, ніж бетони з аналогічними заповнювачами та суперпластифікатором Soudal Soudaplast. Використанні вторинного щебеню вимагає підвищення В/Ц суміші. Одночасне використання вторинного піску додатково підвищує В/Ц. Завдяки меншому В/Ц бетони другої серії мають вищу середню густину, ніж аналогічні бетони першої серії експерименту. Найбільшу середню густину (2369-2465 кг/м^3) мають бетони на основі гранітного гравію і кварцового піску. При використанні щебеню з залізобетонних конструкцій середня густина знижується на 3-5%. При використанні щебеню з цегляної кладки та керамічної плитки – на 8-9%. Бетони на основі вторинного щебеню і піску з залізобетонних конструкцій мають на 6-9% меншу середню густину у порівнянні з бетонами на гранітному гравії. Найменшу середню густину мають бетони на основі вторинного щебеню і піску з переробленої цегляної кладки та керамічної плитки – від 2015 до 2061 кг/м^3.

Завдяки застосуванню цементу вищої марки і більш ефективного суперпластифікатору міцність бетонів другої серії експерименту у віці 3х діб була на 69-190% вище міцності аналогічних бетонів першої серії, у віці 28 діб – вище на 67 до 147%. При використанні кварцового піску найбільшу міцність мають бетоні на основі вторинного щебеню з залізобетонних конструкцій. У віці 3х діб до 17,97 МПа та 30,33 МПа, у проєктному віці до 32,07 і 53,41 МПа для першої і другої серії відповідно. Найменшу міцність (близько 16 МПа у першій серії експерименту і 27 МПа у другій) мали бетони з використанням лише маломіцних вторинних заповнювачів з переробленої цегляної кладки та керамічної плитки.

В цілому всі досліджені бетони на вторинних заповнювачах характеризувалися достатньою міцністю для їх використання в основах жорсткого дорожнього одягу.

Ключові слова: вторинний щебінь, вторинний пісок, вторинні заповнювачі бетону, пластифікатор, основа дорожнього одягу, міцність.

Стаття надійшла до редакції 26.07.2023

UDC 625.855.3 DOI: 10.31650/2786-6696-2023-5-90-99

IMPACT OF DEICING SALT ON THE PERFORMANCE OF ASPHALT MIXTURES IN NORTHWEST CHINA: AN INVESTIGATION INTO MECHANICAL PROPERTIES AND INFLUENTIAL FACTORS

[1]**Mingjun Guo**, Ph.D. Candidate,
guo19920408@hotmail.com, ORCID: 0000-0001-5924-0779
[1]**Kovalskiy V. P.,** Ph.D, Associate Professor,
kovalskiy.vk.vntu.edu@gmail.com, ORCID: 0000-0002-3103-6319
[1]*Vinnytsia National Technical University*
Voiniv-Internatsionalistiv St, 7, Vinnytsia, 21000, Ukraine

Abstract. Currently, the primary form of high-grade highways is constituted by asphalt concrete pavement. Winter conditions often result in ice and snow accumulation on these pavements, precipitating severe traffic incidents. Statistically, around 15%-30% of such incidents are directly linked to icy and snowy conditions. Hence, when roads are laden with ice and snow, the most cost-effective and efficient countermeasure remains the dispersal of deicing salt onto the road surface. Particularly in China's northwestern region, which experiences low precipitation and consistent droughts, the deicing salts applied during winter aren't diluted or transported away by water flow. Consequently, the soil surrounding the roads retains a higher concentration of deicing salts than other regions, leading to a pronounced impact on the pavement's service life.

This investigation aims to experimentally emulate the impact of this high-salt environment on the mechanical properties of asphalt mixtures, followed by an analysis of the crucial factors that influence the asphalt mixtures' durability.

The current study employs measures such as high-temperature rut testing, Marshall water immersion testing, and freeze-thaw splitting testing to investigate the damage patterns of mechanical properties in asphalt mixtures under varying grading, diverse deicing salt solutions, and differing frequencies of dry-wet cycles. In addition, the study employs grey correlation entropy analysis to ascertain the interdependence among factors influencing the performance of asphalt mixtures.

The findings reveal that after undergoing 0, 5, 10, 15, 20, 25, and 30 dry-wet cycles in solutions of 20% industrial salt (NaCl), 15% urea (CH_4N_2O), and 20% anhydrous ethanol (CH_2CH_3OH), both the high-temperature stability and water stability of asphalt mixtures with AC-13 and AC-16 gradings displayed varying levels of decline. Overall, an enhancement in the fine aggregate percentage in asphalt mixtures can augment the asphalt concrete's resistance to deicing salt erosion. As per the grey correlation entropy analysis, gradation variances exerted the most significant impact on diverse mechanical properties, followed by the type of deicing salt solution, with the least significant impact attributed to the frequency of dry-wet cycles. Thus, judicious selection of road materials and structural design can effectively counter the erosive action of deicing salts, thereby enhancing the service life of the road surface.

Key words: road engineering, asphalt mixture, dry-wet cycle, pavement performance, deicing salt.

Introduction. At present, asphalt concrete pavement predominates high-grade highways, necessitating regular maintenance to mitigate or preclude pavement anomalies [1]. During winter,

the manifestation of snow and ice on road surfaces potentially escalates the risk of severe traffic incidents. Statistical data reveal that approximately 15%-30% of traffic accidents are snow and ice-related [2]. Consequently, the most economically efficient strategy for countering snow and ice accumulation continues to be the application of deicing salt [3]. Nonetheless, the prolonged use of deicing salt has been observed to induce substantial alterations in the surrounding ecological environment of the highways [4]. Additionally, this practice has markedly affected the longevity and disease susceptibility of the road infrastructure [5].

Analysis of recent research and publications. To ascertain the effects of deicing salt on asphalt mixtures, pertinent studies have been conducted by various researchers. Juli-Gándara [6] assessed the salt-induced impact on three disparate asphalt mixtures, discovering a higher susceptibility of porous asphalt mixtures to salt degradation. Hassan [7] proposed that freeze-thaw damage inflicted on asphalt mixtures by pure water is less severe compared to when deicing salt is incorporated. Shi's [8] study identified certain deicing salts as prominent culprits of severe asphalt pavement damage, advocating that deicing salt, water, and heat represent essential prerequisites for damage induction. Meanwhile, Wei [9] and Zhou [10] have argued that deicing salt erosion expedites the aging process of asphalt mixtures. Zhou’s [11] work has illustrated that the higher surface tension of deicing salt solutions compared to asphalt allows for easier penetration into the crevices between binder and aggregate, thereby diminishing their interfacial bonding strength. Further, Pan [12] has theorized that deicing salt permeation into the interface between asphalt and aggregate can result in asphalt emulsification, consequently impairing the mixture. Although these studies scrutinize the impact of deicing salt on asphalt mixtures from various viewpoints, they collectively acknowledge that deicing salt can inflict damage of varying magnitudes on asphalt mixtures.

In China's northwest region, the prevailing aridity, marked by scant rainfall and incessant drought, dictates the environmental conditions [13]. During winter, the lack of ample water flow restricts the dilution and displacement of the deicing salt dispersed on the roadways [14]. Consequently, this arid environment induces a higher concentration of deicing salt within the road-adjacent soil compared to other regions. Notably, several scholars have scrutinized the effects of deicer on asphalt mixtures under dry-wet cycles. For instance, Zhang et al. [15] explored the impacts of these cycles on asphalt mortar's micro-mechanical properties in coastal regions, noting an increase in the sulfoxide index and large molecule content coupled with a decrease in surface roughness index as cycle times escalated. Guo's [16] application of the pull-off tensile test to asphalt and aggregates exposed to salt immersion cycles revealed a more significant pull-off tensile strength loss following salt immersion than after immersion in pure water. Luo et al.'s [17] findings indicated a rapid decrease in the splitting strength of asphalt pavement after twelve dry-wet cycles in a deicing salt solution. Yu et al.'s [18] evaluation of the rheological properties of asphalt pavement post immersion in a deicing salt solution revealed diminished low-temperature performance and anti-fatigue properties. However, these pertinent studies have not factored in the unique environmental characteristics of China's northwest region, limiting their applicability as references for road design and maintenance in this particular area.

Goal and objectives. Given the distinctive hydrological and climatic conditions of northwest China, the research team established nine monitoring stations across high-grade highways in Gansu Province, China. These stations facilitated the collection of long-term data on precipitation and atmospheric humidity, as well as temperature readings of asphalt pavement [19]. Concurrently, various commonly utilized deicing salts underwent freezing point analysis at diverse concentrations, yielding ice point data [20]. Building upon these data, the study employs three appropriate

concentrations of deicing salt solutions to execute dry-wet cycle tests on two types of graded asphalt mixtures, taking into account the climatic and hydrological features of northwest China. The high-temperature rut test is employed to explore the high-temperature stability of asphalt concrete, while the Marshall water immersion test and the freeze-thaw splitting test are utilized to investigate the water stability of the same. Various factors influencing the road performance of asphalt mixtures are assessed via grey correlation entropy analysis, aiming to provide guidance for the selection of optimal road surfaces and application of deicing salts during maintenance in road design.

Research methods. In consideration of the snow-melting capabilities of the deicing salts, and taking into account the distinctive climatic and hydrological conditions of Northwest China, solutions for dry-wet cycles were devised with 15% urea (15% CH_4N_2O), 20% industrial salt (20% NaCl), and 20% absolute ethanol (20% CH_2CH_3OH). Preparations for the dry-wet cycle test involved creating Marshall and rut samples of AC-13 and AC-16 gradations. The full dry-wet cycle process involved:

1) The 24h±0.5h immersion of both gradation samples in the deicing salt solutions, as demonstrated in Figure 1.

2) Post-soaking, the samples underwent a 24h±0.5h air-drying process, as presented in Figure 2.

3) Upon completion of the drying phase, the samples were re-introduced to the deicing salt solutions to initiate the ensuing cycle.

Fig. 1. The samples immersed in deicing salt solutions

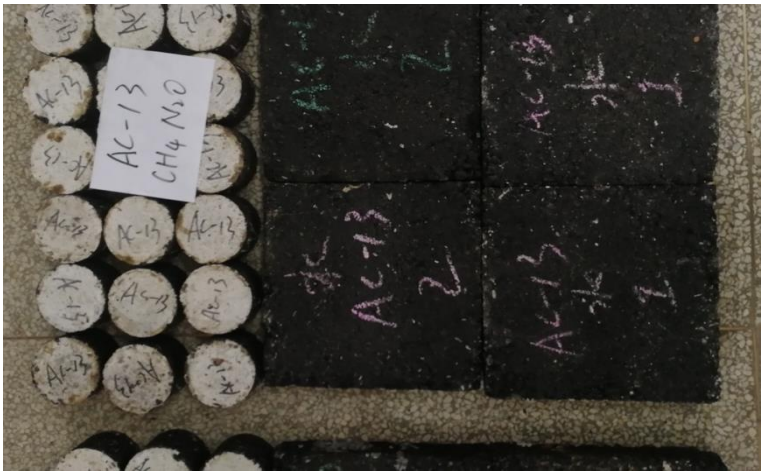

Fig. 2. The samples placed in the air

This methodology denotes a single dry-wet cycle. The experimental procedure encompassed 30 such cycles, with significant indicators assessed at the termination of the 0, 5, 10, 15, 20, 25, and 30 cycles. Given the volatile nature of absolute ethanol, it necessitated the preparation of a fresh anhydrous ethanol solution for each cycle, while the urea and industrial salt solutions were refreshed every three cycles. Upon finalization of the dry-wet cycle, rut samples were subjected to high-temperature rut tests, and Marshall samples evaluated through Marshall water immersion tests and freeze-thaw splitting tests.

Results Analysis Research and Discussion. The alterations in the dynamic stability (DS) and loss rate of the two asphalt mixtures following exposure to dry-wet cycles in three distinct deicing salt solutions are shown in Figure 3.

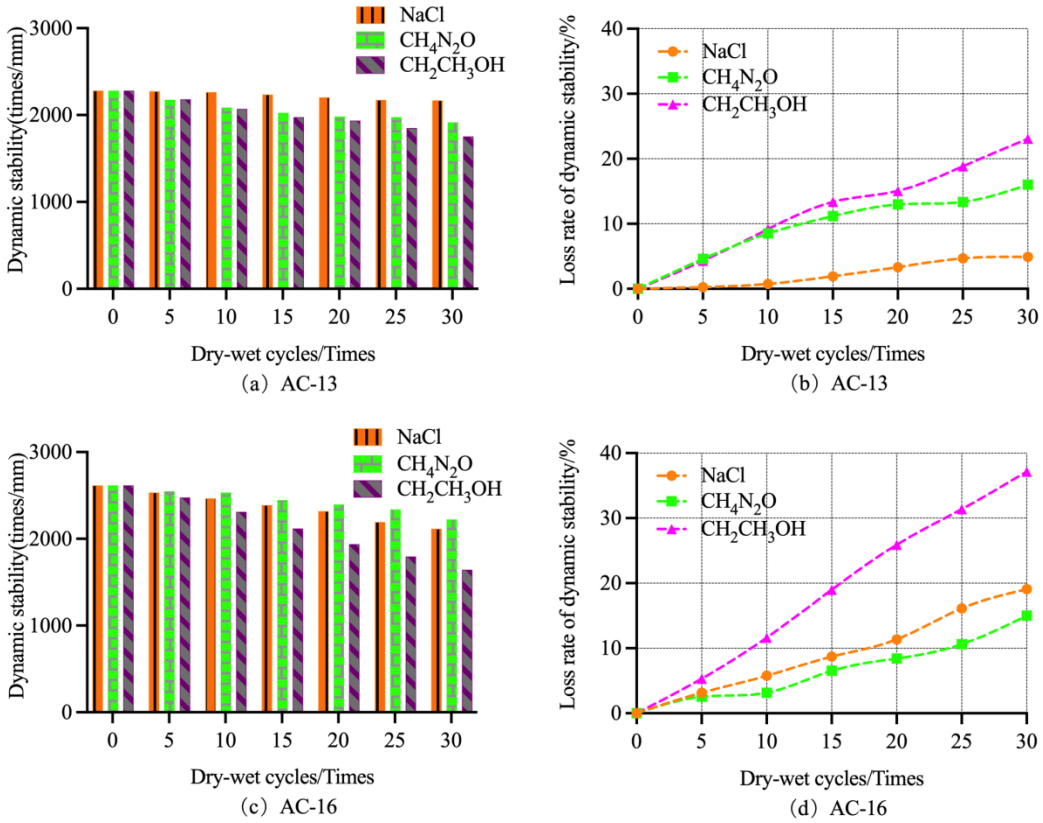

Fig. 3. The alterations in dynamic stability and loss rate after dry-wet cycles

Figures 3(a) and 3(b) demonstrate that, for the AC-13 asphalt mixture, there is an overall downward trend in DS associated with the three different deicing salts as the dry-wet cycles increase. NaCl has the least impact on DS, followed by CH_4N_2O, with CH_2CH_3OH having the most substantial impact. Over the entirety of the dry-wet cycles, DS damage related to NaCl is minimal, at a rate of 4.9%, whereas DS corresponding to CH_4N_2O and CH_2CH_3OH exhibit rates of 16.0% and 23.1%, respectively. Furthermore, within 30 cycles, the lowest dynamic stability values for NaCl, CH_4N_2O, and CH_2CH_3OH are 2168, 1915, and 1754 times/mm, respectively, all surpassing the standard's requirement of 1000 cycles/mm.

From Figures 3(c) and 3(d), it can be deduced that when the gradation of the asphalt mixture is AC-16, the DS corresponding to the three different deicing salts also generally decreases with an increase in dry-wet cycles. Here too, NaCl has the least influence on DS, followed by CH_4N_2O, while CH_2CH_3OH again has the greatest impact. Throughout all the dry-wet cycles, CH_2CH_3OH corresponds to the most pronounced DS damage, at a rate of 37.2%, compared to 19.1% and 15.0%

for NaCl and CH_4N_2O, respectively. Additionally, within 30 cycles, the lowest dynamic stability values for NaCl, CH_4N_2O, and CH_2CH_3OH are 2117, 2223, and 1644 times/mm, respectively, all surpassing the standard's requirement of 1000 cycles/mm.

Upon comparing Figures 3(b) and 3(d), it is evident that the DS decline rate for AC-16 significantly surpasses that for AC-13, suggesting a greater impact of the three salt solutions on AC-16 in terms of DS.

The alterations in the residual stability (MS_0) and loss rate of the two asphalt mixtures following exposure to dry-wet cycles in three distinct deicing salt solutions are shown in Figure 4.

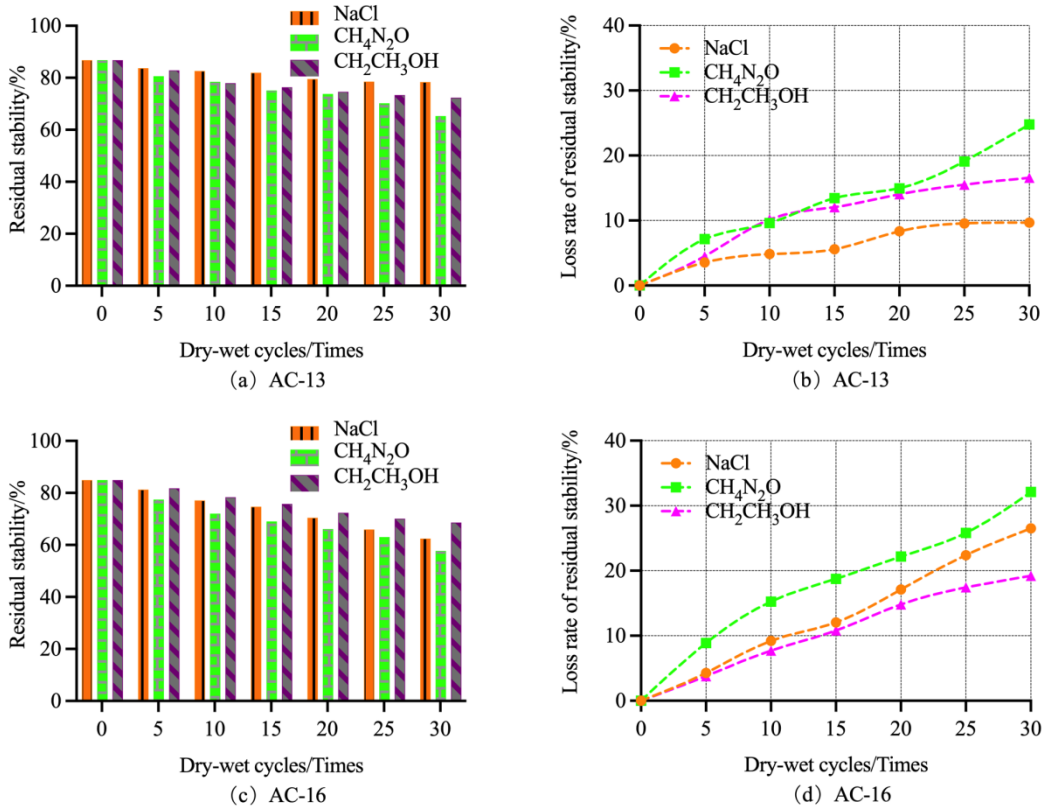

Fig. 4. The alterations in residual stability and loss rate after dry-wet cycles

Upon evaluation of Figure 4(a), it becomes apparent that the MS_0 associated with the three deicing salts undergoes a decline in line with the progressive increase in the number of dry-wet cycles for the AC-13 asphalt mixtures. Further analysis of Figure 4(b) reveals that within a total of 30 dry-wet cycles, NaCl imparts the least effect on MS_0, exhibiting a loss rate less than 10%. The impacts of CH_4N_2O and CH_2CH_3OH on MS_0 show a degree of similarity through the initial 20 cycles, but the 25th and 30th cycles trigger a sudden decline in MS_0 corresponding to CH_4N_2O. The residual stability for CH_4N_2O and CH_2CH_3OH during the 20th cycle is recorded as 73.8% and 74.6% respectively, failing to meet the existing specifications that demand above 75%. Nonetheless, the NaCl-associated MS_0 continues to comply with the current specifications, remaining above 75% throughout the 30 cycles.

From Figure 4(c), similar to the AC-13 mixture, the AC-16 asphalt mixture also demonstrates a downward trend in MS_0 for all three deicing salts as the dry-wet cycles increase. Delving into Figure 4(d), within the 30 dry-wet cycles, CH_2CH_3OH exerts the least effect on MS_0, followed by NaCl, whereas CH_4N_2O imposes the most significant impact. During the initial 20 cycles, the influence of NaCl and CH_2CH_3OH on MS_0 appears comparable, but the 25th and 30th cycles

witness a sharp fall in MS_0 corresponding to CH_2CH_3OH. By the 10th, 15th, and 20th cycles, the MS_0 values corresponding to CH_4N_2O, NaCl, and CH_2CH_3OH are 72 %, 74.7%, and 72.4%, respectively, each of which falls short of the current specifications' demand for a figure above 75%.

On comparing Figure 4(b) and Figure 4(d), it is discernible that the rate of MS_0 reduction for AC-16 marginally surpasses that of AC-13, implying a more pronounced impact of the three salt solutions on AC-16 in terms of MS_0.

The alterations in the tensile strength ratio (TSR) and loss rate of the two asphalt mixtures following exposure to dry-wet cycles in three distinct deicing salt solutions are shown in Figure 5.

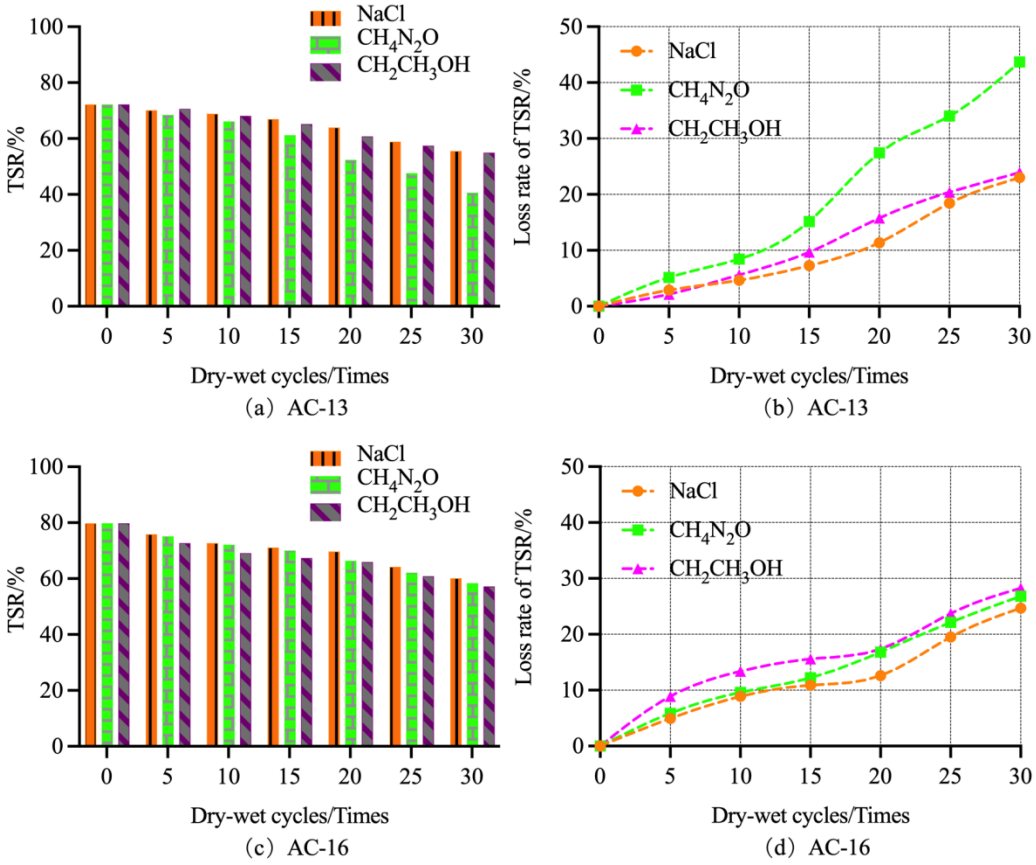

Fig. 5. The alterations in tensile strength ratio and loss rate after dry-wet cycles

As evidenced by Figures 5(a) and 5(b), AC-13 asphalt mixtures present a diminishing trend in TSR in relation to all three deicing salts as the quantity of dry-wet cycles augments. Of these salts, CH_4N_2O exerts a markedly greater influence on TSR compared to the other two, with a less pronounced discrepancy between the effects of CH_2CH_3OH and NaCl on TSR. By the 5th dry-wet cycle, the TSR for CH_4N_2O is 68.5%, and by the 10th cycle, the TSRs for CH_2CH_3OH and NaCl are 68.1% and 68.8%, respectively, failing to achieve the standard's prescribed minimum of 70%.

Referring to Figures 5(c) and 5(d), for AC-16 asphalt mixtures, the TSR shows a similar downward trajectory as the count of dry-wet cycles expands, with no discernible contrast in the impact of the three salts on TSR at equivalent dry-wet cycle numbers. By the 10th cycle, the TSR corresponding to CH_2CH_3OH is 69.1%, and at the 20th cycle, the TSRs for NaCl and CH_4N_2O are 69.7% and 66.4%, respectively, not meeting the required standard of a minimum of 70%.

Upon comparison of Figures 5(b) and 5(d), it emerges that for CH_4N_2O as the deicing salt, the TSR reduction rate for the AC-16 grading outpaces that of AC-13. However, in the case of NaCl or

CH_2CH_3OH being the deicing salts, the TSR decline rate for AC-16 exhibits negligible difference from that of AC-13.

*Grey Correlation Entropy Analysis***.** First proposed by Professor Ju-Long Deng in 1982, Grey Theory is a novel engineering system framework designed to adeptly tackle system issues where information is scant. Over three decades of continued development have seen this theory find applications across various domains. A particular branch of Grey Theory, Grey Correlation Entropy Analysis, allows for a comprehensive assessment of data related to the subject of study in situations of incomplete information, pinpointing the primary and ancillary factors influencing the subject.

The core tenet of Grey Correlation Entropy Analysis is the evaluation of factor relatedness based on the similarity in their geometric shape progression. The similarity in the development trends of factor curves signifies a higher degree of closeness and correlation. Conversely, diverging development trends indicate a lesser degree of correlation and closeness. The process of Grey Correlation Entropy Analysis involves the identification of reference and comparison sequences, sequence initialization, calculation of the difference sequence, determination of the correlation coefficient, and finally, the estimation of the correlation degree.

Utilizing the Grey Correlation Entropy Analysis approach, an examination is conducted to discern the grey correlation between three determinant factors – gradation of the asphalt mixture, type of deicing salt, and the frequency of dry-wet cycles – with the dynamic stability, residual stability, and TSR of the asphalt mixture. This analysis yielded the correlation coefficients between each of these determinant factors and the dynamic stability, residual stability, and TSR respectively, as demonstrated in Table 1.

Table 1 – Results of grey correlation entropy analysis concerning influencing factors

Influencing factor	Gradation	Type of deicing salt	Dry-wet cycles
Dynamic stability	0.7035	0.6568	0.5511
Residual stability	0.6620	0.6341	0.5490
TSR	0.7209	0.6750	0.5648

Table 1 elucidates that the mechanical properties of asphalt mixtures under dry-wet cycles are primarily influenced by the gradation of the mixture. This is followed by the type of deicing salts utilized, with the frequency of dry-wet cycles presenting the least significant impact. This observation suggests that judicious selection of road surface materials can mitigate the erosive effects of deicing salts. Incorporating Liu's research findings on the freezing points of different deicing salts [19], it becomes apparent that the choice of deicing salt type holds diminished significance when the environmental temperature ranges between -5 ℃ and 0 ℃.

Conclusion. Dry-wet cycles were conducted on AC-13 and AC-16 asphalt mixtures using three kinds of deicing salt solutions, and the subsequent alterations in the mixtures' mechanical properties were examined. Data from the high-temperature rut test, the Marshall water immersion test, and the freeze-thaw splitting test were analyzed, leading to the subsequent conclusions:

1. Evaluating from the perspective of high-temperature stability, the detrimental impacts of de-icing salt solutions on AC-13 asphalt mixture can be ordered in a descending sequence as: CH_2CH_3OH > CH_4N_2O > NaCl. Similarly, the adverse effects on AC-16 asphalt mixture due to these de-icing salt solutions follows the decreasing order: CH_2CH_3OH > NaCl > CH_4N_2O.

2. Employing the MS_0 for assessing water stability, the ranking of the damaging effect of deicing salt solutions on AC-13 asphalt mixture is: CH_4N_2O > CH_2CH_3OH > NaCl. For AC-16 asphalt mixture, the order is: CH_4N_2O > NaCl > CH_2CH_3OH.

3. With the TSR as an evaluative parameter for water stability, the sequence of damage for AC-13 asphalt mixture by deicing salt solutions is: CH_4N_2O > CH_2CH_3OH > NaCl. For AC-16 asphalt mixture, the sequence is: CH_2CH_3OH > CH_4N_2O > NaCl.

4. In general, increasing the proportion of fine aggregates in asphalt mixtures enhances their resistance against deicing salt erosion.

5. As per the findings from the grey correlation entropy analysis, the gradation of the asphalt mixture is the leading determinant of its mechanical properties, followed by the type of deicing salt solution. Conversely, the number of dry-wet cycles exerts the least influence on these properties.

The scope of this manuscript is primarily focused on the macroscopic analysis of the impact of deicing salts on the mechanical properties of asphalt mixtures. A comprehensive understanding of these effects also necessitates a microscopic investigation, an aspect not included in the current study. Future investigations will leverage computed tomography (CT) image scanning or scanning electron microscopy (SEM) to inspect the microscopic morphological changes in the asphalt mixtures induced by deicing salt erosion.

References

[1] J.-S. Chen and C. H. Yang, "Porous asphalt concrete: A review of design, construction, performance and maintenance", *Int. J. Pavement Res. Technol.*, vol. 13, no. 6, pp. 601-612, 2020. doi: 10.1007/s42947-020-0039-7.

[2] F. Li *et al.*, "2D-wavelet based micro and macro texture analysis for asphalt pavement under snow or ice condition", *Journal of Infrastructure Preservation and Resilience*, vol. 2, no. 1, p. 14, 2021. doi: 10.1186/s43065-021-00029-y.

[3] H.-C. Dan, J.-W. Tan, Y.-F. Du, and J.-M. Cai, "Simulation and optimization of road deicing salt usage based on Water-Ice-Salt Model", *Cold Regions Science and Technology*, vol. 169, p. 102917, 2020. doi: 10.1016/j.coldregions.2019.102917.

[4] N. Buss, K. N. Nelson, J. Hua, and R. A. Relyea, "Effects of different roadway deicing salts on host-parasite interactions: The importance of salt type", *Environmental Pollution*, vol. 266, p. 115244, 2020. doi: 10.1016/j.envpol.2020.115244.

[5] A. Ebrahimi Besheli, K. Samimi, F. Moghadas Nejad, and E. Darvishan, "Improving concrete pavement performance in relation to combined effects of freeze-thaw cycles and de-icing salt", *Construction and Building Materials*, vol. 277, p. 122273, 2021. doi: 10.1016/j.conbuildmat.2021.122273.

[6] L. Juli-Gándara, Á. Vega-Zamanillo, and M. Á. Calzada-Pérez, "Sodium chloride effect in the mechanical properties of the bituminous mixtures", *Cold Regions Science and Technology*, vol. 164, p. 102776, 2019. doi: 10.1016/j.coldregions.2019.05.002.

[7] Y. Hassan, A. O. Abd El Halim, A. G. Razaqpur, W. Bekheet, and M. H. Farha, "Effects of Runway Deicers on Pavement Materials and Mixes: Comparison with Road Salt", *Journal of Transportation Engineering*, vol. 128, no. 4, pp. 385–391, 2002. doi: 10.1061/(ASCE)0733-947X(2002)128:4(385).

[8] X. Shi, M. Akin, T. Pan, L. Fay, Y. Liu, and Z. Yang, "Deicer impacts on pavement materials: Introduction and recent developments", *The Open Civil Engineering Journal*, vol. 3, no. 1, pp. 16–27, 2009.

[9] H. Wei *et al.*, "Aging mechanism and properties of SBS modified bitumen under complex environmental conditions", *Materials*, vol. 12, no. 7, p. 1189, 2019.

[10] J. Z. Zhou and J. H. Zheng, "Experimental study on low temperature performance of asphalt concrete under chloride salt attack", *Chin. Foreign Highw*, vol. 31, pp. 215–217, 2011.
[11] Z. Zhou, H. Li, X. Liu, and W. He, "Investigation of sea salt erosion effect on the asphalt-aggregate interfacial system", *Int. J. Pavement Res. Technol.*, vol. 13, no. 2, pp. 145–153, 2020. doi: 10.1007/s42947-019-0095-2.
[12] T. Pan, X. He, and X. Shi, "Laboratory investigation of acetate-based deicing/anti-icing agents deteriorating airfield asphalt concrete", *Asphalt Paving Technology-Proceedings*, vol. 77, p. 773, 2008.
[13] Y. Chen, Z. Li, Y. Fan, H. Wang, and H. Deng, "Progress and prospects of climate change impacts on hydrology in the arid region of northwest China", *Environmental Research*, vol. 139, pp. 11–19, 2015. doi: 10.1016/j.envres.2014.12.029.
[14] C. Westerlund and M. Viklander, "Particles and associated metals in road runoff during snowmelt and rainfall", *Science of The Total Environment*, vol. 362, no. 1, pp. 143-156, 2006. doi: 10.1016/j.scitotenv.2005.06.031.
[15] Q. Zhang and Z. Huang, "Investigation of the Microcharacteristics of Asphalt Mastics under Dry–Wet and Freeze–Thaw Cycles in a Coastal Salt Environment", *Materials*, vol. 12, no. 16, Art. no. 16, Jan. 2019. doi: 10.3390/ma12162627.
[16] Q. Guo *et al.*, "Experimental investigation on bonding property of asphalt-aggregate interface under the actions of salt immersion and freeze-thaw cycles", *Construction and Building Materials*, vol. 206, pp. 590-599, 2019. doi: 10.1016/j.conbuildmat.2019.02.094.
[17] Y. Luo, Z. Zhang, G. Cheng, and K. Zhang, "The deterioration and performance improvement of long-term mechanical properties of warm-mix asphalt mixtures under special environmental conditions", *Construction and Building Materials*, vol. 135, pp. 622-631, 2017. doi: 10.1016/j.conbuildmat.2016.12.167.
[18] X. Yu, Y. Wang, Y. Luo, and L. Yin, "The effects of salt on rheological properties of asphalt after long-term aging", *The Scientific World Journal*, vol. 2013, 2013.
[19] Yang liu and Ping Li, *Study on Temperature Field Prediction Model and Anti Icing Technology of Asphalt Pavement in Winter of Gansu Province*, Master, Lanzhou University of Technology, 2018.
[20] Ping Li, Xiying Wei, Tengfei Nian, Yang liu, and Yu Mao, "Freezing Point Test of Deicers on Asphalt Pavement in Seasonal Frozen Region Bulletin of the Chinese Ceramic Society", *Bulletin of the Chinese Ceramic Society*, vol. 38, no. 05. pp. 1561–1567, 2019.

ВПЛИВ ПРОТИОЖЕЛЕДНОЇ СОЛІ НА ЕКСПЛУАТАЦІЙНІ ХАРАКТЕРИСТИКИ АСФАЛЬТОБЕТОННИХ СУМІШЕЙ У ПІВНІЧНО-ЗАХІДНОМУ КИТАЇ: ДОСЛІДЖЕННЯ МЕХАНІЧНИХ ВЛАСТИВОСТЕЙ ТА ФАКТОРІВ ВПЛИВУ

[1]**Мінцзюнь Го**, аспірант,
guo19920408@hotmail.com, ORCID: 0000-0001-5924-0779
[1]**Ковальський В. П.**, к.т.н., доцент,
kovalskiy.vk.vntu.edu@gmail.com, ORCID: 0000-0002-3103-6319
[1]*Вінницький національний технічний університет*
вул. Воїнів-Інтернаціоналістів, 7, м. Вінниця, 21000, Україна

Анотація. На даний час одним з основних матеріалів для влаштування високоякісних автомобільних доріг залишається асфальтобетон. Накопичення льоду та снігу на асфальтобетонних покриттях в зимовий період часто призводять до серйозних дорожньо-транспортних пригод. За статистикою, близько 15-30 % таких інцидентів

безпосередньо пов'язані з ожеледицею та снігопадом. Тому, коли дороги вкриті льодом та снігом, найбільш економічно ефективним і дієвим заходом боротьби з ожеледицею залишається розпорошення протиожеледної солі на дорожньому покритті. Особливо в північно-західному регіоні Китаю, де спостерігається низька кількість опадів і постійні засухи, протиожеледні солі, що застосовуються взимку, не розбавляються і не змиваються потоком води. Як наслідок, дорожнього покриття та ґрунт навколо зберігає високу концентрацію протиожеледних солей, ніж в інших регіонах, що призводить до помітного впливу на термін служби дорожнього покриття.

Метою цього дослідження є експериментальне моделювання впливу високосольового середовища на механічні властивості асфальтобетонних сумішей з подальшим аналізом ключових факторів, що впливають на довговічність асфальтобетонних сумішей.

Для досягнення поставленої мети застосовуються такі методи дослідження, як випробування високотемпературної колії, а також випробування за Маршаллом та випробування на розшарування при замерзанні-відтаванні, що дозволяють дослідити закономірності зміни механічних властивостей асфальтобетонних сумішей в умовах різного гранулометричного складу, різних протиожеледних сольових розчинів та різної частоти циклів зволоження і висушування. Крім того, для встановлення взаємозалежності між факторами, що впливають на експлуатаційні характеристики асфальтобетонних сумішей, у дослідженні використано ентропійний аналіз “сірої кореляції”.

Результати показують, що після проходження 0, 5, 10, 15, 20, 25 і 30 циклів висушування та насичення у розчинах 20% технічної солі (NaCl), 15% карбаміду (CH_4N_2O) і 20% безводного етанолу (CH_2CH_3OH), високотемпературна стійкість і водостійкість асфальтобетону марок АС-13 і АС-16 знизилися в різній мірі. Загалом, збільшення відсоткового вмісту дрібного заповнювача в асфальтобетоні може підвищити стійкість асфальтобетону до сольової ерозії в ожеледицю. Згідно з аналізом ентропії “сірої кореляції” розглянуто вплив трьох факторів. Найбільший вплив на механічні властивості має різниця в гранулометричному складі, потім тип розчину протиожеледної солі, і найменший - частота циклів насичення та висушування. Таким чином, раціональний підбір складу асфальтобетону підвищує експлуатаційні характеристики при негативні дії протиожеледних солей.

Ключові слова: дорожнє будівництво, асфальтобетонна суміш, цикл поперемінного насичення та висушування, експлуатаційні характеристики покриття, протиожеледна сіль.

Стаття надійшла до редакції 28.07.2023

UDC 691:328 DOI: 10.31650/2786-6696-2023-5-100-109

ASSESSMENT OF THE AGGREGATES IMPACT ON THE PROPERTIES OF RECOVERY POLYMER MORTARS

[1]**Savchenko S.V.**, PhD, Associate Professor,
koval_sv@ukr.net, ORCID: 0000-0002-4973-0552
[1]**Antoniuk N.R.**, Ph.D., Associate Professor,
antonuk_nr@ukr.net, ORCID: 0000-0003-1730-0723
[1]*Odessa State Academy of Civil Engineering and Architecture*
4 Didrichson street, Odessa, 65029, Ukraine

Abstract. The peculiarities of polymer mortar application for renovation and restoration are determined on the basis of priority data integration about the destruction mode of valuable historical buildings. The possibilities of controlling technological, physical-mechanical, and operational properties of recovery polymer mortar due to the aggregates of different nature are shown.

For the analysis and optimisation, the quantitative relations between the structure and property factors of recovery polymer mortars and the factors of recipes and technology determining them were obtained in the form of experimental and statistical models calculated using the COMPEX system. The optimisation methods of recipe and technological solutions based on the use of experimental and statistical models are proposed.

The optimisation of polymer mortar composition according to the package of quality indexes and property stability at high temperature has been carried out. The package of "mixture-technology-properties" models has been obtained, with the help of which the change mechanisms of direct and summarizing indexes of mixture technological properties and mechanical properties of recovery polymer mortars have been established when changing the type of aggregates (ceramics, quartz, carbonates, their binary and triple mixtures).

The influence of aggregates on the durability change of polymer mortar under the influence of various temperature-climatic and operational factors (UV-irradiation, alternate action of temperature and aggressive aqueous solutions) has been studied.

It is recommended to use quantity and type optimal aggregates to provide the complex of technological and operational properties of polymer mortar and to reduce the consumption of imported polymer. The rational compositions of polymer mortar with increased stability of properties under changing temperature and climatic conditions are proposed for different restoration technologies.

The series of nomograms have been developed for the initial selection of the "area" of rational polymer mortar compositions, providing for further correction in relation to a specific repairable object. Technological and marketing analysis according to the research results are carried out.

Key words: recovery polymer mortar, aggregates, rheological properties, strength, optimal compositions, operational properties.

Introduction. The preservation of architectural monuments from further destruction is the goal of a number of international programs performed under UNESCO auspices. One of the main tasks of restoration procedures is to provide the life of buildings and structures while preserving their historical and architectural authority [1]. The great amount of restoration and conservation works, complex nature of structural destruction pose new scientific, methodological, and practical challenges. To solve these problems the special technological methods and materials are required. The composite materials in the form of protective and structural polymer mortars, as the world experience shows, are one of the most long-range materials for repair and restoration of stone and concrete structures. The introduction of the aggregates allows to change the technological and operational properties of polymer mortars in a wide range. The development and introduction of

effective polymer mortars based on the use of epoxy oligomers and aggregates of different nature is an urgent task while improving the technology of restoration work [2, 3].

Analyses of recent studies and publications. By means of research, as well as on the materials of international conferences and literature sources, the causes and classification of the main destructions of stone buildings and structures have been considered [4-8]. The first result was the classification of the most characteristic destructions to be repaired and restored according to the following characteristics: loss of monolithicity, delimitation of stone masonry, deep and through cracks, spalling, weathering, stone failure, etc.

The technological peculiarities of restoration works are determined by the variety of object destructions (which requires the use of different restoration materials with variable technological and physical-mechanical parameters), as well as the climatic pattern. The most important engineering tasks (taking into account the quality of engineering staff) include obtaining materials with the required properties, saving critical imported materials, as well as the related issue of decision validity.

According to the world experience, one of the most effective ways of repair, protection and restoration of building structures is the use of polymer-based composite materials [4-7]. One of the main prerequisites for the effective use of polymer mortars for the restoration purposes is the development of the scientific and practical base of polymer composites (V.V. Paturoev, V.I. Solomatov, V.L. Chernyavsky, V.A. Lisenko, I. Nikolov, R.A. Veselovsky, B.N. Strelenko, I.M. Yeshin, etc.).

One of the long-range ways to improve the quality and durability of composite materials and to save the binder is the use of modifying additives and aggregates, optimal both in concentration and in their physical and mechanical parameters. The use of the aggregates becomes extremely important under the conditions of expanding the requirements to the properties of restoration polymer mortars (RPM) (including the achievement of light and texture similarity), regulating the speed of the technological process and the variety of restoration techniques.

Based on the analysis results of characteristic destructions of buildings and structures, the codes and recommendations in the field of restoration of historical monuments, a possible package of technological solutions for the use of polymer mortars for repair and restoration of structures is proposed. The possible package of restoration works includes: reinforcement of existing foundations; monolithicity restoration of structural elements; replacement of destroyed material with new one; bonding of fallen stones and elements; grouting of delaminated masonry; filling of the cracks with decorative polymer mortar; grouting of the cracks with the injection, etc.

The aim of this study is to develop the compositions of recovery polymer mortar with the required complex of technological, physical and mechanical, and operational properties when using the aggregates of different nature and determination of the range of rational compositions that meet the requirements: effective viscosity within $50 \leq \eta_{max} \leq 900$ Pa·s, compressive strength $f_{ctfm} \geq 90$ MPa, bending strength $f_{cm} \geq 60$ MPa, stability coefficient of RPM properties to temperature K_i=100 %.

Objects and methods of research. Epoxy resin ER-20 was used as a binder in the experiments; its parameters are similar to the common foreign analogues (Araldite, Epicol, Epoxy); an amine-type hardener and plasticiser dibutyl phthalate (DBP) were used in the experiments.

The optimisation was carried out using "mixture-technology-properties" models [9]. The properties of filled epoxy polymer mortars were determined by:

V_i – the aggregate fraction of a certain (I-st) kind, with a fractional composition corresponding to fine quartz sand:

V_1 – the ceramic aggregate; V_2 – the carbonate aggregate; V_3 – the quartz aggregate; $\sum Vi = V_1 + V_2 + V_3 = 1$, i.e. the factors are interdependent and form a "mixture";

X_1 – the amount of plasticiser DBP (wt.h) – X_1=30±10 (20, 30, 40);

X_2 – the aggregate degree – X_2=200±100 (100, 200, 300); the factors X_1 and X_2 are interdependent and can be referred to the term "technology". The experiment was implemented according to a specially synthesized plan (Table 1) [9] in the COMREX system.

Table 1 – Experimental plan

№	Fillers, part			The amount of plasticiser DBP, (wt.h)	The filling degree, (wt.h)
	ceramic	carbonate	quartz		
	V_1	V_2	V_3	x_1	x_2
1	0.33	0.33	0.33	1	0
2	0	0	1	1	-1
3	0	0	1	-1	0
4	0	0	1	1	1
5	0	1	0	1	-1
6	0	1	0	1	1
7	0	1	0	-1	-1
8	1	0	0	-1	0
9	1	0	0	1	-1
10	1	0	0	1	1
11	0	0.5	0.5	-1	1
12	0	0.5	0.5	0	-1
13	0.5	0	0.5	-1	-1
14	0.5	0	0.5	0	0
15	0.5	0.5	0	0	1

The models in the form of reduced polynomials were obtained for the technological parameters of mixture quality and physical and mechanical properties of hardened polymer mortars, including the effective viscosity, flexural and compressive strength, and dynamic modulus of elasticity. The effective viscosity η was determined with the rotational viscometer "Polymer RPE-1M", which provided viscosity measurement in the range of 1.8×10^{-3}…3.75×10^{4} Pa·s. Bending strength f_{cm} and compression strength f_{ctfm} (MPa) were determined with test beams 4×4×16 cm; one set of test beams was tested after 10 days after manufacturing, the other one after 60 days stored at the temperature T=80°C. The modulus of elasticity E was determined from the initial linear section of the "load-s" diagram obtained according to step loading with the highest possible average velocity, which provided that strain readings were taken using two lever strain gauges mounted on the opposite edges of the test beams.

Research results. Based on the literature data, the main requirements for recovery polymer mortars were determined. Thus, the viscosity of technological mixtures should vary in a wide range. Its choice depends, first of all, on the method of polymer mortar introduction into the caverns, cracks or open surfaces (injection, hand patching, coating or spraying with the aggregates) [10]. As a rule, the polymer mortars with the bending strength not less than 50-83 MPa and compressive strength 80-100 MPa are used. The important parameters determining the behaviour of polymer mortar in the structure include the bond strength of the RPM with the permanent material, the ratio of elastic moduli and other parameters. The properties of RPM due to the polymer aging can be irreversibly changed under the influence of temperature, humidity, wind loads, ultraviolet irradiation, and other climatic factors [11-14].

Under the conditions of insufficiently studied mechanism of structure formation and destruction of composites and multicriterionality of accepted engineering decisions the most effective approach to the optimisation of their properties is the application of experimental and statistical models (ES-models) [9, 15-17]. There is considerable experience in the application of ES-models in the study and optimisation of composites for various purposes, including polymer mortars for protection, repair and restoration.

At the second stage, the quantitative dependences of the main RPM properties were investigated using ES-models package. Their analysis allowed to choose rational concentrations of the aggregates of different nature for RPM range. The choice of specific types of aggregates (fine brick rubble, limestone grits, fine sands) was determined on the basis of literature data.

The values of effective viscosity η (Pa·s), which characterises the structure-forming ability of the aggregates and was obtained at constant strain (έ=const=1c^{-1}), were comparable characteristic of aggregate surface activity.

The obtained experimental-statistical dependences of the effective viscosity are plotted in Fig. 1 in the form of multicomponent diagrams-tetrahedrons, which were combined with the concentration space "amount of DBP plasticiser – degree of filling".

$$\begin{aligned}\ln\eta = {} & 6.29V_1 + 2.73V_1V_3 - 1.29V_1x_1 + 1.88V_1x_2 + 0.32x_2^2 \\ & + 4.73V_2 - 0.61V_2x_1 + 1.49V_2x_2 + 0.23x_1x_2 \\ & + 2.67V_3 - 0.58V_3x_1 + 0.63V_3x_2\end{aligned}$$

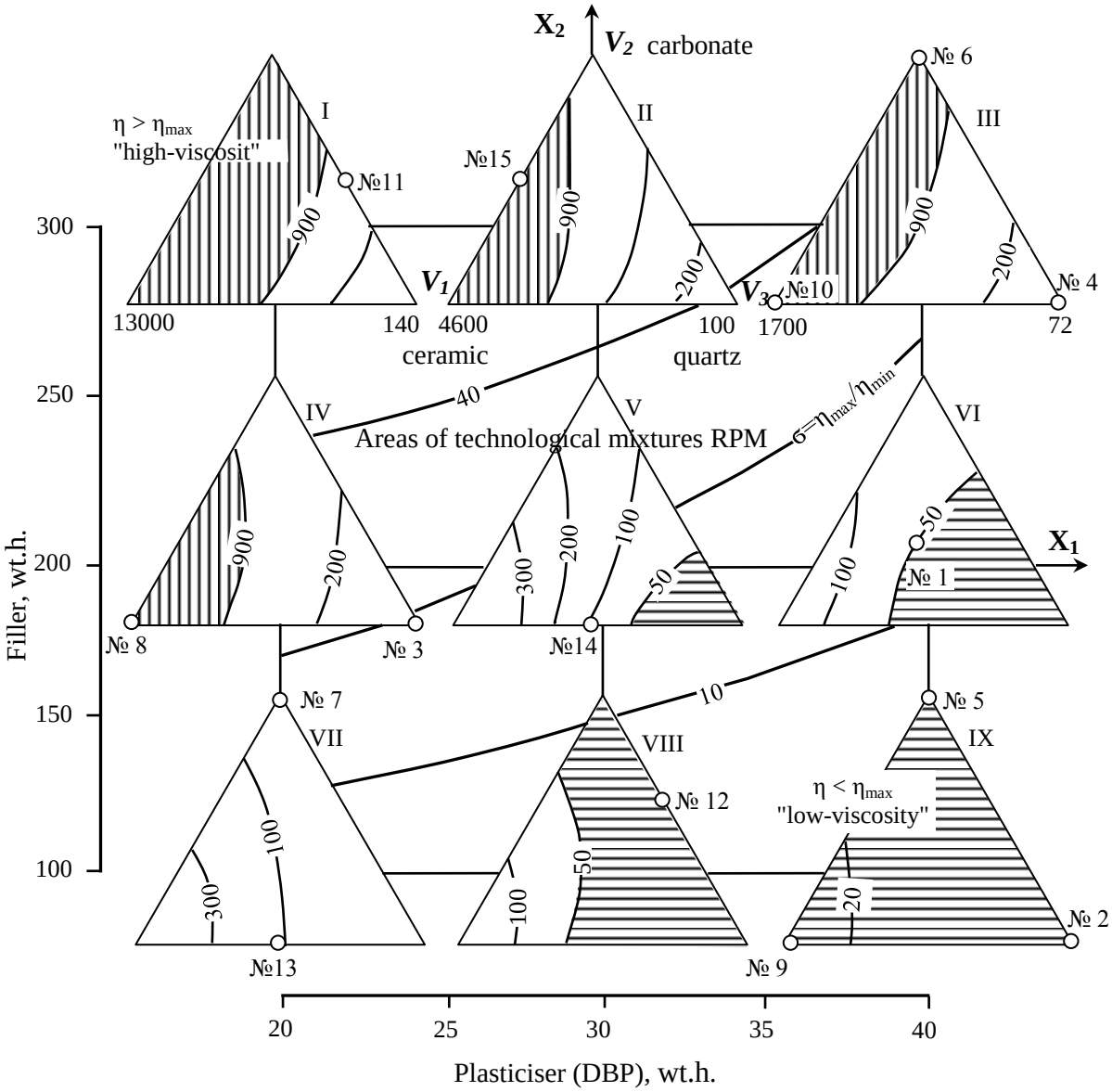

Fig. 1. Nine mixture triangles for the effective viscosity (Pa·s) of the filled polymer mortar constructed according to the model

The base element is a mixture triangle, on which the viscosity isolines η are shown. The "high-viscosity" (η_{max}>900 Pa·s) or "low-viscosity" (η_{max}<50 Pa·s) areas of polymer mortars are shaded inside each of the nine triangles.

From the analysis of the diagram there are the following technological conclusions. They are necessary for the choice of ways to regulate the technological properties of mixtures:

– to obtain technological mixtures ($50 \le \eta_{max} \le 900$ Pa·s) it is necessary, as a rule, to use

average concentrations of aggregates and plasticiser; the working area is limited "at the top" by high-viscosity mixtures with the ceramic aggregate, and "at the top" by low-viscosity mixtures with the quartz aggregate;

– maximum viscosity η_{max} achieved by varying the aggregate type (mixtures do not flow practically) is determined by the ceramic aggregate V_1, which is explained by high surface activity of this aggregate and, as a consequence, by more complete formation of oligomer supramolecular structures;

– the increase of the quartz aggregate proportion leads to a sharp decrease of the viscosity; for the mixtures V_1+V_2, the concentration increase of the carbonate aggregate causes a significant viscosity increase of polymer solutions (on the triangles I-III);

– the interaction of ceramic and quartz aggregates makes it possible to regulate the rheological properties of polymer mortars within the wide limits; the analysis of the model coefficients η shows that the greatest effect of structure formation is achieved with the interaction of V_1 and V_3.

The sensitive shift of viscosity to the variation of aggregate type was investigated using the composite index $=\eta_{max}/\eta_{min}$.

The isolines of the model on the supporting square (Fig. 1) indicate a sharp increase of the system sensitivity to the variations of the concentration and aggregate type – ceramic and quartz.

According to the results of the experiment in 15 experimental points (marked in Fig. 1) the models for the mechanical properties of hardened compositions were calculated. The models described the change of bending strength f_{cm}, the compression f_{ctfm} and the elastic modulus E of polymer mortars depending on the type and amount of considered aggregates. In the whole range of investigated concentrations, with the increase of aggregate degree, the strength factors increase for RPM with ceramic aggregate; they decrease or do not change for RPM with the carbonate, quartz aggregates and their mixture. This difference is explained by the unequal rate of polymer transition from the bulk state to the film state depending on the surface activity of aggregates.

As follows from the analysis of viscosity fluctuation in Fig. 1, the ceramic aggregate has the highest surface activity in the polymer matrix, since $\eta \rightarrow$max. At the same time, it provides the highest compressive strength. Thus, in comparison with quartz, the introduction of the ceramic aggregate into RPW (X_1=30, X_2=200 wt.h.) increases the strength by more than 1.3 times, which follows from the analysis of the mixture triangle in Fig. 2, a. Its mixing with the quartz aggregate is very effective to increase the bending loads resistance; in particular, $f_{cm.max}$ for the same compositions corresponds to the binary mixture V_1+V_3 (53% + 47%).

The elasticity modulus decreases with increasing DBP plasticiser amount, firstly for RPW containing carbonate aggregate. It increases when the quartz aggregate is used. The difference between deformative and elastic properties of permanent materials and polymer mortars significantly affects the workability of RPW. Thus, it is necessary to take into account that at E→min, the polymer mortars have plastic properties which are necessary to reduce internal stresses. Such stresses arise, for example, at the difference between temperature coefficients of the linear expansion of polymer mortar and the construction material (concrete, stone). The stiffening effect (E→max) reduces the difference between the elastic modulus of the materials, which contributes to the reduction of stress concentration in the contact zone "polymer-permanent material".

The secondary analysis allowed to find out the dependence between the recipes and the kinetics of internal stresses development. The studies were carried out on a special measuring complex, which allows to perform simultaneous measurements on 24 samples with the deformation fixation using MI-2 microscope ("cantilever method").

In particular, it was found that regardless of the composition and structure of the polymer morar, the first 4-6 days from the moment of preparation are characterised by a sharp stress increase. In the following 6-10 days a relative stress stabilisation is observed, after which for different compositions the value of internal stresses decreases by 10-50 %. At the age of polymer mortar more than 25 days the level of stresses remains practically unchanged, which indicates the completion of the process of polymer solution structure formation. The compositions, in which quartz sand was used as an aggregate, are characterised by a lower value of internal stresses than compositions with other aggregates.

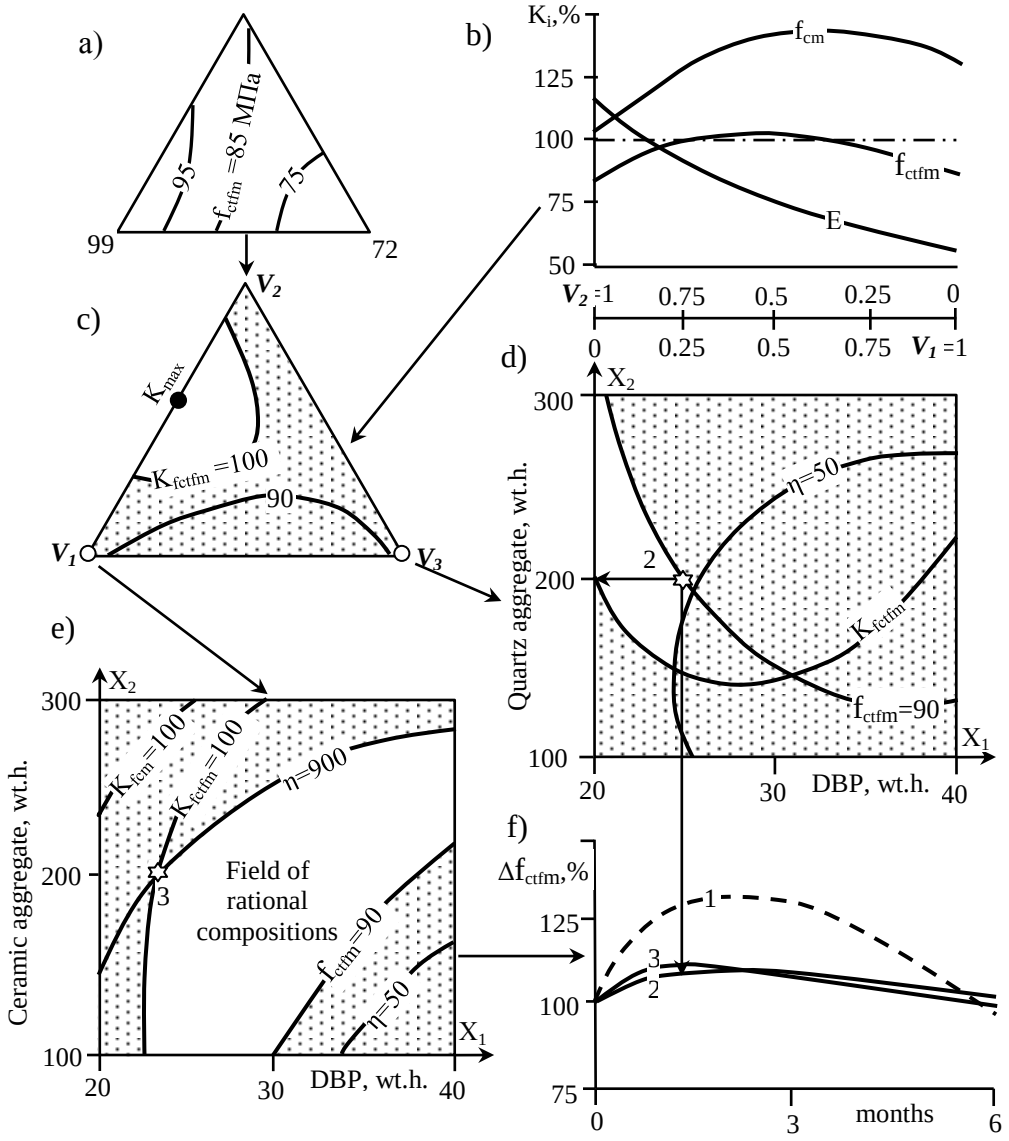

Fig. 2. Complex analysis of aggregates influence on the properties of RPW: (a) compressive strength f_{ctfm} in the mixture diagram; (b) property stability coefficient "K" when going from ceramic (V_1) to carbonate (V_2) aggregate; (c) compressive strength stability coefficient K_{fctfm} for the aggregates V_1, V_2 and V_3; d) optimal region of quartz-filled PRP; e) optimal area with ceramic aggregate; f) fraction change of f_{ctfm} under UV-irradiation (1 – unfilled PRM, 2 – quartz aggregate; 3 – ceramic aggregate)

The properties of restoration polymer mortars must meet the necessary requirements. Since the properties of RPM during the operation can irreversibly change, and this will be reflected on the durability of structures. The most significant external effects include high temperature of the environment. Under the influence of temperature, there are the irreversible physical and chemical transformations, leading to decrease the performance criteria of the material.

In order to assess the resistance of RPM properties to temperature, the comparative analysis of polymer mortars of the initial state (P_0) and after 60 days at the temperature T=80°C (P_T) was carried out. The stability index was determined as:

$$K = \frac{P_T}{P_0} 100\%.$$

In Fig. 2, b there is K coefficient variation for polymer mortars containing ceramic and carbonate aggregates, as well as their mixtures. The greatest variations of RPM properties under the influence of temperature occurred for those compositions in which the carbonate aggregate was used. The analysis of the isolines of K coefficient on the mixture triangle (Fig. 2, c) allowed to conclude from the effectiveness of mixing ceramic and carbonate aggregates to increase the stability of the compressive strength f_{ctfm} of the polymer mortar under the prolonged temperature effect. In the unshaded area (K≥100 %), the polymer mortars are characterised by stable strength.

The joint analysis of the "stability" index models f_{cm} и f_{ctfm} allowed to determine the compositions of polymer mortars that keep the required quality level under the influence of temperature. The appropriateness of mixing aggregates, first of all, ceramic and carbonate aggregates, to increase the stability of RPM properties is shown.

In order to select optimal compositions (Fig. 2. d, e), the isolines of "desirable" viscosity, strength and the boundary isolines of stability of strength parameters were superposed on the general diagrams, in particular, for the polymer mortar with quartz (Fig. 2, d) and ceramic (Fig. 2, e) aggregates. In the field of rational compositions the polymer mortars meet the following requirements: technological mixtures – viscosity 50...900 Pa.s; hardened composites: f_{cm} =60...80 MPa, f_{ctfm} =80...100 MPa, E=1.3...1.6 MPa, K=100 %.

The saving of polymer binder due to simultaneous introduction of two aggregates while maintaining the specified quality and reducing the impact on temperature factors is achieved by increasing the amount of quartz aggregate from 150 to 300 wt.h. (Fig. 2, d) or ceramic aggregate from 100 to 280 wt.h (Fig. 2, e). The narrower variation range of quartz and plasticiser aggregate (20...25 wt.h) increases the requirements to materials proportioning. The characteristic variation ranges of RPM compositions are shown in Table 2.

Table 2 – Variation ranges of RPM compositions

Type of filler (equal parts in the mixture)	Mixture viscosity	Content wt.h.	
		filler	plasticiser
carbonate	average	200…300	23…25
ceramic + carbonate	increased	100…200	30…40
carbonate + quartz	reduced	150…250	20…25
ceramic + quartz	average	100…230	20…25

As follows from the performed analysis, the nomograms for the initial reasons of the recovery polymer mortars recipes with complex filling were developed, which are oriented towards further refinement in relation to specific objects.

In addition to high temperature, the most significant factors causing RRM destruction include sun effect (for exposed surfaces), as well as alternating temperature effect and aggressive aqueous solutions (for building pedestals, foundations, etc.).

The experimental studies to assess the effect of aggregates on the durability of polymer mortars with the rational composition (Fig. 2. d, e) were carried out: a) under UV irradiation for 6 months; b) under moistening in aqueous solution (concentration of sulfate ions – 20 g/l.) and drying under hot blast for 300 cycles. To simulate solar radiation, the irradiation stand of the Agrophysical Institute with the ultraviolet and fluorescent lamps was used, providing the irradiation level of the samples up to 160 W/mt^2.

As the conducted researches have shown, under the influence of UV-irradiation the polymer mortars undergo almost the same changes as under the action of repeated temperature and humidity loads. The decrease of the factors is explained by a very significant role of thermo- and photo-oxidative processes in changing the supramolecular and chemical structures of the polymer. After some increasing during the initial exposure period, the bending strength of unfilled polymer mortar decreases sharply thereafter (curve 1, Fig. 2, e). The short-term process of "burst" strength was

explained by the continuing binder hardening processes under the influence of temperature. The rapid strength decrease may be due to the oxidative breakdown of the polymer binder and aging of the polymer. The introduction of ceramic (curve 2) and quartz (curve 3) aggregates into the polymer mortar prolongs to the strength retention under UV irradiation.

At the same time, the lightfastness of the tested samples was investigated. The most noticeable changes of the colour and gloss after UV-irradiation were in the samples containing carbonate aggregate, to a lesser extent – ceramic and quartz. The samples with carbonate aggregate quickly lose their appearance; "spider lines", as well as chalking, appear on the surface, which is due to intensive destruction of polymer bonds in a thin surface layer.

The use of the studied aggregates allows to stabilise the properties of polymer mortars under the combined effect of temperature and aggressive liquid media. Thus, the tests have shown that the introduction of carbonate aggregate stabilises the elastic modulus E more than ceramic aggregate. The process of properties changing also has an extreme character. The appearance of the extremum depends on the type of aggregate. Some strength increase of polymer mortars during the initial period of exposure is explained by temporary relaxation and more uniform distribution of internal stresses in the material amount.

Conclusions. The source and special features of damage have been determined and a possible package of typical technological solutions for the use of polymer mortar for repair and restoration of damaged structures has been considered.

The model of adjustment nomograms have been developed, which are oriented on further specification of rational compositions of recovery polymer mortars in relation to a specific object of repair – renovation.

The influence of aggregates with different nature on the complex of technological and physical-mechanical properties of recovery polymer mortar has been determined; the possibility of controlling the polymer mortar properties by using aggregates of different nature has been shown.

The rational compositions of technological polymer mortars are proposed for restoration works, in particular, with the compressive strength 80-100 MPa and the bending strength 60-80 MPa at minimum internal stresses, with increased stability of mechanical properties under the influence of high environmental temperature.

The positive influence of rational aggregates on the polymer mortar resistance to the temperature and climatic factors, including UV-irradiation, alternating effects of temperature and aggressive aqueous solutions is shown.

References

[1] Pam'yatniki arhitekturi. Zberegti, ne mozhna znishchiti. [Online]. Avialable: https://biz.nv.ua/experts/arhitekturnoe-nasledie-v-kieve-mozhno-li-zashchitit-novosti-ukrainy-50133205.html. Accessed on: August 19, 2023.

[2] A.P. Prihod'ko, E.S. Harchenko, "Vliyanie tipa modifikatora i ego kolichestva na adgezionnye svojstv polimernyh kompozicij dlya remonta dekorativnyh kompozicij zdanij", *Vestnik DNUZHT*, vol. 36, pp. 117-120, 2011.

[3] V.A. Lisenko, S.V. Savchenko, "Optimizaciya reologicheskih svojstv napolnennyh kompozitov s ispol'zovaniem eksperimental'no-statisticheskih modelej", *Komp'yuternyj poisk optimal'nyh modifikatorov kachestva kompozitov: tez. dokl. seminara*. Odessa, 1992. p. 14.

[4] Inès L. Tchetgnia Ngassam, "A new approach for the mix design of (patch) repair mortars", *Journal of Science, Technology, Innovation and Development*, vol. 10, Iss. 3, pp. 259-265, 2018.

[5] Grażyna Łagoda, Tomasz Gajda, "Change of Mechanical Properties of Repair Mortars after Frost Resistance Rests", *Materials (Basel)*, Iss. 14 (12), p. 3199, 2021.

[6] Qianjin Mao, Jiayi Chen, Wenjing Qi, "Improving Self-Healing and Shrinkage Reduction of Cementitious Materials Using Water-Absorbing Polymer Microcapsules", *Materials (Basel)*, Iss. 15(3), p. 847, 2022.
[7] Tsai-Lung Weng, "Evaluation of cementitious repair mortars modified with polymers", *Sage Journals*. *Applied System Innovation*, vol. 9, Iss. 1, pp. 1578-1586, 2017.
[8] S.V. Savchenko, N.R. Antoniuk, V.V. Bachynckyi, "Assessment of the impact of modifier and filler on the rheological and physical and mechanical properties of plaster solutions", *Bulletin of Odessa State Academy of Civil Engineering and Architecture*, vol. 82, pp. 105-113, 2021. https://doi: 10.31650/2415-377X-2021-82-105-113.
[9] T.V. Lyashenko, V.A. Voznesenskij, *Metodologiya recepturno-tekhnologicheskih polej v komp'yuternom stroitel'nom materialovedenii*: monografiya. Odessa: Astroprint, 2017.
[10] Valentyna Halushko, Alexander Meneilyk, Anatolii Petrovskyi, Denys Uvarov, Anastasiia Uvarova, "Development of technology of mixture application on vertical surface", *Technology Audit And Production Reserves*, vol. 2, no. 1(64), pp. 6-10, 2022. https://doi:10.15587/2706-5448.2022.257050.
[11] V.M. Virovoj, O.O. Korobko, V.G. Suhanov, N.V. Kazmirchuk, S.S. Makarova, *Strukturoutvorennya ta rujnuvannya budivel'nih kompozitiv*: navch. posib. Odesa: ODABA, 2020.
[12] V.N. Vyrovoj, I.V. Dovgan', S.V. Semenova, *Osobennosti strukturoobrazovaniya i formirovaniya svojstv polimernyh kompozicionnyh materialov*. Izd-vo «TES», 2004.
[13] V.G. Suhanov, V.M. Virovoj, O.O. Korobko, *Struktura materialu v strukturi konstrukcii*: monografiya. Odesa: ODABA, 2022.
[14] V. Vyrovoy, O. Korobko, V. Sukhanov, Y. Zakorchemny, "Resistance of concrete and expanded clay concrete under periodic external influences", *MATEC Web of Conferences*, vol. 23016, 03021, 2018. http://doi.org/10.1051/matecconf/201823003021.
[15] T.V. Lyashenko, "Composition-process fields methodology for design of composites structure and properties", *Brittle Matrix Composites 11*. Insitute of Fundamental Technological Research PAS, 2015, pp. 289-298.
[16] T. Lyashenko, S. Kryukovskaya, "Modelling the influence of composition on rheological parameters and mechanical properties of fibre reinforced polymer-cement mortars", *Brittle Matrix Composites 10*. Cambridge: Woodhead Publ. Ltd., Warsaw: IFTR , 2012, pp. 169-178.
[17] T. Lyashenko, "Brittle matrix composites optimisation on the base of structured experimental-statistical models", *Brittle matrix composites 3*: Proc. 3rd Int. Symp. London, New-York: Elsevier Applied Science, 1991, pp. 448-457.

ОЦІНКА ВПЛИВУ НАПОВНЮВАЧІВ НА ВЛАСТИВОСТІ РЕМОНТНО-ВІДНОВЛЮВАЛЬНИХ ПОЛІМЕРРОЗЧИНІВ

[1]**Савченко С.В.,** к.т.н., доцент,
koval_s.v.@ukr.net, ORCID: 0000-0002-4973-0552
[1]**Антонюк Н.Р.,** к.т.н., доцент,
antonuk_nr@ukr.net, ORCID: 0000-0003-1730-0723
[1]*Одеська державна академія будівництва та архітектури*
вул. Дідрихсона, 4, м. Одеса, 65029, Україна

Анотація. На основі пріоритетного узагальнення даних про характер та ступінь пошкодження цінних історичних будівель визначено особливості застосування полімеррозчину для ремонту та реставрації. Показано можливості керування технологічними, фізико-механічними та експлуатаційними властивостями реставраційного

полімеррозчину за рахунок наповнювачів різної природи.

Для аналізу та оптимізації кількісні співвідношення між показниками структури та властивостей ремонтно-відновлювальних полімеррозчинів та визначальними їх факторами рецептури та технології були отримані у вигляді експериментально-статистичних моделей, розрахованих з використанням системи COMPEX. Запропоновано методи оптимізації рецептурно-технологічних рішень, що ґрунтуються на використанні експериментально-статистичних моделей.

Проведено оптимізацію складу полімеррозчину за комплексом показників якості та стабільності властивостей при підвищеній температурі. Отримано комплекс моделей типу "суміш-технологія-властивості", за допомогою яких встановлено закономірності зміни прямих та узагальнюючих показників технологічних властивостей сумішей та механічних властивостей ремонтно-відновлювальних полімеррозчинів при зміні виду наповнювачів (кераміка, кварц, карбонати, їх бінарні та потрійні суміші).

Досліджено вплив наповнювачів на зміну стійкості полімеррозчину при дії різних температурно-кліматичних та експлуатаційних факторів (УФ-опромінення, поперемінний вплив температури та агресивних водних розчинів).

Для забезпечення комплексу технологічних та експлуатаційних властивостей полімеррозчину та зниження витрати імпортованого полімеру рекомендовано використовувати оптимальні за кількістю та видом наповнювачі. Для різних технологій реставраційних робіт запропоновано раціональні склади полімеррозчину з підвищеною стабільністю властивостей за зміни температурно-кліматичних умов.

Розроблено серії номограм для первинного вибору "області" раціональних складів полімеррозчину, що передбачають подальше уточнення стосовно конкретного об'єкта ремонту та реставрації. Проведено технологічні та маркетингові опрацювання за результатами досліджень.

Ключові слова: ремонтно-відновний полімер, наповнювачі, реологічні властивості, міцність, оптимальні склади, експлуатаційні властивості.

Стаття надійшла до редакції 6.07.2023

UDC 691.32 DOI: 10.31650/2786-6696-2023-5-110-116

THE INFLUENCE OF MINERAL ADDITIVES ON THE PROPERTIES OF ULTRA-HIGH STRENGTH CONCRETE

[1]**Sanytsky M.A.,** Doctor of Technical Sciences, Professor,
myroslav.a.sanytskyi@lpnu.ua, ORCID: 0000-0002-8609-6079
[1]**Vakhula O.M.,** PhD, Associate Professor,
orest.m.vakhula@lpnu.ua, ORCID: 0000-0001-8642-4215
[1]**Blikharskyi Z.Z.,** PhD.,
zinovii.z.blikharskyi@lpnu.ua, ORCID: 0000-0001-7555-1980
[1]**Trefler R.Yu.,** Postgraduate student,
romantrf@gmail.com, ORCID: 0000-0001-8478-8090
[1]*Lviv Polytechnic National University*
12, St. Bandery str., Lviv, 79013, Ukraine

Abstract. The article presents the results of a study of the influence of highly active mineral additives on the physical and mechanical properties of ultra-high strength concrete. Currently, according to the classical concept of making ultra-high strength concrete, a significant amount of ultradispersed microsilica is introduced, which determines the increased cost of its preparation. In order to obtain cost-effective ultra-high-strength concrete, the composition of mixtures was evaluated according to the criteria of strength and economy by replacing microsilica with technologically optimized highly dispersed zeolite (SSA=1200 m^2/kg), which belongs to the class of superzeolite. It is shown that for modified concrete with the addition of microsilica, the compressive strength after 2 days is 88.8 MPa, after 28 days – 161.0 MPa. When microsilica is partially replaced by superzeolite, sufficiently high mechanical parameters are achieved: after 2 days the compressive strength is 75.8 MPa, after 28 days the strength increases by 2.1 times and is 163.2 MPa, in this case a flexural strength of 12.1 MPa is achieved. The microsilica has a positive effect due to increased reactivity, especially at an early age. Similarly, the fine fraction of superzeolite is characterized by the acceleration of the pozzolanic reaction, while the coarser fraction contributes to increasing the degree of hydration of the Portland cement due to the desorption of water molecules from micropores and provides internal care for concrete. The cementitious matrix is compacted by filling the intergranular space due to the formation of nanodispersed C-S-H phases. Thermal analysis showed that the amount of calcium hydroxide in the superzeolite cementitious system is 2.75% or 66 kg/m^3, which meets the requirements for ultra-high strength concrete. The synergistic combination of microsilica and superzeolite with high surface activity and polycarboxylate superplasticizer provides high packing density and the necessary strength characteristics of ultra-high strength concretes, as well as contributes to their cost-efficiency, which opens the prerequisites for a large-scale engineering application of such concrete in construction.

Keywords: ultra-high strength concrete, microsilica, superzeolite, polycarboxylate superplasticizer, strength, structure formation, cost-effective design.

Introduction. One of the most important directions in construction is the development of construction materials of a new generation, in particular, ultra-high strength concretes, which are characterized by improved construction and technical properties and belong to the class of ultra-high performance concretes. Such concretes are attracting increasing interest worldwide due to high mechanical properties and durability [1, 2]. Currently, ultra-high strength concrete is mainly used for the construction of high-rise buildings, bridges, tunnels and other structures that require high bearing capacity and durability. At the same time, ultra-high strength concretes have problems that require attention and solutions, in particular, such as fragility, significant heat generation, low crack resistance, high cost, etc.

Analysis of recent research and publications. Ultra-high strength concretes (UHSC) belong to a special class of cementitious materials, which are formed with an optimized gradation of granular components, a low water-to-binder ratio (W/C = 0.20...0.25), and the addition of mineral and chemical additives [3, 4]. As a result, ultra-high strength concrete has a compressive strength that is approximately 3-5 times higher than traditional concrete. The resulting material is characterized by increased workability (slump flow ≥ 200 mm), high mechanical parameters (after 28 days, compressive strength ≥ 150 MPa, tensile strength ≥ 7 MPa, modulus of elasticity 40...60 GPa) [5, 6]. These characteristics of UHSC are mainly based on the high packing density, which is achieved by calculating the amount of fine particles such as cement, microsilica and quartz sand. Due to the increased specific surface of small particles and low water content, the use of significant amounts of superplasticizers is necessary. Ultra-high strength concrete is obtained by modification with surface-active substances and highly dispersed active mineral additives. However, the high preparation cost of ultra-high strength concrete limits its large-scale engineering application [7, 8].

Improving the packing density of cementitious materials by mixing with ultrafine supplementary cementitious materials plays an important role in increasing the physical and mechanical properties of concrete caused by minimizing the void content in the cementitious matrix. Ultrafine particles of active mineral additives are characterized by high values of the interphase zone and surface energy, and also provide a more complete synergistic effect of other components, forming a rheological matrix of the concrete mixture with a minimum water content. That in turn contributes to the directed formation of the microstructure of the cementitious matrix and thanks to its compaction and pozzolanic reactions in the non-clinker part [9]. Therefore, very high packing density is the main attribute in achieving low porosity of cementitious matrix, which leads to significant durability of ultra-high strength concrete compared to conventional concrete [10].

The excellent characteristics of ultra-high strength concrete, such as durability and high mechanical parameters, largely depend on the physical properties and kinds of highly active mineral additives used. One of the commonly used amorphous silicon dioxides is microsilica, a by-product of industrial silicon production with a particle size in the submicrometer range. Microsilica in the early period of hydration plays an important role not only as a microfiller, but also as a superpozzolana. At the same time, the high content of microsilica in the composition of ultra-high strength concretes can lead to an increase in the viscosity of the mixture and agglomeration, which leads to a decrease in the mechanical properties of concrete. On the other hand, the size of amorphous SiO_2 particles in submicrometers is effective for filling the voids present among the particles of cement and other constituent materials, that is, it manifests itself as a microfiller effect [11].

Large reserves of natural pozzolana – zeolite tuffs – are concentrated in Europe. At the same time, zeolites increase the water consumption of cement, which slows down the development of their strength [12]. On the other hand, the use of "super zeolite", which is a natural zeolite crushed to a smaller size than cement, opens up significant prospects. Such a "superpozzolana" provides an increase in the density of laying cement mortar with the same ease of workability [13]. It should be noted that in ultra-high strength concrete, which is developed with a low water-to-binder ratio, the hydration of the cement grains can potentially be limited. To solve the problems related to hydration, the possibility of using superzeolite, which has a high porous structure, should be investigated to ensure the internal care of the cementitious system with the age of hardening [14].

In this regard, it is advisable to conduct research on the replacement of microsilica or its part in the composition of the mixture for ultra-high strength concrete with addition of superzeolite, which will contribute to the improvement of the entire hydration process due to its high pozzolanic activity and ability to internal care with the age of concrete hardening. Modification of cementing systems with an organic component makes it possible, by changing the nature of their surface within wide limits, to activate the processes of structure formation of the cementitious matrix and to improve its microstructure. The improvement of the modern concept of creating ultra-high strength concrete is achieved by using highly effective modifiers and introducing highly dispersed active mineral additive such as superzeolite.

The purpose and tasks of the work – research of the influence of highly active mineral additives of microsilica and superzeolite on the processes of structure formation of the cementitious matrix and mechanical properties of modified fine-grained ultra-high strength concretes.

Research materials and methods. Production of high-quality concrete mixtures is ensured by Portland cement CEM I 42.5 R PJSC "Ivano-Frankivskcement", which meets European standards and is made on the basis of Portland cement clinker with a standardized mineralogical composition.

For designing the grain composition of ultra-high performance concrete, fine sand from the Davydivsky deposit (Lviv region, average density ρ_a=1370 kg/m^3, fineness modulus FM=1.16) and sand from the Slavuta deposit (Khmelnytsky region, ρ_a=1502 kg/m^3, FM=2.0) were used.

Highly active microsilica Elkem Microsilica Grade 940-U (SiO_2 content – 92.3 mass.%, SSA = 16 m^2/g) was used as an artificial mineral additive. As a component of pozzolanic action, zeolite tuff from the Sokyrnytskyi deposit (Transcarpathian region) was used, the main mineral of which is clinoptilolite $(Na, K)_4CaAl_6Si_{30}O_{72}\cdot 24H_2O$. Technologically optimized highly dispersed zeolite (SSA =1200 m^2/kg) belongs to the class of superzeolite, which allows to increase the packing density and improve the cohesion of cement paste. Characteristically, the cost of superzeolite is an order of magnitude lower compared to microsilica, which creates broad prospects for its mass use in concrete technology.

Particle size distribution of samples of finely dispersed active mineral additives was determined using a Malvern Mastersizer 3000 laser granulometer in the range from 0.01 to 3000 μm [15]. For Portland cement CEM I 42.5 R (SSA=350 m^2/kg), particles smaller than 1.0 and 5.0 μm make up 3.90 and 18.92%, respectively. Superzeolite has a bimodal distribution of particles by volume, while the amount of fine fraction up to 5.0 μm is 38 vol. %. This fraction makes the main contribution to the specific surface of superzeolite. Average diameters by specific surface area D[3;2] and volume D[4;3] for portland cement, microsilica, and superzeolite are 5.21 and 24.8 μm, respectively; 0.40 and 10.0 μm; 3.81 and 19.6 μm. The increased content of highly dispersed particles in the range of up to 1.0 μm is characteristic of microsilica determines its significant specific surface and high excess surface energy. An increase in the surface activity of small fractions and the packing density of large grains creates the possibility of increasing the early strength of multicomponent cementing systems.

Highly effective superplasticizers based on polycarboxylate ethers with nanosized molecular chains were used as modifiers to increase strength due to a significant water-reducing effect. The special molecular configuration of Master Glenium ACE 430 from the BASF company promotes the acceleration of cement hydration.

X-ray phase analysis of concrete samples after 28 days of hardening was performed using an Aeris Research Benchtop X-Ray Diffractometer from Malvern Panalytical.

Thermal analysis of the samples was carried out on a derivatograph Q-1500 of the Paulik-Paulik-Erdey system in the temperature range of 20-1000°C. The samples were analyzed in dynamic mode with a heating rate of 10 ^{o}C/min in an air atmosphere. The weight of the sample was 500 mg.

Research results. Research on the mechanical properties of concrete was carried out on the optimized composition of the mixture of components. As a rule, granite aggregate has various defects and microcracks that limit the strength of concrete. Therefore, in the mixture coarse aggregate was replaced by finer aggregate, which has better mechanical properties. Flexural strength was evaluated on 40×40×160 mm prisms, and compressive strength on halves of these prisms in accordance with EN 1015-11. Workability was tested in accordance with EN 1015-3. The composition of the concrete mixture was characterized by the quantitative content of components with a consumption of materials per 1 m^3: C = 800 kg, A = 1165 kg (sand with FM=2.0 – 1000 kg + sand with FM=1.16 – 165 kg), active mineral additives – 200 kg, superplasticizer Master Glenium ACE 430 (2.5%) – 20 kg, water 195...205 kg (W/C=0.25). A high-speed mixer was used for the production of ultra-high strength concrete, while the movement time was optimized to achieve homogeneity and quality of the mixture and was 8-10 minutes. The mobility of the mixture was characterized by the spreading of 300 mm cone. In order to improve the quality indicators of ultra-high strength concrete, the compositions were adjusted by replacing microsilica with the addition of superzeolite by 50% and 100%, respectively.

Tests were carried out for concrete through 2; 7 and 28 days of hardening.

As can be seen from Fig. 1, for concrete with additive of microsilica the compressive strength at an early age is R_{c2} = 88.8 MPa, after 28 days –161.0 MPa and the flexural strength – 12.1 MPa. For concrete with the addition of superzeolite, the compressive strength after 2 days – 57.6 MPa, after 28 days – 163.2 MPa. With the introduction of active mineral additives in the amount of 100 kg of microsilica and 100 kg of superzeolite, slightly higher strength indicators are achieved in the early stages of hardening compared to concrete with superzeolite additive; in this case the flexural strength – 12.3 MPa.

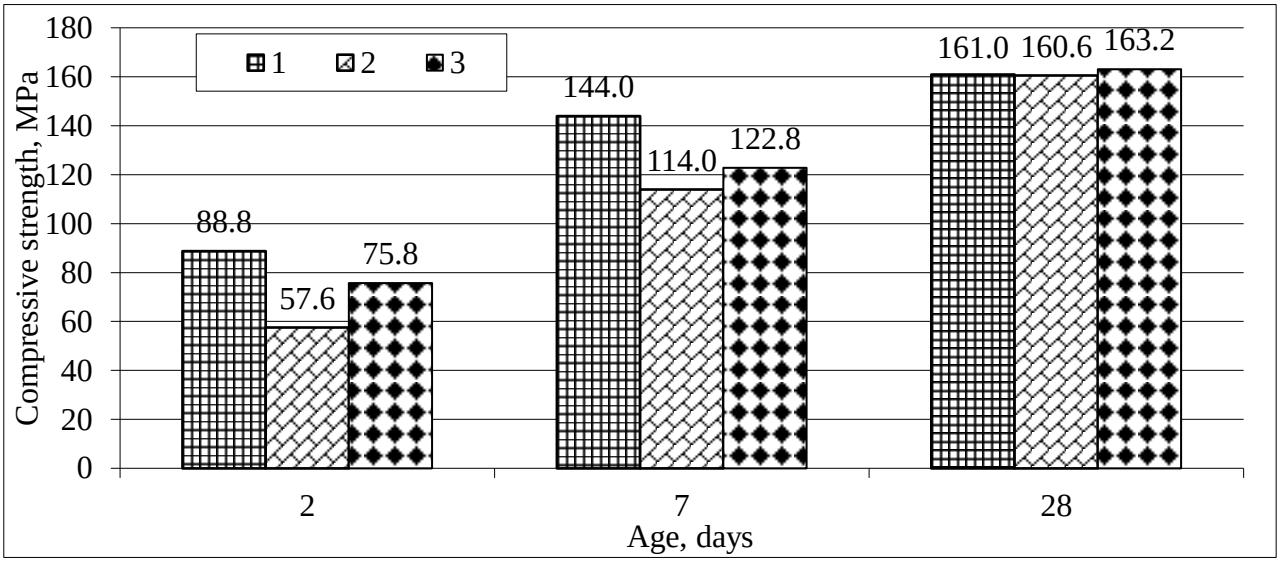

Fig. 1. Compressive strength of concretes with additives of microsilica (1), superzeolite (2) and microsilica + superzeolite in a ratio of 1:1 (3) dditives of microsilica (1), superzeolite (2) and microsilica + superzeolite in a ratio of 1:1 (3)

According to the X-ray analysis data the diffraction patterns of the cementitious matrix with the addition of microsilica show lines of calcite (d/n=0.303; 0.249 nm) and hydrated phase – calcium hydroxide (d/n=0.490; 0.263 nm). The introduction of microsilica with increased reactivity contributes to the acceleration of the pozzolanic reaction with the additional formation of C-S-H gel clusters. After 28 days of hardening of concrete with addition of superzeolite a decrease in the intensity of calcium hydroxide lines is observed (Fig. 2); at the same time, intense lines of quartz appear (d/n=0.334, 0.244, 0.223; 0.212; 0.181 nm) and line of calcite are fixed.

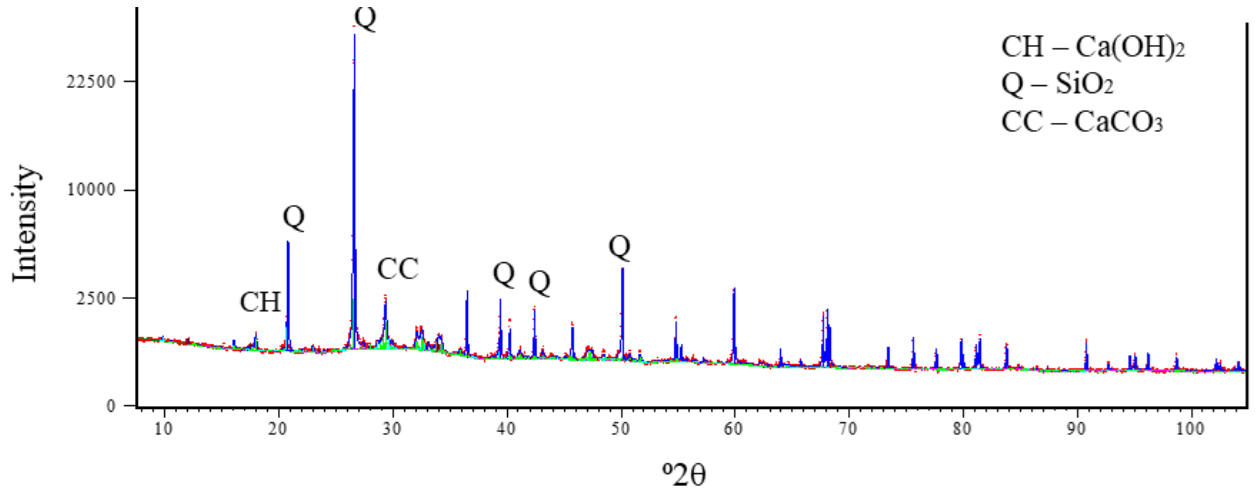

Fig. 2. Diffractogram of cementitious matrix with superzeolite additives after 28 days of hardening

As can be seen from the thermogravimetric analysis data (Fig. 3), the amount of calcium hydroxide in the cementitious matrix with microsilica does not exceed 1.5%, while the amount of $Ca(OH)_2$ in the composite with the addition of superzeolite is 2.75% or 66 kg/m^3, which meets the requirements for ultra-high performance concrete. In this case, the amount of bound water in fine-grained concrete with the addition of superzeolite (4.66 mass. %) is slightly higher than with the addition of microsilica (4.48 mass.%). As a result of the pozzolanic reaction of superzeolite, the cementitious matrix is compacted by filling the intergranular space.

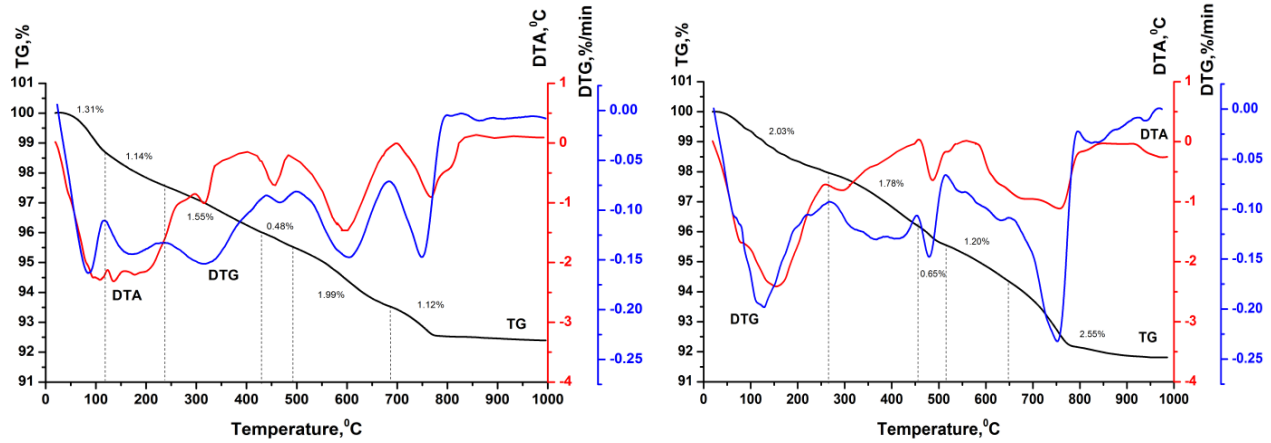

a) b)

Fig. 3. Thermograms of concrete with the addition of microsilica (a) and superzeolite (b) after 28 days of hardening

The results show that microsilica has a positive effect, mainly due to increased reactivity, especially at an early age. The fine fraction of superzeolite is characterized by the acceleration of the pozzolanic reaction, and the coarser fraction helps to increase the degree of hydration of the cementing system due to the desorption of water molecules from micropores, which provides internal care for concrete. The combination of microsilica and superzeolite with a polycarboxylate superplasticizer to a greater extent ensures the maximum density of the cementitious matrix and strength properties of ultra-high-strengh concretes, and also contributes to their cost-effectiveness.

Conclusions:

1. Cost-effective ultra-high strength concrete is developed using a multi-level particle packing approach to maximize the density of mixture of multi-fraction fine aggregates and polymineral cementing systems. It was established that modified concrete with additives of microsilica and superzeolite is characterized by increased mechanical properties: at an early age the compressive strength is R_{c2} = 75.8 MPa, and after 28 days increases by 2.1 times and is 163.2 MPa, while the flexural strength R_{f28} =12.3 MPa is achieved.

2. It is shown that superzeolite allows to reduce bleeding, sedimentation, increase the water-holding capacity of the mixture, as well as to provide internal care, as a result of which the strength of concrete increases with the age of hardening. The amount of calcium hydroxide in the cementitious matrix with the addition of superzeolite is 2.75% or 66 kg/m^3, which meets the requirements for ultra-high strength concrete. The replacement of microsilica with superzeolite provides a reduction in the production cost of ultra-high-strength concrete, which largely determines the practical feasibility of its large-scale engineering application in construction.

Prospects for further research. To increase the efficiency and durability of ultra-high strength concrete, it is advisable to continue research in the direction of developing compositions with additives of nanosilica and various types of reinforcing fiber materials.

Gratitude. The authors express their gratitude to the Ministry of Education and Science of Ukraine for supporting the project (registration number 0123U101832), which is being implemented at the expense of budget funding in 2022-2023.

References

[1] Li-Shan Wu, Zhi-Hui Yu, Cong Zhang, Toshiyuki Bangi, "Design approach, mechanical properties and cost-performance evaluation of ultra-high performance engineered cementitious composite (UHP-ECC): A review", *Construction and Building Materials*, vol. 340, 127734, 2022. doi.org/10.1016/j.conbuildmat.2022.127734.

[2] M. Sadiq, P. Soroushian, M. Bakker, "Ultra high performance cementitious composites with enhanced mechanical and durability characteristics", *SN Applied Sciences*, vol. 3, pp. 676, 2021. doi.org/10.1007/s42452-021-04628-y.

[3] S. Kroviakov, V. Volchuk, M. Zavoloka, "Fractal model of the influence of expanded clay concrete macrostructure on its strength", *Key Engineering Materials*, vol. 864, pp. 43-52, 2020. doi:10.4028/www.scientific.net/KEM.864.43.

[4] O.V. Sumariuk, V.F. Romankevych, O.D. Halunka, O.V. Kutsyk, V.V. Polevetsky, S.M. Novikov, I.M. Fodchuk, "Influence of polyfunctional nanomodificators on the microstructure of concrete composites of high strength and density", *Physics and Chemistry of Solid State*, vol. 21(1), pp. 19-26, 2020. doi org//scijournals.pnu.edu.ua /index.php/pcs s /article/view/2250.

[5] M.A. Johari, J.J. Brooks, Sh. Kabir, P. Rivard, "Influence of supplementary cementitious materials on engineering properties of high strength concrete", *Construction and Building Materials*, vol. 25, pp. 2639-2648, 2011. doi:10.1016/j.conbuildmat.2010.12.013.

[6] W. Zemei, H. Kh. Kamal, Sh. Caijun, "Changes in rheology and mechanical properties of ultra-high performance concrete with silica fume content", *Cement and Concrete Research*, vol. 23(6), 105786, 2019. doi.org/10.1016/j.cemconres.2019.105786.

[7] K. L. Nam, K.T. Koh, K. Min Ook, G.S. Ryu, "Uncovering the role of micro silica in hydration of ultra-high performance concrete (UHPC)", *Cement and Concrete Research*, vol. 104, pp. 68-79, 2018. doi.org/10.1016/j.cemconres.2017.11.002.

[8] X. Xing, W. Miaomiao, Sh. Weiguo, L. Jiangwei, "Performance and microstructure of ultra-high-performance concrete (UHPC) with silica fume replaced by inert mineral powders", *Construction and Building Materials*, vol. 327, 126996, 2022. doi.org/10.1016/j.conbuildmat.2022.126996.

[9] M. Sanytsky, T. Kropyvnytska, I. Heviuk. *Rapid hardening clinker-efficient cements and concretes*. Lviv, 2021.

[10] A. Aashay, A. Matthew, H. Hannah, C. Cesar, "Microstructural packing- and rheology-based binder selection and characterization for Ultra-high Performance Concrete (UHPC)", *Cement and Concrete Research*, vol. 103, pp. 179-190, 2018. doi.org/10.1016/j.cemconres.2017.10.013.

[11] X. Juyu, J. Liu. K. Yang. Sh. Zhang, "Role of silica fume on hydration and strength development of ultra-high performance concrete", *Construction and Building Materials*, vol. 338, 127600, 2022. doi.org/10.1016/j.conbuildmat.2022.127600.

[12] M. Sanytsky, T. Kropyvnytska, R. Trefler, "Modified sulfate-resistant Portland cements with zeolite addition", *Visnik Odes'koï derzhavnoï akademiï budivnictv ta arhitekturi*, vol. 87, pp. 100-107, 2022. doi.org/10.31650/2415-377X-2022-87-100-107.

[13] J.J. Chen, L.G. Li, P.L. Ng, "Effects of superfine zeolite on strength, flowability and cohesiveness of cementitious paste", *Cement and Concrete Composites*, vol. 83, pp. 101-110, 2017. doi.org/10.1016/j.cemconcomp.2017.06.010.

[14] K. Maziar, Sh. Behrouz, "Internal curing capabilities of natural zeolite to improve the hydration of ultra-high performance concrete", *Construction and Building Material*s, vol. 340, 127452, 2022. doi.org/10.1016/j.conbuildmat.2022.127452.

[15] M. Sanytsky, A. Usherov-Marshak, T. Kropyvnytska, I. Heviuk, "Performance of multicomponent Portland cements containing granulated blast furnace slag, zeolite and limestone", *Cement Wapno Beton*, vol. 25(5), pp. 416-427, 2020. doi.org/10.32047/ CWB.2020.25.5.7.

ВПЛИВ АКТИВНИХ МІНЕРАЛЬНИХ ДОБАВОК НА ВЛАСТИВОСТІ НАДВИСОКОМІЦНОГО БЕТОНУ

[1]**Саницький М.А.,** д.т.н., професор,
myroslav.a.sanytskyi@lpnu.ua, ORCID: 0000-0002-8609-6079
[1]**Вахула О.М.**, к.т.н., доцент,
orest.m.vakhula@lpnu.ua, ORCID: 0000-0001-8642-4215
[1]**Бліхарський З.З.,** к.т.н.,
zinovii.z.blikharskyi@lpnu.ua, ORCID: 0000-0001-7555-1980
[1]**Трефлер Р.Ю.**, аспірант,
romantrf@gmail.com, ORCID: 0000-0001-8478-8090
[1]*Національний університет «Львівська політехніка»*
вул. Ст. Бандери, 12, м. Львів, 79013, Україна

Анотація. У статті наведено результати дослідження впливу високоактивних мінеральних добавок на фізико-механічні властивості надвисокоміцних бетонів. На даний час, згідно з класичною концепцією виготовлення надвисокоміцного бетону, вводиться значна кількість ультрадисперсного мікрокремнезему, що зумовлює підвищену вартість його приготування. Для отримання рентабельних надвисокоміцних бетонів проведено оцінку складу сумішей за критеріями міцності та економічності шляхом заміни мікрокремнезему на технологічно оптимізований високодисперсний цеоліт (SSA=1200 м2/кг), який належить до клас суперцеоліту. Показано, що для модифікованого бетону з додаванням мікрокремнезему міцність на стиск через 2 доби становить 88,8 МПа, через 28 діб - 161,0 МПа. Встановлено, що при частковій заміні мікрокремнезему суперцеолітом досягаються достатньо високі механічні показники: через 2 доби міцність при стиску становить 75,8 МПа, через 28 діб міцність зростає в 2,1 рази і складає 163,2 МПа, при цьому досягається міцність на вигин 12,1 МПа. Мікрокремнезем вносить позитивний ефект завдяки підвищеній реакційній здатності, особливо в ранньому віці. Аналогічно дрібна фракція суперцеоліту характеризується прискоренням реакції пуцоланізації, тоді як грубша фракція сприяє підвищенню ступеня гідратації цементної системи за рахунок десорбції молекул води з мікропор, тобто забезпечує внутрішній догляд за бетоном. В результаті пуцоланової реакції мікрокремнезему та суперцеоліту відбувається ущільнення цементуючої матриці шляхом заповнення міжзернового простору за рахунок утворення нанодисперсних C-S-H фаз. Термічний аналіз свідчить, що кількість кальцію гідроксиду в цементуючій системі з суперцеолітом становить 2,75% або 66 кг/м^3, що відповідає вимогам для надвисокогоміцного бетону. Представлені результати свідчать про те, що синергетичне поєднання мікрокремнезему та суперцеоліту з високою поверхневою активністю та полікарбоксилатного суперпластифікатора забезпечує підвищену щільність упаковки зерен цементуючої матриці, необхідні міцнісні характеристики надвисокоміцного бетону, а також сприяє зниженню вартості його приготування, що відкриває передумови для більш широкомасштабного застосування такого бетону в будівництві.

Ключові слова: бетон надвисокої міцності, мікрокремнезем, суперцеоліт, полікарбоксилатний суперпластифікатор, міцність, структуроутворення, економічне проектування.

Стаття надійшла до редакції 9.08.2023

UDC 628.16 DOI: 10.31650/2786-6696-2023-5-117-125

THE STUDY ON THE IRREGULARITY OF WATER COLLECTION AND DISTRIBUTION BY POROUS PIPES IN FREE-FLOW WATER MOVEMENT

[1]**Progulny V.,** D.Sc., Professor,
varkadia@ukr.net, ORCID: 0000-0001-8310-3823
[1]**Grachov I.,** Senior Lecturer,
giawork@ukr.net, ORCID: 0000-0002-4173-4452
[2]**Bulhakov R.,** PhD,
od_va_kaf_rao@ukr.net, ORCID: 0000-0002-8825-718X
[2]**Frolov A.,** Senior Instructor,
sanec418@ukr.net, ORCID: 0000-0002-0941-4299
[1]*Odessa State Academy of Civil Engineering and Architecture*
4, Didrikhson str., Odessa, 65029, Ukraine
[2]*Odesa Military Academy*
10, Fontanska doroga str., Odessa, 65009, Ukraine

Abstract. One of the main utilities used to obtain drinking water in households and drinking water supply in towns are filters with drainage distribution and diversion systems in their main structural elements. The filters are equipped with porous pipes for distributing and collecting water to increase efficiency and reliability. Therefore, obtaining reliable methods for their calculation is of scientific and practical interest.

The article notes that water in distribution and collection pipelines moves with a variable flow rate along the way. Moreover, the inflow or outflow of water depends on the pressure variable along the length of the pipe. If the movement is free-flowing, it depends on the variable water level. While for porous pipes, this movement is continuous.

The subject of fluid moving with a variable flow rate has been studied by many authors; however, the dependences obtained in those cases mainly concerned perforated pipelines and open trays.

The authors study the operation of a porous pipe under the conditions of free-flow movement, which is described by two equations, the movement of fluid inside the pipe and the movement of fluid through the pipe's walls. The article indicates the complexity of this problem. Namely, the fact that these equations are interconnected. That is, the fluid flow through the pipe walls depends on the depth of the water layer in the pipe, which is determined by the equation of motion inside the pipe. Similarly, the law of depth change is defined, particularly by the laws of the inflow.

A mathematical model was obtained during the investigation of the uneven distribution and collection of water by a porous pipe. Based on this model, an approximate calculation method was developed, which makes it possible to get the value of the average flow depth in the pipe from the critical depth of water installed at the end of the pipe. To simplify the calculations, the article gives the corresponding nomograms.

The validation of the model was carried out on an experimental setup. The analysis of the experimental data showed good correspondence to the calculation results performed according to the approximate method, i. e. the deviation of the flow depth in the middle section does not exceed 1.5%.

Keywords: porous pipe, free-flow movement, filters, collection (outflow) of water, hydraulic calculation.

Introduction. One of the priority tasks of the state is to provide settlements with high-quality drinking water, which is established by the Law of Ukraine "On Drinking Water and Drinking Water Supply". Ukraine wants to adjust its regulatory documents on drinking water supply with

regulatory acts of the European countries [1]. It requires an increased efficiency of water treatment facilities and improvement of both the construction and hydraulic calculation methods [2].

Usually, to obtain water of the required quality, it is necessary to connect with the technological scheme of water purification in filtering facilities. At water treatment plants, filters are the most expensive and complex structures. The quality of the water supplied to the consumer, the practical productivity, and even the economic indicators of the entire station depend on them [3, 4]. In recent years, systems of porous pipes have been widely used in drainages and flushing water removal systems to intensify the work of fast filters [5, 6]. Therefore, improving the methods of hydraulic calculation and optimization is a vital task.

The analysis of recent research and publications. Water in porous distribution and collection pipelines (channels) moves with a variable flow rate, so it is impossible to describe the movement using the usual Bernoulli equation. Moreover, the inflow or outflow of water depends on the pressure variable along the length of the pipe. If the movement is free-flowing, it depends on the variable water level. The inflow or outflow of water can be continuous (if the pipe wall is porous) or discrete.

Many authors have studied fluid movement patterns with a variable flow rate. Numerous studies concern the movement of fluid with a variable flow path in perforated pipelines and open trays [7-12].

The research conducted by G.A. Petrov is devoted to the movement of fluid with a variable flow rate. From the equation of the amount of flow, he obtained the equation for a pressureless prismatic channel [13]:

$$\frac{2a_k Q}{gw^2}dQ = \frac{a_k Q^2}{gw^2}\frac{\partial w}{\partial h}dh + dh + dx\left(i_0 - i_f\right) = 0 \quad (1)$$

The closest to this question is studying fluid movement in channels covered by porous plates [14].

It appeared that the equations for the dynamics of variable mass differ from those for constant mass. It happens mainly because of the loss of energy due to the so-called "mixing" of masses or vortex resistance. During the flow of liquid these losses, in many cases, reach values that significantly exceed the usual losses due to internal friction. Vorticity is formed during outflow or inflow of water when the liquid is moving with a variable flow rate in perforated distribution pipes. This is caused by turbulent jets. It is these vortices that provide additional support to the main mass of the moving liquid. When collecting or draining water through porous pipes, vortices may also form at the boundary between the main flow and the porous layer. However, their size will be smaller compared with perforated pipes, since the pore sizes are much smaller than the diameter of the holes in the collection and distribution pipes. Accordingly, the speed of water entry (exit) is much lower than that of the transit flow.

The purpose and objectives of the research. The article is dedicated to the study of the porous pipes operating in pressureless movement. The task of these studies is to obtain an approximate method of calculation when collecting and draining water.

Research materials and methods. Let us consider a porous pipe (Fig. 1) with a constant radius R laid with a slope i_0 in the direction of the flow.

A decline curve is created in the pipe and the depth of this flow (h) will vary along its length, while the water level outside the pipe (H) is constant. Inflow of water to the pipe can occur in two zones, namely in the area below the water level in the pipe ($z \leq h$), where the specific inflow is q_1, and in the area above the water level in the pipe – inflow q_2. The mathematical model of the work of a porous pipe is defined by two main equations [15]:

1) movement of liquid inside the pipe;

2) fluid movement through the pipe walls.

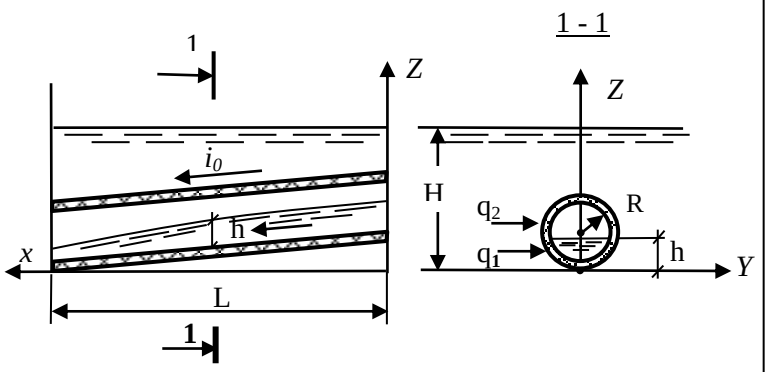

Fig. 1. Scheme of collecting water using a porous pipe

These equations are interconnected, i.e., the flow of liquid through the walls of the pipe depends on the movement of the liquid in the middle of the pipe with a layer (h), which is variable in length. Similarly, the law of change of depth h(x) is determined, in particular, by regularities of the water inflow.

Consider the equation defining the internal flow.

The liquid inside the pipe moves with a change in flow rate along its length, namely at the beginning of the flow (x = 0), flow rate Q = 0, and at the end (x = L) – Q = Q_k. Thus, movement with a variable flow rate in a prismatic channel is considered. To describe such a movement, the equation obtained by G. L. Petrov (1) was chosen, since it was obtained using a minimum of assumptions, and the results were verified experimentally.

If, for the sake of simplification, the losses of frictional pressure along the length are neglected, then the equation of motion in complete differentials is written in the following way:

$$\frac{\alpha}{g} d\left(\frac{Q^2}{\omega}\right) + \omega dh = \omega i_0 dx, \tag{2}$$

Q, ω is the flow rate and cross-sectional area of the flow at a distance *x* from its beginning;

h is the depth of the flow; i_0 is the slope of the pipe; α is the Coriolis coefficient; *g* is the acceleration of free fall.

The boundary conditions of equation (2) are the following:

$$\left.\begin{array}{l} x = 0,\ \ Q = 0,\ \ h = h_1 \\ x = L,\ \ Q = Q_k,\ \ h = h_k \end{array}\right\}. \tag{3}$$

In the integral form the equation (2) looks the following way:

$$\frac{\alpha Q^2}{g\omega} + \int \omega dh + \widetilde{C} = i_0 \int_0^x \omega dx, \tag{4}$$

$\widetilde{C}$ – is the constant of the integration.

To integrate (4), it is necessary to have the dependence of the flow cross-sectional area on its depth *h*. To integrate (4), it is necessary to have the dependence of the flow cross-sectional area on its depth h. The volume of liquid in the pipe from the initial cross-section to the cross-section *X* is determined by the integral on the right-hand side of (4). This volume can be roughly calculated from the average cross-section of the stream, i.e.:

$$\int_0^x \omega dx \cong \omega_{cp} x. \tag{5}$$

The dependence *ω(h)* is also needed to calculate ω_{cep}.

As the analysis and performed calculations showed, the dependence *ω(h)* can be represented with sufficient accuracy by a power function:

$$\overline{\omega}(\overline{h}) = \beta \overline{h}^{\kappa}, \tag{6}$$

β and *κ* are empirical coefficients calculated by the method of least squares;

$\overline{w} = w/R^2$, $\overline{h} = h/R$ – is the dimensionless area of the stream and its depth.

Satisfactory approximation of formula (6) is achieved by using two curves: at $h \le R$ – $\beta_1 = 1.68$, κ_1 = 1.47 (the maximum deviation of calculated data from formula (6) does not exceed Δ = 3.9%, and the relative root mean square deviation – σ = 0.026).

Substituting (6) into (4), we have the following result after the integration:

$$\frac{\alpha Q^2}{g\omega} + \frac{\beta}{\kappa+1} h^{\kappa+1} + \widetilde{C} = i_0 \beta \frac{h_1^{\kappa} + h^{\kappa}}{2} x \cdot \tag{7}$$

To determine $\widetilde{C}$ we use the first boundary condition from (3): $x=0$, $Q=0$, $h=h_1$. Then

$$\widetilde{C} = -\frac{\beta}{\kappa+1} h_1^{\kappa+1}, \tag{8}$$

where:

$$\frac{\alpha Q^2}{g\omega} + \frac{\beta}{\kappa+1}(h^{\kappa+1} - h_1^{\kappa+1}) = i_0 \beta \frac{h_1^{\kappa} + h^{\kappa}}{2} x \cdot \tag{9}$$

Let's include the coefficient $\kappa_h = h_1/h_\kappa$, which determines the ratio of the depths of the stream at the beginning and at the end. Then, using the second boundary condition from (3) – $x = L,\ Q = Q_\kappa,\ h = h_\kappa$, we obtain:

$$\frac{\alpha Q^2}{g\omega_\kappa^2 h_\kappa} + \frac{1}{\kappa+1}(1 - \kappa_h^{\kappa+1}) = \frac{i_0 L}{2h_\kappa}(1 + \kappa_h^{\kappa}) \cdot \tag{10}$$

In equation (10), the coefficient κ_h is a function of two dimensionless parameters. The first of them determines the ratio of the doubled velocity pressure at the end of the stream to its depth:

$$A_1 = \frac{\alpha Q_\kappa^{\ 2}}{g\omega_\kappa^2 h_\kappa} = \frac{\alpha V_\kappa^{\ 2}}{g h_\kappa}, \tag{11}$$

and the second parameter determines the flow geometry:

$$A_2 = \frac{i_0 L}{2h_\kappa}. \tag{12}$$

Then equation (10) can be represented as follows:

$$A_1 + \frac{1}{\kappa+1}(1 - \kappa_h^{\kappa+1}) = A_2(1 + \kappa_h^{\kappa}) \tag{13}$$

or in a form convenient for iterative calculations:

$$\kappa_h = \left\{1 - \left[A_2(1 + \kappa_h^{\kappa}) - A_1\right](1+\kappa)\right\}^{\frac{1}{\kappa+1}}. \tag{14}$$

When $h>R$ $\kappa=1$, the equation for κ_h is simplified:

$$\kappa_h = \sqrt{(A_2 - 1)^2 + 2A_1} - A_2. \tag{15}$$

By determining the K_h coefficient, you can find the average flow depth in the pipe. Thus, an approximate method of calculating for porous pipes was obtained, which allows to determine the depth of the flow in the middle cross-section and to calculate the inflow along this cross-section. For this, it is not necessary to know the law of change of depth inside the pipe, but only the parameters of the flow at its end (parameter A_1) and the geometry of the channel (A_2). Then, by determining the ratio of the depths of the stream at the beginning and at the end, you can find the depth of the stream in the middle section.

In the case of free flow of water from the end section of the pipe, a depth equal to the critical depth is set in it [16]. This depth, which corresponds to the minimum specific flow energy for round pipes is calculated by the following formula [17]:

$$\frac{h_{кр}}{R} = 0{,}844\left(\sqrt{\frac{\alpha}{g}}\frac{Q}{R^{2,5}}\right)^{0{,}511}, \tag{16}$$

valid upon fulfillment of the following conditions:

$$0{,}0023 < \sqrt{\frac{\alpha}{g}}\frac{Q}{R^{2,5}} < 4{,}53. \tag{17}$$

Research results. To simplify the following calculations the Fig. 2 shows the *h (Q,R)* dependence graph. The Fig. 3 is a graph for calculating the A_1 parameter. The Fig. 4 shows the nomograms for calculating the ratio of flow depths in the pipe at the beginning and at the end of κ_h for the cases $h \le R$ and $h > R$.

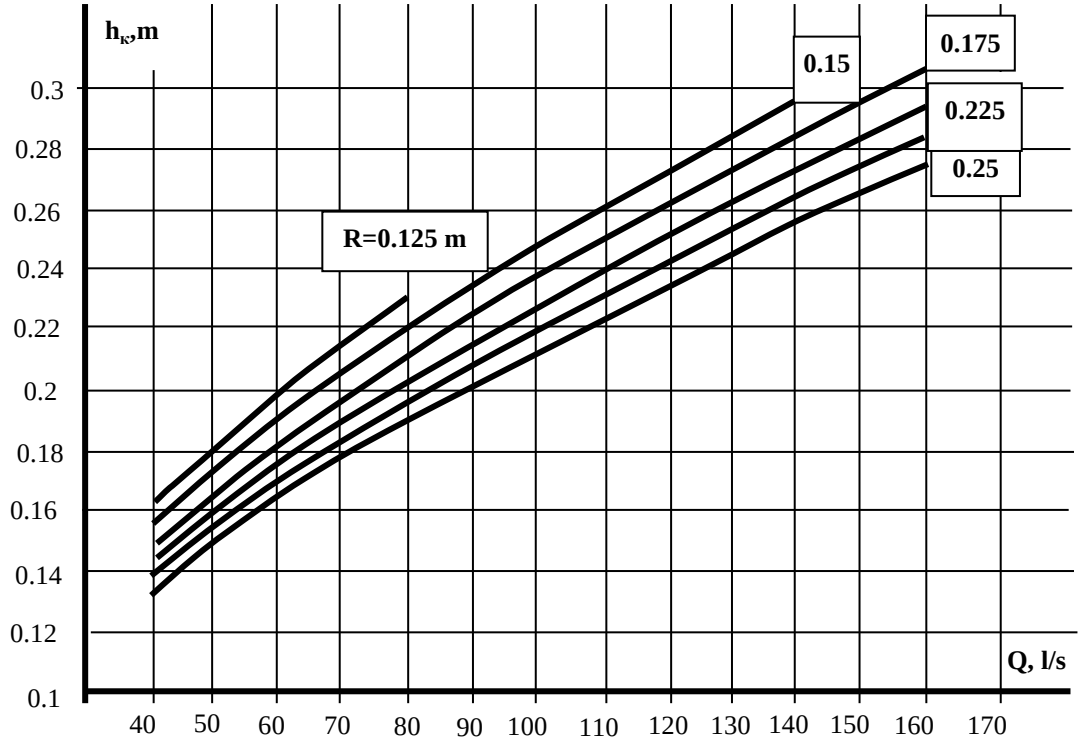

Fig. 2. Graph for determining the critical flow depth

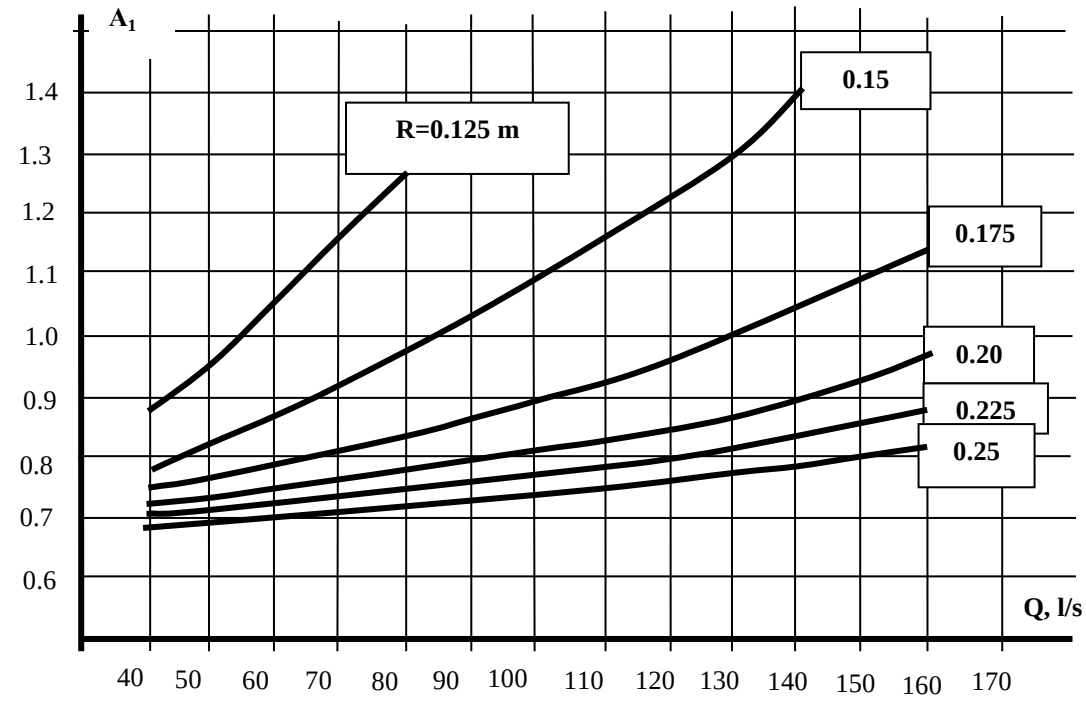

Fig. 3. Graph for calculating parameter A_1

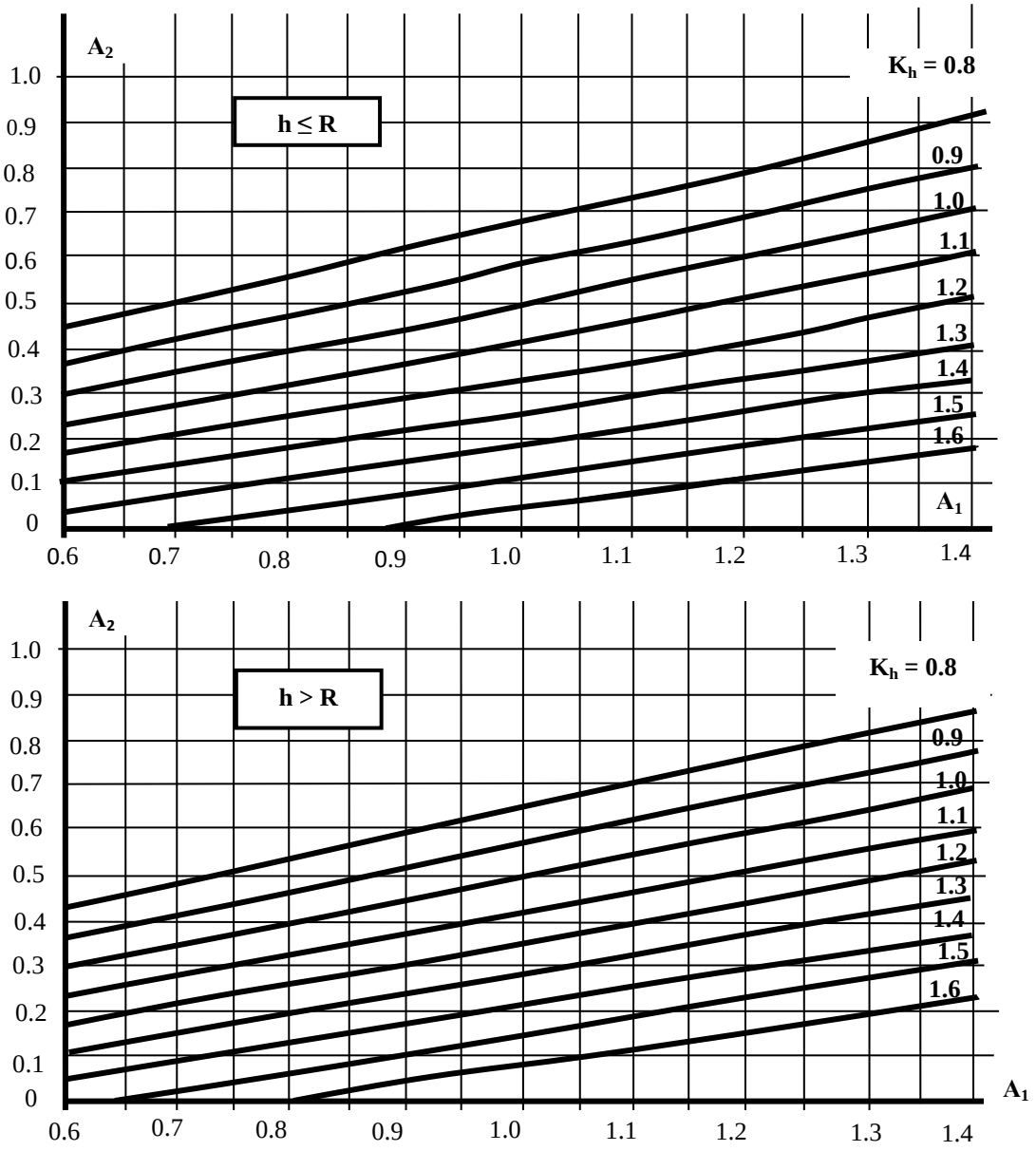

Fig. 4. Graph of determination of K_h for cases $h \leq R$ & $h > R$

The order of calculations using Fig. 2 – 4 is the following:

1. According to the specified radius of the pipe and the calculated flow rate according to Fig. 2, one can determine the critical depth at the end of the pipe $h_{кр}$, and according to Fig. 3 parameter A_1 can be determined.

2. A_2 is calculated by formula (12), then using the nomogram in Fig. 4 κ_h is determined, after that the average depth of the flow is found.

The validation of the model was carried out on an experimental setup which includes a porous polymer concrete pipe with an outer diameter of 150 mm, a length of 1000 mm, a wall thickness of 20 mm, which was installed in a tank with a height of 2 m and a diameter of 1.2 m.

On one side, the porous pipe was connected by means of a flange with a 120 mm diameter outlet pipe, and on the other end, it was closed with a blank plug.

5 piezometers were installed in the pipe with a step of 200 mm to measure the depth of the flow along its length. Water was supplied to the installation using a pump.

Analysis of the graph (Fig. 5) shows a good correspondence between the experimental data and the results of the calculation performed according to the approximate method. That is, the deviation of the flow depth in the average cross-section obtained experimentally from the calculated

data does not exceed 1.5%. This allows us to conclude that the developed approximate method of calculating porous pipes is reliable.

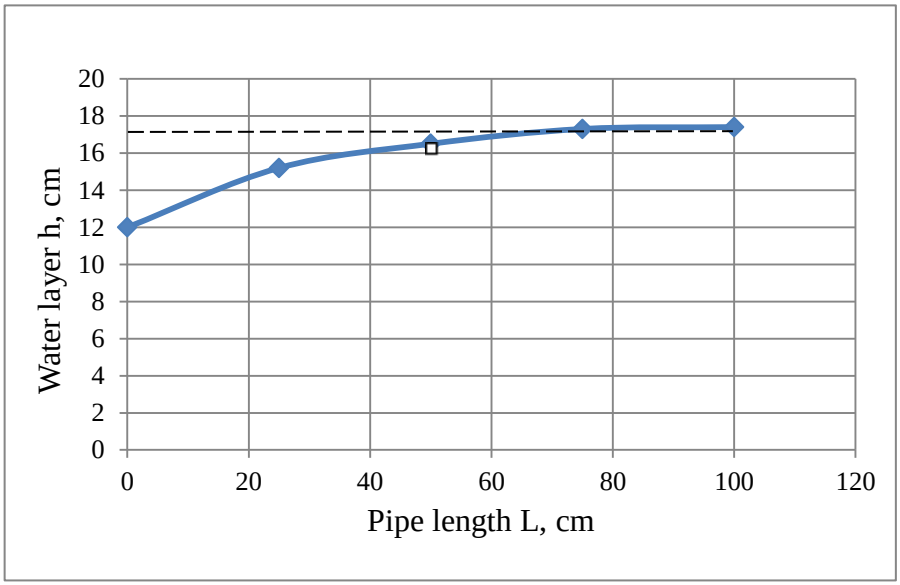

Fig. 5. Change in the flow depth in the pipe:
◇ – experimental data; □ – – calculation results;
---- – average flow depth obtained from
experimental data

Conclusions:

1. It is shown that to describe the operation of a porous collection pipe, it is necessary to use the equations of fluid movement in the pipe and fluid movement through the pipe walls at the same time, since these equations are interconnected.

2. To describe the movement of liquid in the pipe, the G. A. Petrov equation was used, the conclusion of which was made with a minimum number of assumptions, and which was verified experimentally. It is shown that when collecting water through a porous pipe, the projection of the speed of the connecting flow onto the direction of the main flow can be accepted $\theta=0$. In this case, the equation of motion is simplified, however, in this case, it will not be possible to integrate it. Therefore, in order to obtain the engineering method of calculations, it was necessary to neglect frictional pressure losses along the length of the flow for pressureless movement of water in the pipe.

3. To integrate the obtained equation (2), the dependence of the flow area in the pipe on the depth was approximated by the static formula (6), the coefficients of which were determined by the method of least squares. In addition, the ratio of depths at the beginning and at the end of the flow is introduced. The iterative formula (13) was obtained to calculate the ratio.

4. The procedure for calculating flow depths in the pipe has been developed. This makes it possible to determine the depth at the beginning and middle of the pipe with a known depth at the end (assumed equal critical depth).

5. The task of further research is to check the method of calculation of porous pipes in production conditions.

References

[1] Natsional′na dopovid′ pro yakist′ pytnoyi vody ta stan pytnoho vodopostachannya v Ukrayini u 2016 rotsi. Baza danykh "Minrehion Ukrayiny". [Online]. Available: http://www.minregion.gov.ua/napryamki-diyalnosti/zhkh/teplovodopostachannya-ta-vodovidvedennya/natsionalnadopovid/proekt-natsionalnoyi-dopovidi-pro-yakistpitnoyi-vodi-ta-stan-pitnogo-vodopostachannya-vukrayini-u-2016-rotsi/

[2] P.D. Horuzhy, T.P. Homutetska,V.P. Horuzhy, *Resursozberigayuchi tehnologii vodopostachannya*. K.: 2008.

[3] *Voda ta vodoochysn itekhnolohiyi. Naukovo-tekhnichni visti*, K.: 2016. no. 2.

[4] S.M. Epoyan,, V.D. Kolotilo, O.G. Drushlyak, G.I. Suhorukov, T.C. Ayrapetyan, *Vodopostachannya ma ochistka prirodnih vod*. H.: 2010.

[5] V. Progulnyi, M. Ryabkov, "Application of porous drainage in filters with floating media", *Naukovo-tekhnichnyy zbirnyk*, no. 2 (19), pp. 143-146, 2015.

[6] V. Progulnyi, "Poristyi konstruktsii filtrovalnykh sooruzheniy", *Zbirnik II Mizhnarodnoi naykovoi konpherensyi z naukovo–praktichnikh tekhnologiy*, Luksenburg, pp. 32-35, 2021.

[7] A. Kravchuk, G. Kochetov, O. Kravchuk, "Improving the calculation of collecting perforated pipelines for water treatment structures", *Eastern-European Journal of Enterprise Technologies*, vol. 6, no. 10(108), pp. 23–28, 2020.

[8] B. Schultz, "Irrigation and drainage systems research and development in the 21st century", *Irrigation and Drainage,* vol. 51, no. 4, pp. 311–327, 2002.

[9] L.K. Smedema, S. Abdel-Dayem, W.J. Ochs, "Drainage and agricultural development", *Irrigation and Drainage Systems*, no.14, pp. 223–235, 2000.

[10] V.V. Chernuk, V.V. Ivaniv, M.B. Shenukh, "Nerivnomirnist pritoku void do napirnogo truboprovodu-zbiracha zhalezhno vid kuta priednannya vkhidnikh strumeniv", *Naukovyivisnik NLTUU Ukraine,* T. 29, no. 9, pp. 116–120, 2019.

[11] P.I. Mendus, S.P. Mendus, V.O. Turchenuk, B.A. Philipchuk, A.M. Rokochinskiy, "Drenazhna risovikhsistemakh та komleksna osinka yogo ephektivnosti", *Visnik NUVGP. «Tekhnichninauki»,* T.3, no. 71, pp. 248–251, 2015.

[12] I.V.Bigun, "Osoblivosti zastosuvannya napirnikh rozpodilnikh truboprovodiv uriznikh tekhnichnikh sistemakh", *Theory and Building Practice*, T.1, no. 2, pp. 14–20, 2019.

[13] G.A. Petrov, *Gidravlika peremennoy massi*. L.: 1964.

[14] M.V. Ryzbkov, "Poristi konsruksii drenazhiv v shvidkikh vodoochisnikh filtrakh z plavayuchoyu zasipkoyu", avtoref. dis. na zdobuttya nauk. stupenya k-ta tekhn. nauk: 05.23.04, Odes'ka derzhavna akademiya budivnictva ta arhitekturi. Odesa 2018.

[15] P.A. Grabovskiy, G.M. Larkina,V.I. Progulnyi, "Intensifikasiya vodoochisnikh filtriv", *Vodopostachannya ta vodovidvedennya,* no. 6, pp. 38-48, 2012.

[16] D.M. Mins, S.A. Shubert, *Filtri AKH i raschoti promivki skorikh filtriv*. M.: 1951.

[17] A.M. Kurganov, N.F. Fyodorov, *Gidravlicheskie raschoti system vodopostachannya ta vodovidvedennya*. L.: 1986.

ДОСЛІДЖЕННЯ НЕРІВНОМІРНОСТІ ЗБОРУ ТА РОЗДАЧІ ВОДИ ПОРИСТИМИ ТРУБАМИ В УМОВАХ БЕЗНАПІРНОГО РУХУ

[1]**Прогульний В.Й.,** д.т.н., професор,
varkadia@ukr.net, ORCID: 0000-0001-8310-3823
[1]**Грачов І.А.,** ст. викладач,
giawork@ukr.net, ORCID: 0000-0002-4173-4452
[2]**Булгаков Р.В.,** к.т.н.,
od_va_kaf_rao@ukr.net, ORCID: 0000-0002-8825-718X
[2]**Фролов О.С.,**ст. викладач,
sanec418@ukr.net, ORCID: 0000-0002-0941-4299
[1]*Одеська державна академія будівництва та архітектури*
вул. Дідрихсона, 4, м. Одеса, 65029, Україна
[2]*Військова академія*
вул. Фонтанська дорога, 10,м. Одеса, 65009, Україна

Анотація. Однією з основних споруд, що застосовуються для отримання води питної якості у схемах господарсько-питного водопостачання населених пунктів, є фільтри, головні конструктивні елементи яких включають дренажно-розподільні та відвідні системи. Для підвищення ефективності та надійності фільтри обладнуються пористими трубчастими системами для розподілу та збирання води. У зв'язку з цим отримання достовірних методик їх розрахунку представляє науковий та практичний інтерес.

У статті зазначається, що вода у розподільчих та збірних трубопроводах рухається зі змінною по шляху витратою. Причому приплив або відтік води залежить від змінного по довжині труби тиску, і якщо рух безнапірний – від змінного рівня води, а для пористих труб цей рух безперервний.

Задача руху рідини зі змінною по шляху витратою вивчалася багатьма авторами, проте залежності які при цьому були отримані в основному стосувалися перфорованих трубопроводів і відкритих лотків.

Авторами розглядається робота пористої труби за умовами безнапірного руху, що описується двома рівняннями – руху рідини всередині труби і руху рідини через стінки труби. Зазначається складність цієї задачі, яка обумовлена тим, що це рівняння взаємопов'язані. Тобто витрата рідини через стінки труби залежить від глибини шару води в трубі, яка визначається рівнянням руху всередині труби. Аналогічно закон зміни глибини визначається, зокрема, закономірностями припливу.

Досліджуючи нерівномірність розподілу та збору води пористою трубою отримано математичну модель, на підставі якої розроблено наближену методику розрахунку. Це дозволяє по критичній глибині води, яка встановлюється в кінці труби, отримати значення середньої глибини потоку в трубі. Для спрощення розрахунків в статті наведені відповідні номограми.

Перевірка достовірності моделі проводилася на експериментальній установці. Аналіз отриманих дослідних даних показав добру відповідність їх результатам розрахунку, виконаних за наближеною методикою – відхилення глибини потоку в середньому перерізі не перевищує 1,5%.

Ключові слова: пориста труба, безнапірний рух, фільтри, збирання (відтік) води, гідравлічний розрахунок.

Стаття надійшла до редакції 12.07.2023

UDC 699.844.1 DOI: 10.31650/2786-6696-2023-5-126-133

FIELD TESTS OF IMPACT NOISE INSULATION OF THE FLOOR USING PLANNING THEORY

[1]**Babii I.,** Ph.D., Associate Professor,
igor7617@gmail.com, ORCID: 0000-0001-8650-1751
[1]**Bichev I.,** Ph.D., Associate Professor,
bichev@ukr.net, ORCID: 0000-0002-3000-2600
[1]**Kalchenia Y.,** Graduate student,
yevhenii.kalchenya@gmail.com, ORCID: 0000-0003-0653-1171
[1]*Odessa State Academy of Civil Engineering and Architecture*
Didrikson str., 4, Odessa, 65029, Ukraine

Abstract. In modern construction, one of the main indicators of the quality of housing for users of multi-storey buildings is still noise. The task of preventing the noise that occurs in the house itself needs to be given more attention when designing and soundproofing. It is known that extraneous sounds penetrating into a living space cause a negative impact not only on the psychological state of a person, but also on the physical one. In this regard, each user of the premises wants to receive comfortable conditions for staying in them. To achieve this condition, it is necessary to develop effective structural and technological schemes for soundproofing the floor from impact noise, as well as their verification and evaluation using the theory of planning experiments.

This article is devoted to solving an important issue of sound insulation of floors in monolithic reinforced concrete multi-storey residential buildings, namely from impact noise. The article considers the structural and technological schemes of sound insulation of the floor of fifteen types, using different materials and their combinations to achieve regulatory requirements for sound insulation from impact noise.

It was determined that the thickness of the layer of materials and the density have a significant effect on the insulation performance against shock noise. The work investigated floor constructions based on layers of changing materials. Specifically, such parameters as the thickness (50±10 mm) and density (300±50 kg/m^3) of polystyrene concrete "Izolkap" and the thickness of the semi-dry screed (50±10 mm).

When choosing the most rational design and technological scheme used the results of planning theory, as well as indicators of reduced impact noise, obtained as a result of field tests, it allowed to choose the most rational and effective version of "floating" floor – based on materials "Akuflex" and "Izolkap" (polystyrene concrete) – scheme №11, the index of the reduced level of impact noise is Lnw = 52 dB.

The arrangement of the structural and technological scheme of floor sound insulation №11 allows to reduce the level of initial impact noise in the room by 37.5%.

Keywords: sound insulation, impact noise, "floating" floor, multilayer system.

Introduction. In modern construction, one of the main indicators of the quality of housing for users of multi-storey buildings is still noise. Noises can be heard both from the street – technogenic and biogenic (noise from transport, stadium, open entertainment clubs), and from housemates. Massive or multi-layer building envelopes and efficient window systems help to prevent outside noise. In turn, the tasks of preventing noise that occurs in the house itself must be given more attention when designing and soundproofing. Since it is known that extraneous sounds penetrating into a living space cause a negative impact not only on the psychological state of a person, but also on the physical one, therefore, in this regard, each user of the premises wants to receive comfortable conditions for staying in them. To create such conditions, it is necessary to develop effective design and technological schemes for soundproofing the floor, as well as their verification and evaluation.

Recent research researches and publications results. There are two main types of noise in the construction industry: airborne and structural. It should be noted that noise is understood as a chaotic mixing of sounds. Airborne noise is transmitted through air, while structural noise is transmitted through a solid body. One of the types of structural noise is shock [1]. So, in most of the series of houses that were built in the last century, central heating was arranged. In such systems, metal pipes were used to supply the coolant to the heating radiators. At the same time, strikes on the central heating radiator, for example, during repairs on the ground floor of the house, are most likely to be heard by residents, even at a considerable distance from the source.

An analysis of sources showed that during the construction of frame-monolithic buildings, for the most part, sound insulation by the developer is not provided for housing, especially economy or comfort class [2-4]. But, at the same time, it largely depends on the materials that were chosen for the construction of buildings. Thus, internal inter-apartment walls, which in the vast majority of buildings are made of aerated concrete, have a lower rate of sound insulation from airborne noise than walls made of ceramic bricks. At the same time, walls with ceramic walls have similar indicators in terms of airborne noise insulation, which, due to the structural features of buildings, are made of monolithic reinforced concrete. However, this significantly increases the impact noise penetration rate.

In turn, for developers who position themselves as builders of luxury real estate, the use of high-quality and effective sound insulation in buildings is required. At the same time, the issue of additional soundproofing of premises from the developer comes to the fore. In this case, the fact that at the stage of building construction, the complex sound insulation of floors, walls, communications, reduces the level of penetration of various types of noise is not ruled out.

In many new residential complexes and old buildings, residents have to independently carry out construction work that is aimed at getting rid of noise [5-7]. At the same time, they, first of all, need to decide which type of noise they need to deal with. Because for different types of noise and insulated structures there are their own design and technological solutions. In most cases, only complex insulation of ceilings and walls will help to solve issues related to sound insulation and achieve comfortable conditions in the premises.

It is known that the level of insulation of airborne noise of an interfloor ceiling or load-bearing walls is determined, first of all, by the massiveness and thickness of the structure. However, this solution is not always economically feasible. In the case of insulation from impact noise, in most cases it is necessary to apply special technological solutions using additional structures. Thus, for isolation from the types of noise discussed above, it is necessary to apply unique design and technological solutions.

One of the structures through which structural noise is transmitted are floor slabs, monolithic or prefabricated. This is especially true for frame-monolithic or prefabricated buildings, which have been built in large numbers since the beginning of the 21st century. One of the most effective ways to deal with this type of noise is, from the point of view of building acoustics, the construction of a "floating" floor [7, 8].

This design is a massive screed of fine-grained concrete (often with a semi-dry cement-sand mixture) or lightweight concrete, which are laid on the interfloor overlap over a layer of material with elastic properties. At the same time, the "floating" floor screed should not have rigid connections with both the load-bearing and enclosing structures of the building [9]. To do this, it is separated from the side surfaces of walls, diaphragms and partitions with elastic gaskets (damper tape). As the material of the insulating layer, in most cases, slabs of acoustic mineral wool on a basalt or fiberglass base are used. It is also possible to use various types of foamed polymeric or fibrous roll materials.

The sound insulation index of a floating floor depends on the thickness and structure of the screed material and the elastic properties of the gasket material. In some cases, the use of various types of soundproofing materials can achieve a reduction in impact noise by more than 40 dB. Therefore, the search for optimal design and technological solutions and materials that are aimed at obtaining structures that provide standard sound insulation indicators becomes an urgent task.

Materials and methods of study. In the structures under study, the thickness of the monolithic reinforced concrete floor slab was 180 mm. In turn, for isolation from impact and structure-borne noise, a simple thickening of the structure is not effective. Therefore, it is necessary to use specially developed and more effective design and technological solutions for floor soundproofing.

The studies were carried out in natural conditions, in apartments of houses built according to a frame-monolithic scheme. Two apartments are allocated for each type of floor soundproofing construction. This is necessary for the reliability of the results obtained and the elimination of the error factor in the performance of works [10]. The following materials were used in the research:

– "Izolkap" – polystyrene concrete, which is a light mixture for the installation of heat and sound insulating screed, which consists of Portland cement and filler treated with a special additive. As a filler, inert expanded polystyrene granules (Ø 6-8 mm) are used, with high thermal insulation ability. The material belongs to the class of lightweight concrete.

– "Akuflex" is a rolled material based on specially processed polyester fibers, developed in accordance with modern requirements for room acoustics and working to absorb impact noise. The material is used as a soundproofing base in the construction of "floating" floors. It is a layer between the screed and the floor finish. In addition, "Akuflex" can be used as a damping layer under the screed for additional insulation against impact noise.

Experimental planning theory was used to conduct experimental studies. In accordance with this theory, a 15-point plan of experimental studies was used. In it, each of the factors changes at three different levels [11]. They are conditionally designated -1, 0 and +1.

The following factors and levels of their variation were adopted in the work, Table 1:

– thickness of the layer "Izolkap" (X_1) – (50 ± 10) mm;

– thickness of the c/p screed (X_2) – (50 ± 10) mm;

– density of "Izolkap" (X_3) – (300 ± 50) kg/m^3.

Table 1 – Factors and levels of their variation

Levels of variation	Factors		
	X_1	X_2	X_3
	Thickness of the layer "Izolkap", mm	Thickness of the layer c/s screed, mm	Density of "Izolkap", kg/m^3
-1	40	40	250
0	50	50	300
+1	60	60	350

Factors of the thickness of the material "Izolkap" (polystyrene concrete) and the thickness of the c/p screed can affect the impact and airborne sound insulation, and also affect the complexity and time of work.

The density factor of the "Izolkap" material directly affects the impact noise index, since the greater the density, the more cement in the material, which increases the impact noise index, and this also affects the complexity of laying the material and the time of work.

The studies were carried out using a 15-point three-factor experiment plan, which is shown in Table 2.

Table 2 – Experiment plan

№ Scheme	x_1	x_2	x_3	"Izolkap", mm	C/s screed, mm	Density «Izolkap», kg/m^3
1	+1	-1	-1	60	40	250
2	+1	-1	+1	60	40	350
3	+1	0	0	60	50	300
4	+1	+1	-1	60	60	250
5	+1	+1	+1	60	60	350
6	-1	-1	0	40	40	300
7	-1	0	-1	40	50	250
8	-1	0	0	40	50	300
9	-1	0	+1	40	50	350
10	-1	+1	0	40	60	300
11	0	0	0	50	50	300
12	0	-1	+1	50	40	350
13	0	-1	-1	50	40	250
14	0	+1	-1	50	60	250
15	0	+1	+1	50	60	350

Research results. Work performance technology. Organizational and technological processes of the device of constructive and technological schemes of the floor.

1. Preparatory work. Leveling the floor slab (filling depressions and caverns, beating off large influxes of concrete), as well as grouting the fixings of the facade slab to the floor slab with mortar and grouting geodesic holes in the floor slab.

Installation of a damper tape around the perimeter of the premises Fig. 1, and cleaning the surface from debris, as well as dedusting the surface.

Fig. 1. Installation the damper tape

2. The installation of the material "Izolkap". Preparatory work (kneading and supply of material, lifting tools, equipment to the floor). The material device process is shown in Fig. 2.

Fig. 2. The installation of "Izolkap"

3. The device of the material "Akuflex".

3.1. Preparatory work for the device material "Akuflex":

A) Partial sealing of the surface of the coating in places of formation of cavities and junctions of heating pipes with "Izolkap" material, cleaning of sags on a previously made surface.

B) Cleaning the damper tape from contamination with "Izolkap" material.

3.2. Laying material "Akuflex". It is produced by gluing rolls of material to each other with reinforced tape, with an overlap of 5-10 cm, as well as gluing the roll to a damper tape. The process of laying the "Akuflex" material is shown in Fig. 3.

Fig. 3. Laying material "Akuflex"

4. Installation of a cement-sand screed Fig. 4.

Fig. 4. Installation of a cement-sand screed

Measurements of sound insulation of reduced impact noise consist of the following stages: preparation for testing premises; measurement of the level of impact noise under the ceiling when creating shock effects on it; processing of measurement results.

Research equipment. For acoustic studies, the following set of measuring equipment was used:

- Acoustic multifunctional counter "Octava-ECOPHYSICS";
- Standard percussion machine "UM-10";
- Microphone dBx;
- Software package for measurement of reverberation time based on PC;
- Preamp P200;
- Acoustic system dB Technologies OPERA 605D.

Measurement of impact noise insulation was carried out according to the methods of DSTU B V.2.6-86:2009 (Fig. 5), calculation according to DSTU B V.2.6-85:2009.

The results of field tests are shown in Table. 3. Floor structures No. 1, 2, 4, 7, 11, 14 – comply with regulatory requirements, floor structures No. 2, 3, 5, 6, 8, 9, 10, 12, 13, 15 – do not comply with regulatory requirements.

Table 3 – The results of field tests

№№ p/p	Plan line number														
	1	2	3	4	5	6	7	8	9	10	11	12	13	14	15
L’nw, dB	54	57	56	52	56	55	53	56	56	57	52	57	56	52	57

Fig. 5. Measurement of impact noise insulation

Prospects for further research. It should be noted that it is necessary to study the cost of arranging such floors. This will make it possible to optimize these works not only in terms of structural features, but also in terms of the economic component.

Conclusions:

1. The results of full-scale studies of structures for impact noise using the theory of planning experiments made it possible to choose the most rational option for sound insulation.

2. It has been established that the arrangement of the structural-technological scheme for soundproofing floor no. 11 makes it possible to reduce the level of the initial (uncoated reinforced concrete slab) impact noise in the room by 37.5%.

3. Floor structures with thicknesses of "Izolkap" materials (with a density of 250 and 300 kg/m^3) and a c/s screed of 40 mm are not sufficient and will not satisfy the strength indicators, which in the future may lead to rapid wear and destruction of the structure.

4. Floor structures with thicknesses of "Izolkap" materials (with a density of 300 and 350 kg/m^3) and a 50 mm c/s screed are sufficient and meet the necessary sound insulation and strength requirements.

5. Floor structures with thicknesses of "Izolkap" materials (with a density of 300 and 350 kg/m^3) and a cement/sand screed of 60 mm are sufficient and meet the necessary requirements for sound insulation and strength, but are more difficult to manufacture and are not economically viable.

6. The work requires further research, thanks to which the optimal insulation parameters will be determined, taking into account the cost of installing such floors.

References

[1] O.I. Meneylyuk, I.M. Babiy, H.D. Bochorishvili, K.I. Bochevar, *Materialy ta tekhnolohiyi izolyatsiynykh robit v budivnytstvi*. Monohrafiya. Odesa: Vydavnytstvo FOP Bondarenko M.O., 2020.

[2] A.R. Murzakova, U.Sh. Shayakhmetov, K.A. Vasin, V.S. Bakunov, "Razrabotka tehnologyi polucheniya efektivnogo stroitelnogo yacheistogo teplo i zvukoizolyatsionnogo konstrukcionnogo materiala", *Stroitelnye materialy*, no. 5, p. 65-66, 2011.

[3] DBN V.1.1-31:2013. Zahist terutoriy, budivel' ta sporud vid shumu. Kyiv, Ministerstvo regional'nogo rozvitku, budivnictva ta zhitlovo-komunal'nogo gospodarstva Ukraïni, 2014.

[4] V.L. Angelov, L.V. Angelov, "Zvukoizolyatsiya mezhetazhnikh perekrytiy sovremennykh krupnopanel'nykh zdaniy", *Materialy mezhdunarodnoy nauchno-prakticheskoy konferencii "Energosberezhenie i ekologiya v stroitelstve i ZhKKh, transportnaya i promyshlennaya tekhnologiya*". Moskva-Budva, 2010, p. 195-197.

[5] V.S. Didkovsky, V.P. Hare, N.A. Samoylenko, "Ocenka izolyatsii vozdushnogo shuma ograzhdayuschikh konstruktsiy v rasshirennom diapazone chastot", *Electronika i svyaz'*, no. 1, pp. 164-168, 2011.

[6] A.S. Polevshchikov, "Zvukoizolyatsiya mezhetazhnikh perekritiy v zhilikh zdaniyakh", *Zhilishchnoe stroitel'stvo*, no. 7, pp. 55-57, 2015.

[7] O.O. Popov, I.M. Babiy, YE.Y. Kal′chenya, A.M. Hostryk, "Vybir ratsional′noho konstruktyvno-tekhnolohichnoho rishennya ulashtuvannya teplo- ta zvukoizolyatsiyi pidlohy", *Mizhvidomchyy naukovo-tekhnichnyy zbirnyk (tekhnichni nauky) «Budivel'ne vyrobnytstvo» NDIBV*, vol. 65, pp. 41-44, 2019.

[8] V.A. Gorin, V.V. Klimenko, E.P. Shnurnikova, "Izolyatsiya udarnogo shuma mezhetazhnimy perekritiyami s parketnimy polamy", *Academia. Arkhitectura i stroitelstvo*, no. 3, pp. 200-203, 2010.

[9] DSTU-N B V.1.1-34:2013. Postanovleniye po raschetu i proektirovaniyu zvukoizolyatsii ograzhdayuschikh konstruktsiy zhulikh I obschestvennikh zdaniy, 2014.

[10] DSTU B V.2.7-183:2009. Stroitel'nie materialy. Materialy i izdeliya stoitel'nie zvukopogloschaushchie i zvukoizolyatsionnie. Klasifikatsiya I obchie tekhnicheskie trebovaniya. Kiïv, Minregionbud Ukraïni, 2010.

[11] V.A. Voznesenskyy, T.V. Lyashenko, B.L. Oharkov, *Chyslennye metody reshenyya stroytel'no-tekhnolohycheskykh zadach na ÉVM*. K.: Vyshcha shkola, 1989.

НАТУРНІ ДОСЛІДИ ІЗОЛЯЦІЇ УДАРНОГО ШУМУ З ВИКОРИСТАННЯМ ТЕОРІЇ ПЛАНУВАННЯ

[1]**Бабій І.М.,** к.т.н., доцент,
igor7617@gmail.com, ORCID: 0000-0001-8650-1751
[1]**Бічев І.К.,** к.т.н., доцент,
bichev@ukr.net, ORCID: 0000-0002-3000-2600
[1]**Кальченя Є.Ю.,** аспірант,
yevhenii.kalchenya@gmail.com, ORCID: 0000-0003-0653-1171
[1]*Одеська державна академія будівництва та архітектури*
вул. Дідріхсона, 4, м. Одеса, 65029, Україна

Анотація. У сучасному будівництві одним з основних показників якості житла для користувачів приміщень багатоповерхових будинків залишається шум. Завданням перешкоджання шуму, що виникає в самому будинку, необхідно приділити більшу увагу при проектуванні та влаштуванні звукоізоляції. Відомо, що сторонні звуки, що проникають у житлове приміщення, стають причиною негативного впливу не лише на психологічний стан людини, а й на фізичний. У зв'язку з цим кожен користувач приміщень хоче отримати комфортні умови перебування в них. Для досягнення цієї умови необхідно розробити ефективні конструктивні та технологічні схеми звукоізоляції підлоги від ударного шуму, а також їх перевірки та оцінки з використанням теорії планування експериментів.

Дана стаття присвячена вирішенню важливого питання звукоізоляції перекриттів монолітних залізобетонних багатоповерхових житлових будинків, а саме від ударного шуму. У статті розглянуто конструктивно-технологічні схеми звукоізоляції підлоги п’ятнадцяти типів із застосуванням різних матеріалів та їх комбінацій для досягнення нормативних вимог до звукоізоляції від ударного шуму.

Визначено, що на показники ізоляції від ударного шуму досить вагомо впливає товщина шару матеріалів та щільність. В роботі досліджувалися конструкції підлоги на основі шарів матеріалів, що змінювалися. А саме такі показники як товщина (50±10 мм) та щільність (300±50 кг/м^3) полістиролбетону «Izolkap» та товщина напівсухої стяжки (50±10 мм).

При виборі найбільш раціональної конструктивно-технологічної схеми використовувалися результати теорії планування, а також показники зниженого ударного шуму, отримані в результаті натурних випробувань, що дозволило вибрати найбільш раціональний і ефективний варіант «плаваючої» підлоги – на основі матеріалів «Акуфлекс» та «Ізолкап» (полістиролбетон) – схема №11, показник приведеного рівня ударного шуму Lnw = 52 дБ, що на 9,1% менше за нормативний.

Влаштування конструктивно-технологічної схеми звукоізоляції підлоги №11 дозволяє знизити рівень початкового (залізобетонна плита без покриття) ударного шуму в приміщенні на 37,5%.

Ключові слова: звукоізоляція, ударний шум, «плаваюча» підлога, багатошарова система.

Стаття надійшла до редакції 30.07.2023

ВИМОГИ ДО ОФОРМЛЕННЯ СТАТЕЙ
у збірнику наукових праць
“Сучасне будівництво та архітектура”

До опублікування у фаховій збірці наукових праць приймаються раніше не опубліковані наукові статті, із зазначеною нижче **тематикою публікацій**:

1. Архітектура.
2. Будівельні конструкції.
3. Будівельні матеріали та технології.
4. Гідротехнічне та транспортне будівництво.
5. Інженерні мережі та обладнання.
6. Основи та фундаменти.
7. Технологія та організація будівельного виробництва.

Стаття повинна відповідати тематиці збірника, публікуватися вперше і включати такі елементи:

• актуальність та постановку проблеми у загальному вигляді, її зв'язок із важливими науковими чи практичними завданнями;
• аналіз останніх досліджень і публікацій, у яких представлено вирішення даної проблеми і на які спирається автор; виділення невирішених раніше частин загальної проблеми, яким присвячується дана стаття;
• формулювання цілей статті (постановка завдання);
• виклад основного матеріалу дослідження з повним обґрунтуванням отриманих наукових результатів;
• висновки з даного дослідження і перспективи подальшого розвитку у даному напрямку;
• список літератури.

Загальні вимоги до оформлення тексту

Статті подаються в електронному вигляді файлом Word 97 − 2003 в форматі .doc. Назва файлу має містити номер тематики публікації та прізвище першого автора (наприклад, 5 Іванов.doc).

Статті подаються українською чи англійською мовою і друкуються мовою оригіналу.

Текстова частина статті набирається на аркушах формату **А4** шрифтом **Times New Roman 12 пт** через одинарний інтервал, вирівнюється по ширині сторінки, поля по 2 см з усіх боків, абзацний відступ − 1,0 см. **Обсяг статті 7-16 повних сторінок разом з анотаціями.**

Структура статті:

− ***індекс УДК*** (вирівняно по лівому краю без абзацного відступу, прописний, напівжирний);
− ***назва статті*** (відцентрована, усі літери прописні, напівжирні, переноси не допускаються);
− ***прізвище, ініціали всіх авторів, науковий ступінь, вчене звання*** (вирівняно по правому краю, прізвище – напівжирний; ступінь і звання – рядковий);
− ***повна назва вищого навчального закладу чи організації*** (курсив, вирівняно по правому краю; якщо автори з різних навчальних закладів, то кожен автор з окремого рядка);

− ***електрона пошта*** (вирівняно по правому краю та поряд унікальний номер ORCID);

− ***анотації до статті*** (абзацний відступ, назва напівжирна, анотації пишуться двома мовами: українською і англійською.

Текст першої анотації пишеться мовою основного тексту статті та повинен бути **не менш як 1800 знаків.**

Текст другої анотації, якщо видання не є повністю англомовним, кожна публікація не англійською мовою супроводжується анотацією англійською мовою обсягом **не менш як 1800 знаків**. Якщо видання не є повністю україномовним, кожна публікація не українською мовою супроводжується анотацією українською мовою обсягом **не менш як 1800 знаків**. Друга анотація розміщується в кінці статті після списку літератури на англійській мові.

Дві анотації повинні коротко повторювати структуру статті, що включає введення, ціль, методику, результати, висновок. Машинний переклад **не дозволяється.**

− ***ключові слова*** (міжрядковий інтервал не робиться, абзацний відступ, назва напівжирна, текст ключових слів не більше 6–8 слів).

Назва статі, прізвище і ініціали, науковий ступінь, вчене звання, місце роботи, анотація і ключові слова – повторюються українською та англійською мовами.

Між рядками з індексом УДК, назвою статі, прізвищем авторів, анотацією, основним текстом і переліком літератури, літературою на англійській мові та другою анотацією одинарний інтервал.

− ***Основний текст статті.***

Структура основного тексту статті згідно з постановою ВАК України № 7-05/1 від 15.01.2003 р. (Бюлетень ВАК України №1, 2003 р.) повинна мати такі необхідні елементи (***назви структурних елементів в тексті статті потрібно виділити напівжирно***)**:**

– вступ (постановка проблеми у загальному вигляді та її зв’язок з важливими науковими чи практичними завданнями);

− аналіз останніх джерел досліджень і публікацій, у яких започатковано розв’язання проблеми (бажано, щоб це був аналіз останніх публікацій у фахових журналах) і на які опирається автор, виділення не розв'язаних раніше частин загальної проблеми, яким присвячується стаття;

– постановка мети та завдання (формулювання мети та завдань досліджень);

– матеріали та методи дослідження (опис використаних матеріалів та методів дослідження проблеми, що розглядається у статті);

– основний матеріал і результати (виклад основного матеріалу дослідження з повним обґрунтуванням отриманих наукових результатів);

− висновки (наукова новизна, наукове та практичне значення результатів дослідження, перспективи подальших наукових розроблень);

− ***література*** (відцентрована, напівжирна; посилання в тексті подають у квадратних дужках [2]; список літератури наводиться відповідно порядку посилань у тексті згідно з ДСТУ 8302:2015 та записується в стовпчик; написання «Джерела інформації», «Перелік літератури» **не допускається**). Бібліографічний список наводиться мовою оригіналу та транслітерується.

− ***бібліографічний список (References).*** Для відтворення українських власних назв засобами англійської мови при перекладі публікації англійською мовою застосовується транслітерація. Найменування організацій та установ, що не перекладаються на англійську мову, також транслітеруються. Транслітерація прізвищ авторів виконується залежно від мови оригіналу джерела відповідно до вимог Постанови Кабінету Міністрів України від 27.01.2010 р. № 55 «Про впорядкування транслітерації українського алфавіту латиницею». Бібліографічний список повинен бути оформлений з використанням стиля ***IEEE STYLE*** згідно з «Міжнародним стилем цитування та посилання в наукових роботах», Київ, 2016.

Таблиці слід виконувати в редакторах Word без заливання. Кожна таблиця має бути надрукована з відповідним заголовком та нумерацією після першого посилання на неї. Ширина таблиць не повинна перевищувати поля сторінки. Шрифт в таблиці повинен відповідати шрифту статті.

Формули мають бути виконані в редакторі формул *Equation 3.0* чи *MathType* з використанням тільки загальноприйнятих шрифтів (Times New Roman; Symbol). Кожна формула набирається як один об'єкт, нумерація формул арабськими цифрами справа в дужках вирівняна по ширині сторінки.

Рисунки (діаграми, фото), подаються у чорно-білому, кольоровому варіанті або у градаціях сірого кольору після першого посилання на них; мають бути згруповані та являти собою один графічний об'єкт; мати нумерацію та підпис позначення ось координат. Розміри підписів на рисунку повинні відповідати шрифту Times New Roman 12 пт.

Разом зі статтею подаються:

− відомості про автора (авторська довідка): прізвище, ім'я, по батькові (повністю); вчене звання, вчений ступінь; посада, місце роботи; контактні адреси й телефони; поштова адреса, на яку надсилати примірник збірника

– рецензія на статтю, якщо автором є аспірант без співавторів з вченим ступенем та вченим званням.

Статті, які не відповідають наведеним вимогам, до розгляду не приймаються.

Подані матеріали підлягають додатковому рецензуванню членами редколегії або провідними фахівцями за науковими напрямами, тому можуть бути повернені авторам на доопрацювання.

Остаточне рішення щодо публікації статті приймає редакційна колегія видання.

Відхилений оригінал не повертається.

Оплата здійснюється тільки після підтвердження прийняття статті до друку.

Вартість публікації статті **1100 грн.** Збірник виходить 4 рази на рік щоквартально, в кінці кожного кварталу. Статті необхідно надсилати до 1 числа останнього кварталу (наприклад, якщо збірник виходить в кінці червня, то статті приймаються до 1 червня). Але прийом статей може закінчитись раніше вказаного терміну, якщо буде набрано необхідну кількість сторінок.

Матеріали надсилати за адресою:
Редакція «Сучасне будівництво та архітектура»
Одеська державна академія будівництва та архітектури,
вул. Дідрихсона, 4
м. Одеса, 65029, Україна
Контактна особа: Антонюк Надія Романівна
тел. роб. (048) 70-00-608
e-mail: visnuk_odaba@ogasa.org.ua
Сайт збірника: http://visnyk-odaba.org.ua/

Платіжні реквізити:
Центр НТТМ по АБ, код **21028281**,
МФО **320478**, Р/р **UA 103204780000026009924861812** в ПАТ АБ «Укргазбанк»,
Призначення платежу: «Сучасне будівництво та архітектура, ПІБ першого автора»

Просимо після відправлення матеріалів обов'язково зателефонувати або зв'язатися електронною поштою, щоб упевнитися в отриманні матеріалів та рішенні редакційної колегії щодо публікації статті.

Наукове видання

СУЧАСНЕ БУДІВНИЦТВО ТА АРХІТЕКТУРА

ЗБІРНИК НАУКОВИХ ПРАЦЬ

Випуск № 5
вересень 2023

Головний редактор *Вировой В.М.*

Технічний редактор *Антонюк Н.Р.*

Підписано до друку 15.09.2023 р.
Формат 60×84/8. Папір офсетний. Гарнітура Times.
Цифровий друк. Ум.-друк. арк. 14,4.
Наклад 100 прим. Зам. №20-29Е

Видавець і виготовлювач:
Одеська державна академія будівництва та архітектури
Свідоцтво ДК № 4515 від 01.04.2013 р.
Україна, 65029, м. Одеса, вул. Дідріхсона, 4.
тел. (048) 729-85-34, e-mail: rio@ogasa.org.ua

Надруковано в авторській редакції з готового оригінал-макету
в редакційно-видавничому відділі ОДАБА